



HAL
open science

Climate and sea level variations in the Gulf of Lion : coupling stable and radiogenic isotopes proxies

Virgil Pasquier

► **To cite this version:**

Virgil Pasquier. Climate and sea level variations in the Gulf of Lion : coupling stable and radiogenic isotopes proxies. Earth Sciences. Université de Bretagne occidentale - Brest, 2017. English. NNT : 2017BRES0094 . tel-01738260v2

HAL Id: tel-01738260

<https://theses.hal.science/tel-01738260v2>

Submitted on 20 Mar 2018

HAL is a multi-disciplinary open access archive for the deposit and dissemination of scientific research documents, whether they are published or not. The documents may come from teaching and research institutions in France or abroad, or from public or private research centers.

L'archive ouverte pluridisciplinaire **HAL**, est destinée au dépôt et à la diffusion de documents scientifiques de niveau recherche, publiés ou non, émanant des établissements d'enseignement et de recherche français ou étrangers, des laboratoires publics ou privés.

Thèse préparée à l'Université de Bretagne Occidentale
pour obtenir le diplôme de DOCTEUR délivré de façon partagée par
L'Université de Bretagne Occidentale et l'Université de Bretagne
Loire

Spécialité : Géosciences Marine

École Doctorale Sciences de la Mer et du Littoral

présentée par

Virgil Pasquier

Préparée au Laboratoire Géosciences
Océan

Variations climatiques et glacio-eustatiques dans le Golfe du Lion: Une approche couplée des isotopes stables et radiogéniques

Climate and sea-level variations in the Gulf of Lion: coupling stable and radiogenic isotopes proxies.

Thèse soutenue le 17 novembre 2017
devant le jury composé de :

Frank BASSINOT

Directeur de recherche, CEA - LSCE / *Rapporteur*

Galen Pippa HALVERSON

Associate Professor, McGill university / *Rapporteur*

Aurélie PENAUD

Maître de conférence, Université de Bretagne Occidentale /
Examinatrice

Francisco Javier SIERRO

Professor, Universidad of Salamanca / *Examineur*

Christophe THOMAZO

Maître de conférence, Université de Bourgogne / *Examineur*

Christophe HEMOND

Professeur, Université de Bretagne Occidentale / *Examineur*

Marina RABINEAU

Chargée de recherche, Université de Bretagne Occidentale /
Directrice de thèse

Pierre SANS-JOFRE

Maître de conférence, Université de Bretagne Occidentale /
Tuteur

Sidonie REVILLON

Chercheuse Associée, Université de Bretagne Occidentale /
Tutrice

David FIKE

Professor, Washington University in St Louis / *Invited tutor*

Samuel TOUCANNE

Cadre de recherche, IFREMER / *invité*



Sur les épaules de Darwin,
Sur les épaules des Géants.
Se tenir sur les épaules des Géants,
et voir plus loin, voir dans l'invisible,
à travers l'espace et à travers le temps.

Plonger notre regard dans le passé,
pouvoir remonter le temps à contre courant,
parcourir des âges depuis longtemps révolus,
où nos ancêtres arpentaient le monde,
mais où nous étions pas encore.

Entrevoir ces monde disparus qui nous ont donnés naissance,
découvrir des éclats de passé qui, soudain, resurgissent de l'oubli
et ressentir un vertige ...

Le vertige du voyage,
d'innombrables voyages depuis la nuit des temps,
aussi loin que nous remontons dans le passé,
notre Histoire est une histoire en chemin,
en partance ...

J-C Ameisen

Contents

	Page
1 Chapter I: Sediment on the move: How margin sediments reflect processes from the mountains to the sea?	1
1.1 Preamble	7
1.2 Source to sink: a multidisciplinary scope	9
1.3 Source to Sink: Natural interactions and feedback between surface and deep Earth processes ..	9
1.4 Orbital climate cycles: From landscape to sedimentary responses	12
1.5 The influence of climate on early and burial diagenesis	19
1.6 The organic matter: the driving Force during early diagenesis	20
1.7 Diagenetic regimes and depositional environment	23
1.8 The Gulf of Lion: PROMESS for new insights for early diagenesis?	25
1.9 Climate's impact on the Gulf of Lion sedimentation	28
1.10 Organic carbon source, fluxes and burial in the Gulf of Lion	29
1.11 Keeping the PROMESS	31
1.12 Scope of this thesis	34
2 Chapter II: Materials and Methods	43
2.1 PRGL 1-4 borehole	47
2.1.1 PRGL1-4 description	47
2.1.2 Available dataset	48
2.1.3 PRGL 1-4 age model	51
2.1.4 Sampling strategy	53
2.2 Methods	55
2.2.1 Multi-element concentration determination	55
2.2.2 S-C-N content in bulk sediments	59
2.2.3 Mass spectrometry	79
3 Chapter III: Increase runoff in the North Mediterranean borderland during deposition of anoxic events (sapropels): the emerging role of the North Atlantic climate	89
3.1 Modern Mediterranean state	92
3.1.1 Climate	92
3.1.2 Oceanic circulation	94
3.2 What are 'Sapropels'	94
3.2.1 Appearance and duration	96
3.2.2 Sapropel formation: Anoxia and/or Productivity	98
3.2.3 The emergence of a North Borderland freshwater contribution to sapropel formation	100
3.2.4 Mediterranean climate response to North Atlantic climate variability	102
3.3 New evidences of enhanced rainfall activity in the Gulf of Lion	104
3.4 Implication for sapropel history	118
4 Chapter IV: When Milankovitch cycles induce overprints on global pyrite records: Toward a better understanding of the sulfur cycle	129
4.1 Biological Sulfur cycling	134
4.1.1 Sulfate reduction	134
4.1.2 Sulfur oxidation	137
4.1.3 Sulfur disproportionation	137
4.2 Geological Sulfur cycle	139
4.2.1 Generalities	139
4.2.2 The mineral record of the sulfur cycle	141
4.2.3 Variability in Sulfur isotopes proxies	145
4.3 Variability in modern environments	150
4.3.1 Study case of Papua New Guinea [Aller et al., 2008]	150
4.3.2 Model prediction under sea-level changes [Fike et al. in review]	153
4.4 Pyrite sulfur isotopes: a new proxy of glacial interglacial environmental changes	154
4.5 Implications for past sulfur records	161
4.6 Perspectives	161

Contents

	Page
Chapter V: How climate affects early diagenesis?	171
5.1 Organic matter content, origin and reactivity effect on early diagenetic processes [microbial view]	174
5.1.1 Organic carbon content	175
5.1.2 Organic carbon origin	176
5.1.3 Organic carbon reactivity and preservation state	178
5.2 Indirect regulation of early diagenesis by climate changes [sedimentary control]	181
5.3 Looking forward	184
Appendix 1: The use of laser ablation: A New Hope in Brest	185
A1.1 Scope of this project	186
A1.2 Material	187
A1.3 Objectives	188
A1.4 Set-up of foraminifera cleaning in Brest	188
A1.5 Set-up of the laser ablation technic in Brest	189
A1.6 What about my TE/Ca PhD project?	194
Appendix 2: CarboFlux: detritic versus biogenic	201
A2.1 Scope of this project	202
A2.2 Geochemical approach	205
A2.3 Identification of carbonates preserved in Gulf of Lion marine sediments	207
A2.4 Characterization of detrital carbonates in the Gulf of Lion marine sediment	209
A2.4 Characterization of carbonates from the watershed	210
A2.5 Looking forward	212

Sediments on the move: How margin sediments reflect processes from the mountains to the sea?

Sédiments en mouvement: Comment les
sédiments intègrent les processus de la
montagne à l'océan?

Abstract

Ce chapitre introductif a pour but de donner aux lecteurs les notions nécessaires à la compréhension d'un système de transfert Terre-Mer, mais également comment les sédiments déposés sur les marges continentales peuvent être utilisés comme des indicateurs des variations passées de ces systèmes. L'un des acteurs principaux des transferts de sédiments est le climat. Pour cette raison, nous exposerons brièvement les causes, puis également les conséquences des variations climatiques sur la sédimentation des marges (passive). L'influence du climat sur la diagenèse, et plus particulièrement sur l'export du carbone organique, est introduit. En effet, ce dernier est un acteur principal des processus post-deposition (diagenèse). Nous verrons donc comment ce dernier la régule.

Puisque ce travail de thèse a été réalisé sur un forage prélevé dans le Golfe du Lion (Sud de la France), nous focaliserons cette introduction sur les caractéristiques sédimentaires de ce dernier. Mais également sur l'impact du climat sur sa sédimentation, et sur l'export de carbone organique dans le bassin sédimentaire.

Ce chapitre est conclu par une présentation générale de l'organisation du manuscrit.

Contents

1 Preamble	7
2 Source to sink: a multidisciplinary scope	9
3 Source to Sink: Natural interactions and feedback between surface and deep Earth processes.....	9
4 Orbital climate cycles: From landscape to sedimentary responses	12
5 The influence of climate on early and burial diagenesis	19
6 The organic matter: the driving 'Force' during early diagenesis	20
7 Diagenetic regimes and depositional environment	23
8 The Gulf of Lion: PROMESS for new insights for early diagenesis?	25
9 Climate's impact on the Gulf of Lion sedimentation	28
10 Organic carbon source, fluxes and burial in the Gulf of Lion	29
11 Keeping the PROMESS	31
12 Scope of this thesis.....	34

List of Figures

1	Conceptual view of a sediment rooting system. Sediment is transferred from a source region to a sink along trajectories shown by rivers (solid blue lines). Some trajectories involves short transit times with brief periods of storage in the sediment rooting system (floodplain buffering zone), whereas others involve long times with prolonged periods of storage (i.e. river bars, shore accumulation). Transport and storage of sediment imply buffering of incoming sediment flux signals.	7
2	Schematic and blurred representation of factors controlling sedimentation. From Rabineau, 2001.	9
3	Time scales of 'Source to Sink' concept. Longer times scales are embedded in shorter sedimentological response, redrawn from Ruddiman 2001.	10
4	(A) Schematic of a sedimentary supply (Q) signal from the erosion zone and how that signal propagates through the rooting system. The leftmost Q_s signal represents as measured at the exit of the erosion zone and for simplification is the same that the original forcing. The transfer zone Q_s signal is measured within the transfer zone at some distance from the exit of the source zone. The rightmost cartoon show the propagated signal at the accumulation zone (sink) as an input for stratigraphic record. Dashed lines illustrate that the signal is modified during propagation processes. (B) 2D profile of 'classic' rooting sediment system composed of a source zone prone to erosion, transfer and accumulation zones (yellow areas highlight potential storage zone). Important control factors are indicated on the profile such as tectonics, climate, sea level base-line and potential anthropogenic activities. From Romans et al. 2016.	11
5	(A) Major climatic variations recorded in marine benthic oxygen isotope (LR04 curve) during the last 5 Ma from Lisieki and Raymo, 2005. (B) LR04 zoom over the last 700,000 years with Railsback et al. (2015a) marine isotope scheme which was used in the following studies of this manuscript. Periodic variation of orbital parameters collectively known as Milankovitch parameters: (C) Eccentricity, (D) axial tilt and (E) precession. Taken in unison variation of these three cycles creates alterations in the seasonality of solar radiation reaching the Earth's surface (i.e. insolation curve in Watt/m^2).	14
6	Milankovitch parameters. (A) Earth's eccentricity orbit: Earth's orbit around the Sun is slightly elliptical inducing 100,000 and 400,000 years periodicities. (B) Earth's tilt: Earth's rotation axis is currently tilted at an angle of 23.5° away from a line perpendicular to the plane of its orbit around the Sun with resulting periodicity (41,000 years). (C) Precession of Earth's axis: Earth's slow wobbling motion cause its rotational axis to point in different direction through time. Adapted from Imbrie and Imbrie 1980.	16
7	Relative sea level over the last 550,000 years. Data came from marine benthic foraminifera oxygen isotope, coral-reefs for highstands and delta for lowstands. First order cycles (i.e.100,000 years) are clearly identified as inducing approx 100 meters sea level changes, with superimposed 20 and 40,000 cyclicities. Red bands correspond to interglacials periods with warm substages (i.e. sensu stricto) highlighted in dark pink. Termination (T.) according to Barker et al. (2011). Scheme of marine stage according to Railsback et al. (2015a). Redrawn from Rabineau et al. (2006); Jouet (2007).	17

8	Timing of sequence boundaries and systems tracts in relation to time and base level changes. HST: Highstand system tract, TST: Transgressive system tract, LST: Lowstand System Tract, FSST: Falling sea level stage system tract, SB: Sequence boundary, MFS: Maximum flooding surface, TS: Transgressive surface. Redrawn from Vail et al. (1977).	18
9	Stratigraphy conceptual model. (A) The equilibrium profile of a rooting system. In order to maintain the equilibrium profile erosion and/or deposition of alluvial sediment place if there is no sea-level changes and/or tectonic vertical movements. (B) Erosion of sediment due to uplift in the source zone. (C) Erosion and deposition of sediments along the transfer zone due to subsidence of the source zone. (D) Deposition of sediment in the sink zone due to a relative sea-level rise. (E) erosion and transfer of sediment in a deeper sedimentary unit due to sea-level fall. From http://www.cambridge.org/	19
10	Schematic in vertical cross section of major diagenetic processes involved in the remineralization of organic matter in marine deposits. After deposition, reactive organic matter is decomposed and oxidized. The rate of decrease organic matter with time and depth is a function of the initial reactivity and burial condition, as the quantity of buried organic carbon in sedimentary sequence. A set of oxydation processes naturally occur leading to the production of dissolved products which are used by the benthic community and reduced authigenic minerals. From Aller (2014).	22
11	Few examples of steady and unsteady diagenetic regimes commonly observed in margin environments. Individual regimes differ in boundary condition, sediment mass properties, and interior transport-reaction processes. (A) Steady state accumulation assumed in most diagenetic regime (Bernier et al. 1980); (B) bioturbated surface region; (C) highly mobil and periodically reworked sediment layer uncomformably overlying older, relic deposits; (D) Permeable sediment and bioturbated zones that controlled exchanges; (E) un-steady environment controlled by re-oxidation after erosional processes. Modified from (Aller 2014).	25
12	Location of the study area delimited by a red rectangle on the general map of the Mediterranean region.	26
13	Seismic dataset and bathymetry of the Gulf of Lion (modified from Leroux et al., 2015). Red triangles correspond to industrial wells, blues triangles correspond to the two PROMESS European boreholes. Big green dots represents the ESP data, small green dots represent OBS data on Sardinia profiles. From Leroux et al. (2017).	27
14	Synthetic stratigraphic section across the Gulf of Lions, illustrating the overall progradation of the deltaic system during MIS3 and MIS2 and retrogradation during the deglaciation. Coastal deltaic deposits are shown in yellow, while pelitic prodeltaic sediments are shown in gray. The red line from the inner shelf to the slope indicates the recent condensed layer. The position of borehole/core PRGL1-MD99-2348 is indicated. Names of seismic reflectors and seismic units together with their ages are shown in the figure. Although many of these units are not mentioned in the text they are shown to facilitate comparisons with other papers referenced in the text. Note that the vertical scale is strongly exaggerated. The figure was modified from Rabineau (2001), Jouet et al. (2006).	28
15	Range of $\delta^{13}\text{C}$ and C/N values reported in the literature for characteristic organic matter sources (i.e. living flora and fauna) that accumulate in marine sedimentary sequences in coastal environment. Compile data from Lamb et al. (2006) and references therein.	30

16	Stable isotopic composition of organic carbon vs total nitrogen:carbon ratio from superficial sediments in the Gulf of Lion. The range of composition of four organic carbon sources (C3 vascular plant detritus, C3 soil derived organic matter riverine/estuarine phytoplankton detritus and marine phytoplankton detritus) are also plotted in the graph to illustrate their relative influences. Data from Tesi et al. (2007).....	30
17	(Bottom left) Bathymetrical map of the Gulf of Lion with location of PRGL1-4 borehole in the interfluvium of Boucart and Herault canyons, BC and HC respectively, and main coastal rivers. Part of high resolution seismic reflection profile P-1036a crossing the borehole in a NW-SE direction across the outer shelf and upper slope (modified from Rabineau (2001)). Schematic seismic section illustrate the stacking of the last five sedimentary sequences bounded by major discontinuities (red) attributed to 100 kyr glacio-eustatic cycles. The shelf morphology allows preservation of low-stand accumulation (yellow). The thick yellow line represent the shoreline position during the Last Glacial Maximum. PRGL1-4 location and sampling depth are projected within the seismic schematic framework.	32

List of Tables

1	Annual budget for the mineralization of organic matter and consumption of oxidants in Aarhus bay, Danish coastal sediment. The basic reaction and exchange in oxidation step are shown for the element involved. The rates of processes were determined for one m ² of sediment and where all recalculated to carbon equivalent. Data compiled in Jørgensen (1996).	23
---	--	----

1. Preamble

Continental margins are peculiar places to study the modern sedimentary cycle because sediment in margin regions has been routed from mountains (source) through river systems (transfer) to the sea (sink). In the sea, sediment can be deposited in deltas or coastal areas or further offshore on the shelf, slope and deep basin. In some cases, sediment is by-passed across continental shelves and is being delivered directly to the deep sea (often through submarine canyons and deep-sea fan channels, see **Figure 1**). This is what we call a '**routing system**': i.e. the system that transport sediment from mountains to the deep sea. Therefore, when looking at sediment records, we can see it as a 'storyteller' of the Earth's history.

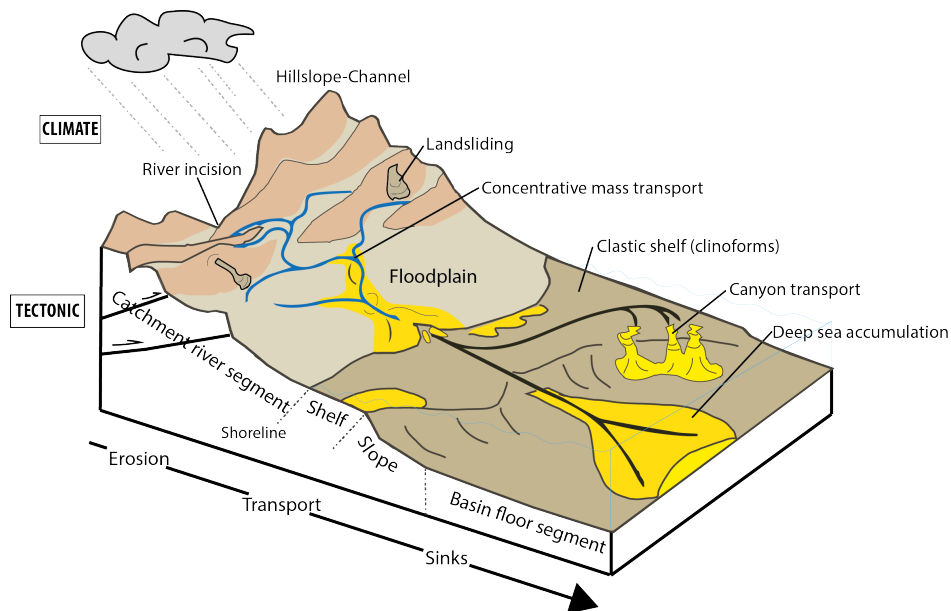


Figure 1

Conceptual view of a sediment routing system. Sediment is transferred from a source region to a sink along trajectories shown by rivers (solid blue lines). Some trajectories involves short transit times with brief periods of storage in the sediment routing system (floodplain buffering zone), whereas others involve long times with prolonged periods of storage (i.e. river bars, shore accumulation). Transport and storage of sediment imply buffering of incoming sediment flux signals.

The goal of this chapter is to let readers better understand what is a routing system, and how sedimentary archives on continental margin (i.e. the pile of sediment that will be sampled thanks to long boreholes) can be used to trace past variations of this 4 dimensions system (i.e. in space, but also in time). Many questions remain to be answered.

Which areas are eroding, when and why? Can we identify the first-order factors that controls sediment supply, in the present and in the past? How do the characteristics of river systems affect sediment's properties? Are we able to predict sediment origin and sediment maturity for a given source-to-sink system? Does it depends on regional climatic characteristics? How induced changes in a routing system affect the biosphere? What are post-depositional processes? How and when post-depositional processes happened and what are their effects on sediment's characteristics? On a broader scale, how can we reconstruct the geological history of a routing system, keeping in mind the different parameters that controlled the sedimentation (i.e. tectonic, climate, worldwide change in

sea level and shelf hydrodynamic, and post deposition processes).

This chapter will also try to highlight the question of time integration of the physical, chemical and biological processes that shape Earth's surface and that drive sedimentary fluxes using an unconventional scale that is out of our human timescale; over large spatial and geological times (in our case: the last 500 ka). Making the **connection** between these two-time levels is an exciting part of our natural science domain.

2. Source to sink: a multidisciplinary scope

The story of Earth's landscapes changes requires assimilation of **many disciplines**: geology, biogeochemistry, oceanography, atmospheric and hydrology chemistry, meteorology, ecology, glaciology, climate modeling, and many others. This range of discipline is very large and quite challenging for all new students in Earth's landscape evolution for whom each of these science is new and require very specific topics on many research fields and time scales.

3. Source to Sink: Natural interactions and feedback between surface and deep Earth processes

One of the main goal in a sedimentology approach is to access the link in sedimentary systems, between erosional, and depositional processes. Earth's landscape, shaped by the interplay between tectonic and climate, is a dynamic interface over which biogeochemical cycles operate, see **Figure 2**. This figure highlights that the sedimentation is associated with physical, biological, and chemical processes acting across the continent-ocean interface, and involves transport of particulate and dissolved sediments.

Sediment is moved from a **source to a sink**, from erosional processes on topographic highs and associated foreland, to the depositional processes in bathymetric lows ending in the deep oceanic basins. The long-term preservation of sediment in such routing system produces the narrative of the geological history through times, which is in fact driven by Earth's lithosphere motion that creates both relief in mountains and basins in oceans.

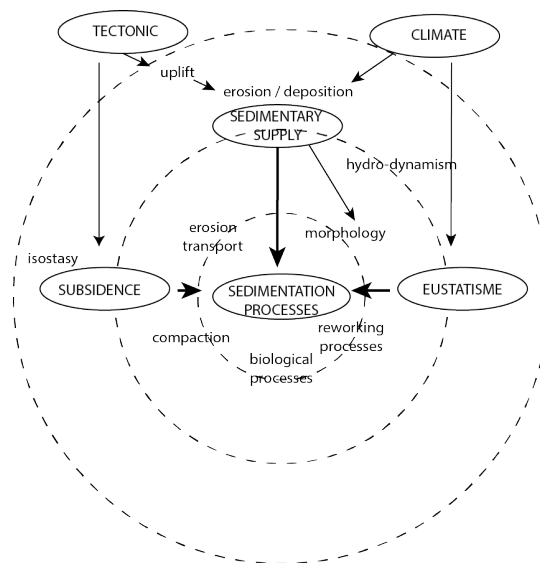


Figure 2

Schematic and blurred representation of factors controlling sedimentation. From Rabineau, 2001.

Earth's surface is the critical interface across which the bulk of Earth's chemical and biological exchanges take place. Most biological cycles involve the transport of material, either as particles, or dissolved by fluids. This transport represents more than 20 billion tons of sediments delivered to the ocean each year (Allen 2008). And about the same mass is delivered to the ocean as solute elements allowing the perpetuation of the ocean bulk chemistry, nutrient loading and biological productivity.

20 billion tons:
approx. 2 times the
mass of
67P/Churyunmov-
Gerasimenko
comet

Order of magnitude of tectonic surface processes: Mont Blanc is growing by 1 millimeter per year because of tectonic uplift, Godon et al. (2013)

Orogenic regions are permanently under the action of strong erosion processes, they therefore act as **generator for sediment**. Because erosion depends strongly on climatic conditions, a goal in geosciences is to decipher past imprints of climate on mountainous landscapes. But, this is complicated by the difference of response time, the different temporal resolution of these two components, see **Figure 3**, and also the concomitant impact of tectonics. Changes in tectonic settings are very slowly transmitted to the Earth's surface. As an example mountain belts are continuously adjusting their mass-balance to the new tectonic conditions. This is a very low process. Nevertheless, tectonic contributes to erosion through long term processes (i.e. uplift) which allows unceasing production of newly formed sediment particles.

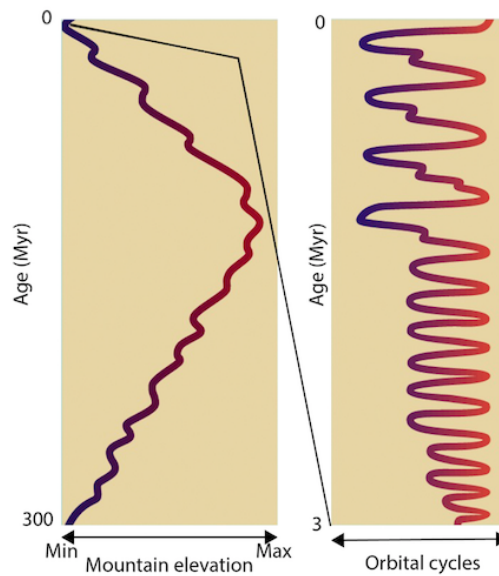


Figure 3

Time scales of 'Source to Sink' concept. Longer times scales are embedded in shorter sedimentological response, redrawn from Ruddiman 2001.

Climate, by contrast, is changeable and by the time that tectonic effects has affected the mountain belt, the climate has changed from cold to warm, wet to arid many times. This is well known for the late Pleistocene which shows a periodicity of approximate 100,000 years. These changes alter the amount of solar radiation (i.e. sunlight energy) arriving on Earth's surface and subsequent chemical and physical weathering rates, sediment transport processes and their deposition and post-deposition history. As a result, long-term estimation of such weathering processes is difficult to estimate at geological timescales, and we should keep a critical view on such estimations.

Nevertheless, deciphering the relative importance between tectonic and climate on erosional drivers is a longstanding and passionate debate where two scientific thought are arguing in support of Tectonic or Climate . There is something of the chicken and egg in this debate, because our Earth planet is a strongly coupled system. It is critical to answer the question of which one is the main trigger because of the complex interlinks between the 'signal' and the 'response'.

Moreover, external forcing (i.e. Tectonic among others) are initially transformed into an

'Earth surface signature' through the production of a mobile mass (i.e. sediment) which is transported and redistributed (i.e. totally or partially, and affected by transport processes) within the downward system (i.e. Sink; Allen et al. 2013). Those 'Earth surface signal' propagation, and subsequent preservation in stratigraphic sequences, are dependent of initial conditions (i.e. magnitude and frequency of the initial forcing), inherent characteristics of the sediment routing-system (i.e. the response of the different compartments of the routing system, their morphology, size of the transfer zone, presence of buffer zone, etc), and the signal to noise ratio (Romans et al. 2016 and references within for a throughout review), **Figure 4**. Continental shelves, slopes and deep ocean basin are generally viewed as the ultimate sinks, but their records are variably preserved as a result of variable post-depositional reworking (i.e. bioturbation, mixing depth, and layer thickness for example; Milligan et al. 2003; Tesi et al. 2012; Aller 2014). Therefore, deciphering the trigger of erosional processes using stratigraphic and/or marine sediment sequences can be challenging to unravel.

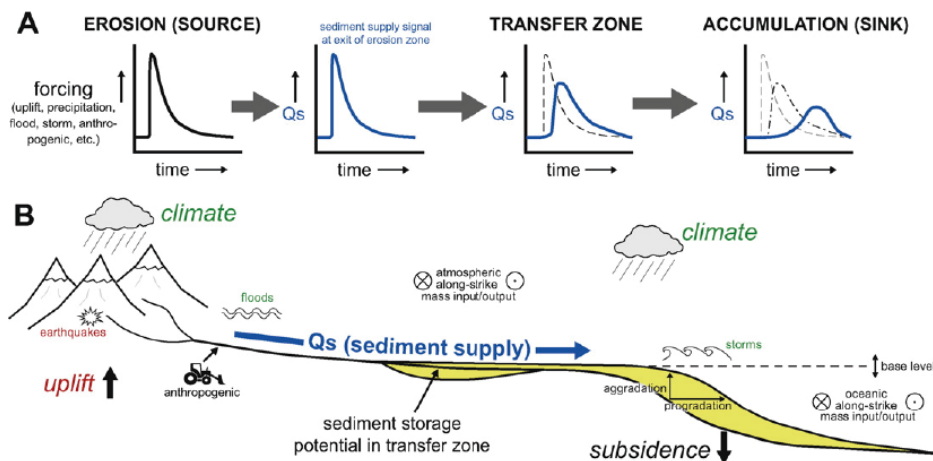


Figure 4

(A) Schematic of a sedimentary supply (Q) signal from the erosion zone and how that signal propagates through the routing system. The leftmost Q_s signal represents as measured at the exit of the erosion zone and for simplification is the same that the original forcing. The transfer zone Q_s signal is measured within the transfer zone at some distance from the exit of the source zone. The rightmost cartoon show the propagated signal at the accumulation zone (sink) as an input for stratigraphic record. Dashed lines illustrate that the signal is modified during propagation processes. (B) 2D profile of 'classic' routing sediment system composed of a source zone prone to erosion, transfer and accumulation zones (yellow areas highlight potential storage zone). Important control factors are indicated on the profile such as tectonics, climate, sea level base-line and potential anthropogenic activities. From Romans et al. 2016.

Let's take the example late Cenozoic global cooling (~ 5 Ma) that has experienced the Earth's surface during the past 5 million years, and the worldwide associated increase rate of sedimentation (Donnelly 1982; Hay et al. 1988, 2002; Molnar 2004; Peizhen et al. 2001; Willett 2010; Leroux et al. 2017 among others). In such case, the factor controlling 'short-term' sediment production was mainly driven by variable and large amplitude climatic fluctuations through the mid-Pleistocene. This cooling trend led to the onset of North Hemisphere glaciation around 2.5 Ma (Raymo 1994), and affected all mid-latitude mountains (i.e. the Alps). However, it is hard to date the beginning of erosional processes which led to the increased sedimentation flux on oceanic margin. Nevertheless, Leroux and collaborators (2017) have recently quantified the evolution of sedimentary volumes for the last 6 Ma in the Gulf of Lion, and shown an increase of the sedimentation rates since the Messinian salinity crisis. One difficulty with the Alps, as with all active regions, is to decipher erosion rate changes induced by climate and those induced by tectonic activity (i.e. especially in

Messinian salinity crisis: the desiccation of the Mediterranean Sea between 5.96 and 5.33 Ma. It resulted from the closure of marine gateways between the Atlantic Ocean and the Mediterranean Sea, the causes of which remain enigmatic.

the Alps because it is a compressive zone which shows various deformation activities: compression in the East; opening and rotation in the West and complex poly-deformation in the central Alps; Selverstone 2005). Nevertheless, there are evidences for high **exhumation rates** measured in the internal and external massifs (Fügenschuh and Schmid 2003; Malusà and Vezzoli 2006; Persaud and Pfiffner 2004). This important tectonic activity is a potential explanation for increased sedimentation supply because it affects the way how mountains reacted to climate changes. Tectonics also controls deep Earth movement (e.g. crust and mantle processes) which affects vertical movements and geodynamic processes. Therefore, the factor controlling the long-term sediment production seems to be closely dependent on the tectonic context. Moreover, long-term vertical movements also governed the **accommodation space**, and therefore sediment accumulation in the Western Mediterranean Sea (i.e. in the sense of preservation; Rabineau et al. 2005). The accommodation space can be defined as a simple volume balance between processes that controlled the amount of space that can be occupied by sediments (or water) and how much sediments (and water) fills this accommodation space. One of the main controlling parameter of the accommodation space is the **tectonic subsidence**. As its name implies, is driven by tectonic forces in opposition to isostatic vertical movements induced by sediment and water loads. Tectonic subsidence in the case of the Gulf of Lion results from the cooling of hot lithosphere during the opening of the Liguro-Provençal basin (i.e. Corso-Sarde rotation around 23 - 21 Ma). During the stretching, the continental lithosphere was heated and therefore uplifted. As oceanic lithosphere cools, it becomes denser and subsides. The cooling subsidence decreases exponentially with times (Leeds et al. 1974; Furlong and Chapman 2013 for a thorough review). Nevertheless, during several millions of years, verticals movements are generated, creating new available space for sediment accumulation. Changes in sea level also contribute to the available potential space for sedimentation, because the accommodation space results from the interplay of subsidence and eustatic sea-level variations. At tectonic scale their effects are strong only over very large times-scale. On the contrary sea-level changes and sediment loading create rapid changes in accommodation (Peizhen et al. 2001).

Because of the **strong feedback** mechanisms of deep Earth processes on surface routing system, tectonic processes allow sediment creation but also sediment trapping. Consequently, the realms of **subsidence** driven by tectonic processes **are the key to the transformation of erosion and depositional processes into sedimentary record** over the Geologic History. Whatever the upland release of sediment into the system, their preservations depend on space available for accumulation over long timescales.

4. Orbital climate cycles: From landscape to sedimentary responses

Erosion (and subsequent sedimentary fluxes) depends strongly on **climatic factors**. Climatic variations therefore are an essential key to understand physical, chemical, and biological processes that shape the Earth's surface. For understanding the climate effects on Earth's surface, we **move from the tectonic to the orbital timescale**, at least during the last several million years, when continent and ocean were reaching their present-day position. Note that orbital-scales changes have occurred during all of Earth's history, but our focus here is on the last 2 million years where well-dated climate records are available.

The dominant mode of climate variability during the Quaternary/Pleistocene has been characterized by oscillation between glacial and interglacial climate states. Based on comparison of land sequence, marine and ice cores, it seems clear that these cycles have affected the entire Earth surface, including the world oceans (e.g. Imbrie et al. 1984; Johnsen et al. 1992; Shackleton 2000; Lisiecki and Raymo 2005). This variability is at the origin of the

Orbital Scale:
Climatic fluctuations related to Earth's orbit around the Sun.

establishment of isotopic stratigraphic charts: (i) the highly used SPECMAC curve (Imbrie et al. 1984; Martinson et al. 1987) and (ii) LR-04 published in 2005 by Lisiecki and Raymo, as prominent examples. The reference curve LR04, **Figure 5A and B**, presents a 5.3 Myr stack of benthic $\delta^{18}\text{O}$ from 57 well dated and globally distributed sites around the world. Since this publication in 2005, this curve is commonly used to highlight glacial and interglacial variability, see **Figure 5**. On this figure the scheme of lettered Marine Isotope substages of Railsback and colleagues (2015b) is applied, as in all studies reported in this thesis manuscript.

Introduction to Quaternary climate nomenclature

The Quaternary nomenclature and stratigraphy are mainly based on the use of continuous oxygen isotopes of benthic marine foraminifera, such as LR04 stack. These records show large isotopic fluctuations interpreted as changes in ice volume and temperature that are inherently global and therefore used for global correlation.

First Arrhenius (1952) introduced the term climatostratigraphic '**stage**'. A 'stage' referred to intervals of sediment or time. Later, Emiliani (1955) characterized the oxygen isotopic variability as **Marine Isotopic Stage** (i.e. MIS), and defined the present and previous interglacials with odd numbers (i.e. MIS1, 5, 7, 9, 11, etc) and glacials with even numbers (i.e. MIS2, 4, 6, 8, 10, etc). With an exception for MIS3 which is no longer considered as an interglacial (Sirocko et al. 2006).

Later, because 'stage' periods are not isotopically homogeneous the term '**sub-stage**' was introduced by Shackleton (1969). He defined those isotopes sub-stages as intervals of times with isotopic maxima and minima of lesser relative magnitude than those defining stages. Also, Shackleton (1969) named those sub-stages (or substages) with a lettered nomenclature, notably in MIS 5 as substages MIS 5a, 5b, 5c, 5d, 5e.

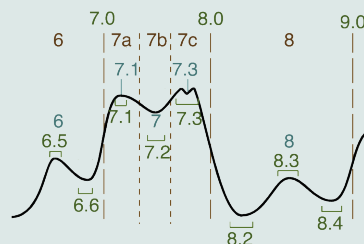
However, other sub-stage nomenclatures have been employed in many different papers, and sometimes with conflicting and/or different designations, see Box figure. That is why Railsback and collaborators (2015a) recently published a single and unified lettered scheme for paleoclimatology studies.

Stage and substages as defined in:

Style of Emiliani (1955, 1961) and Shackleton (1969)

Style of Arrhenius (1952)

Style of Prell et al. (1986)



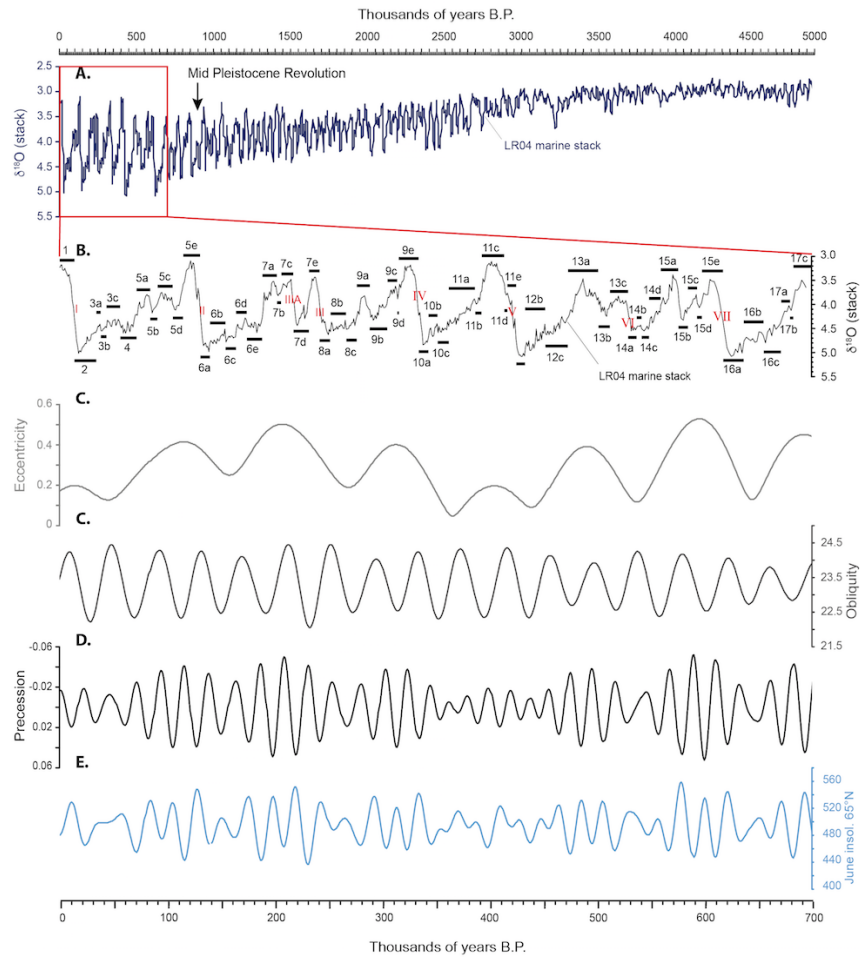


Figure 5

(A) Major climatic variations recorded in marine benthic oxygen isotope (LR04 curve) during the last 5 Ma from Lisieki and Raymo, 2005. (B) LR04 zoom over the last 700,000 years with Railsback et al. (2015a) marine isotope scheme which was used in the following studies of this manuscript. Periodic variation of orbital parameters collectively known as Milankovitch parameters: (C) Eccentricity, (D) axial tilt and (E) precession. Taken in unison variation of these three cycles creates alterations in the seasonality of solar radiation reaching the Earth's surface (i.e. insolation curve in Watt/m^2).

But first, we must understand what drives the climate changes, in other terms what are the mechanisms that lead to successive glacial (i.e. cold) and interglacial (i.e. warm) periods ? Since the mid 17-th century, when Johannes Kepler investigated the Earth's orbit, we know that the Earth is moving around the Sun within an elliptic plane. However, the Earth's orbit around the sun is not constant over long-time intervals. Instead, it varies in a cyclic way due to gravitational interaction with other bodies in the solar system. These variations are complex, but some dominant cycles were theorized by Milutin Milankovitch during the 1920's. Milankovitch highlighted changes in the orbital eccentricity, obliquity and precession, which alter the amount of solar radiation reaching the Earth, creating astronomical seasons.

- (i) Earth's orbit is not a perfect circle: it has a slight elliptical or eccentric shape, see **Figure 5.C** and **Figure 6**. Basic geometry shows that Earth's distance from the Sun changes according to this position in the elliptical orbit, inducing variation in the amount of solar radiation that Earth receives. Those slight changes in the Earth-Sun distance are described as the **Eccentricity (e)**. Changes in orbital eccentricity are concentrated mainly at two periods. One shows 100,000 years variations, while the other has a wavelength of approx. 400,000 years and alter the 100,000 years cycles between larger and smaller peak values. A third one also exists at a period of 2.1 Myr but it is much weaker.
- (ii) Earth rotates (on itself) around an axis that passes through its poles. This axis is tilted at an angle of 23.5° , called **Earth's Obliquity (ϵ)**, see **Figure 5.D** and **Figure 6**. Variation in the degree of Earth's axial tilt varies between 22.1° and 23.5° , over a cycle around 41,000 years. Increased tilt increases the amplitude of the seasonal cycle in insolation, providing more solar energy during summer, especially at higher latitudes. Note that, the actual trend of decreasing tilt is supposed to induce milder seasons, as well as a global cooling and should encourage the onset of a new ice age on Earth.
- (iii) **Precession (ω)** is the Earth's slow wobble as it spins on its axis, see **Figure 5.E** and **Figure 6**. The wobbling of the Earth on its axis is caused by the gravitational pull of the Moon and the Sun on the irregular Earth's diameter at the equator. It can be visualized as a slow turning of Earth's axis of rotation through a circular path, which one full turn every 25,700 years. A second kind of precessional motion is known as precession of the ellipse, resulting from the entire rotation of the elliptically Earth's orbit around the Sun. The combined effect of the two motions causes solstices (i.e. longer days occur during the summer, and shorter ones during winter time) and equinoxes (at equinox : day and night are of approximately equal duration everywhere on the planet). Because the positions of the solstices and equinoxes in relation to Earth's eccentric orbit have not always been fixed, there are two sub-cycles around 19,000 and 23,000 years.

It is now widely demonstrated, and commonly accepted, that these astronomical cycles influence seasonal and latitudinal distribution of incident solar radiation, that drive major climate changes (Berner et al. 1980), even if some phase of oscillation are also driven internally by ocean – atmosphere climate coupling.

Milutin Milankovitch: 28 May 1879 - 12 December 1958. Milutin was a Serbian mathematician, astronomer, climatologist, geophysicist, civil engineer, and popularizer of science. Milankovitch gave two fundamental contributions to global science. The first contribution is the **Canon of the Earth's Insolation**, which characterizes the climate of all the planets of the Solar system. The second contribution is the explanation of Earth's long-term climate changes caused by changes in the position of the Earth in comparison to the Sun, now known as **Milankovitch cycles**.

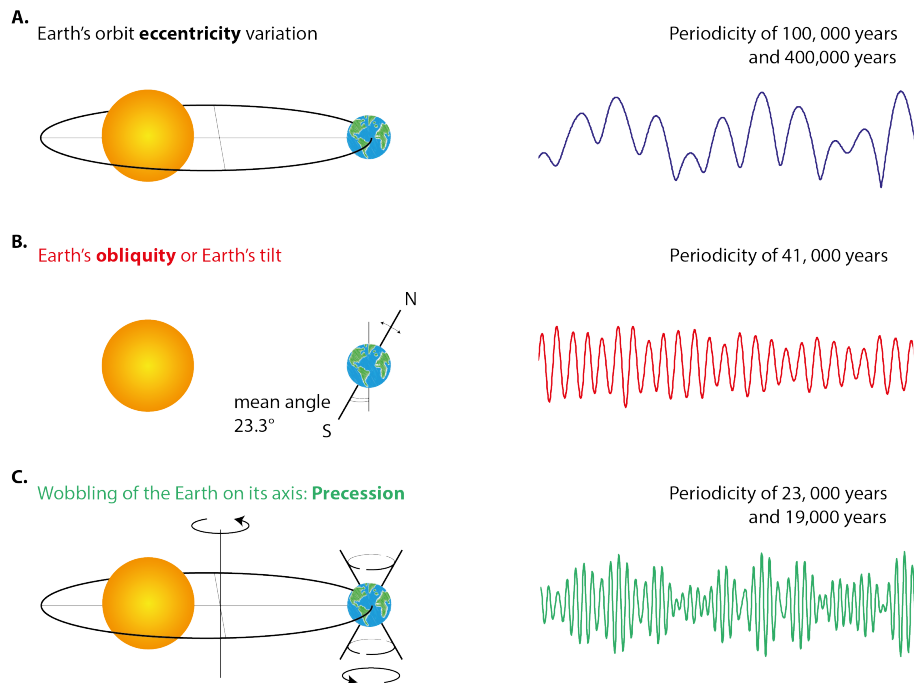


Figure 6

Milankovitch parameters. **(A)** Earth's eccentricity orbit: Earth's orbit around the Sun is slightly elliptical inducing 100,000 and 400,000 years periodicities. **(B)** Earth's tilt: Earth's rotation axis is currently tilted at an angle of 23.5° away from a line perpendicular to the plane of its orbit around the Sun with resulting periodicity (41,000 years). **(C)** Precession of Earth's axis: Earth's slow wobbling motion cause its rotational axis to point in different direction through time. Adapted from Imbrie and Imbrie 1980.

Mid-Pleistocene Revolution: is now more commonly named Mid-Pleistocene transition; MPT. It is define by two characteristics around the Brunhes/Matuyama transition: (i) the increase in amplitude and (ii) the decrease in frequency of the marine $\delta^{18}\text{O}$ signal in marine archives.

Finally, what are the real impacts of those Milankovitch cycles on Earth's climate? In 1976, James D Hays, John Imbrie and Nicolas J Shackleton highlighted that major climate changes, over the last 500,000 years, followed changes in Earth's orbit variations. Indeed, cross-spectral analyses between astronomical and sedimentary parameters were carried out and three discrete peaks (at 23,000, 42,000, and approximately 100,000 years) were found and correspond to the dominant periods of Earth's orbit around the Sun (Hays et al. 1976). Authors concluded that changes in Earth's geometry orbit are the fundamental cause of **Quaternary ice ages**, confirming Milankovitch's summer predictions at 65° (Milankovitch 1920). These results were rapidly confirmed by other workers, such as Kominz et al. 1979; Morley and Hays 1981; Ruddiman and McIntyre 1981 among others.

The Earth's climate became cooler through the Tertiary (65 Myr) with frequent oscillations that increased in amplitude and led to the succession of major ice ages during the Quaternary (2.6 Myr to present day). During the first part of the Quaternary from 2.6 Myr to 0.9 Myr ago, ice-sheets advanced and retreated with an approximate 41,000 yr cycles. During Late Quaternary (after 0.9 Myr) they followed a 100,000 yr dominant cyclicity and became more severe (Shackleton and Hall 1984; Raymo 1994). This change (i.e. initially named the Mid-Pleistocene Revolution; MPR) is clearly visible on oxygen isotopic composition of many calcifying organisms but the exact cause(s) and exact dating remains unclear and debated (Raymo and Huybers 2008; Elderfield et al. 2012; Head

and Gibbard 2015). Whatever its origin, the MPT marks the beginning of the ice-sheet dynamic over the North Hemisphere, known as the Laurentine (i.e. North America) and European Ice sheets. After the MPT, glacial - interglacial cycles show an asymmetric evolution between long glaciation and short deglaciation phases of each cycle (Gildor and Tziperman 2000). These cycle's asymmetric signature, features a long cooling interval (see **Figure 5.A. and B.** the global $\delta^{18}\text{O}$ trend) marked by an oscillating buildup of ice sheets to a maximum volume (i.e. glacial maximum) during approx 60 to 90,000 years; followed by a relatively short warming interval (i.e. interglacial of approx 10 000 years).

Since the onset of Pleistocene, the ice sheet dynamic triggered huge **transfers of water** between the two largest reservoirs on Earth: the ice sheets and the oceans. As the ice sheets waxed and waned, the concomitant fall and rise of sea level highlight the direct consequences of glacial cycles (Lambeck et al. 2002). Because ice sheets represent a huge volume of ice (i.e. 50-60 million km^3), they induced large amplitude **glacio-eustatic changes** of circa 120 to 140 m (i.e. sea-level changes related to ice-sheet fluctuations; Raymo and Ruddiman 1992). It is generally agreed that oxygen isotope, recorded in deep sea sediment, gives insight of global ice volume and hence of glacio-eustatic component of sea-level (Imbrie et al. 1984; Shackleton 1987, 2000; Waelbroeck et al. 2002; Siddall et al. 2003; Grant et al. 2012, 2014). Moreover, direct and accurate geological imprints of past sea levels exist around the world, for example coral reef altitudes and siliciclastic paleoshoreline observations are good and independent indicators of sea-level, that give reference values for the conversion of oxygen isotope to sea level changes in meters (after corrections for isostasy and subsidence; Siddall et al. 2013; Bard et al. 1990; Chappell and Shackleton 1986; Rabineau et al. 2006; Jouet 2007). Thus, Late Quaternary is characterized by major high amplitude sea-level variations occurring at $\sim 100,000$ yrs (**Figure 6**), with superimposed shorter cycles (i.e. few meters to several decimeters sea-level changes corresponding to 20 and 40,000 years cyclicities).

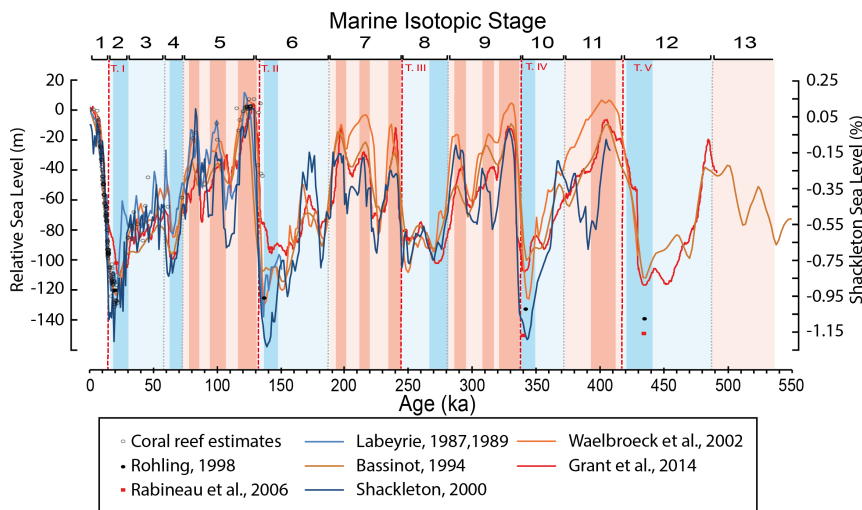


Figure 7

Relative sea level over the last 550,000 years. Data came from marine benthic foraminifera oxygen isotope, coral-reefs for highstands and delta for lowstands. First order cycles (i.e.100,000 years) are clearly identified as inducing approx 100 meters sea level changes, with superimposed 20 and 40,000 cyclicities. Red bands correspond to interglacials periods with warm substages (i.e. sensu stricto) highlighted in dark pink. Termination (T.) according to Barker et al. (2011). Scheme of marine stage according to Railsback et al. (2015a). Redrawn from Rabineau et al. (2006); Jouet (2007).

Sediment preservation in a sedimentary basin is the result of the interplay between accommodation (as discussed earlier) and sediment supply that governs the **geometries of the deposits**. During Late Quaternary, a fundamental parameter in sediment's preservation is the magnitude of sea-level changes which affect the vertical stacking of sedimentary facies. Stratigraphy sequence models linked the stratigraphic sequences geometries to a cycle of variation of relative sea-level (**Figure 8**; e.g. Vail et al. 1977; Posamentier and Allen 1993). Indeed, sea-level changes controlled the sediment geometries and preservation/erosion of sediment over the shelf. Changes in sea-level induce seaward/landward migration of coastal rivers and shorelines, therefore highly impact the sediment distribution and thickness, **Figure 8**.

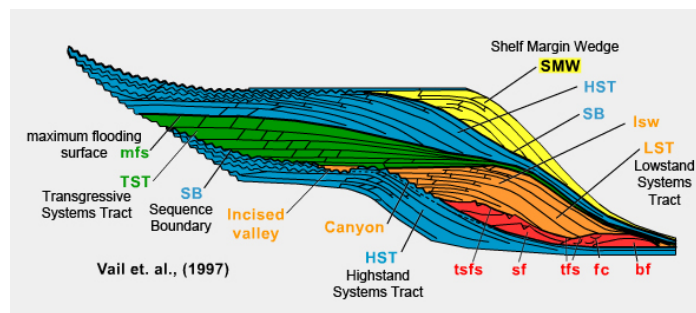


Figure 8

Timing of sequence boundaries and systems tracts in relation to time and base level changes. HST: Highstand system tract, TST: Transgressive system tract, LST: Lowstand System Tract, FSST: Falling sea level stage system tract, SB: Sequence boundary, MFS: Maximum flooding surface, TS: Transgressive surface. Redrawn from Vail et al. (1977).

Sedimentary facies are also dependent on the water depth, and preservation of shallow-water part of a stratigraphic cycle is extremely dependent on water depth evolution. Because, sediment cannot accumulate for long period of times on the same graded profile (i.e. lack of space), relative sea level variations are very important because they allowed bypass or erosion of sediment in some parts and deposition in other parts of the sedimentary system. The balance between the rate of accommodation created by tectonic processes and the long-term sediment accumulation rate determines whether a succession of cycles will be preserved in sediment records (**Figure 9**). When preserved, these cycles are imprinted in the stratigraphy and are very sensitive to sea-level changes.

Storm rainfalls, ice-sheet or ice-cap movements, aridity, and many other factors have an important influence on the rate of land erosion, natural land-cover (i.e. forest, etc) and biological cycles. Upland catchment releases sediment into adjacent sedimentary basins, but the preservation and the characteristics of sediment in those sedimentary-systems depend on the space available and therefore are highly dependent of both tectonic and eustatic changes.

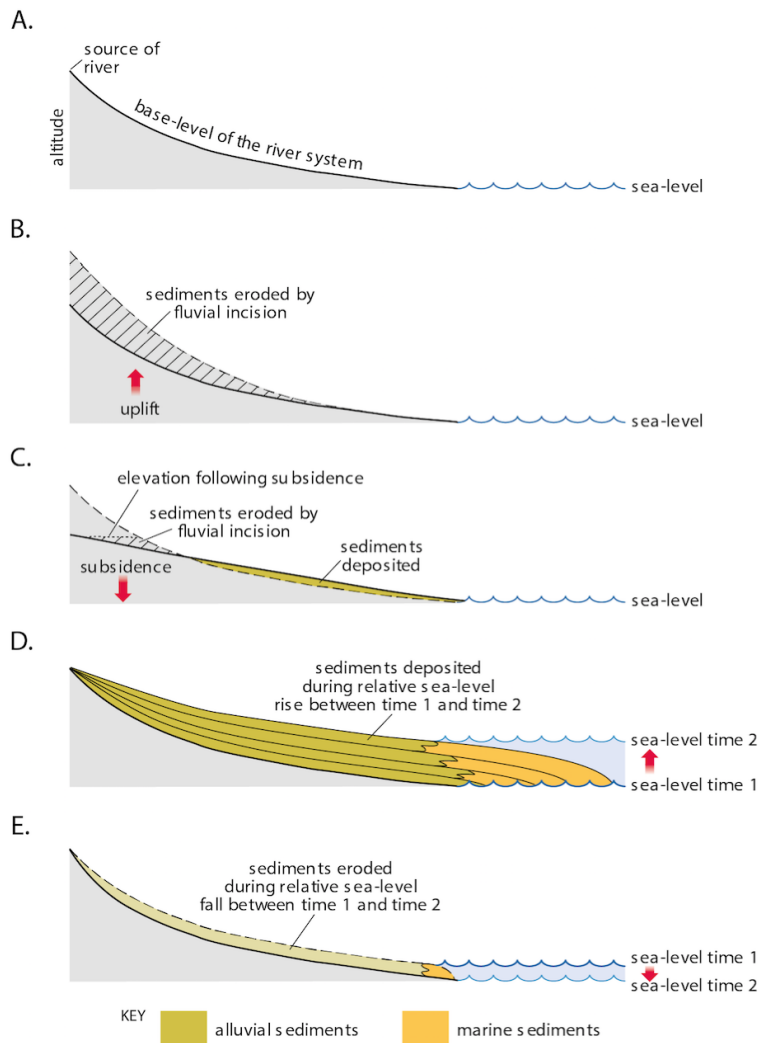


Figure 9

Stratigraphy conceptual model. **(A)** The equilibrium profile of a river system. In order to maintain the equilibrium profile erosion and/or deposition of alluvial sediment place if there is no sea-level changes and/or tectonic vertical movements. **(B)** Erosion of sediment due to uplift in the source zone. **(C)** Erosion and deposition of sediments along the transfer zone due to subsidence of the source zone. **(D)** Deposition of sediment in the sink zone due to a relative sea-level rise. **(E)** erosion and transfer of sediment in a deeper sedimentary unit due to sea-level fall. From <http://www.cambridge.org/>.

5. The influence of climate on early and burial diagenesis

Climate conditions, such as temperature and precipitation intensity, and geomorphology of sediment in the watershed define the intensity of weathering, as well as the composition of the weathering products through physical and chemical erosion (Parrish 1993; Jeans et al. 2001). Besides determining the composition of the material supplied into the basin, the climate controls the water availability and geochemical conditions in the **post-depositional**

Open system: In chemistry an open system is a system that can exchange freely reactant with its surroundings.

environment.

One of the main climate's control results in the deposition and build-up of sedimentary sequences, as well as dynamic changes in physical and chemical interactions of these deposits with the overlying water column and underlying substratum. Sea bed geochemical cycles are driven by components of the sediment which undergo a wide range of reaction, including hydrolysis, dissolution, oxidation/reduction, precipitation, recrystallization among others. Many of these reactions are **rapid, biologically mediated**, and occur within the **first centimeters** of the sediments, where reactants and products are abundant and easily exchangeable. Physical and chemical changes associated with these reactions happen during early stage of sediment deposition at low temperature ($< 50\text{ }^{\circ}\text{C}$) and define the **early diagenesis**. Factors and mechanisms that control early diagenetic processes are often associated to transport of solutes, fluids, and particulate material across the water-sediment interface (Burdige and Lerman 2006; Schulz 2006). They are usually viewed as open systems and therefore have major impact on the global ocean chemistry. Diagenetic processes significantly affect sediment composition and modify the initial inputs that would be crucial for paleo-environmental reconstructions (e.g. S and Fe cycles; Goldhaber 2003; Lyons and Gill 2010; Raiswell and Canfield 1998). Therefore, recognition and accurate understanding of paleo-environments depends on our understanding of early diagenetic processes, and their evolution with climate (i.e. depositional conditions and environments).

However, field compilation reveals that organic matter degradation is not constant and that organic carbon burial vary significantly in **space and times** (Canfield 2005; Blair and Aller 2012; Aller et al. 2008, 2010; Aller 2014). Many factors can explain observed disparities such as **deposition rates** (Calvert and Pedersen, 1992; Tromp et al. 1985), **microbenthic activity** (Aller 1982; Jørgensen and Gallardo 1999; Jørgensen and D'hondt 2006), **physical sediments proprieties** (see next section), electron donor availability (Canfield and Thamdrup 1994), and other factors that have a **direct effect on organic matter source**, transport, and deposition which are closely dependent of changes in the climatic conditions.

For instance, it is widely accepted that **organic carbon is the primary driver** of the early diagenesis (Lehmann et al. 2002; Habicht and Canfield 1997; Froelich et al. 1979; Jørgensen 1982), therefore the amount of organic matter in the sediment and its preservation/degradation mechanisms will have strong impacts (Demaison and Moore 1980). Episodes of reduced bottom O_2 concentration enhanced the preservation of organic matter, this occurred in the recent Mediterranean history (Rohling et al. 2015 for a thorough review). Such cyclic and repeated episodes result in the formation of so called **sapropel** layers which should have affected early diagenetic processes in the Mediterranean Sea.

6. The organic matter: the driving 'Force' during early diagenesis

Almost all organic matter deposited in marine sediments originates from biological photosynthesis activity in the terrestrial or marine biosphere. During photosynthetic activity, dioxide carbon molecules and water molecules combine together and form a multitude of organic compounds, according to the various photosynthetic organisms (De Leeuw and Largeau 1993), following the equation n° 1.



In this very simplified reaction 'CH₂O' represents an idealized chemical formula representing the **multitude of the different organic compounds** naturally produced by photosynthetic organisms. Although a large fraction of newly formed carbon is rapidly recycled, the amount of organic matter that ultimately settles on sea-floor reveals significant regional

variability (Lutz et al. 2002; Tesi et al. 2007). At a global scale, the amount of newly formed carbon reaching the sediments represents a very small fraction of the production (Bernier 2006). As a mean value, some 25-50 % of primary productivity products reach the sea floor in coastal environments whereas the fraction is only around 1 % in the deep sea (Suess 1980).

Once settled at the sea / water interface, the susceptibility of organic matter to microbial degradation processes is commonly defined as its '**degradability**', but it is important to note, as highlighted by Mayer (1995), that the degradability is "*not an inherent, or absolute, property of the organic matter itself, but results from the interaction between organic matter and its environments*". Also, the terms '**refractory**' and '**labile**' are usually used to describe relative difference in organic matter degradability. The relative post-depositional degradation of organic matter strongly depends on the characteristics of the depositional settings and the timescales of interest. However, despite the difference in original composition and degradation, detrital organic matter in sediments are typically formed of: 10-20 % carbohydrates, 10 % nitrogenous compounds (mostly amino acids) and 5-15 % of lipids (Hedges and Oades 1997; Burdige and Lerman 2006). A remaining fraction of chemically complex compounds is known to be relatively resistant to biological degradation is commonly name humic substances (Schnitzer 1991). Capturing and defining this complexity in natural sediment is very challenging due to very limited availability of organic compounds and bias during chemical sediment preparation. Nonetheless, it is recognized that most bio-polymers (i.e. proteins and nucleic acids) are particularly labile contrary to biomacromolecules (i.e. algeenan and cutan) which are more resistant. Between these two end-members lie divers organic compounds such as carbohydrate which are relatively labile, or ester-linked macromolecules like cutin or aromatic lignin which tend to be less degradable.

Two significant consequences arise from this chemical heterogeneity.

- i First the relative degradability of organic matter differs in function of the depositional context: **terrestrial organic matter** is relatively more refractory than **marine derived organic matter** (Hedges et al. 2000) due to difference in chemical composition. Also, the refractory nature of terrestrial organic matter could be related to pre-burial phase in soil and degradation processes during transport, i.e. organic matter settled in marine environment have already undergone extensive degradation processes compared to relatively newly formed phytoplankton derived organic matter. However, recent work suggests a more complex relationship between the origin of organic matter and degradability (i.e. encapsulation or physical protection in aggregates; Bianchi 2011; Huguet et al. 2008).
- ii The second intuitive aspect of the chemical heterogeneity is that: less degradable organic matter persists through time; or in other words aerobic and anaerobic degradation leads to an **increase of the refractory material**. However other processes can lead to a decrease of organic matter degradability and may play an important role in the preservation of organic carbon with depth. Several processes, such as geopolymerization and sulfidization, are known to change labile compounds toward degradation resistant products and facilitate their preservation over geological timescales (Burdige 2007; Raven et al. 2016).

Organic matter decomposition rate and remineralization in marine sediments is accomplished by billions of individual **microorganisms**. All these microbial cells have a critical role in diagenetic processes, especially in organic matter degradation and associated redox reactions. One of the fundamental concept in our understanding of early diagenetic processes associated with organic matter is that **oxidation-reduction reactions** follow a regular evolution with time, and as a consequence with depth (in most of the case where steady state conditions are observed; Claypool and Kaplan 1974; Froelich et al. 1979; Aller

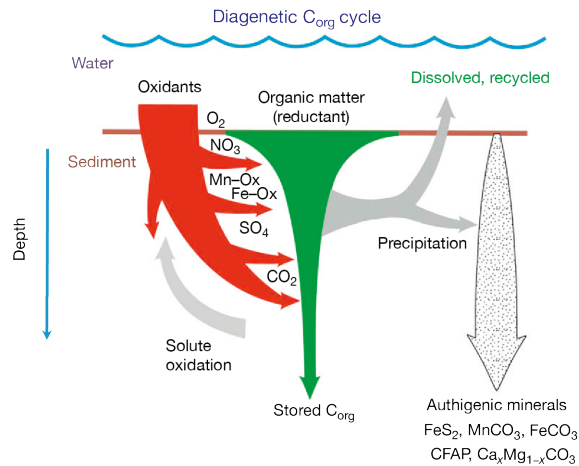


Figure 10

Schematic in vertical cross section of major diagenetic processes involved in the remineralization of organic matter in marine deposits. After deposition, reactive organic matter is decomposed and oxidized. The rate of decrease organic matter with time and depth is a function of the initial reactivity and burial condition, as the quantity of buried organic carbon in sedimentary sequence. A set of oxidation processes naturally occur leading to the production of dissolved products which are used by the benthic community and reduced authigenic minerals. From Aller (2014).

Steady state conditions: deposits are modeled as laterally homogeneous bodies, in an open system with the overlying water reservoir, and accreting upward in a vertical dimension at a regular rate equivalent to net sedimentation.

2014; Berner et al. 1980; Tesi et al. 2012). The primary oxidants naturally found in marine environments are O_2 , NO_3^- , Mn-Fe oxides, SO_4^{2-} and CO_2 . These oxidants are preferentially and sequentially used by heterotrophic bacteria to oxidize organic carbon substrate as a function of free energy yield, for optimization of their growth; see **Figure 10**.

The quantitative importance of these oxidants for degradation of organic matter, or mineralisation of organic carbon has been extensively studied during the last decade in both culture experiments and diagenetic modelling. It is generally admitted that oxygen and sulfate play a major role in shelf sediments whereas nitrate seems to play a minor role in oxidation of organic matter. Manganese and Iron reduction mostly occurs close to the surface and are relatively rapidly consumed. Moreover, these solid-phase oxidants (i.e. Mn and Fe oxides) are dependant of bioturbation processes to bring them down to their zone of reaction. **Table I.1** shows an example of process rate happening in coastal sediment as compiled in Jørgensen (1996).

In such exercise, it is important to keep in mind that the different oxidants are not equivalent to their oxidation capacity. For example, when iron in Fe(III) is reduced, the product is Fe^{2+} and the iron atoms have been reduced only by one oxidation step, from +3 to +2. When sulfur atom in sulfate (SO_4^{2-}) are reduced, eight oxidation steps are required, from +6 to -2, to produced H_2S . Therefore, one mol of sulfate has 8-fold higher oxidation capacity than one mol of iron.

In order to compare oxidants role in organic carbon oxidation, their reduction rates have been converted to carbon equivalents on the basis of their change in oxidation step. It is now clear that oxygen and sulfate are the predominant oxidants in coastal sediments, sulfate oxidizing about 44 % of the organic carbon buried in sediment. Once H_2S formed, approx. 15 % is buried as pyrite (i.e. widely variable across depositional environments) while the rest was re-oxidized and could potentially consume one - third of the oxygen uptake (Jørgensen and Nelson 2004).

Reaction	Δ oxidation steps	Measured rate mol.m ⁻² .yr ⁻¹	Estimated carbon equivalents
[CH ₂ O] -> CO ₂	C: 0 → +4 = 4	9.9	9.9
O ₂ -> H ₂ O	O: 0 → -2 = 2	9.2	9.2
NO ₃ ⁻ -> N ₂	N: +5 → 0 = 5	0.15	0.19
Mn(IV) -> Mn ₂ ⁺	Mn: +4 → +2 = 2	0.8	0.4
Fe(III) -> Fe ₂ ⁺	Fe: +3 → +2 = 1	1.6	0.4
SO ₄ ²⁻ -> HS ⁻	S: +6 → -2 = 8	1.7	3.4

Table 1 Annual budget for the mineralization of organic matter and consumption of oxidants in Aarhus bay, Danish coastal sediment. The basic reaction and exchange in oxidation step are shown for the element involved. The rates of processes were determined for one m² of sediment and where all recalculated to carbon equivalent. Data compiled in Jørgensen (1996).

Organic matter decomposition and remineralization play a **central role** in early diagenesis because of its necessary implication in the redox reaction succession. The latter significantly controls the pH and redox potential within sediments. Although previous studies have shown that redox pattern in surface sediments is not the only factor controlling the early diagenesis. Recent modeling studies have highlighted other processes affecting early diagenetic processes, especially in margin sedimentation where the upward steady state is not the most representative.

7. Diagenetic regimes and depositional environment

Numerous integrated coastal research approaches have been conducted to understand the processes governing the input, transport and fate of sediment from terrestrial to oceanic environments (Nittrouer and Wright 1994; Wheatcroft and Borgeld 2000; Geyer et al. 2004; Tesi et al. 2007; Kim et al. 2006; Gaillardet et al. 1999 among others). These efforts led to the construction of conceptual models for investigations of diagenetic processes, geochemistry, and physical environmental changes and mass fluxes calculation (Berner et al. 1980; Burdige and Lerman 2006; Emerson and Hedges 2003 among others). Five types of conceptual models are used:

- **Thermodynamic models** to evaluate solution speciation, saturations states, reaction probability, mineral precipitation and stability,
- **Stoichiometric models** to examine reaction balance and reaction between products and reactants,
- **Transport models** to look at the system time dependence and mass fluxes,
- **Kinetic models** to examine extent of reaction and mechanistic reactions through time,
- **Ecological model** which combines theories of microbial substrate, bioturbation, transport and biogeochemical cycles.

I will not enter into the details of the modelling approach (i.e. see (Aller 2014) and Arndt et al. (2013) for a thorough synthesis) but proper utilisation of any of these models requires a thorough understanding of the depositional environment and ecosystem context in which diagenesis occurs. Indeed, diagenetic reaction and their interconnectivity with the overlying column are strongly dependent of the depositional environments because this one defines the boundary conditions and the transport reaction.

Depending on the environmental settings and history, sediment may be composed of various sediment size and can be more or less permeable to advective flows, they can be relatively permanent and accrete steadily upward or subject to strong exchange with adjacent region. They may be inhabited or prone to intense bio-reworking of particles and/or bio-irrigate, in the photic zone or interacting with mats, etc... Each of these scenarios can produce very different boundary condition, internal transport and/or reactions which will affect the burial of organic matter and the precipitation of authigenic minerals.

Over the years, basic models have become progressively more and more complicated, numerically based and used for global scale extrapolation of diagenetic patterns and allowed identification of several important parameters involved in early diagenetic history:

1. **Energetic condition** at the water – sediment interface. In high energetic environments, surface sediment layers are subject to periodic or stochastic reworking that lead to episodically re-oxidization, erosion and re-equilibration (**Figure 11.E**). In fine grained environments, such perturbations induce formation of a surface mobile layer, overlying a more consolidated, relict, deposit (Allen 2008; **Figure 11.C**), which affects redox zonation and therefore diagenetic processes. Low-energy environments show laterally homogeneous sediment bodies, composed of fine grained sediments, low O₂ concentrations and minimum benthic fauna concentration (**Figure 11.A**),
2. **The biogenic effect**. During early diagenetic processes, benthic fauna rework and irrigate sediments mostly in the first 10 to 50 cm, but may extent several meters into the seabed. Bioturbation creates complex, time-dependent, three-dimensional heterogeneities that can dramatically affect diagenetic processes and distribution by facilitating particle exchange between the sediment and the water column (Meysman et al. 2006; Fan et al. 2011; Knaust 2013; Koretsky et al. 2002), **Figure 11.B**,
3. **Physical sediment proprieties** control the permeability and therefore affect advective flow of fluids. Coarse grained deposits have high permeabilities and overlying water readily flow through them in response to pressure gradient, and interaction with bottom currents (Huettel and Webster 2001). Therefore, a large amount of suspended particules, typically composed of small organic rich debris, are carried and re-supplied to those sandy environments independently of net sedimentation (Huettel et al. 1996; Cook et al. 2007; **Figure 11.D**),
4. **Deposition rate**. The observed correlation between average organic matter degradation and sediment accumulation rate has led to hypothesis that sedimentation rate exerts an important influence on early diagenetic processes. This causal relationship has often been explained by the rapid burial of freshly deposited material below the biologically active, mixed sediment surface (Blair et al. 2003).

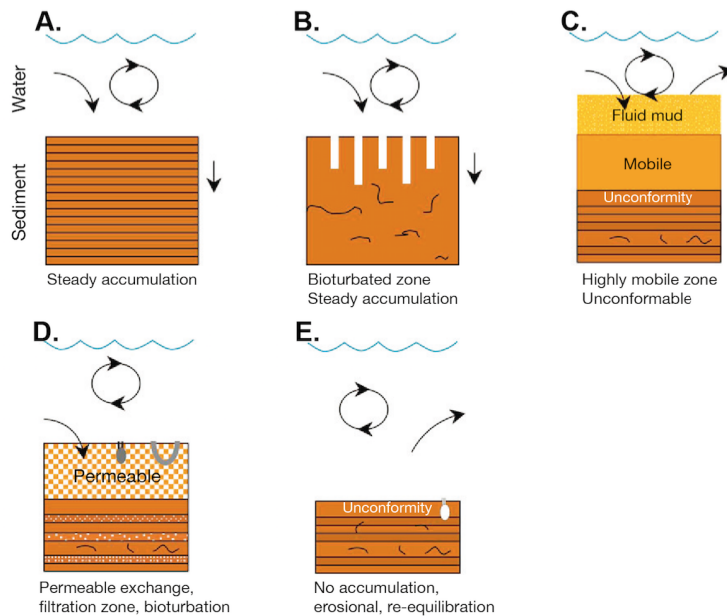


Figure 11

Few examples of steady and unsteady diagenetic regimes commonly observed in margin environments. Individual regimes differ in boundary condition, sediment mass properties, and interior transport-reaction processes. **(A)** Steady state accumulation assumed in most diagenetic regime (Berner et al. 1980); **(B)** bioturbated surface region; **(C)** highly mobil and periodically reworked sediment layer unconformably overlying older, relic deposits; **(D)** Permeable sediment and bioturbated zones that controlled exchanges; **(E)** un-steady environment controlled by re-oxidation after erosional processes. Modified from (Aller 2014).

8. The Gulf of Lion: PROMESS for new insights for early diagenesis?

As we just saw, early diagenetic processes in marine sediment are one of the major long-term sinks to reduced carbon on Earth (Berner 1982; Hedges 1992). Also, burial rates are small compared to estimation of global primary production (0.1 %; Hedges and Oades 1997), and the long-term sink of particulate organic carbon in marine sediment contribute to regulate the atmospheric CO₂ levels over geologic time scales (Berner 1989; Canfield and Teske 1996; Claypool et al. 1980 among others). For this reason, many efforts have been made to understand how organic carbon burial occurs in ocean and what controls the burial fluxes (Canfield 1994; Galy et al. 2007; Gordon and Goni 2004). Most biogeochemical approach have considered the flux of organic carbon to the seafloor to be steady, and to decay exponentially below the surface sediment due to microbial degradation and remineralization. However, most burial occurs in river-dominated coastal margins, where steady-state conditions are not always the case and organic burial flux is strongly tied to climate changes (Hedges and Keil 1995; Aller et al. 2008; Tesi et al. 2007). During this PhD study, we take advantage of an extraordinary opportunity to refine our understanding of the influence of climate on biogeochemical cycling and burial of organic carbon in coastal margin (i.e. early diageneses), using the **Gulf of Lion** which reveals a unique record of **migrations of an entire shelf sedimentary system** during the last five circa 100 kyr glacial/interglacial cycles.

The Gulf of Lion is located in the **western Mediterranean basin**, see **Figure 12**. Its main drainage basin is the Rhodanian basin, and its major river, the Rhone (the second biggest Mediterranean river after the Nile), which carried sediments eroded mainly from the French Alps. Much smaller watersheds and rivers come from the Pyrenees (Aude, Agly, Tet and Tech rivers) and from the Massif central in the central region of the Languedoc (Herauld river). This area also presents a wide continental margin allowing storage of sediment under high sea level (on the inner shelf), but also during glacial times (on the outer shelf) despite the sea-ward migration of the shore position due to sea-level lowering and the subsequent sub-aerial exposure of the inner and middle shelf (Rabineau et al. 2006; Bassetti et al. 2008; Jouet et al. 2006; Berner 2006).

Because the Gulf of Lion is a **young margin**, strongly impacted by river inputs in its coastal zone, connected to several **mountain watersheds** and preserving sediment whatever the climatic context (glacial and interglacial), it is one of the **most attractive natural laboratories** in the world to study recent geodynamic and paleoclimatic processes.

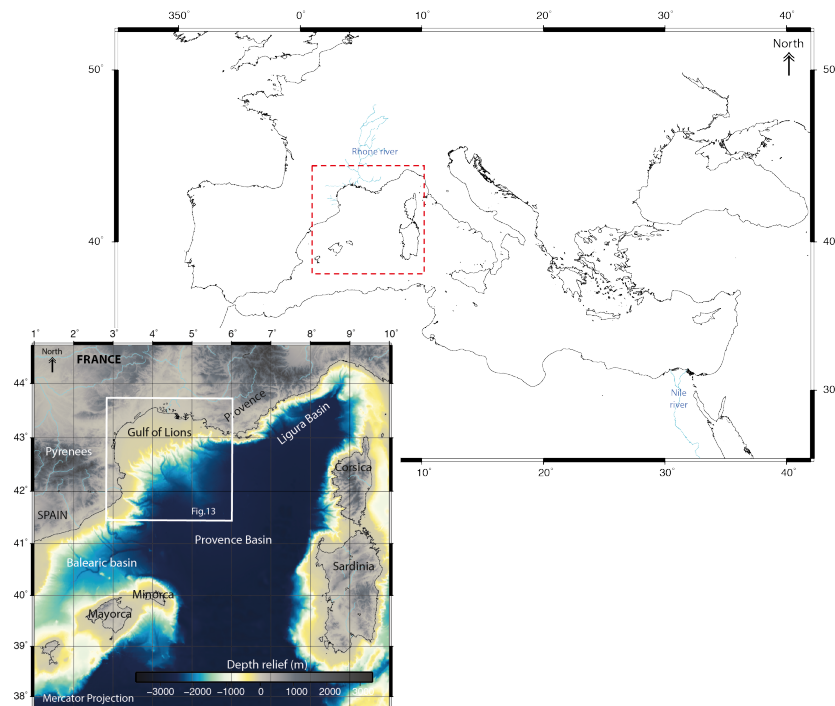


Figure 12
Location of the study area delimited by a red rectangle on the general map of the Mediterranean region.

Previous studies devoted to the better understanding of post-rift subsidence (Rehault et al. 1984; Burrus 1989) showed strong and continuous vertical movement (i.e. total subsidence); related to the recent (Neogene) opening of the Liguro-Provençal basin. Indeed, this strong subsidence results from the Late Oligocene-Aquitainian rifting, and later counter-clockwise rotation of the Corsica-Sardinia block (e.g. Séranne et al. 1995; Olivet 1996). The stratigraphy of the Liguro-Provençal basin has been studied at various timescales, from the syn-rift series (Gorini et al. 1993; Guennoc et al. 2000 among others) to the Plio-Quaternary sequences (Bache 2008; Baztan et al. 2005; Droz et al. 2006; Rabineau et al. 2005, 2006,

2014; Leroux et al. 2015, 2017; Mauffrey et al. 2015). Taking advantage of the extensive seismic dataset available on the Gulf of Lion shelf, Rabineau and collaborators in 2005 highlighted the effect of the ‘total’ subsidence of the platform. Seismic erosional surfaces show angles of inclination increasing with age enabling tilt measurement of well characterized and dated strata (i.e. numerous petroleum boreholes give access to precise depths and dates, see **Figure 13**). Therefore, (Rabineau et al. 2005) proposed a continuous seaward tilt of **250 m/Ma** at 70 km of the coast, for the last 0.5 Ma. Using a numerical stratigraphic model, Rabineau et al. 2014 and Leroux et al. 2017 confirmed the total subsidence rate, and extended this rate until 5.3 Ma. Giving this characteristic, the Gulf of Lion represents an ideal area to study past variation of a rooting system and feedback between climate, sedimentation and diagenetic processes at various times timescales.

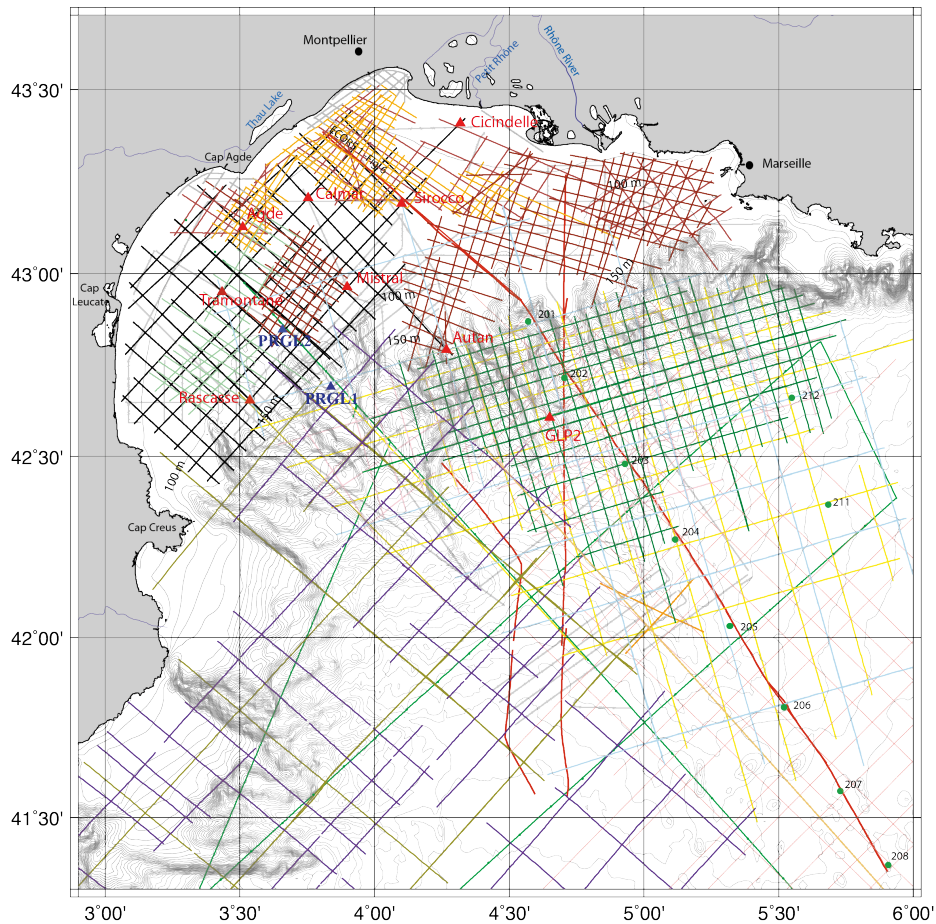


Figure 13

Seismic dataset and bathymetry of the Gulf of Lion (modified from Leroux et al., 2015). Red triangles correspond to industrial wells, blues triangles correspond to the two PROMESS European boreholes. Big green dots represents the ESP data, small green dots represent OBS data on Sardinia profiles. From Leroux et al. (2017).

9. Climate's impact on the Gulf of Lion sedimentation

Quaternary glaciations are known for their extreme glacio-eustatic changes which strongly control the partitioning of sediments in systems tracts on margins.

After several decades of intense seismic investigation, progress in coring technics and intense scientific debates (see Rabineau, 2001 for a thorough review), Rabineau and collaborators (2001) present a coherent stratigraphic model for the shelf sedimentation organization in the Gulf of Lion. In two dimensions, the seismic data presents a complex superposition of seismic units showing some typical sigmoidal prisms corresponding to various energy environments implying different sedimentary processes. The combination of faunal and grain size analyses from shallow cores from inner shelf to shelf break allows a complete understanding of the sedimentary history. Indeed, each sequence consists of a seaward thickening wedge, showing progradation of the prodeltaic system in response to sea-level falls of the glacial-interglacial periods (100 kyr climatic cycles; Rabineau et al. 2005).

For example, **Figure 14** shows the uppermost sedimentary sequence formed during the last glacial cycle. Here we clearly see propagation of the deltaic system (U147) during MIS 3, and the rapid progradation of coastal sand deposits during the maximum of sea-level fall of the last glacial periods (U151/U151). These coastal sand deposits pass rapidly to the silty-clay pro-deltaic sediments at the shelf break (Jouet et al. 2008). The regressive para-sequence, U147/U151/U152, is overlain by a series of transgressive units that indicate a rapid retro-gradation of the sedimentary system from the outer to the inner shelf in response to sea-level rise during the deglaciation (Jouet et al. 2006). During the Holocene the pro-deltaic system retreated landward and a new pro-deltaic accumulation developed in the inner shelf. As the result, terrigenous fine-grains no longer reached the upper slope, initiating a long period of sediment starvation and the deposition of a condensed layer mainly composed of the slow flux of pelagic biogenic material (e.g. foraminifera, Sierro et al. 2009).

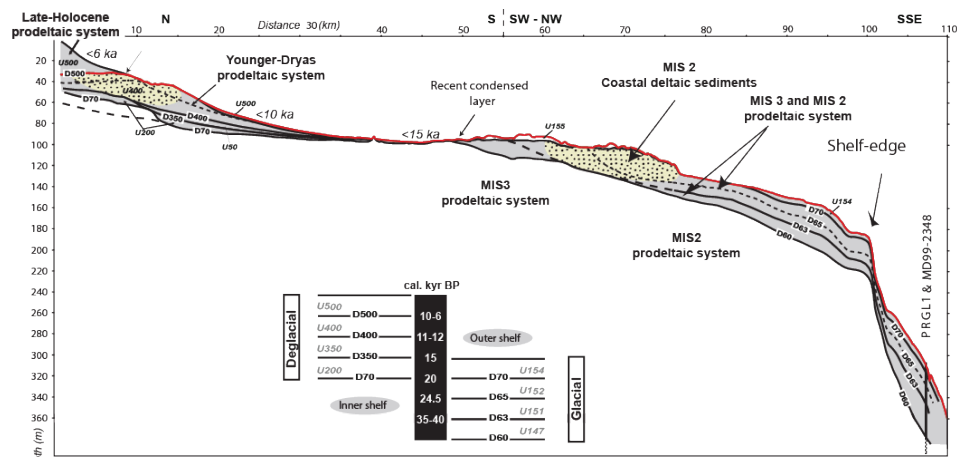


Figure 14

Synthetic stratigraphic section across the Gulf of Lions, illustrating the overall progradation of the deltaic system during MIS3 and MIS2 and retrogradation during the deglaciation. Coastal deltaic deposits are shown in yellow, while pelitic prodeltaic sediments are shown in gray. The red line from the inner shelf to the slope indicates the recent condensed layer. The position of borehole/core PRGL1-MD99-2348 is indicated. Names of seismic reflectors and seismic units together with their ages are shown in the figure. Although many of these units are not mentioned in the text they are shown to facilitate comparisons with other papers referenced in the text. Note that the vertical scale is strongly exaggerated. The figure was modified from Rabineau (2001), Jouet et al. (2006).

Our understanding of paleohydrological, and paleoclimatic conditions in the Mediterranean basin show a strong influence of African monsoon in the Mediterranean sedimentation (Rohling et al. 2015 and references therein). The prominent example is the cyclic occurrence of sapropel deposits caused by precessional extensive Nile discharges, disruptions in the basin's hydrology and reduced bottom water ventilations (see Chapter IV for a more detailed description). Recently and for the first time in the western Mediterranean basin (i.e. GDEC borehole, Corsica, eastern boundary of the Gulf of Lion), direct evidence of pluvial phases coinciding with sapropel times were evidenced (Toucanne et al. 2015; Dixit et al. 2017). During these high rainfall periods, an enhanced proportion of terrestrial organic matter were observed; equivalent or higher than that observed during glacial times where the GDEC site is closer of the river mouth; Toucanne et al. 2015; Dixit et al. 2017. This suggests that significant organic matter occurs at GDEC site during periods of high sea-level. Such exportation of terrestrial organic matter has been related to enhanced discharge of the Golo river in response to atmospheric re-arrangement during northward extension of the African summer monsoon at times of minima in the precession index (i.e. during northern hemisphere summer insolation maxima).

Using an intercomparison of marine, lacustrine and cave records, Toucanne and collaborators highlighted the regional character of rainfall. Therefore, the Gulf of Lion sedimentation may have experienced similar increase of terrestrial organic carbon. This is one aspect that we will discuss in this manuscript, see Chapter III for discussion.

10. Organic carbon source, fluxes and burial in the Gulf of Lion

One of the main issues in studying sedimentary organic matter on continental margins is to accurately estimate the relative proportion of terrestrial vs marine organic matter (i.e. degradability). Accurate information relative to the origin of organic carbon will considerably improve our knowledge of sedimentary processes, transport from the continent to sediment accumulations, and therefore, improve our understanding of early diagenetic processes.

In coastal environment, the **stable organic carbon isotopes** ($\delta^{13}\text{C}_{\text{org}}$) and **organic carbon to total nitrogen ratio** (C/N) have been widely used (Meyers 1994; Lamb et al. 2006; Kim et al. 2006; Tesi et al. 2007) because they have the potential to provide information on the origin of organic material preserved in sediments, see **Figure 15**. The distribution of $\delta^{13}\text{C}_{\text{org}}$ and C/N of various sources of carbon in estuarine sediments has led to its use as a tracer of carbon pathways and storage in sediments. For example, there are significant preferential uptake from atmospheric ^{12}C during plant photosynthesis, therefore we observe large variations in $\delta^{13}\text{C}$ between C3- and C4- photosynthetic pathway (14 ‰); terrestrial vs marine (5 - 8 ‰), particulate, and dissolved organic carbon (~ 9 ‰); see **Figure 15**. On the basis of $\delta^{13}\text{C}$ alone, there is strong overlap between possible origin which may induce wrong organic carbon origin attributions. Although, the use of C/N ratio can significantly help with the distinction between those sources (see Lamb et al. 2006 for a thorough review).

In any case, interpretation of these proxies is often complicated by the fact that bulk material (i.e. sediment) presents mixture from several sources, history and thus their isotopic ratio are weighted averages. Furthermore, selective degradation of organic carbon during early diagenesis, or during chemical sample preparation can substantially alters $\delta^{13}\text{C}_{\text{org}}$ and/or C/N ratio. The latter point will be discussed in details within the Chapter II.

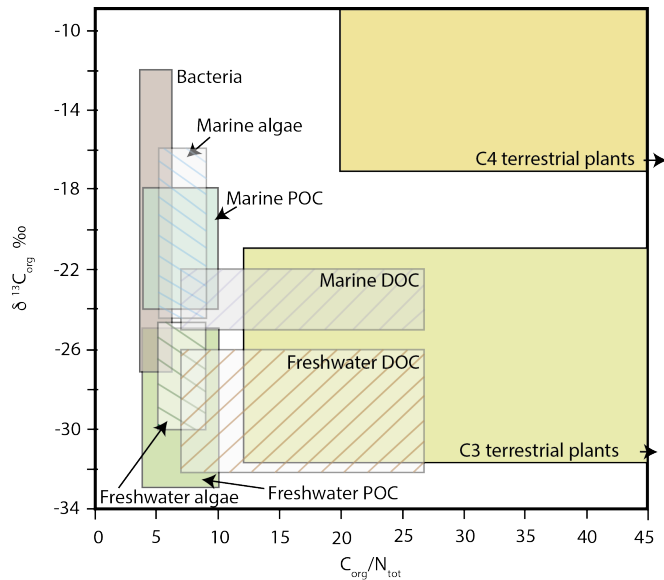


Figure 15

Range of $\delta^{13}\text{C}$ and C/N values reported in the literature for characteristic organic matter sources (i.e. living flora and fauna) that accumulate in marine sedimentary sequences in coastal environment. Compil data from Lamb et al. (2006) and references therein.

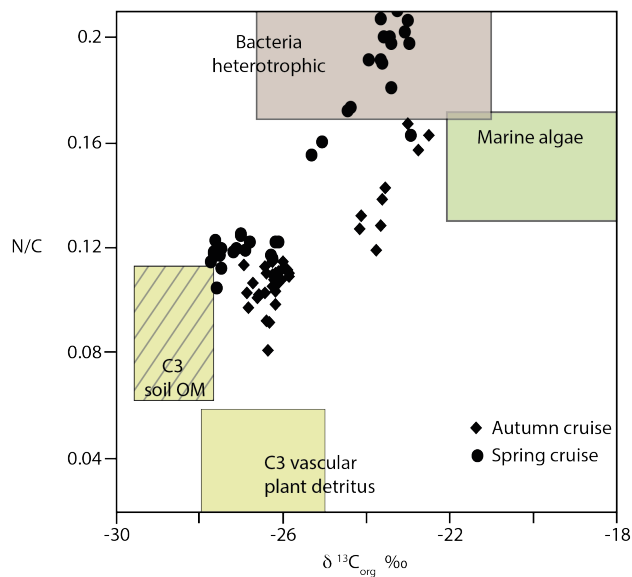


Figure 16

Stable isotopic composition of organic carbon vs total nitrogen:carbon ratio from superficial sediments in the Gulf of Lion. The range of composition of four organic carbon sources (C3 vascular plant detritus, C3 soil derived organic matter, riverine/estuarine phytoplankton detritus and marine phytoplankton detritus) are also plotted in the graph to illustrate their relative influences. Data from Tesi et al. (2007).

In the Gulf of Lion this approach has already been done in soils, riverbeds from the land, as well as surface sediments over the entire shelf, and within transect from river mouths to canyons (Kim et al. 2006; Tesi et al. 2007; Cathalot et al. 2010); see **Figure 16**. Those studies used core tops of sediment cores from the entire shelf (i.e. from prodeltaic to open shelf environments) obtained during various offshore cruises, at various season and/or hydrological regime (i.e. low water level vs flood). As expected, high C/N values and low organic carbon isotopic values were measured in soils and river beds (Kim et al. 2006). In the pro-delta region, organic content was inversely related to the distance from the Rhone, and showed a clear seasonal variability (i.e. highest organic content during wet months). A clear decrease in organic content is observed along the shelf, where offshore station located at the shelf break reached the lower organic content values. The C/N ratio decreases seaward. Depleted isotopic values were measured in prodelta regions, with values as low as -27 ‰, and the $\delta^{13}\text{C}_{\text{org}}$ showed enrichment along the shelf. The heaviest value was measured at the shelf break and showed a value in the range of typical marine phytoplanktonic derived organic matter (Tesi et al. 2007; Hedges and Oades 1997). All these results are summarized as in **Figure 16** where $\delta^{13}\text{C}_{\text{org}}$ is plotted against the N/C ratio rather than the classical C/N because the N/C ratio parameter behaves linearly in a mixing model (Goñi et al. 2003). (Note also that land values were not plotted as the N content is not available). The **Figure 16** shows a clear mix between marine (i.e. bacteria heterotrophic and marine algae end members) and terrestrial organic carbon (i.e. C3 soil organic matter and C3 vascular plant detritus end-members). This trend highlights a possible mixing of soil-derived material, isotopically depleted, rich in organic carbon with marine phyto-detritus characterized by lower organic content and heavier isotopic composition. Such a mixture is supported by elevated coefficient of correlation (R^2 : 0.82 and 0.86 respectively for autumn and spring samples). Along the dispersal system (i.e. Gulf of Lion shelf), the remaining fraction of terrestrial organic carbon that not settled in the prodelta, can be transported seaward and then be diluted by (i.e. mixed with) marine organic carbon further seaward, before reaching the sea-bed and start degradation by microbial activity (i.e. early diagenesis). In other words, the advected material that reaches the shelf break has lost its original terrestrial signature and is dominantly marine.

On another hand, those studies also confirmed the major role of the Rhone river during the present day interglacial in terms of amount of material inputs compared to western rivers (Tech, Tet, Agly, Aude, Herault, Orb). Today, the Rhone catchment represents the major fresh water and organic carbon input to the Mediterranean Sea (Sempéré et al. 2000). Also, the Rhone river is the dominant source of terrigenous material, it represents 80 % of the total sedimentation in the Gulf of Lion which represent 19.2 ± 6 ton of carbon per year (Sempéré et al. 2000).

11. Keeping the PROMESS

The PROMESS project was part of large European research programs with varied studies on deltaic margins from source to sink (Eurodelta, Eurostrataform, Promess, Hermes, etc). The original objectives were to obtain comprehensive transects and sampling over the last 500 kyr across two Mediterranean deltaic margin located in the northwest Mediterranean Sea (i.e. the Gulf of Lion) and in the Adriatic Sea (Berné 2004; Trincardi et al. 2004; Cattaneo et al. 2004; and other papers in a special issue of *Oceanography*, Vol.17, N° 4). The project successfully drilled boreholes at the two locations in 2004 which helped to better understand the interaction between sediment supply, sea-level changes, and climate changes over the last 500 kyr.

For both Adriatic and Gulf of Lion, a revisited seismic stratigraphic analysis was proposed on the based on multi-proxy analysis that provided a **precise chrono-**

stratigraphic framework. The interpretation of **100 kyr glacial-interglacial cycles** governing the sedimentary architecture of both margin (Rabineau et al. 2005 and Ridente et al. 2008, respectively) were verified over the last 500 kyr. Paleo-depth of shoreface proposed by (Rabineau et al. 2006) have also been verified.

In this PhD study, we focused on **PRGL 1-4 borehole** drilled on the interfluvium of the Bourcart and Herault canyons at a water depth of 298 m. The location of this site is close to the **shelf break**, making it ideal for recording spatial variation of the Gulf of Lion sedimentary system (See paragraph: Climate's impact on Gulf of Lion sedimentation), as well as organic carbon variations and fluxes in the past. The exceptional position of PRGL1-4 at the shelf edge, under influence of coastal rivers supply and between well-developed canyons (BC and HC) makes PRGL1-4 well suited for **continuously recording sediments inputs** from coastal rivers during high- and low- sea level (i.e. low sea-level shoreface associated with low sea-level (the yellow sediment prisms on seismic profile, see **Figure 17**, which have also been reported with the yellow thick line in the bathymetrical map).

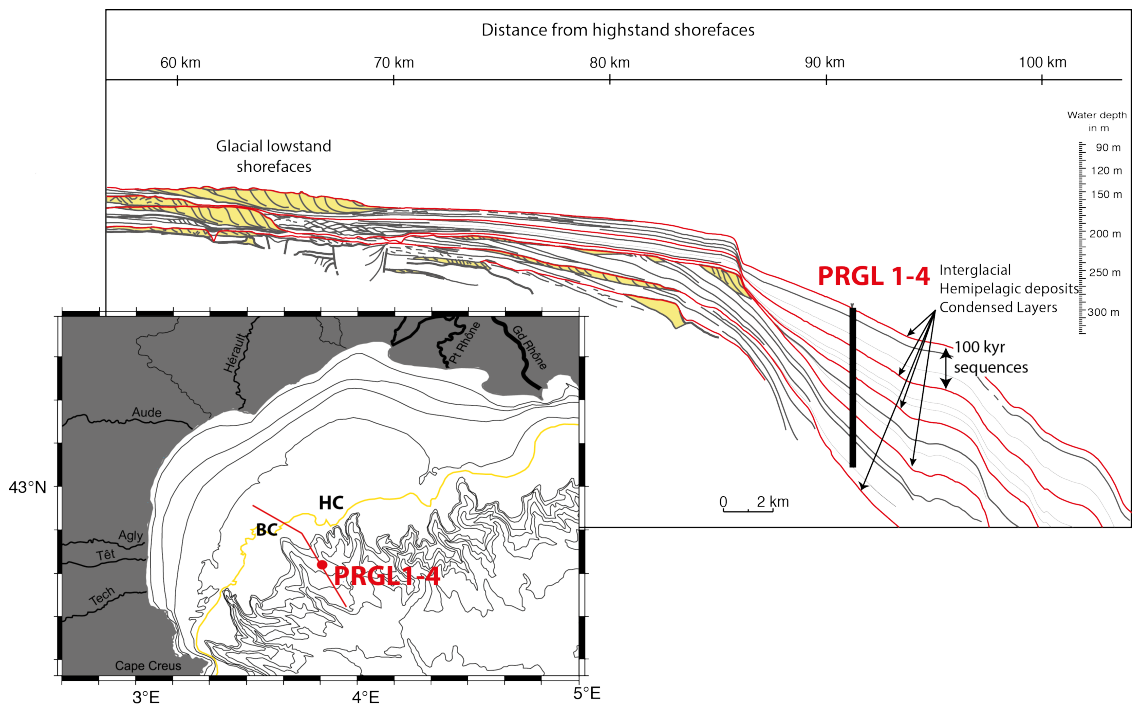


Figure 17

(Bottom left) Bathymetrical map of the Gulf of Lion with location of PRGL1-4 borehole in the interfluvium of Boucart and Herault canyon, BC and HC respectively, and main coastal rivers. Part of high resolution seismic reflection profile P-1036a crossing the borehole in a NW-SE direction across the outer shelf and upper slope (modified from Rabineau (2001)). Schematic seismic section illustrate the stacking of the last five sedimentary sequences bounded by major discontinuities (red) attributed to 100 kyr glacio-eustatic cycles. The shelf morphology allows preservation of low-stand accumulation (yellow). The thick yellow line represent the shoreline position during the Last Glacial Maxima. PRGL1-4 location and sampling depth are projected within the seismic schematic framework.

Previous foraminifera analysis conducted by Sierro and collaborators (2009) on PRGL1-4, allowed the establishment of the first continuous oxygen isotopic curve in the Gulf of Lion over the last 5 climatic cycles. Such dataset considerably helps to recognize the imprint of sea level changes and allows the definition of a robust chronological framework. A close examination of grain size distribution within the borehole, mainly composed of fine grain sediments (i.e. muds), revealed specific sandy-size intervals, foraminifer-rich, during interglacial times. Using radiocarbon datings, oxygen isotopes preserved in foraminifera and seismic correlation, Sierro et al. (2009) also confirmed the presence of condensed layers at times of sea level rises over the last 270 kyr as observed during the retreat of the last glacial maxima Rhone prodelta. Most studies based on PRGL 1-4 (or earlier studies at the same location) have shown strong modulations of oceanic physical parameters (i.e. sea surface temperature, bottom water oxygenation and ventilation, biogenic production), land-ocean export (i.e. sediment provenance, terrigenous export) and physical sediment grain's parameters (i.e. granulometry, porosity, and composition) by climate changes at various times scales (i.e. glacial/interglacial - millennial to centennial: Frigola et al. 2012; Cortina et al. 2011, 2013, 2015, 2016a,b; Révillon et al. 2011; more details are available in the second chapter of this manuscript). Precessional features have also been recognized in $\delta^{18}\text{O}$ foraminifera and C/N ratio by Cortina and collaborators (2012), re-enforcing the close climatic control on Gulf of Lion sedimentation.

On another hand, pockmarks distribution, spread along major sequences discontinuities, as well as on the sea-floor, suggested the presence of fluid migration (Riboulot et al. 2014). Such fluids sedimentary features seem to indicate the production of biogenic gas, probably methane resulting from the microbial degradation of organic matter rapidly accumulated at the sea floor, and preserved in clay material (as observed during low sea-level). The presence of bacteria and Archea was demonstrated at the same location by Ciobanu et al. (2012). However, no direct chemical sampling attested the gases production. In the case of the Gulf of Lion, this biogenic origin could have been enhanced and/or favored by 'artificial' gas confinement in layers enriched with foraminifera shells accumulation (i.e. condensed layers with high porosity, see paragraph 'Climate's influence on the Gulf of Lion' for further explanation).

12. Scope of this thesis

This work focuses on climate's effect on organic carbon source, and burial, and therefore on early diagenetic processes in sediments. In order to unravel the intertwined climate – early diagenesis dynamics, sediments from PRGL 1-4 are investigated, including (i) interglacial coarse (sand-size) samples that have experienced low organic carbon inputs due to high sea level (i.e. coastal rivers disconnection), that we suppose mainly originating from the marine bio-production as observed nowadays at the shelf break, (ii) fine clastic glacial sediments deposited close to prodeltaic accumulation (or within?) under very high rate of terrigenous sedimentation Sierro et al. (2009), and therefore high organic carbon flux and (iii) samples located within termination that underwent a transition from a prodeltaic to an open marine depositional regime due to post-glacial sea-level rise.

To tackle the climate – early diagenesis interaction in the Gulf of Lion, a **wide range of geochemical tools** was applied, including (i) different multi-elements (trace and major) determinations (HR-ICP-MS and ICP-AES); (ii) Elemental Analyzer and Isotope Ratio Mass Spectrometry (EA-IRMS) for detailed analysis of organic matter composition and source, and pyrite; (iii) microscopic and spectrometric techniques such as laser-ablation interfaced with ICP-MS for direct solid sampling; and (iii) Thermal Ionization Mass Spectrometry for marine carbonate origin.

Chapter 2 explores the methods used during this PhD. A focus on the effect of acid type (i.e. hydrochloric and acetic), but also strength (from 0.2 to 10 N) on $\delta^{13}\text{C}_{\text{org}}$, $\delta^{15}\text{N}$, organic carbon and total nitrogen content is reported. This study led to a recent acceptance to *Rapid Communication in Mass Spectrometry*, that highlighted that glacial and interglacial sediment do not behave the same to acid pre-treatment. Also, these results indicate that high HCl strengths (>1.5 N) induce significant bias in organic carbon isotopic ratio and content determination due to preferential leaching of an isotopically light pool of organic matter. This calls for precautions when using $\delta^{13}\text{C}_{\text{org}}$ and C/N ratio for organic matter origin and subsequent uses (i.e. paleo-environmental reconstruction and/or early diagenetic processes).

Chapter 3 examines the nature and the timing of preserved organic matter in PRGL 1-4, but also focuses on the impact of climate changes on buried organic carbon in the Gulf of Lion over the last 200 kyr. Using a multi-proxy approach, we highlight episodes of high land-derived organic carbon, resulting from high river inputs, during sapropel depositions in the Eastern Mediterranean basin. Such findings are consistent with previous observations for high rainfall activity in Corsica (Toucanne et al. 2015), and confirmed the regional character of atmospheric humidity and precipitation over the North Mediterranean borderland at times of precession minima. Taking advantage of PRGL 1-4, we suggest enhanced (i.e. frequency) passage of North Atlantic lows in the Western Mediterranean. Our evidence for high rainfall activity along the North Mediterranean borderland provides additional constraint on the role of mid-latitude atmospheric circulation on the forcing leading to sapropel deposition: (i) increasing carbon organic flux from continent through Mediterranean basins with potential consequence on the primary production and the subsequent marine organic matter flux to the sea-floor, and (ii) hydrological changes leading to disruption of hydrological circulation and subsequent reduction of bottom water during sapropel deposition. This work has been submitted to *Quaternary Science Reviews*.

Chapter 4 discusses early diagenetic processes involved in pyrite formation associated with the bacterial sulfate reduction. Indeed, past studies have shown that the sulfur isotopes fractionning varies as a function of the metabolic activity of the sedimentary microbial community and the growth conditions. The others primary control are (i) the

flux of pyrite burial, which is considered as the proportion of the total sulfur from the ocean, or (ii) change in the marine sulfate reservoir. As such, variations of sulfur isotopic composition of sedimentary sulphide phases (i.e. pyrite) are inferred to reflect evolution of the ocean chemistry and global redox conditions.

However, PRGL 1-4 sediments show anomalous sulfur isotope fractionations (> 76 ‰) that is not consistent with variation of sulfate in the modern ocean (i.e. sulfate residence time in the ocean is much longer 13 My). Therefore, we proposed in a *Proceedings of National Academy of Sciences* published paper that pyrite sulfur isotopic measurement in PRGL 1-4 reflect local processes involved in early diagenesis (i.e. changes in microbial processes related to organic carbon flux and/or sediment physical proprieties induced by climate changes), see Pasquier et al. (2017).

Chapter 5 is devoted to a discussion on how climate affects early diagenesis, trying to decipher the relative importance of changes in organic carbon content, origin and degradability versus sedimentological parameters such as porosity and water content.

Because a significant part of my time was not devoted to deciphering relation between climate and early diagenetic processes, others project were investigated and are reported in annexe of this manuscript

Appendix 1 explains the un-successful trial to develop a laser ablation on foraminifera shells using a HR-ICP-MS in Brest. Indeed, trace elements in foraminifera shells are wildly used because they allow high resolution reconstructions of sea-water parameters, such as salinity or temperature. The idea was to:

- reconstruct Rhone river hydrology over the last 200 kyr using Mg/Ca and Ba/Ca ratios preserved in planktonic foraminifera shells and then compared with the organic carbon isotopic dataset (i.e. Chapter 3),
- reconstruct sea-level variations in the Gulf of Lion using multi foraminifera species.

However, because of the high sensibility of HR-ICP-MS, the set-up of micro laser ablation if foraminifera calcite was not easy, and would have needed many years of mass spectrometry experimentations, therefore, in agreement with my supervisors, I decided to stop this investigation.

Appendix 2 shows how we wanted to use radiogenic isotopes ($^{87}\text{Sr}/^{86}\text{Sr}$) to trace export of terrigenous carbonates in sedimentary basin. In this project, **still in progress**, we measured $^{87}\text{Sr}/^{86}\text{Sr}$ isotopic composition of bulk PRGL 1-4 carbonated fraction assuming to find the actual strontium sea-water signature ($^{87}\text{Sr}/^{86}\text{Sr}_{\text{seawater}} = 0.7092$). Indeed, in marine environment carbonates precipitate calcite with little, or negligible, strontium isotopic fractionation from ambient sea-water. Down-core fluctuations of $^{87}\text{Sr}/^{86}\text{Sr}$ range between 0.708090 and 0.708580, and follow regional sea-level reconstruction. According to this, and because 50 % of the Rhone watershed is composed of carbonated lithologies, this carbonate signal cannot reflect pure in-situ biogenic calcite production, and must reflect a mixing with older detrital carbonate outcropping in the drainage basin.

LITERATURE CITED

- Allen, P. A., 2008. From landscapes into geological history. *Nature* 451 (7176), 274.
- Allen, P. A., Armitage, J. J., Carter, A., Duller, R. A., Michael, N. A., Sinclair, H. D., Whitchurch, A. L., Whittaker, A. C., 2013. The qs problem: sediment volumetric balance of proximal foreland basin systems. *Sedimentology* 60 (1), 102–130.
- Allen, R. C., 1982. The Effects of Macrobenthos on Chemical Properties of Marine Sediment and Overlying Water. Springer US, Boston, MA, pp. 53–102.
- Allen, R. C., 2014. *Sedimentary Diagenesis, Depositional Environments, and Benthic Fluxes*, 8th Edition. Vol. 11. Elsevier Ltd.
- Allen, R. C., Blair, N. E., Brunskill, G. J., 2008. Early diagenetic cycling, incineration, and burial of sedimentary organic carbon in the central Gulf of Papua (Papua New Guinea). *Journal of Geophysical Research*.
- Allen, R. C., Madrid, V., Chistoserdov, A., Aller, J. Y., 2010. Unsteady diagenetic processes and sulfur biogeochemistry in tropical deltaic muds: implications for oceanic isotope cycles and the sedimentary record. . . et *Cosmochimica Acta*.
- Arndt, S., Jørgensen, B. B., LaRowe, D. E., Middelburg, J., Pancost, R., Regnier, P., 2013. Quantifying the degradation of organic matter in marine sediments: a review and synthesis. *Earth-science reviews* 123, 53–86.
- Bache, F., Feb. 2008. Oligocene-Miocene evolution of the Gulf of Lion continental margin (Provencal Basin). Theses, Université de Bretagne occidentale - Brest.
- Bard, E., Hamelin, B., Fairbanks, R. G., Zindler, A., 1990. Calibration of the 14c timescale over the past 30,000 years using mass spectrometric u-th ages from barbados corals. *Nature* 345 (6274), 405–410.
- Barker, S., Knorr, G., Edwards, R. L., Parrenin, F., 2011. 800,000 years of abrupt climate variability. *Science* 334, 347–351.
- Bassetti, M. A., Berné, S., Jouet, G., Taviani, M., 2008. The 100-ka and rapid sea level changes recorded by prograding shelf sand bodies in the Gulf of Lions (western Mediterranean Sea). *Geochemistry, Geophysics, Geosystems* 9 (11), 1–27.
- Baztan, J., Berné, S., Olivet, J. L., Rabineau, M., 2005. Axial incision: the key to understand submarine canyon evolution (in the western Gulf of Lion). *Marine and Petroleum Geology* 22, 805–826.
- Berné, S., 2004. Promess 1: past global changes investigated by drilling mediterranean continental margins. In: *AGU Fall Meeting Abstracts*.
- Berner, R. A., 1982. Burial of organic carbon and pyrite sulfur in the modern ocean: its geochemical and environmental significance. *Am. J. Sci.:(United States)* 282.
- Berner, R. A., 1989. Biogeochemical cycles of carbon and sulfur and their effect on atmospheric oxygen over phanerozoic time. *Palaeogeography, Palaeoclimatology, Palaeoecology* 75 (1-2), 97–122.
- Berner, R. A., 2006. Geocarbsulf: a combined model for phanerozoic atmospheric o₂ and co₂. *Geochimica et Cosmochimica Acta* 70 (23), 5653–5664.
- Berner, W., Oeschger, H., Stauffer, B., 1980. Information on the co₂ cycle from ice core studies. *Radiocarbon* 22 (2), 227–235.
- Bianchi, T. S., 2011. The role of terrestrially derived organic carbon in the coastal ocean: A changing paradigm and the priming effect. *Proceedings of the National Academy of Sciences* 108 (49), 19473–19481.
- Blair, N. E., Aller, R. C., 2012. The fate of terrestrial organic carbon in the marine environment. *Annual Review of Marine Science* 4, 401–423.
- Blair, N. E., Leithold, E. L., Ford, S. T., Peeler, K. A., Holmes, J. C., Perkey, D. W., 2003. The persistence of memory: the fate of ancient sedimentary organic carbon in a modern sedimentary system. *Geochimica et Cosmochimica Acta* 67 (1), 63–73.
- Burdige, D. J., 2007. Preservation of organic matter in marine sediments: controls, mechanisms, and an imbalance in sediment organic carbon budgets? *Chemical reviews* 107 (2), 467–485.
- Burdige, D. J., Lerman, A., 2006. *Geochemistry of marine sediments*. Vol. 41. Princeton University Press Princeton.
- Burrus, J., 1989. Review of geodynamic models for extensional basins; the paradox of stretching in the gulf of lions (northwest mediterranean). *Bulletin de la Société géologique de France* (2),

377–393.

- Canfield, D. E., 1994. Factors influencing organic carbon preservation in marine sediments. *Chemical Geology* 114 (3), 315–329.
- Canfield, D. E., 2005. The early history of atmospheric oxygen: homage to robert m. garrels. *Annual Revue of Earth and Planetary Sciences* 33, 1–36.
- Canfield, D. E., Teske, A., Jul. 1996. Late Proterozoic rise in atmospheric oxygen concentration inferred from phylogenetic and sulphur-isotope studies. *Nature* 382 (6587), 127–132.
- Canfield, D. E., Thamdrup, B., 1994. The production of (34) S-depleted sulfide during bacterial disproportionation of elemental sulfur. *Science*.
- Cathalot, C., Rabouille, C., Pastor, L., Deflandre, B., 2010. Temporal variability of carbon recycling in coastal sediments influenced by rivers: assessing the impact of flood inputs in the Rhône River prodelta. *Biogeosciences* 7, 1187–1205.
- Cattaneo, A., Trincardi, F., Langone, L., Asioli, A., Puig, P., 2004. Cliniform generation on mediterranean margins. *Oceanography* 17 (4), 104–117.
- Chappell, J., Shackleton, N., 1986. Oxygen isotopes and sea level. *Nature* 324 (6093), 137–140.
- Ciobanu, M., Rabineau, M., Droz, L., Révillon, S., Ghiglione, J. F., Dennielou, B., Jorry, S. J., Kallmeyer, J., Etoubleau, J., Pignet, P., et al., 2012. Sedimentological imprint on subseafloor microbial communities in western mediterranean sea quaternary sediments. *Biogeosciences* 9, 3491–3512.
- Claypool, G. E., Holser, W. T., Kaplan, I. R., Sakai, H., Zak, I., 1980. The age curves of sulfur and oxygen isotopes in marine sulfate and their mutual interpretation. *Chemical Geology* 28, 199–260.
- Claypool, G. E., Kaplan, I., 1974. The origin and distribution of methane in marine sediments. In: *Natural gases in marine sediments*. Springer, pp. 99–139.
- Cook, P. L., Wenzhöfer, F., Glud, R. N., Janssen, F., Huettel, M., 2007. Benthic solute exchange and carbon mineralization in two shallow subtidal sandy sediments: Effect of advective pore-water exchange. *Limnology and Oceanography* 52 (5), 1943–1963.
- Cortina, A., Grimalt, J. O., Martrat, B., Rigual-Hernández, A., Sierro, F. J., Flores, J. A., 2016a. Anomalous sst warming during mis 13 in the gulf of lions (northwestern mediterranean sea). *Organic Geochemistry* 92, 16–23.
- Cortina, A., Grimalt, J. O., Rigual-Hernández, A., Ballegeer, A.-M., Martrat, B., Sierro, F. J., Flores, J. A., 2016b. The impact of ice-sheet dynamics in western mediterranean environmental conditions during terminations. an approach based on terrestrial long chain n-alkanes deposited in the upper slope of the gulf of lions. *Chemical Geology* 430, 21–33.
- Cortina, A., Sierro, F. J., Filippelli, G., Flores, J. A., Berné, S., 2013. Changes in planktic and benthic foraminifer assemblages in the gulf of lions, off south france: Response to climate and sea level change from mis 6 to mis 11. *Geochemistry, Geophysics, Geosystems*.
- Cortina, A., Sierro, F. J., Flores, J. A., 2015. The response of SST to insolation and ice sheet variability from MIS 3 to MIS 11 in the northwestern Mediterranean Sea (Gulf of Lions). *Geophysical Research Letters* 42, 10366–10374.
- Cortina, A., Sierro, F. J., Gonzalez-Mora, B., Asioli, A., 2011. Impact of climate and sea level changes on the ventilation of intermediate water and benthic foraminifer assemblages in the Gulf of Lions, off South France, during MIS 6 and 7. *Palaeogeography, Paleoclimatology, Paleoecology* 309, 215–228.
- De Leeuw, J., Largeau, C., 1993. A review of macromolecular organic compounds that comprise living organisms and their role in kerogen, coal, and petroleum formation. In: *Organic Geochemistry*. Springer, pp. 23–72.
- Demaison, G. J., Moore, G. T., 1980. Anoxic environments and oil source bed genesis. *Organic Geochemistry* 2 (1), 9–31.
- Dixit, Y., Toucanne, S., Tripathi, A., Lora, J., Fontanier, C., Pasquier, V., Bonnin, L., Jouet, G., 2017. Eccentricity forcing on the precession-derived Mediterranean rainfall during the past interglacials. In preparation.
- Donnelly, T. W., 1982. Worldwide continental denudation and climatic deterioration during the late tertiary: Evidence from deep-sea sediments. *Geology* 10 (9), 451–454.
- Droz, L., Dos Reis, A., Rabineau, M., Berne, S., Bellaiche, G., 2006. Quaternary turbidite systems on the northern margins of the balearic basin (western mediterranean): a synthesis. *Geo-Marine Letters* 26 (6), 347–359.

- Elderfield, H., Ferretti, P., Greaves, M., Crowhurst, S., McCave, I., Hodell, D., Piotrowski, A., 2012. Evolution of ocean temperature and ice volume through the mid-pleistocene climate transition. *Science* 337 (6095), 704–709.
- Emerson, S., Hedges, J., 2003. Sediment diagenesis and benthic flux. *Treatise on Geochemistry* 6, 625.
- Emiliani, C., 1955. Pleistocene temperatures. *The Journal of Geology* 63 (6), 538–578.
- Fan, Y., Zhu, Q., Aller, R. C., Rhoads, D. C., 2011. An in situ multispectral imaging system for planar optodes in sediments: examples of high-resolution seasonal patterns of ph. *Aquatic geochemistry* 17 (4-5), 457.
- Frigola, J., Canals, M., Cacho, I., Moreno, A., Siero, F. J., Flores, J. A., Berné, S., Jouet, G., Dennielou, B., Herrera, G., Pasqual, C., Grimalt, J. O., Galavazi, M., Schneider, R., 2012. A 500 kyr record of global sea-level oscillations in the Gulf of Lion, Mediterranean Sea: new insights into MIS 3 sea-level variability. *Climate of the Past* 8 (3), 1067–1077.
- Froelich, P., Klinkhammer, G., Bender, M. L., Luedtke, N., Heath, G. R., Cullen, D., Dauphin, P., Hammond, D., Hartman, B., Maynard, V., 1979. Early oxidation of organic matter in pelagic sediments of the eastern equatorial atlantic: suboxic diagenesis. *Geochimica et cosmochimica acta* 43 (7), 1075–1090.
- Fügenschuh, B., Schmid, S., 2003. Late stages of deformation and exhumation of an orogen constrained by fission-track data: a case study in the western alps. *Geological Society of America Bulletin* 115 (11), 1425–1440.
- Furlong, K. P., Chapman, D. S., 2013. Heat flow, heat generation, and the thermal state of the lithosphere. *Annual Review of Earth and Planetary Sciences* 41, 385–410.
- Gaillardet, J., Dupré, B., Louvat, P., Allegre, C., 1999. Global silicate weathering and co₂ consumption rates deduced from the chemistry of large rivers. *Chemical geology* 159 (1), 3–30.
- Galy, V., France-Lanord, C., Beyssac, O., Faure, P., Kudrass, H., Palhol, F., 2007. Efficient organic carbon burial in the bengal fan sustained by the himalayan erosional system. *Nature* 450 (7168), 407.
- Geyer, W., Hill, P., Kineke, G., 2004. The transport, transformation and dispersal of sediment by buoyant coastal flows. *Continental Shelf Research* 24 (7), 927–949.
- Gildor, H., Tziperman, E., 2000. Sea ice as the glacial cycles' climate switch: Role of seasonal and orbital forcing. *Paleoceanography* 15 (6), 605–615.
- Godon, C., Mugnier, J.-L., Fallourd, R., Paquette, J.-L., Pohl, A., Buoncristiani, J.-F., 2013. The bossons glacier protects europe's summit from erosion. *Earth and Planetary Science Letters* 375, 135–147.
- Goldhaber, M., 2003. Sulfur-rich sediments. *Treatise on Geochemistry* 7, 407.
- Goñi, M. A., Teixeira, M. J., Perkey, D. W., 2003. Sources and distribution of organic matter in a river-dominated estuary (winyah bay, sc, usa). *Estuarine, Coastal and Shelf Science* 57 (5), 1023–1048.
- Gordon, E. S., Goni, M. A., 2004. Controls on the distribution and accumulation of terrigenous organic matter in sediments from the mississippi and atchafalaya river margin. *Marine Chemistry* 92 (1), 331–352.
- Gorini, C., Le Marrec, A., Mauffret, A., 1993. Contribution to the structural and sedimentary history of the gulf of lions (western mediterranean) from the ecores profiles, industrial seismic profiles and well data. *Bulletin de la Société géologique de France* 164 (3), 353–363.
- Grant, K., Rohling, E., Bar-Matthews, M., Ayalon, A., Medina-Elizalde, M., Ramsey, C. B., Satow, C., Roberts, A., 2012. Rapid coupling between ice volume and polar temperature over the past 150,000 years. *Nature* 491 (7426), 744.
- Grant, K. M., Rohling, E. J., Ramsey, C. B., Cheng, H., 2014. Sea-level variability over five glacial cycles. *Nature Communications* 5.
- Guennoc, P., Gorini, C., Mauffret, A., 2000. Histoire géologique du golfe du lion et cartographie du rift oligo-aquitainien et de la surface messinienne. *Géologie de la France* 3, 67–97.
- Habicht, K. S., Canfield, D. E., 1997. Sulfur isotope fractionation during bacterial sulfate reduction in organic-rich sediments. *Geochimica et Cosmochimica Acta* 61 (24), 5351–5361.
- Hay, W. W., Sloan, J. L., Wold, C. N., 1988. Mass/age distribution and composition of sediments on the ocean floor and the global rate of sediment subduction. *Journal of Geophysical Research: Solid Earth* 93 (B12), 14933–14940.
- Hay, W. W., Soeding, E., DeConto, R. M., Wold, C. N., 2002. The late cenozoic uplift-climate

- change paradox. *International Journal of Earth Sciences* 91 (5), 746–774.
- Hays, J. D., Imbrie, J., Shackleton, N. J., 1976. Variations in the earth's orbit: pacemaker of the ice ages. *Science* 194 (4270), 1121–1132.
- Head, M. J., Gibbard, P. L., 2015. Early–middle pleistocene transitions: linking terrestrial and marine realms. *Quaternary International* 389, 7–46.
- Hedges, J., Oades, J., 1997. Comparative organic geochemistries of soils and marine sediments. *Organic geochemistry* 27 (7), 319–361.
- Hedges, J. I., 1992. Global biogeochemical cycles: progress and problems. *Marine chemistry* 39 (1-3), 67–93.
- Hedges, J. I., Eglinton, G., Hatcher, P. G., Kirchman, D. L., Arnosti, C., Derenne, S., Evershed, R. P., Kögel-Knabner, I., De Leeuw, J., Littke, R., et al., 2000. The molecularly-uncharacterized component of nonliving organic matter in natural environments. *Organic geochemistry* 31 (10), 945–958.
- Hedges, J. I., Keil, R. G., 1995. Sedimentary organic matter preservation: an assessment and speculative synthesis. *Marine chemistry* 49 (2-3), 81–115.
- Huettel, M., Webster, I. T., 2001. Porewater flow in permeable sediments. The benthic boundary layer. Oxford University Press, New York, 144–179.
- Huettel, M., Ziebis, W., Forster, S., 1996. Flow-induced uptake of particulate matter in permeable sediments. *Limnology and Oceanography* 41 (2), 309–322.
- Huguet, C., de Lange, G. J., Gustafsson, Ö., Middelburg, J. J., Damsté, J. S. S., Schouten, S., 2008. Selective preservation of soil organic matter in oxidized marine sediments (madeira abyssal plain). *Geochimica et Cosmochimica Acta* 72 (24), 6061–6068.
- Imbrie, J., Hays, J. D., Martinson, D. G., McIntyre, A., Mix, A. C., Morley, J. J., Pisias, N. G., Prell, W. L., Shackleton, N. J., 1984. The orbital theory of pleistocene climate: support from a revised chronology of the marine $\delta^{18}O$ record.
- Imbrie, J., Imbrie, J. Z., 1980. Imbrie, j and imbrie, k. p. 1979. ice ages: Solving the mystery. *Geological Magazine* 117 (2).
- Jeans, C., Mitchell, J., Fisher, M., Wray, D., Hall, I. R., 2001. Age, origin and climatic signal of english mesozoic clays based on k/ar signatures. *Clay minerals* 36 (4), 515–539.
- Johnsen, S., Clausen, H. B., Dansgaard, W., Fuhrer, K., Gundestrup, N., Hammer, C. U., Iversen, P., Jouzel, J., Stauffer, B., et al., 1992. Irregular glacial interstadials recorded in a new greenland ice core. *Nature* 359 (6393), 311–313.
- Jørgensen, B. B., Apr. 1982. Mineralization of organic matter in the sea bed—the role of sulphate reduction. *Nature* 296 (5858), 643–645.
- Jørgensen, B. B., 1996. Case study—aarhus bay. Eutrophication in coastal marine ecosystems, 137–154.
- Jørgensen, B. B., D'hondt, S., 2006. A starving majority deep beneath the seafloor. *Science* 314 (5801), 932–934.
- Jørgensen, B. B., Gallardo, V. A., 1999. *Thioploca* spp.: filamentous sulfur bacteria with nitrate vacuoles. *FEMS Microbiology Ecology* 28 (4), 301–313.
- Jørgensen, B. B., Nelson, D. C., 2004. Sulfide oxidation in marine sediments: geochemistry meets microbiology. *Geological Society of America Special Papers* 379, 63–81.
- Jouet, G., Nov. 2007. Stratigraphic records of climatic and glacio-eustatic cycles during the Late Quaternary - Modelling the Gulf of Lions continental margin. Theses.
- Jouet, G., Berné, S., Rabineau, M., Bassetti, M. A., Bernier, P., Sep. 2006. Shoreface migrations at the shelf edge and sea-level changes around the Last Glacial Maximum (Gulf of Lions, NW Mediterranean). *Marine Geology* 234, 21–42.
- Jouet, G., Hutton, E. W., Syvitski, J. P., Berné, S., 2008. Response of the rhône deltaic margin to loading and subsidence during the last climatic cycle. *Computers & Geosciences* 34 (10), 1338–1357.
- Kim, J. H., Schouten, S., Buscaill, R., 2006. Origin and distribution of terrestrial organic matter in the NW Mediterranean (Gulf of Lions): Exploring the newly developed BIT index. *Geochemistry, Geophysics, Geosystems* 7 (11), 1–20.
- Knaust, D., 2013. Bioturbation and reservoir quality: towards a genetic approach. *AAPG Search and Discovery Article* 50900.
- Kominz, M., Heath, G., Ku, T.-L., Pisias, N., 1979. Brunhes time scales and the interpretation of climatic change. *Earth and Planetary Science Letters* 45 (2), 394–410.

- Koretsky, C. M., Meile, C., Van Cappellen, P., 2002. Quantifying bioirrigation using ecological parameters: a stochastic approach. *Geochemical Transactions* 3 (3), 17–30.
- Lamb, A. L., Wilson, G. P., Leng, M. J., 2006. A review of coastal palaeoclimate and relative sea-level reconstructions using $\delta^{13}C$ and C/N ratios in organic material. *Earth-Science Reviews* 75 (1), 29–57.
- Lambeck, K., Esat, T. M., Potter, E.-K., 2002. Links between climate and sea levels for the past three million years. *Nature* 419 (6903), 199.
- Leeds, A. R., Knopoff, L., Kausel, E. G., 1974. Variations of upper mantle structure under the Pacific ocean. *Science* 186 (4159), 141–143.
- Lehmann, M. F., Bernasconi, S. M., Barbieri, A., McKenzie, J. A., 2002. Preservation of organic matter and alteration of its carbon and nitrogen isotope composition during simulated and in situ early sedimentary diagenesis. *Geochimica et Cosmochimica Acta* 66 (20), 3573–3584.
- Leroux, E., Aslanian, D., Rabineau, M., Moulin, M., Granjeon, D., Gorini, C., Droz, L., 2015. Sedimentary markers in the provençal basin (western mediterranean): a window into deep geodynamic processes. *Terra Nova* 27 (2), 122–129.
- Leroux, E., Rabineau, M., Aslanian, D., Gorini, C., 2017. High-resolution evolution of terrigenous sediment yields in the Provence Basin during the last 6 Ma: relation with climate and tectonics. *Basin Research*, 1–35.
- Lisiecki, L. E., Raymo, M. E., 2005. A Pliocene-Pleistocene stack of 57 globally distributed benthic $\delta^{18}O$ records. *Paleoceanography* 20 (1).
- Lutz, M., Dunbar, R., Caldeira, K., 2002. Regional variability in the vertical flux of particulate organic carbon in the ocean interior. *Global Biogeochemical Cycles* 16 (3).
- Lyons, T. W., Gill, B. C., 2010. Ancient sulfur cycling and oxygenation of the early biosphere. *Elements* 6 (2), 93–99.
- Malusà, M. G., Vezzoli, G., 2006. Interplay between erosion and tectonics in the western alps. *Terra Nova* 18 (2), 104–108.
- Martinson, D. G., Pisias, N. G., Hays, J. D., Imbrie, J., Moore, T. C., Shackleton, N. J., 1987. Age dating and the orbital theory of the ice ages: development of a high-resolution 0 to 300,000-year chronostratigraphy. *Quaternary research* 27 (1), 1–29.
- Mauffrey, M. A., Berné, S., Jouet, G., Giresse, P., Gaudin, M., 2015. Sea-level control on the connection between shelf-edge deltas and the Bourcart canyon head (western Mediterranean) during the last glacial/interglacial cycle. *Marine Geology* 370, 1–19.
- Mayer, L. M., 1995. Sedimentary organic matter preservation: an assessment and speculative synthesis. *Marine chemistry* 49 (2-3), 123–126.
- Meyers, P. A., 1994. Preservation of elemental and isotopic source identification of sedimentary organic matter. *Chemical Geology* 114, 289–302.
- Meysman, F. J., Middelburg, J. J., Heip, C. H., 2006. Bioturbation: a fresh look at Darwin's last idea. *Trends in Ecology & Evolution* 21 (12), 688–695.
- Milankovitch, M., 1920. *Théorie mathématique des phénomènes thermiques produits par la radiation solaire*.
- Milligan, T., Hill, P., Wheatcroft, R., Fox, J., 2003. Post flood evolution of grain size in surficial sediments on the prodelta of the Po river. In: EGS-AGU-EUG Joint Assembly.
- Molnar, P., 2004. Late Cenozoic increase in accumulation rates of terrestrial sediment: How might climate change have affected erosion rates? *Annu. Rev. Earth Planet. Sci.* 32, 67–89.
- Morley, J. J., Hays, J. D., 1981. Towards a high-resolution, global, deep-sea chronology for the last 750,000 years. *Earth and Planetary Science Letters* 53 (3), 279–295.
- Nittrouer, C. A., Wright, L. D., 1994. Transport of particles across continental shelves. *Reviews of Geophysics* 32 (1), 85–113.
- Olivet, J., 1996. La cinématique de la plaque ibérique. *Bull. Cent. Rech. Explor. Prod. Elf Aquitaine* 20 (1), 131–195.
- Parrish, J. T., 1993. Climate of the supercontinent Pangea. *The Journal of Geology* 101 (2), 215–233.
- Pasquier, V., Sansjofre, P., Rabineau, M., Houghton, J., Fike, D. A., 2017. Pyrite sulfur isotopes reveal glacial–interglacial environmental changes. *Proceedings of the National Academy of Sciences of the United States of America* 114 (23), 5941–5945.
- Peizhen, Z., Molnar, P., Downs, W. R., 2001. Increased sedimentation rates and grain sizes 2–4 Myr ago due to the influence of climate change on erosion rates. *Nature* 410 (6831), 891.
- Persaud, M., Pfiffner, O.-A., 2004. Active deformation in the eastern Swiss alps: post-glacial faults,

- seismicity and surface uplift. *Tectonophysics* 385 (1), 59–84.
- Posamentier, H., Allen, G., 1993. Siliciclastic sequence stratigraphic patterns in foreland, ramp-type basins. *Geology* 21 (5), 455–458.
- Rabineau, M., Mar. 2001. A geometric and stratigraphic model of Quaternary sedimentary in the Gulf of Lion margin: A record of 100,000 years climatic cycles. Theses, Université Rennes 1.
- Rabineau, M., Berné, S., Aslanian, D., Olivet, J. L., 2005. Sedimentary sequences in the Gulf of Lion: a record of 100,000 years climatic cycles. *Marine Petroleum Geology* 22, 775–804.
- Rabineau, M., Berné, S., Olivet, J. L., Aslanian, D., 2006. Paleo sea levels reconsidered from direct observation of paleoshoreline position during Glacial Maxima (for the last 500,000 yr). *Earth and Planetary Science Letters* 252, 119–137.
- Rabineau, M., Leroux, E., Aslanian, D., Bache, F., Gorini, C., Moulin, M., Molliex, S., Droz, L., dos Reis, A. T., Rubino, J. L., Guillocheau, F., Olivet, J. L., Feb. 2014. Quantifying subsidence and isostatic readjustment using sedimentary paleomarkers, example from the Gulf of Lion. *Earth and Planetary Science Letters* 388 (C), 353–366.
- Railsback, L. B., Gibbard, P. L., Head, M. J., 2015a. An optimized scheme of lettered marine isotope substages for the last 1.0 million years, and the climatostratigraphic nature of isotope stages and substages. *Quaternary Science Reviews* 111, 94–106.
- Railsback, L. B., Gibbard, P. L., Head, M. J., 2015b. An optimized scheme of lettered marine isotope substages for the last 1.0 million years, and the climatostratigraphic nature of isotope stages and substages. *Quaternary Science Reviews* 111, 94–106.
- Raiswell, R., Canfield, D. E., 1998. Sources of iron for pyrite formation in marine sediments. *American Journal of Science* 298 (3), 219–245.
- Raven, M. R., Sessions, A. L., Fischer, W. W., Adkins, J. F., Aug. 2016. Sedimentary pyrite d34S differs from porewater sulfide in Santa Barbara Basin: Proposed role of organic sulfur. *Geochimica et Cosmochimica Acta* 186 (C), 120–134.
- Raymo, M., 1994. The initiation of northern hemisphere glaciation. *Annual Review of Earth and Planetary Sciences* 22 (1), 353–383.
- Raymo, M. E., Huybers, P., 2008. Unlocking the mysteries of the ice ages. *Nature* 451 (7176), 284.
- Raymo, M. E., Ruddiman, W. F., 1992. Tectonic forcing of late cenozoic climate. *Nature* 359 (6391), 117–122.
- Rehault, J.-P., Boillot, G., Mauffret, A., 1984. The western mediterranean basin geological evolution. *Marine Geology* 55 (3-4), 447–477.
- Révillon, S., Jouet, G., Bayon, G., 2011. The provenance of sediments in the Gulf of Lions, western Mediterranean Sea. *Geochemistry, Geophysics, Geosystems* 12 (8), 1–20.
- Riboulot, V., Thomas, Y., Berné, S., Jouet, G., Cattaneo, A., 2014. Control of quaternary sea-level changes on gas seeps. *Geophysical Research Letters* 41 (14), 4970–4977.
- Ridente, D., Trincardi, F., Piva, A., Asioli, A., Cattaneo, A., 2008. Sedimentary response to climate and sea level changes during the past 400 ka from borehole prad1-2 (adriatic margin). *Geochemistry, Geophysics, Geosystems* 9 (9).
- Rohling, E. J., Marino, G., Grant, K. M., 2015. Mediterranean climate and oceanography, and the periodic development of anoxic events (sapropels). *Earth Science Reviews* 143, 62–97.
- Romans, B. W., Castellort, S., Covault, J. A., Fildani, A., Walsh, J., 2016. Environmental signal propagation in sedimentary systems across timescales. *Earth-Science Reviews* 153, 7–29.
- Ruddiman, W. F., 2001. *Earth's Climate: past and future*. Macmillan.
- Ruddiman, W. F., McIntyre, A., 1981. The north atlantic ocean during the last deglaciation. *Palaeogeography, Palaeoclimatology, Palaeoecology* 35, 145–214.
- Schnitzer, M., 1991. Soil organic matter-the next 75 years. *Soil Science* 151 (1), 41–58.
- Schulz, H. D., 2006. Quantification of early diagenesis: dissolved constituents in pore water and signals in the solid phase. In: *Marine Geochemistry*. Springer, pp. 73–124.
- Selverstone, J., 2005. Are the alps collapsing? *Annual Review of Earth and Planetary Sciences* 33.
- Sempéré, R., Charrière, B., Van Wambeke, F., Cauwet, G., 2000. Carbon inputs of the rhône river to the mediterranean sea: biogeochemical implications. *Global Biogeochemical Cycles* 14 (2), 669–681.
- Séranne, M., Benedicto, A., Labaum, P., Truffert, C., Pascal, G., 1995. Structural style and evolution of the gulf of lion oligo-miocene rifting: Role of the pyrenean orogeny. *Marine and Petroleum Geology* 12 (8), 809–820.
- Shackleton, N., 1969. The last interglacial in the marine and terrestrial records. *Proceedings of the*

- Royal Society of London B: Biological Sciences 174 (1034), 135–154.
- Shackleton, N., 1987. Oxygen isotopes, ice volume and sea level. *Quaternary Science Reviews* 6 (3), 183–190.
- Shackleton, N., Hall, M., 1984. Oxygen and carbon isotope stratigraphy of deep-sea drilling project hole-552a-plio-pleistocene glacial history. *Initial Reports of the Deep Sea Drilling Project* 81 (DEC), 599–609.
- Shackleton, N. J., 2000. The 100,000-year ice-age cycle identified and found to lag temperature, carbon dioxide, and orbital eccentricity. *Science* 289 (5486), 1897–1902.
- Siddall, M., Hindmarsh, R., Thompson, W., Dutton, A., Kopp, R., Stone, E., 2013. Sea level variations during the last interglacial. *Inside PAGES*.
- Siddall, M., Rohling, E. J., Almogi-Labin, A., Hemleben, C., et al., 2003. Sea-level fluctuations during the last glacial cycle. *Nature* 423 (6942), 853.
- Sierro, F. J., Andersen, N., Bassetti, M. A., Berné, S., 2009. Phase relationship between sea level and abrupt climate change. *Quaternary Science Reviews* 28, 2867–2881.
- Sirocko, F., Claussen, M., Litt, T., Sanchez-Goni, M., 2006. *The climate of past interglacials*. Vol. 7. Elsevier.
- Suess, E., 1980. Particulate organic carbon flux in the oceans—surface productivity and oxygen utilization. *Nature* 288 (5788), 260–263.
- Tesi, T., Langone, L., Goñi, M., Wheatcroft, R., Miserocchi, S., Bertotti, L., 2012. Early diagenesis of recently deposited organic matter: A 9-yr time-series study of a flood deposit. *Geochimica et Cosmochimica Acta* 83, 19–36.
- Tesi, T., Miserocchi, S., Goñi, M. A., Langone, L., 2007. Source, transport and fate of terrestrial organic carbon on the western Mediterranean Sea, Gulf of Lions, France. *Marine Chemistry* 105, 101–117.
- Toucanne, S., Minto'o, C., Fontanier, C., 2015. Tracking rainfall in the northern Mediterranean borderlands during sapropel deposition. *Quaternary Science Reviews* 129, 178–195.
- Trincardi, F., Cattaneo, A., Correggiari, A., Ridente, D., 2004. Evidence of soft sediment deformation, fluid escape, sediment failure and regional weak layers within the late quaternary mud deposits of the adriatic sea. *Marine Geology* 213 (1), 91–119.
- Vail, P. R., Mitchum Jr, R., Thompson III, S., 1977. Seismic stratigraphy and global changes of sea level: Part 3. relative changes of sea level from coastal onlap: section 2. application of seismic reflection configuration to stratigraphic interpretation.
- Waelbroeck, C., Labeyrie, L., Michel, E., Duplessy, J. C., McManus, J., Lambeck, K., Balbon, E., Labracherie, M., 2002. Sea-level and deep water temperature changes derived from benthic foraminifera isotopic records. *Quaternary Science Reviews* 21 (1), 295–305.
- Wheatcroft, R., Borgeld, J., 2000. Oceanic flood deposits on the northern california shelf: large-scale distribution and small-scale physical properties. *Continental Shelf Research* 20 (16), 2163–2190.
- Willett, S. D., 2010. Late neogene erosion of the alps: a climate driver? *Annual Review of Earth and Planetary Sciences* 38, 411–437.

Materials and Methods

Matériel et Méthodes

Abstract

Au cours de ce travail, nous avons utilisé les outils de la sédimentologie, et de la géochimie sédimentaire sur le forage PRGL1-4. Ce chapitre est divisé en deux parties principales:

(i) La première se focalise sur la description du forage, afin de mieux appréhender les variations sédimentaires qui le composent. Nous exposerons également les différentes méthodes relatives aux outils (i.e. sédimentaire, et géochimique) utilisés lors de ce travail de doctorat. Enfin, nous exposerons la méthode utilisée pour l'élaboration du modèle d'âge utilisé lors de ce travail de thèse ; et les principales différences avec le modèle précédent établi par Sierro et al. 2009.

(ii) La deuxième partie de ce chapitre expose les diverses méthodes géochimiques utilisées. Je n'ai pas souhaité présenter les concepts de la géochimie isotopique car cette dernière est maintenant couramment utilisée. Cependant, je me concentrerai plus longuement sur l'effet de la préparation des échantillons en vue des analyses isotopiques du carbone organique et de l'azote puisque ce dernier a fait l'objet d'une publication dans *Rapid Mass Communication in Mass Spectrometry*.

Contents

1	PRGL 1-4 borehole	47
1.1	PRGL1-4 description	47
1.2	Available dataset	48
1.3	PRGL 1-4 age model	51
1.4	Sampling strategy	53
2	Methods	55
2.1	Multi-element concentration determination	55
2.2	S-C-N content in bulk sediments	59
2.3	Mass spectrometry	79

List of Figures

18	PRGL1-4 schematic log with associated high-resolution pictures. (A to D) show interglacial silty-clay sedimentary facies with relative high porosity associated with high foraminifera abundance. (E to J) correspond to glacial sedimentation facies recorded in PRGL1-4 showing clay sedimentation with abundant organic matter spots and low porosity. From Pasquier et al. (2017) Supplementary Information S3.	47
19	Examples of the pre-existing data used during this PhD. All curves shown in this figure show variation in depth. (A) Schematic log of the borehole, (B) The purple curve show density variation whereas the grey one represent the porosity variations, (C) Calcium and Iron records from X-ray fluorescence core scanning, black and orange curves respectively, (D) Variation of the $>63 \mu\text{m}$ size grains, (E) Oxygen isotopic composition of planktonic specie <i>G. bulloides</i> , and benthic specie <i>H. balthica</i> , (F) Sea Surface Temperature reconstruction from alkenones, (G) ϵNd and $^{87}\text{Sr}/^{86}\text{Sr}$, (H) Synthetic pollen diagram.	50
20	Age model comparison between (A) GL_T -syn from Barker et al. (2011); (B) PRGL1-4 age model from Pasquier et al. (2017); (C) PRGL1-4 age model from Sierro et al. (2009); (D) Specmac curve used by Sierro et al. (2009) and curve (E) show the difference in kyr between B and C and (E) Marine Accumulation rate for PRGL1-4 using the age model shown in B	52
21	Trace and major elements chemistry, modified after Rongemaille et al. (2011).	55
22	Schematic diagram of the standard Inlet system of HR-ICP-MS.	56
23	Calculated standard deviation for trace elements measured in a multi-element standard solution at 5 ppb. RSD is define as: $\text{RSD} = \text{standard deviation} / \text{average}$	57
24	(A) Schematic of laser ablation setup. Inserts show the ICP-MS signal intensity behaviour with the pulse smoothing manifold, for a laser pulse of 1/s. The transition between 1laser pulse per second to 2laser pulse per second is also shown with a smoothing behaviour. From Eggins et al. (1998); (B) SEM images of laser ablation in a <i>O. universalis</i> using 10, 20, 50, 100, 500 laser pulses, and (C) fossil <i>N. dutertrei</i> test which have been analysed using LA-ICP-MS.	58
25	Sulfur extraction line used at Washington University in St Louis.	59
26	EA montage of organic carbon and nitrogen isotopes schematic.	79
27	Nier type Mass Spectrometer schematic, modified after the DeltaV plus Operating Manual.	79
28	Diagram of an EI source (adapted from Hoffman and Stoobant 2002).	80
29	Sr purification protocol from Révillon et al. 2011.	83
30	TIMS TRITON ionic source and samples magazine.	85

List of Tables

2	Radiocarbon ages used during this PhD investigation.	49
3	Chronological framework for PRGL1-4. 0-60 kyr age of isotope events from North-GRIP ice core (GICC05 chronology, Rasmussen and Andersen 2006; Svensson et al. 2008) and 60-500 kyr from the synthetic Ice Greenland record of Barker et al. (2011). GI refer to Greenland Interstadials.	54
4	EA configuration used during EA-IRMS sequences.	78
5	Table of standards used for the isotopic calibration certified and house standard, and mean isotopic composition obtained during this PhD.	81
6	Table of reproducibility on standards during each nitrogen/carbon analytical sequence obtain during his PhD.	82
7	Calculated reproducibility on Washington University house standards (BS / BaS / SZn) and certified standard (IAEA-S1 / IAEA-S2 / IAEA-S3).	82
8	Sr elution step using Eichrom [®] Sr SPEC resin.	84

1. PRGL 1-4 borehole

During the European project PROMESS, two boreholes were sampled in the Gulf of Lion. One was drilled through the sandy paleo- shoreface on the shelf (PRGL1-2), and the other through the distal part, near the shelf edge. The latter is composed of silty-clay materials (PRGL1-4). We focused our study on the latter.

1.1. PRGL1-4 description

The Borehole PRGL1-4 and the core MD99-2348 have been recovered at approximately the same location, at 298-meters depth on the shelf edge of the Gulf of Lion. The borehole is 300 m long in total and is predominantly composed of homogeneous grey silty-clay clastic material, which contains abundant organic matter spots and few bioturbation evidences, see **Figure 18**. Interglacial deposits are characterized by sandy biogenic sediments mainly dominated by biogenic shells, including foraminifera tests (see pictures A to D in the **Figure 18**). Contrary to glacial deposits which are composed of clastic fine grains containing rare foraminifera tests and numerous organic matter spots (pictures E to J in the **Figure 18**). The grain-size distribution within the borehole is therefore closely related to the percentage of calcium carbonate (i.e. biogenic sandy layers are composed of foraminifera shells which are pure calcium carbonates).

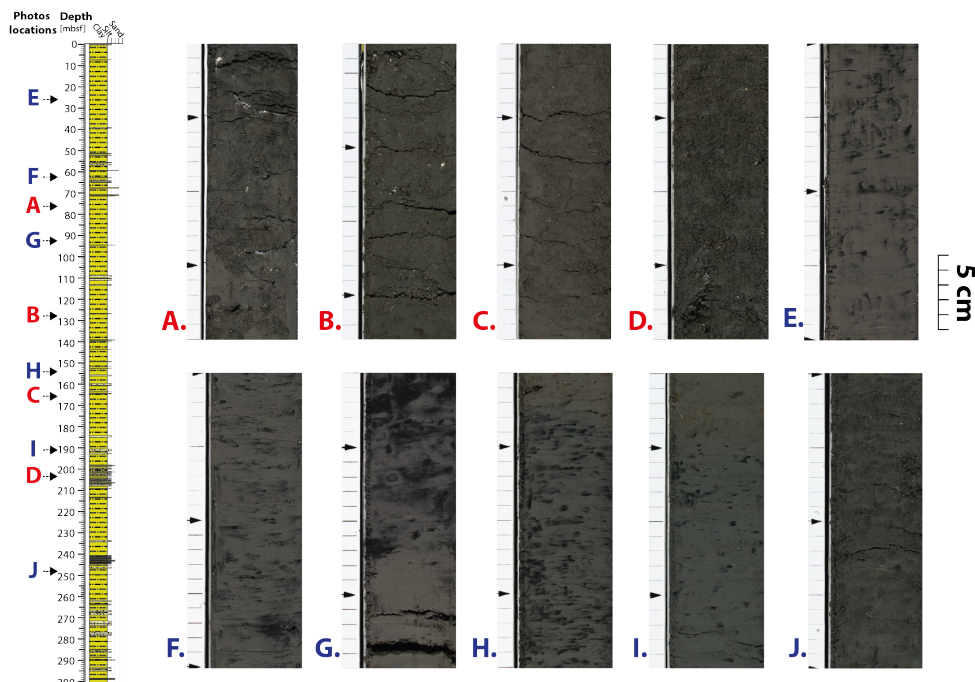


Figure 18

PRGL1-4 schematic log with associated high-resolution pictures. (A to D) show interglacial silty-clay sedimentary facies with relative high porosity associated with high foraminifera abundance. (E to J) correspond to glacial sedimentation facies recorded in PRGL1-4 showing clay sedimentation with abundant organic matter spots and low porosity. From Pasquier et al. (2017) Supplementary Information S3.

1.2. Available dataset

A large set of data is already available for those cores. Most of the results obtained on PRGL1-4, or MD99-2348, are freely available on the Pangea website: <https://www.pangea.de/?q=PROMESS1>

Here I present an overview of the different methodologies and results already published on PRGL1-4 (see **Figure 19**):

The core description, analysis of physical proprieties, and semi quantitative measurement of major element concentrations (XRF core-scanner) were completed onboard the vessel during the drilling processes and/or in the 'Geosciences Marines' research unit at Ifremer during the consortium period.

The physical proprieties, such as the density, magnetic susceptibility, velocity of P waves were initially measured at high resolution (1 cm) using a non-destructive technique: Geotek-MSCL (Multi Sensor Core Logger). After the MSCL measurements, the core was split in two. One section was used for destructive analyses, while the other was archived for future investigations. The 'work' section sampled for destructive analyses was photographed and visually described according to the grain size, color, and sedimentary structures.

Semi-quantitative analysis of major elements (Ca, Fe, Ti and K) was carried out at 4 cm resolution using the first generation Avaatech non-destructive X-ray fluorescence (XRF) core scanner at Ifremer. Measurements were completed at the University of Bremen.

Grain size analyses on bulk and decarbonated sediments were carried out at 20 cm sampling intervals using a Coulter LS 100 Laser Diffraction Particle Size Analyzer after removing the organic matter and carbonates by treatment with H₂O₂ and HCl, respectively. Decarbonated measurements with a laser technique allow the determination of the silt/clay ratio which was used as a proxy for environmental energy during sediment deposition (Frigola et al. 2012).

PRGL1-4 was sampled every 10 cm for isotope analyses and foraminifera counting. Both were carried out on residues of sediments subjected to a 150 μm sieve. The >150 μm fraction was split to obtain an aliquot of 300 species prior to be counted. Approximately 2-20 species of *G. bulloides* (i.e. planktonic foraminifera) and *H. balthica* (i.e. benthic species) larger than 150 μm were hand-picked to measured oxygen and carbon isotope ratios. Foraminifera tests were soaked in 15 % H₂O₂ to remove any organic matter remaining, and ultrasonically cleaned in ethanol to remove any infill material. Samples were analyzed using a MAT 251 mass spectrometer at Kiel university, the analytical error was better than 0.07 ‰ of $\delta^{18}\text{O}$ ratio (Sierro et al. 2009).

Several AMS ¹⁴C analyses were performed at Poznan Radiocarbon Laboratory (Poland) using a mixture of calcareous shells (mainly foraminifera and/or mollusk shells). During this PhD study, the dates were corrected for a marine reservoir effect of 400 kyr (Siani et al. 2001), and radiocarbon ages were calibrated to calendar years using CALIB 7.0.0 and the IntCAL13 calibration curve of Reimer et al. (2013); see **Table 2**.

A total of 700 samples were collected from the borehole for biomarker extraction based on the procedure of Villanueva et al. (1997) and reported in Cortina et al. (2015). Briefly, 2.5 g of bulk sediment was chemically treated to extract organic long chain of type n-alkane (C21 to C33), therefore analyzed using a Varian 3800 mass spectrometer equipped with specific inlet for liquid injection. Long chain di- and tri- unsaturated alkenones (C37) are

Accelerator Mass Spectrometry

(AMS): AMS detects ¹⁴C and ¹²C in a given sample, determining the ¹⁴C/¹²C ratio. The ¹⁴C/¹²C ratio is used to calculate the fractionation modern which define the age of the samples compare to modern (i.e.1950). See McNichol et al. 2016 for detailed overview of AMS data acquisition, and conversion to radiocarbon age.

Site	Sample depth	Lab analytical #	C-14 age	±	Calibrated age	Average calibrated age	Reservoir age
PRGL1-4	19.643	Poz-16580	20330	120	[23 708-24 054]	23881	400
PRGL1-4	25.682	Poz-14910	24070	140	[28 129 - 28 547]	28338	400
PRGL1-4	26.664	Poz-16581	24200	150	[28 268-28 700]	28484	400
PRGL1-4	27.54	Poz-16563	24000	150	[28 041-28 479]	28260	400
PRGL1-4	29.68	Poz-14911	25660	140	[30 182-30 592]	30387	400
PRGL1-4	31.1	Poz-16582	26180	180	[30 735-31 201]	30968	400
PRGL1-4	32.427	Poz-16583	28000	200	[32 635-33 201]	32918	400
PRGL1-4	34.036	Poz-16584	29690	260	[34 387-34 981]	34684	400
PRGL1-4	35.652	Poz-14912	30760	250	[35 451-35 985]	35718	400
PRGL1-4	36.7	Poz-16586	33800	400	[38 344-39 182]	38763	400
PRGL1-4	40.884	Poz-14913	38200	600	[42 254-43 340]	42797	400
PRGL1-4	42.024	Poz-16571	35800	500	[40 196-41 184]	40690	400
PRGL1-4	44.067	Poz-16587	39500	800	[43 197-44 637]	43917	400
PRGL1-4	45.956		41100	900	[44 503-46 127]	45315	400
PRGL1-4	47.891		45100	2800	[46 341-53 381]	49861	400
PRGL1-4	49.079		46300	1700	[46 960-52 036]	49498	400

Table 2 Radiocarbon ages used during this PhD investigation.

produced by phytoplankton, and commonly interpreted as a paleo productivity indicator in marine environments. This is contrary to long-chain n-alkanes (C21 to C33), which are terrestrial waxes easily removed from leaf surfaces and transported by wind and/or rivers. Determination of n-alkanes provides good indications related to the preservation and degree of maturation of terrestrial organic matter (Eglinton and Hamilton 1967).

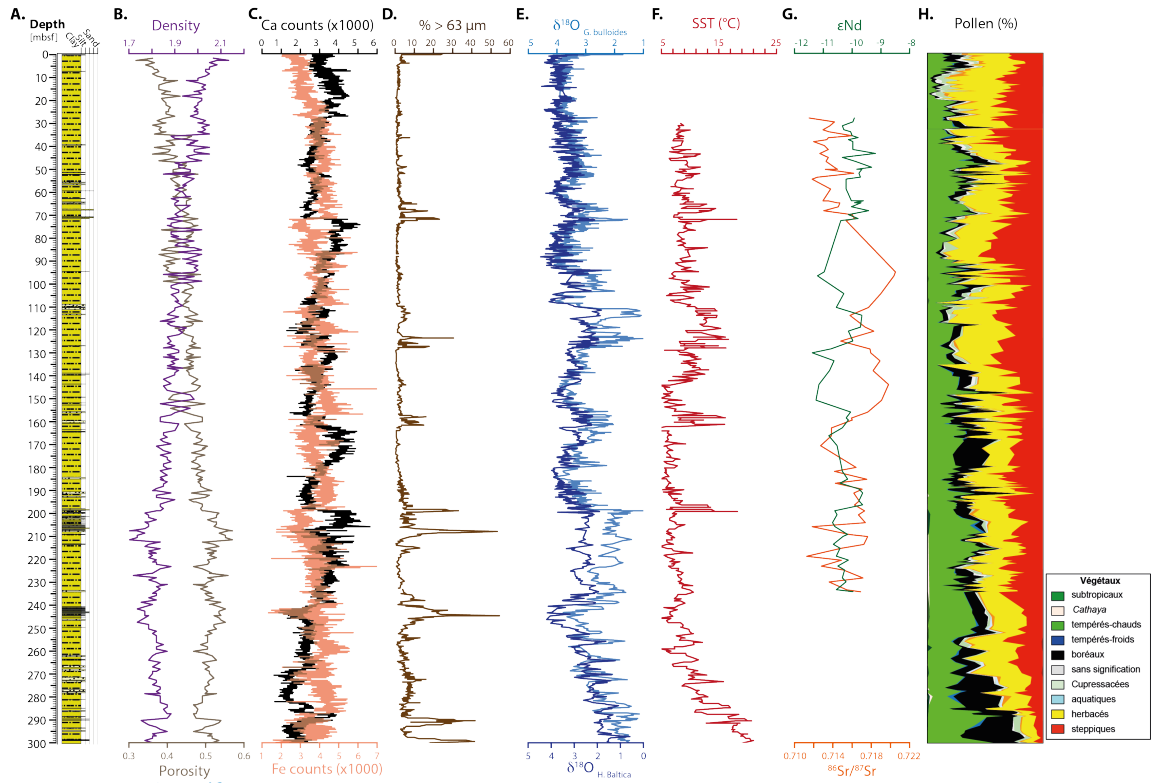
Sea surface temperatures (SST) were also calculated based on the proportion of long chain n-alkenones (C37). See Cortina et al. (2015) supplementary Information Text1 for a thorough calculation explanation.

A total of 120 samples were also analyzed to better understand the sediment provenance and the alteration conditions using ϵNd , $^{87}\text{Sr}/^{86}\text{Sr}$ ratio, and trace elements within the decarbonated $<63 \mu\text{m}$ clay fraction (Révillon et al. 2011). Indeed, since the 80's it has been suggested that Neodymium (Nd) isotopes can be used as a robust proxy to trace sediment provenance (Goldstein and O'Nions 1981; Grousset et al. 1988; White et al. 1985) without any influence of sedimentation weathering processes. Strontium (Sr) isotopes can also be used as source tracers (i.e. transmission of the parent $^{87}\text{Sr}/^{86}\text{Sr}$ composition to the alteration products), but during chemical weathering this ratio can change due to preferential uptake of radiogenic strontium by the surrounding fluids. As a consequence, the $^{87}\text{Sr}/^{86}\text{Sr}$ of the sediment is lowered during the transport process (Jeong et al. 2006; Blum and Erel 1997).

Botanical identification of pollen grains based on detailed morphological analyses and comparison with modern taxa have been performed along the entire core by Jean Pierre Suc, and on the MD99-2348 by Beaudouin et al. (2007). Pollen grains were chemically extracted from bulk sediment using different acid treatments, then sieved prior to counting (i.e. a minimum of 150 pollen grain) under microscope. Several palynozones were defined based on the change of major taxa, as well as their evolution and abundance through the borehole. For example, in PRGL1-4 borehole, the presence of reworked palynomorphs has been linked to major sea-level fluctuation and/or melting of the Alps ice-sheet (Beaudouin et al. 2007).

Sea Surface temperature (SST):

The C37 alkenones is known to be mainly produced by the microalgae *Emiliania huxleyi* which live in the upper few meters of the ocean, therefore alkenone-based temperature give annual average water column temperatures between 0 and 40 m depth (Cacho et al. 1999).



Examples of the pre-existing data used during this PhD. All curves shown in this figure show variation in depth. **(A)** Schematic log of the borehole, **(B)** The purple curve show density variation whereas the grey one represent the porosity variations, **(C)** Calcium and Iron records from X-ray fluorescence core scanning, black and orange curves respectively, **(D)** Variation of the $>63 \mu\text{m}$ size grains, **(E)** Oxygen isotopic composition of planktonic specie *G. bulloides*, and benthic specie *H. balthica*, **(F)** Sea Surface Temperature reconstruction from alkenones, **(G)** ϵNd and $^{87}\text{Sr}/^{86}\text{Sr}$, **(H)** Synthetic pollen diagram.

1.3. PRGL 1-4 age model

High resolution micro-paleontological and geochemical studies at PRGL1-4 were completed during the consortium duration. The uppermost portion (21.5 m) was precisely correlated with MD99-2348, where a robust age model was previously established by Sierro et al. (2009).

The chronostratigraphic framework of PRGL1-4 used in this PhD, is based on $\delta^{18}\text{O}$ measurements which show distinct end-members characterizing interglacials (low $\delta^{18}\text{O}$ values) and glacials (higher $\delta^{18}\text{O}$), similar to the approach used in Sierro et al. (2009), see **Figure 20** and **Table 3**. Indeed, both age models are based on the close similarities between PRGL1-4 planktonic *G.bulloides* $\delta^{18}\text{O}$ and the NGRIP ice core isotopes from Greenland for the last 60 ka (GICC05 chronology, Rasmussen and Andersen 2006; Svensson et al. 2008). Up to 60 ka, I used the synthetic Greenland record reported in Barker et al. (2011), whereas Sierro et al. (2009) used the Specmac isotopic stack from Martinson et al. (1987). I have chosen to use the ice-core $\text{GL}_T\text{-syn}$ curve because it is well established that Greenland (and Antarctica) is very sensitive to climate changes, which is clearly demonstrated by the existence of repeated, large, abrupt shifts in $\delta^{18}\text{O}$ or δD of polar ice. These shifts are one expression of a global system that drives major global climate changes, known as the bipolar seesaw model. We also know that the bipolar seesaw model is one expression of the ocean-atmosphere climate system as an integrated and synergistic system. We note that the overall concept of bipolar seesaw is not restricted to oceanic processes (i.e. AMOC), but also includes atmospheric shifts (i.e. controlling global atmospheric chemistry and subsequent polar precipitation) that occurred more abruptly and quickly. Moreover, Barker et al. (2011) used the precise and absolutely dated Chinese and Alpine speleothems records to place $\text{GL}_T\text{-syn}$ curve on an absolute time scale for the last 400 ka. This approach provides a refinement of the PRGL1-4 age model and gave an alternative to the ultimate dependence on orbital tuning. Furthermore, it allows us to use the absolute 'Speleo-Age' chronology based on the Uranium-Thorium isotopic dating system during the last 400 ka, which is important when comparing marine and terrestrial paleoclimate records (e.g. speleothems $\delta^{18}\text{O}$, see Chapter III). Such synchronization was already used to produce accurate chronologies in the Iberian and Corsican margins (Hodell et al. 2013; Margari et al. 2014; Toucanne et al. 2015). Based on the use of the $\text{GL}_T\text{-syn}$ curve, some discrepancies between both age models appeared (see **Figure 20**). Most differences are located on abrupt transition zones. Indeed, these differences are much sharper in the $\text{GL}_T\text{-syn}$ curve than in the global $\delta^{18}\text{O}$ stack (i.e. Specmac curve shows gradual transition due to longer time response of the ocean related to climate changes). Interglacial age models are also quite discordant, but this is easily explained by the fact that they are very condensed, and a small change in the chronology of tie points induces large changes.

Because isotope substage labelling has been subject to debate over the last decade, in this study we have chosen to use the marine stage scheme published in detail in Railsback et al. (2015) for identification of glacio-climatic events; see **Figure 20**.

Bipolar seesaw theory: is initially based on ice cores records from Greenland and Antarctica where millennial temperature changes have opposed during warning timing. That mean cold periods in Greenland occurred during warning trend in Antarctica, and their opposite. Together with climate simulations showed that the north-south coupling stemmed from changes in the thermohaline circulation of the Atlantic Ocean, ?.

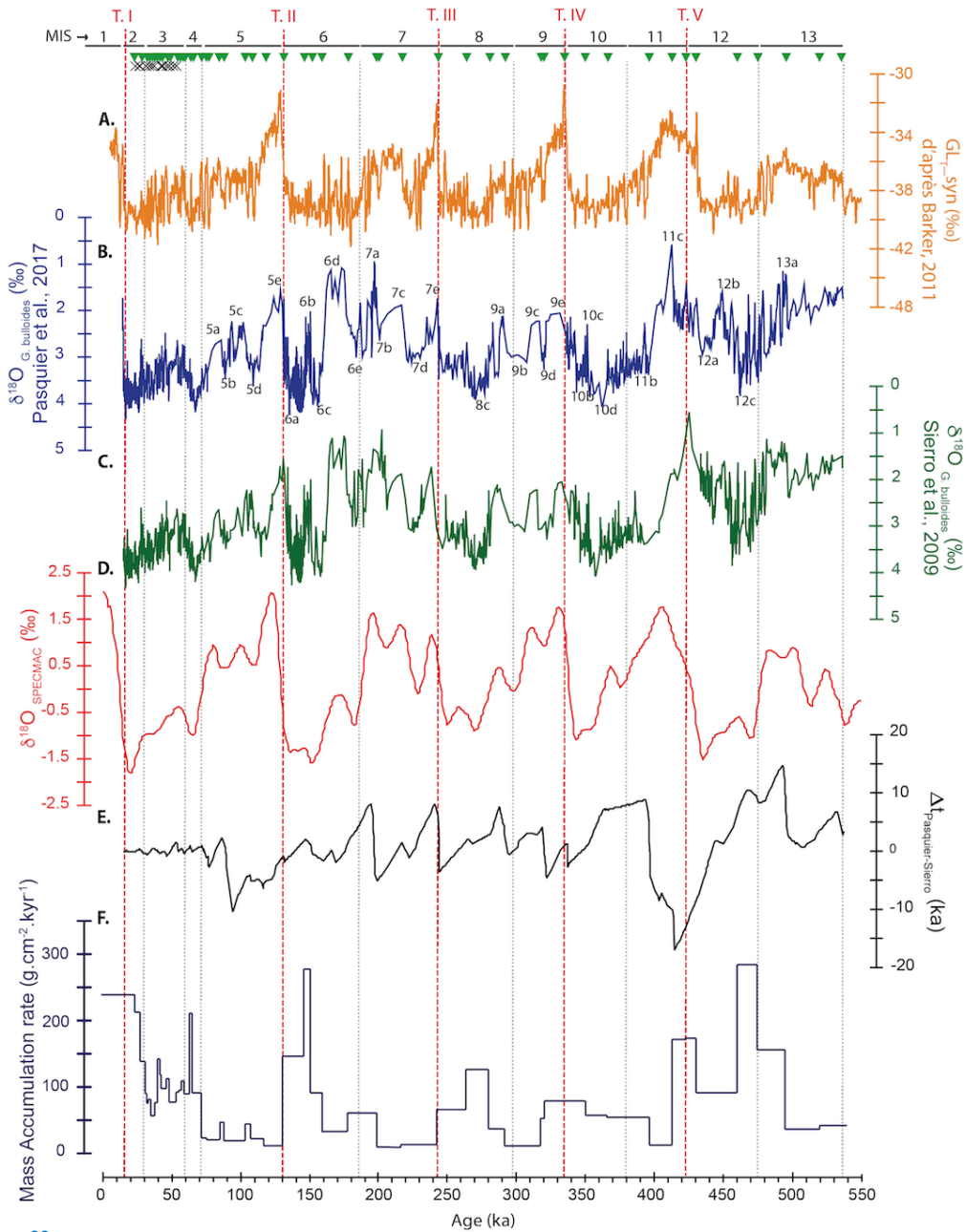


Figure 20

Age model comparison between (A) GL_T-syn from Barker et al. (2011); (B) PRGL1-4 age model from Pasquier et al. (2017); (C) PRGL1-4 age model from Sierro et al. (2009); (D) Specmac curve used by Sierro et al. (2009) and curve (E) show the difference in kyr between B and C and (E) Marine Accumulation rate for PRGL1-4 using the age model shown in B.

Mass accumulation rate Marine accumulation rate in $\text{g.cm}^{-2}.\text{kyr}^{-1}$, have been calculated after estimation of the dry density (D_{dry}) of the sediment. This last parameter was determined indirectly from the MSCL estimation of the wet density of the sediment (D_{wet}). Considering a density of 1.024 g.cm^{-3} for the interstitial water saturating space between grains and 2.65 g cm^{-3} for the mean grain density (e.g. Auffret et al. 2002), the dry density was calculated from the following equation 2

$$D_{\text{dry}} = 2.65 \times (1.024D_{\text{wet}})/(1.024 - 2.65) \quad (2)$$

The mass accumulation rate (MAR) is define using equation 3:

$$MAR = LSR \times D_{\text{dry}} \times (1 - IC) \quad (3)$$

Where LSR refers to linear sedimentation rate in cm.kyr^{-1} , calculated using a simple linear relationship between depth in the borehole and the age model; D_{dry} correspond to bulk density in g.cm^{-3} , and IC refers to the carbonated content in %. The marine accumulation rate is calculated between the tie-points defined in the age model (**Table 3**). Marine accumulation rate from PRGL1-4 range between 3.0 and 244.5, with an average of ca $75.5 \text{ g.cm}^{-2}.\text{kyr}^{-1}$. This also clearly suggest that glaciations enhanced the rate of physical erosion, which promote more rapid silicate weathering. Glaciations may also affect the weathering of non-silicate minerals. Because quantification of the non-silicate weathering is hard to quantify most authors do not take them in account. The latter is discuss in more details in the Appendix 2.

1.4. Sampling strategy

This work focuses on climate changes over the last 500 000 years and its impacts on early diagenesis processes and sediment composition in the Gulf of Lion. In order to unravel the intertwined climate - sediment deposition early diagenesis dynamics, sediments from different time intervals are investigated including (i) high resolution of the last 200 000 years, and (ii) glacial-interglacial transition (i.e. terminations) which have experienced some of the largest and most important natural climate changes in Earth's recent history. Compared to the initial one, my sampling party was less spectacular, but allows extraction of 775 sediment slice (1 cm thick) during about 5 days (15 to 19 December 2014). Once the borehole had been subsampled, sediments were freeze-dried prior to any treatment.

The interval covering the last 200 000 years was sampled every 20 centimeters, except the last glacial periods (i.e. 23 to 70 m) where I used remaining sediments from Sidonie Revillon previous works and/or available samples in Brest. Terminations IV and V (respectively center around 170 and 210 m) were subsampled with a sampling step of 30 cm. Due to low sedimentation rates, and presence of condensed layer during interglacial times, the proportion of samples corresponding to warm conditions in the Gulf of Lion is very low compared to glacial and termination times (with an approx. ratio of 1:4).

Stratigraphic Event	NorthGRIP Age (ka BP)	GLT _{syn}	
		GICC05/NALPPSpeleo Age (ka BP)	PRGL-1-4 - depth (mbsf)
Top PRGL 1-4	14.16		0
Onset GI-1 / T.I	14.8		0.25
Onset GI-2	23.2		19.8
Onset GI-3	27.7		27.99
Onset GI-4	28.63		29.6
End GI-4	31.49		33
Onset GI-5	32.14		33.55
Onset GI-6	33.57		34.32
Onset GI-7	35.72		35.69
Onset GI-8	38.83		37
Onset GI-9	40.1		38.3
Onset GI-10	41.05		40.08
Onset GI-11	43.02		41.96
Onset GI-12	46.1		44.79
Onset GI-13	48.35		46.66
Onset GI-14	54.06		49.44
Onset GI-15	55.88		50.71
Onset GI-16	57.95		52.24
Onset GI-17	59.09		53.59
End GI-18		62.95	56.63
Onset GI-18		64.2	58.95
Onset GI-19		71.95	63.83
Onset GI-20		75.74	64.39
End GI-20		75.58	65.13
Onset GI-21 / MIS5.a		86.46	65.52
MIS5.c-MIS5.b transition		89.82	66.8
Onset GI-22		103.66	68.7
Onset MIS5.c / GI-23		106.92	70.2
Onset MIS5.d		116.29	71.6
Onset MIS5.d / T.II		131	72.4
MIS6.c-MIS6.b transition		146.51	93.8
Onset MIS6.c		151.01	104.45
Onset 6.d		160	110.8
Onset MIS6.e		178	115.27
Onset MIS7.a		199	125.18
Onset MIS7.b		201.17	125.46
Onset MIS7.c		217	125.75
Onset MIS7.e / T.III		243	127.6
Onset MIS8.c		264.3	139.19
MIS8.d-MIS8.e transition		280.5	155.5
Onset MIS8.e		291.5	158.35
MIS9.c-MIS9.b transition		321	160.91
Onset MIS9.c / T.IV		336	161.7
End MIS-10		351	179.9
MIS11-MIS10 transition		396.5	198.4
Mid-MIS11.b		413	199.38
Mid-MIS11.c		423	212.37
Onset MIS11.c / T.V		431	223.25
Mid-MIS12		460.5	242.31
MIS13.b-MIS13.a transition		495.5	290.7
MIS13.c-MIS13.b transition		520.5	296.3
Base PRGL 1-4		536	300.5

Table 3 Chronological framework for PRGL1-4. 0-60 kyr age of isotope events from North-GRIP ice core (GICC05 chronology, Rasmussen and Andersen 2006; Svensson et al. 2008) and 60-500 kyr from the synthetic Ice Greenland record of Barker et al. (2011). GI refer to Greenland Interstadials.

2. Methods

The analysis of sediment chemistry is performed under various forms according to techniques, sedimentary fraction analyzed (i.e. bulk, clay and/or carbonates) and measurements used. During this PhD, the stable isotopes analysis on organic matter (carbon and nitrogen) and reduced sulfur phases preserved in bulk sediment were measured after sample's combustion; whereas major and traces elements concentrations in carbonate samples (e.g. from the catchment area and/or biogenic carbonate) has been done under solution form after acetic acid dissolution.

In this part I present (i) first the method used for Trace and major element on the carbonated fraction, (ii) therefore the technic used for S-C-N content preserved in bulk sediments and, (iii) finally the mass spectrometry techniques used for stables isotopes (Sulfur, Carbon and Nitrogen) and radiogenic isotopes (Strontium) acquisition using TIMS methods.

2.1. Multi-element concentration determination

2.1.1. Protocol for extraction of trace and major elements. 160 analyses of trace and major elements concentrations in biogenic carbonates contained in bulk samples were performed during this PhD, following the method presented in **Figure 21**, and described in details in Rongemaille et al. (2011).

All these experiments were carried out in a class 1000 clean laboratory with cleaned apparatus, twice distilled or commercially purchased ultra-pure acids. All the experimental operations describe bellow were conducted at room temperature.

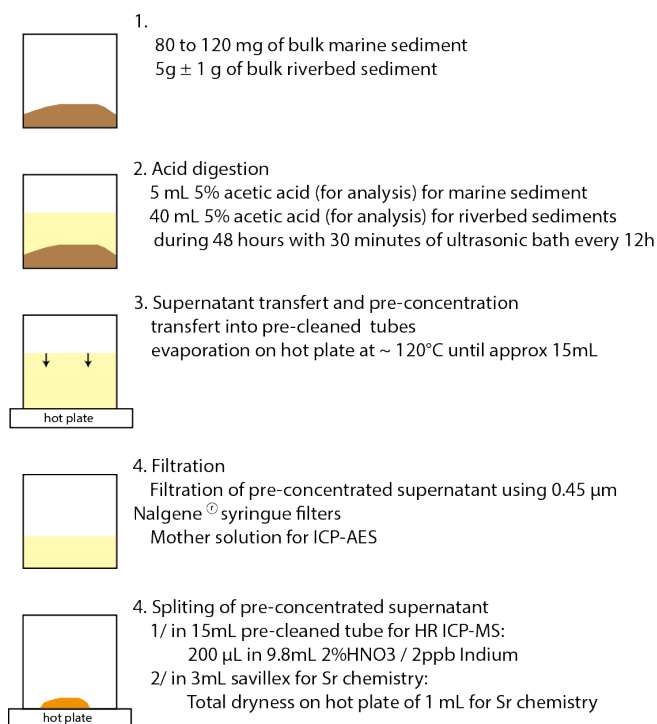


Figure 21

Trace and major elements chemistry, modified after Rongemaille et al. (2011).

Mass Spectrometry:
A detailed explanation of the Mass Spectrometry technique is reported below in a specific section.

2.1.2. Trace elements concentrations determination. Inductively Coupled Plasma Mass Spectrometry (ICP-MS) was used to measure trace elements concentrations using a HR ICP-MS (High Resolution ICP-MS) in Brest. ICP-MS is the most powerful technique for the quantification of trace elements, allowing quantitative multi-element analyses at trace levels, with minimal sample preparation. The PSO is equipped with a Finnigan Thermo Electron Element II, hosted within the IUEM.

This instrument uses an inlet system consists of:

- (i) A peristaltic pump, used to pump liquid sample to the nebulizer
- (ii) A nebulizer is used to convert the liquid sample into a fine aerosol which is a mixture of sample gas (Argon) and the sample solution. The aerosol is sprayed directly to the spray chamber.

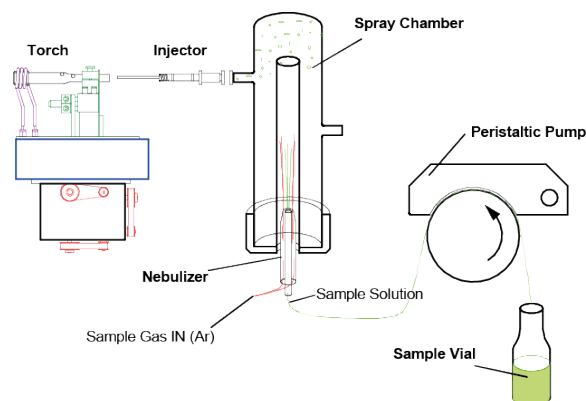


Figure 22

Schematic diagram of the standard Inlet system of HR-ICP-MS.

- (iii) A spray chamber which is used to remove large droplet and ensures that only droplets small enough to remain in suspension in the gas flow are carried into the plasma through the injector.
- (iv) A torch which allow injection of the aerosol sample through the center of the plasma (where the temperature is as high as 6000 to 8000 °C), where it is completely dissolved and the elements in the aerosol are converted first into gaseous atoms and then ionized towards the end of the plasma. At the plasma rims, the temperature is lower allowing creation of oxide and/or hydroxide with masses near to measured elements. These chemical complexes lead to interferences which must be corrected.

The plasma interface is the link between the 'outside world' (i.e. open atmosphere environment) and the clean and high vacuum inside of the Element II. The end of the burning plasma, ions are directly entering the extraction lens of the mass spectrometer through several cones interfaces.

The data processing of HR ICP-MS is based on the use of indium (In) as internal benchmark, because Ca rich matrix often creates small obstructions within the sample cone. When this happens, there is a decrease in transmitted ions into the MS, then an artificially decrease in recorded intensities. Using In we can investigate and correct this artificially decrease by normalizing recorded In counts to the average of the sequence.

Every HR ICP-MS sequence also contains several set of multi-element standard solutions covering a wide range of elements (major and traces), with different concentrations (i.e. in our case: 0.5, 1, 5, 50 and 100 ppb). Repeated and systematic measurements

Plasma: It means 'moldable substance' or 'jelly' in ancient greek. It is one of the four fundamental states of matter, while the others are solid, liquid, and gas. Unlike these three states of matter, plasma does not naturally exist on the Earth under normal surface conditions, and can only be artificially generated from neutral gases.

of these solutions allow (1) the calibration of unknown samples and (2) calculation of reproducibility, see **Figure 23**.

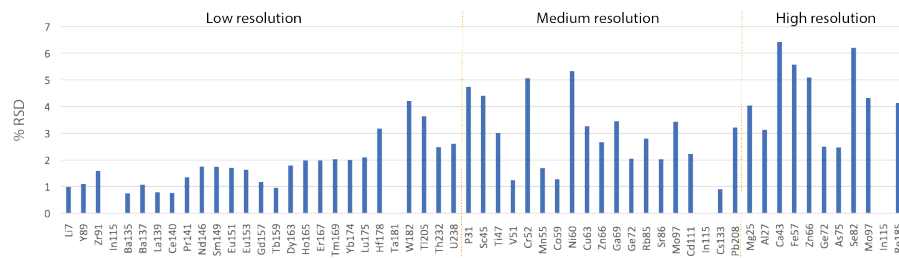


Figure 23

Calculated standard deviation for trace elements measured in a multi-element standard solution at 5 ppb. RSD is defined as: $RSD = \text{standard deviation} / \text{average}$.

Laser ablation Approximately 200 laser ablations using ICP-MS have been done to measure trace elements on foraminifera calcite. The detailed summary is reported in Appendix 1 of this thesis.

Laser ablation works by focusing a laser onto substrate (i.e. in my case foraminifera shells) to remove material that is on its surface, or samples of the entire substrate during depth profiles through foraminifera shells.

The experiment set-up is schematically represented on **Figure 24**, where ablation occurring under a controlled atmosphere within the 'ablation cell'. It is contained by a mixture of Argon and Helium gases. Ablation products are transported to the mass spectrometer (ICP-MS) via the same mixture gases to reduce losses during transport and contamination from the 'outside world'. Most importantly, the transport step smooths the signal which greatly reduces the pulsations in samples delivery resulting from ablation with a pulse-laser and allow stable signal during analyses, see **Figure 24**. Highly controlled and precise foraminifera shell sampling has been achieved with a pulse 193 nm laser system, which limit absorption of laser energy on calcite during the sampling periods (Eggins et al. 1998). The laser system illuminates a mask which is imaged at 20-folds demagnification onto the sample surface using optical lens. The focus step is re-adjusted for each ablation and allows laser pulse energy to focus on the samples.

Each laser pulse removed a uniform layer of calcite ($\sim 0.1 \mu\text{m}$ thick; Eggins et al. 2003) and application of multiple laser impulsion at the same spot allows sampling of entire foraminifera calcite, see **Figure 24**.

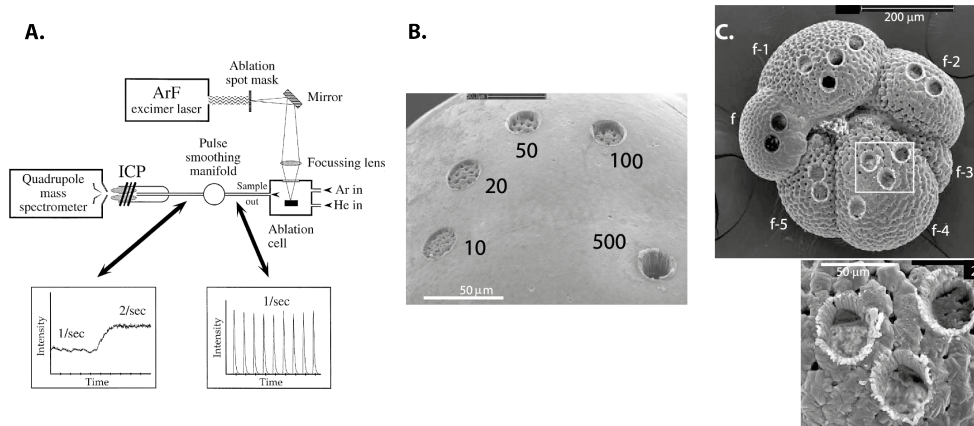


Figure 24

(A) Schematic of laser ablation setup. Inserts show the ICP-MS signal intensity behaviour with the pulse smoothing manifold, for a laser pulse of 1/s. The transition between 1 laser pulse per second to 2 laser pulse per second is also shown with a smoothing behaviour. From Eggins et al. (1998); (B) SEM images of laser ablation in a *O. universalis* using 10, 20, 50, 100, 500 laser pulses, and (C) fossil *N. dutertrei* test which have been analysed using LA-ICP-MS.

2.1.3. Major element determination. Major elements determination uses the Inductively Coupled Plasma Atomic Emission Spectrometry (ICP-AES). Again during this PhD, I used the PSO mass spectrometer: Horiba Jobon Yvon Ultima 2 which allows the determination of all major elements, and some traces (Rb, Sr, Sc, V, Cr, Co, Ni, Y, Zr, Nb, La, Ce, Nd, Sm, Gd, Dy, Er, Yb, Th, Li, Cu, Zn, Be).

ICP-EAS uses the fact that excited electrons emit energy at a given wavelength when returning to 'normal' state. The fundamental characteristic of this process is that each element emits energy at specific wavelengths related to its chemical character. In the ICP-AES technique it is common to select a single wavelength (or a very few) for a given element (depending of existing interferences). The intensity of the energy emitted at the chosen wavelength is proportional to the concentration of that element in the analyzed sample. Thus, by determining which wavelengths are emitted by a sample and by determining their intensities, the analyst can quantify the elemental composition of the given sample relative to a reference standard.

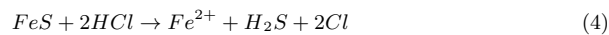
As for HR ICP-MS, major elements determination requires samples to be in solution which will be flown into a nebulizer using a peristaltic pump. Then, the aerosol is injected into the torch, the light emitted from the plasma enter an optical channel is then focused through a lens and passed through an entranced slit into the spectrometer. The spectrometer is analogous to a prism that refracts visible light into its colors component, rotation of the diffraction allows sequential moves of each wavelength into the detector. The energy intensity at each wavelength is measured to provide a quantitative result that can be compared to a reference standard (i.e. analyzed at different concentrations to create a calibration curve).

The data processing also uses a wide range of concentration of multi-element standard solution; see HR ICP-MS for details. Calculated standard deviation calculated on repeated standard solutions are around 1 %, except of K which is up to 3 %.

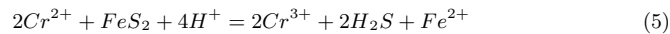
2.2. S-C-N content in bulk sediments

2.2.1. Extraction of sedimentary sulfur form. Pyrite sulfur from 131 samples was extracted using the chromium reduction method (Canfield et al. 1986; Burton et al. 2008) which is illustrated in **Figure 25**. This method allows a total recovering of all reduced inorganic sulfur present in sedimentary samples (pyrite, element sulfur and iron monosulfide phases).

During extraction, 1.0 ± 0.05 g of sample powders were reacted with ~ 25 mL of 6M HCl solution to reduced sulfur forms to H_2S , following the equation 4



Then, 25 mL of 1M reduced chromium chloride ($CrCl_2$) was added over four hours in a specialized extraction line under a Nitrogen atmosphere at temperature around $100^\circ C$. This step produces sulfuric acid and destroy the pyrites within the sediment following equation n° 5



The liberated hydrogen sulfide was reacted in a silver nitrate (0.1 M) trap. In such solution, the hydrogen sulfide precipitate as Ag_2S following equation n° 22:



The residual Ag_2S was rinsed three times using Mili-Q water, centrifuged then dried until complete dryness.

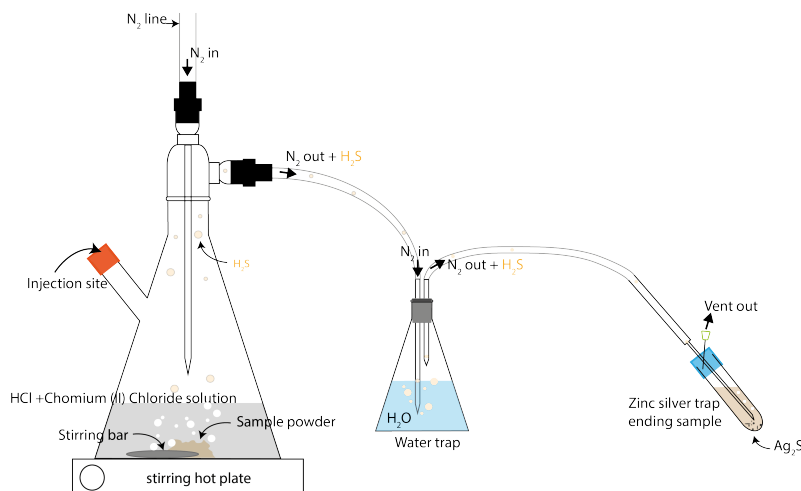


Figure 25
Sulfur extraction line used at Washington University in St Louis.

This chemical step was realized in the Stable Isotopes Laboratory of the University of Washington in St Louis, Missouri, where lab equipment's allows us to extract 7 samples simultaneously. Pyrite concentrations are deduced from extracted Ag_2S masses. All chemical reagents were prepared by myself.

2.2.2. Acid digestion on river influenced shelf sediment organic matter: Carbon and nitrogen contents and isotopic values.



Acid digestion on river influenced shelf sediment organic matter: Carbon and Nitrogen contents and isotopic values

Journal:	<i>Rapid Communications in Mass Spectrometry</i>
Manuscript ID	Draft
Wiley - Manuscript type:	Research Article
Date Submitted by the Author:	n/a
Complete List of Authors:	Pasquier, Virgil; UMR 6538, Institut Universitaire Européen de la Mer, Laboratoire Géosciences Océan Sansjofre, Pierre; UMR 6538, Institut Universitaire Européen de la Mer Lebeau, Oanez; Pole Spectrométrie Océan, Institut Universitaire Européen de la Mer, Université de Bretagne Occidentale Liorzou, Céline; Pole Spectrométrie Océan, Institut Universitaire Européen de la Mer, Université de Bretagne Occidentale Rabineau, Marina; UMR 6538, Institut Universitaire Européen de la Mer, Laboratoire Géosciences Océan
Keywords:	TOC, C/N ratio, Organic matter, pre-analysis treatment method, $\delta^{13}\text{C}_{\text{org}}$
Abstract:	Natural stable isotopes ratios ($\delta^{13}\text{C}_{\text{org}}$ and $\delta^{15}\text{N}$) and associated elemental concentrations (i.e. total organic carbon and total nitrogen contents) preserved in marine sediments are frequently used for the determination of paleoenvironmental processes such as the organic matter origin. Previous studies highlighted bias in the determination of such geochemical proxies due to pre-analysis acid treatment methods. This study is the first systematic comparison of the effect of acid treatment methods on bulk organic matter using a unique sedimentary system, under two contrasting climatic contexts (i.e. glacial vs interglacial). We used the most common method for pre-treatment analysis, which consists of acidification followed by several de-ionised water rinses. We investigated the effect of acid type (i.e. Hydrochloric acid and Acetic acid), but also acid strength (from 0.2 to 10N) on the $\delta^{13}\text{C}_{\text{org}}$, $\delta^{15}\text{N}$, TOC, TN and C/N ratio on three samples from the Gulf of Lion (GoL). Two of them (i.e. S.302 and S.102) were deposited during glacial maxima (i.e. high sedimentation rate, low porosity and high terrestrial inputs) whereas S.157 characterizes interglacial conditions (high porosity, low sedimentation rates, low terrestrial inputs and high foraminifera content). We show that acid type did not significantly affect results. We also find that (i) glacial and interglacial samples do not react similarly to acid pre-treatment, (ii) high acid strength (>1.5N) induce significant bias on $\delta^{13}\text{C}_{\text{org}}$, TOC values and therefore on C/N ratio; (iii) 25% of an isotopically distinct pool of organic carbon was lost between the use of 0.2N and 1.5N affecting $\delta^{13}\text{C}_{\text{org}}$ values by more than 1.5‰; (iv) geochemical evidences indicate that the leachable organic carbon pool is preferentially composed of terrestrial organic matter. These findings call for

1
2
3
4
5
6
7
8
9
10
11
12
13
14
15
16
17
18
19
20
21
22
23
24
25
26
27
28
29
30
31
32
33
34
35
36
37
38
39
40
41
42
43
44
45
46
47
48
49
50
51
52
53
54
55
56
57
58
59
60

	precautions when using C/N ratios and associated $\delta^{13}\text{C}_{\text{org}}$ values for paleoenvironmental and climate reconstructions.

SCHOLARONE™
Manuscripts

For Peer Review

1
2
3
4
5
6
7
8
9
10
11
12
13
14
15
16
17
18
19
20
21
22
23
24
25
26
27
28
29
30
31
32
33
34
35
36
37
38
39
40
41
42
43
44
45
46
47
48
49
50
51
52
53
54
55
56
57
58
59
60

1 **Acid digestion on river influenced shelf sediment**
2 **organic matter: Carbon and Nitrogen contents and isotopic**
3 **values**

4
5 PASQUIER Virgil ^a; SANS JOFRE Pierre ^a; LEBEAU Oanez ^b; LIORZOU Celine ^b;
6 RABINEAU Marina ^a;

7
8 ^a UMR 6538, Institut Universitaire Européen de la Mer, Place Nicolas Copernic,
9 29280 Plouzané, France

10 ^b Pole Spectrométrie Océan, Institut Universitaire Européen de la Mer,
11 Université de Bretagne Occidentale, Place Nicolas Copernic, 29280 Plouzané,
12 France

13 *Corresponding author: virgil.pasquier@univ-brest.fr

14
15 **Keywords** (5): $\delta^{13}\text{C}_{\text{org}}$, TOC, C/N ratio, Organic matter, pre-analysis treatment
16 method

17
18 **ABSTRACT: (288/500 w)**

19 Natural stable isotopes ratios ($\delta^{13}\text{C}_{\text{org}}$ and $\delta^{15}\text{N}$) and associated elemental
20 concentrations (i.e. total organic carbon and total nitrogen contents) preserved in
21 marine sediments are frequently used for the determination of paleoenvironmental
22 processes such as the organic matter origin. Previous studies highlighted bias in the
23 determination of such geochemical proxies due to pre-analysis acid treatment
24 methods. This study is the first systematic comparison of the effect of acid treatment
25 methods on bulk organic matter using a unique sedimentary system, under two
26 contrasting climatic contexts (i.e. glacial vs interglacial). We used the most common
27 method for pre-treatment analysis, which consists of acidification followed by several
28 de-ionised water rinses. We investigated the effect of acid type (i.e. Hydrochloric acid
29 and Acetic acid), but also acid strength (from 0.2 to 10N) on the $\delta^{13}\text{C}_{\text{org}}$, $\delta^{15}\text{N}$, TOC,
30 TN and C/N ratio on three samples from the Gulf of Lion (GoL). Two of them (i.e.
31 S.302 and S.102) were deposited during glacial maxima (i.e. high sedimentation rate,
32 low porosity and high terrestrial inputs) whereas S.157 characterizes interglacial

1
2
3
4
5
6
7
8
9
10
11
12
13
14
15
16
17
18
19
20
21
22
23
24
25
26
27
28
29
30
31
32
33
34
35
36
37
38
39
40
41
42
43
44
45
46
47
48
49
50
51
52
53
54
55
56
57
58
59
60

33 conditions (high porosity, high foraminifera content, low sedimentation rates and low
34 terrestrial inputs). We show that acid type did not significantly affect results. We also
35 find that (i) glacial and interglacial samples do not react similarly to acid pre-
36 treatment, (ii) high acid strength (>1.5N) induce significant bias on $\delta^{13}\text{C}_{\text{org}}$, TOC
37 values and therefore on C/N ratio; (iii) 25% of an isotopically distinct pool of organic
38 carbon was lost between the use of 0.2N and 1.5N affecting $\delta^{13}\text{C}_{\text{org}}$ values by more
39 than 1.5‰; (iv) geochemical evidences indicate that the leachable organic carbon
40 pool is preferentially composed of terrestrial organic matter. These findings call for
41 precautions when using C/N ratios and associated $\delta^{13}\text{C}_{\text{org}}$ values for
42 paleoenvironmental and climate reconstructions.

43 44 **1. Introduction**

45 Sedimentary organic matter (OM) in marine environments is typically composed
46 of a mixture of in-situ marine and land exported particles. Autochthonous grains
47 derive from land erosion, land plant detritus and outcropping older marine deposits
48 which have already been degraded to various degrees. The accurate determination
49 of past total organic carbon content (TOC), total nitrogen content (TN), carbon and
50 nitrogen isotopic composition ($\delta^{13}\text{C}_{\text{org}}$ and $\delta^{15}\text{N}_{\text{tot}}$) of OM naturally preserved in
51 coastal marine sediments have been widely used for past environmental processes
52 interpretation. C/N ratios are commonly used as a tracer for OM sources and
53 alteration during weathering processes (1-5). Combined with $\delta^{13}\text{C}_{\text{org}}$, C/N ratio is also
54 a powerful proxy to discriminate carbon sources and different photosynthetic
55 pathways (e.g. C3- vs C4-photosynthesis (6)). Nitrogen isotopes and content allow
56 determination of trophic levels but can also be used as proxy for primary productivity
57 and redox state of past-environments (7-11).

58 In most coastal sediments, the carbon fraction is commonly divided in two forms: the
59 organic carbon (OC) and inorganic carbon (IC) which is usually enriched in ^{13}C
60 relative to OC because of the isotopic fractionation induced by photosynthesis (12).
61 The accurate determination of OC content and its carbon isotopic composition
62 involves the complete removal of the IC fraction from the bulk sediment. This is
63 performed using acid treatment methods which may also introduce artificial
64 modifications of the natural OC mix preserved in old sediments.

1
2
3
4
5
6
7
8
9
10
11
12
13
14
15
16
17
18
19
20
21
22
23
24
25
26
27
28
29
30
31
32
33
34
35
36
37
38
39
40
41
42
43
44
45
46
47
48
49
50
51
52
53
54
55
56
57
58
59
60

65 There are several studies which have investigated the effects of acid types on
66 specific terrestrial or aquatic products with contradictory induced effects (13-17).
67 Several, but fundamentally different acid pre-treatment methods have been reported,
68 within a range of acid reagents and strengths, type of capsule or chemistry
69 environment (i.e. wet or fumigation chemistry). The results of these studies show that
70 the acidification step can influence elemental and isotopic composition of both C and
71 N and therefore their subsequent interpretations. Brodie and collaborators (13,14)
72 have shown that a non-linear and unpredictable biases on OM characterization can
73 be related to the acid pre-treatment. Loss or gain of C and N appear to vary
74 according to acidification type, characteristic of the depositional environment and IC
75 content (18). Therefore, there is no consensus on the effect of such essential pre-
76 analyses treatments, which is commonly considered as negligible or within the
77 instrumental precision. For $\delta^{13}\text{C}_{\text{org}}$, bias up to 7‰ lowered values have been reported
78 in (13), ruling out the possibility to distinguish between C3 and C4 photosynthetic
79 pathways. Therefore, environmental interpretation of OM data in both modern and
80 paleoenvironments can be highly questionable.

81 This paper presents the first systematic comparison for the most common acid
82 treatment, IC removal using both hydrochloric and acetic acids (HCl and AA), on a
83 wide range of acid strength on quaternary sediments. We examine the effect of
84 increased acid strength on the reliability of TOC, TN, C/N ratio, $\delta^{13}\text{C}_{\text{org}}$ and $\delta^{15}\text{N}$ for
85 three samples from the Gulf of Lion (GoL).

86
87

88 2. Experimental

89 2.1. Samples origin and paleo-climatic context

90 The studied sediment originate from the GoL, Western Mediterranean Sea,
91 which is characterised by a wide continental shelf (70 km), that was sub-aerially
92 exposed during Quaternary glacial times (19,20). Spatial and temporal distribution of
93 sediment in the studied area are mostly governed by sea level changes (Figure 1).
94 The present day spatial composition of OM in the GoL has already been studied in
95 detail (1-3) showing that origin and spatial distribution of OM are strongly related to
96 sediments deposited at river mouths. These pro-deltaic sediments are characterized
97 by low $\delta^{13}\text{C}_{\text{org}}$ values (around -25‰) and high sedimentation rates (i.e. 20 cm.years⁻¹,

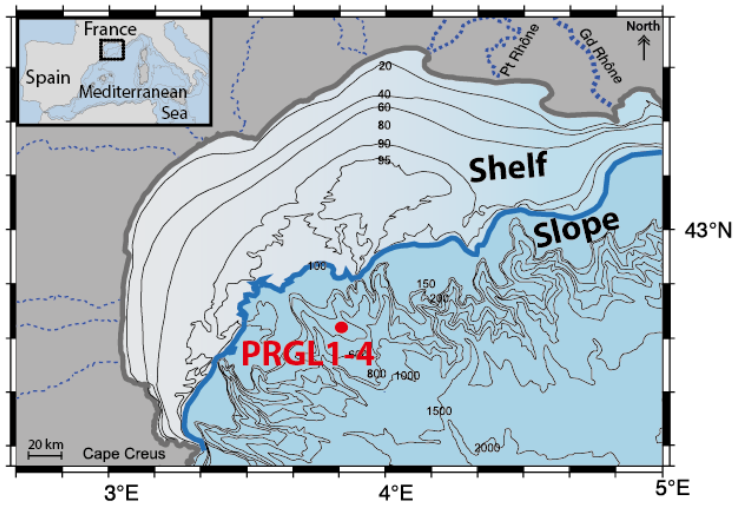


Figure 01: Map of the Gulf of Lion with the position of the PRGL1-4 core (42.690N; 3.838E). The bold grey line highlights the present shoreline position and the contours reflect modern water depths. The bold blue line corresponds to the shoreline position during the last-glacial period (low sea level).

1
2
3 98 (21)), contrasting with open ocean sedimentation (i.e. very low sedimentation rate
4
5 99 bellow 0.3 m.ka⁻¹, (26)) characterized by higher $\delta^{13}\text{C}_{\text{org}}$ values around -21‰ at the
6
7 100 shelf break (originating from primary producers and derived outcomes). According to
8
9 101 the shelf distribution, organic carbon isotopes ($\delta^{13}\text{C}_{\text{org}}$) preserved in sediments can
10
11 102 be interpreted as reflecting the relative proportion of terrestrial *versus* marine OC (i.e.
12
13 103 seaward dilution; Pasquier et al., in prep).

14
15 104 Samples come from PRGL 1-4 borehole (42.690N; 3.838E), a 300m continuous
16
17 105 record drilled on the upper slope (298 meters water depth) of the GoL, on the
18
19 106 interfluvium between the Bourcart and Herault canyons. Borehole PRGL 1-4 was drilled
20
21 107 in the framework of the European Union project PROMESS1
22
23 108 (<http://www.pangaea.de/Projects/PROMESS1/>). Whatever the climatic context (i.e.
24
25 109 glacial or interglacial), GoL sediments are significantly rich in carbonates (> 40%
26
27 110 wt/wt), and mainly composed of silty-clay sediments which are poor in organic
28
29 111 compounds (0.6 % and 0.08 % wt/wt for Total Organic Carbon (TOC) and Total
30
31 112 Nitrogen (TN) respectively, n= 382 analyses; 22, Pasquier et al., in prep).

32
33 113 According to the age model (22) and paleoenvironment reconstructions, the
34
35 114 present study is based on 3 samples originating from two contrasted climatic and
36
37 115 sedimentological settings:

- 38
39 116 - Sample S.157 is a typical interglacial sediment deposited under high sea
40
41 117 level context, during Marine Isotope Stage 7.d (~224 ka). Sediments
42
43 118 deposited under such context are associated with low sedimentation rate
44
45 119 due to the landward migration of coastal rivers (i.e. Rhône and Pyrenean
46
47 120 rivers) and increased foraminiferal abundance, resulting in higher
48
49 121 porosity.
50
51 122 - Samples S.102 and S.304 correspond to low sea-level during the
52
53 123 Penultimate glacial maximum MIS 6.2 (~138 ka) and MIS 12.4 (~468 ka)
54
55 124 respectively. These sediments were deposited in typical deltaic
56
57 125 environment characterized by rapid sedimentation allowing higher
58
59 126 preservation of labile sediment (22).
60

53 128 2.2. Pre-analyses protocol and acid treatment

54
55 129 Once the borehole has been subsampled, sediments were freeze-dried prior to
56
57 130 any treatment. A well-known portion of dried samples (1.5 ± 0.1g) was ground in
58
59 131 agate mortar, and transferred to pre-cleaned 15 ml centrifuge tubes. Prior to
60

1
2
3
4
5
6
7
8
9
10
11
12
13
14
15
16
17
18
19
20
21
22
23
24
25
26
27
28
29
30
31
32
33
34
35
36
37
38
39
40
41
42
43
44
45
46
47
48
49
50
51
52
53
54
55
56
57
58
59
60

132 elemental and isotopic analyses, carbonate (IC) fraction was removed by dissolution,
133 using an excess of hydrochloric acid (HCl) or acetic acid (AA) during 24 hours at
134 room temperature. In detail, homogenized sediments were split in numerous aliquots
135 of 30 +/- 0.5 mg. Seventeen different leaching procedures were employed, using HCl
136 or acetic acid (AA) at different acid strength: 0.2N, 0.5N, 1N, 1.5N, 2N, 2.5N, 3N, 4N,
137 5N, 6N, 7N, 8N, 9N, 10N, 10N (and 2h at 80°C), 5% AA, 10% AA. During digestion,
138 centrifuge tubes were placed in ultrasonic bath during 3h at room temperature to
139 increase the mechanical separation of clay and calcium carbonates. After digestion,
140 residues were washed three times with distilled water, centrifuged and dried at 50°C
141 overnight. Samples were then weighted in tin capsules and kept in a desiccator.

142

2.3. C and N elemental and isotopic analysis

143 All analyses were performed using an elemental analyser (EA, Flash 2000 -
144 Thermo Scientific) coupled to an isotope ratio mass spectrometer (Delta V+, Thermo
145 Scientific) at the Pôle de Spectométrie Océan (PSO, Brest, France). Samples were
146 first loaded into an autosampler then dropped automatically into the oxidation furnace
147 maintained at 1020°C. The flash combustion was performed using an 8 second
148 injection time of dioxygen at a flux of 240ml/min. Oxidation reactor was filled with
149 chromium(III) oxide and silver-plated cobalt oxide to ensure the complete oxidation of
150 flash combustion products. The resulted gas was then transferred, by continuous
151 Helium flow (100 ml/min), to a reduce column filled with activated copper, heated at
152 650°C. This reducing step allow both the removal of excess oxygen and reduction of
153 NO_x to N₂. Water vapour was removed from the gas stream by anhydrous Mg(ClO₄)₂
154 trap, the remaining gas phases were separated by gas chromatography and
155 introduced into mass spectrometer via a Conflo IV system (Thermo Scientific).

156 Carbon and Nitrogen isotopes ratio were obtained against reference standards
157 SED-IVA (IVA reference number: 33802151) and house standards (Acetanilide:
158 CH₃CONHC₆H₅ reference number: 274462, CAP: leaf litter and LIPG: yeast). House
159 standards were calibrated against certified materials, such as IAEA-N1, IAEA-N2,
160 IAEA-CH6 and IAEA-600. $\delta^{13}\text{C}_{\text{org}}$ and $\delta^{15}\text{N}$ are given as the per mil deviation from the
161 PDB standard and atmospheric N₂, respectively. Routine replicate measurements on
162 standards had internal deviations of $\pm 0.15\text{‰}$ and $\pm 0.30\text{‰}$ (2σ), respectively for
163 nitrogen and carbon. TN and TOC percentage were measured using the Thermal
164 Conductivity Detector (TCD) of the Flash EA 2000, ThermoScientific. Routine
165

1
2
3
4
5
6
7
8
9
10
11
12
13
14
15
16
17
18
19
20
21
22
23
24
25
26
27
28
29
30
31
32
33
34
35
36
37
38
39
40
41
42
43
44
45
46
47
48
49
50
51
52
53
54
55
56
57
58
59
60

166 replicate measurements had internal deviations less than 4% and 5%, respectively
167 for TN and TOC.

168
169
170

171 3. Results

172 Results are presented in Figures 2, 3 and 4 and Table 1.

173 3.1. Organic Carbon: content and isotopic results

174 For all samples (i.e. including all the experiments), the TOC ranges between
175 0.56 and 0.84 %wt/wt and isotopic values between -21.7 and -24.4‰. These values
176 are in the classic range of organic poor sediments deposited in coastal marine
177 environments (22) .

178 Inter Glacial sample S157, present an average $\delta^{13}\text{C}_{\text{org}}$ value of $-22.04 \pm 0.13\text{‰}$
179 with a TOC of $0.79 \pm 0.03\%$ wt/wt. No trend nor deviation was observed with the use
180 of different acid attacks.

181 Glacial samples S304 and S102 show averages $\delta^{13}\text{C}_{\text{org}}$ of $-24.62 \pm 0.31\text{‰}$ and -
182 $24.31 \pm 0.33\text{‰}$ respectively and TOC of $0.63 \pm 0.07\%$ and $0.63 \pm 0.04\%$ respectively.
183 An effect of acid strength on TOC values is clearly visible between 0.2 and 1.5N HCl
184 acid attack, where we can observe a decreasing trend from values around 0.8%
185 down to 0.6% (Figure 2a). This loss of 0.2% of TOC is accompanied by an increase
186 of 1.5‰ of $\delta^{13}\text{C}_{\text{org}}$ values (from -25.6‰ to -24.1‰), explaining the slightly higher
187 standard deviation obtained for these two samples (Figure 2b). Above 1.5N HCl acid
188 concentration, neither OC content nor isotopic values present any trends.
189 Interestingly, TOC and isotopic values are not affected by the type of acid used for
190 decarbonation step (i.e. HCl or AA): AA values (both TOC and isotopic values) are
191 similar to HCl attack above 1.5N for these two samples.

192 The interglacial sediment sample S157 shows thus higher TOC and higher
193 $\delta^{13}\text{C}_{\text{org}}$ compared to the two glacial samples S305 and S102 (0.8 versus 0.6% in
194 average, and -22.0‰ vs -24.5‰ in average).

195

196 3.2. Total nitrogen content and isotopic ratio

197 The mean TN values for the three samples with the different decarbonation
198 methods is $0.08 \pm 0.002\%$ wt/wt (Table 1). The TN appears stable and low whatever

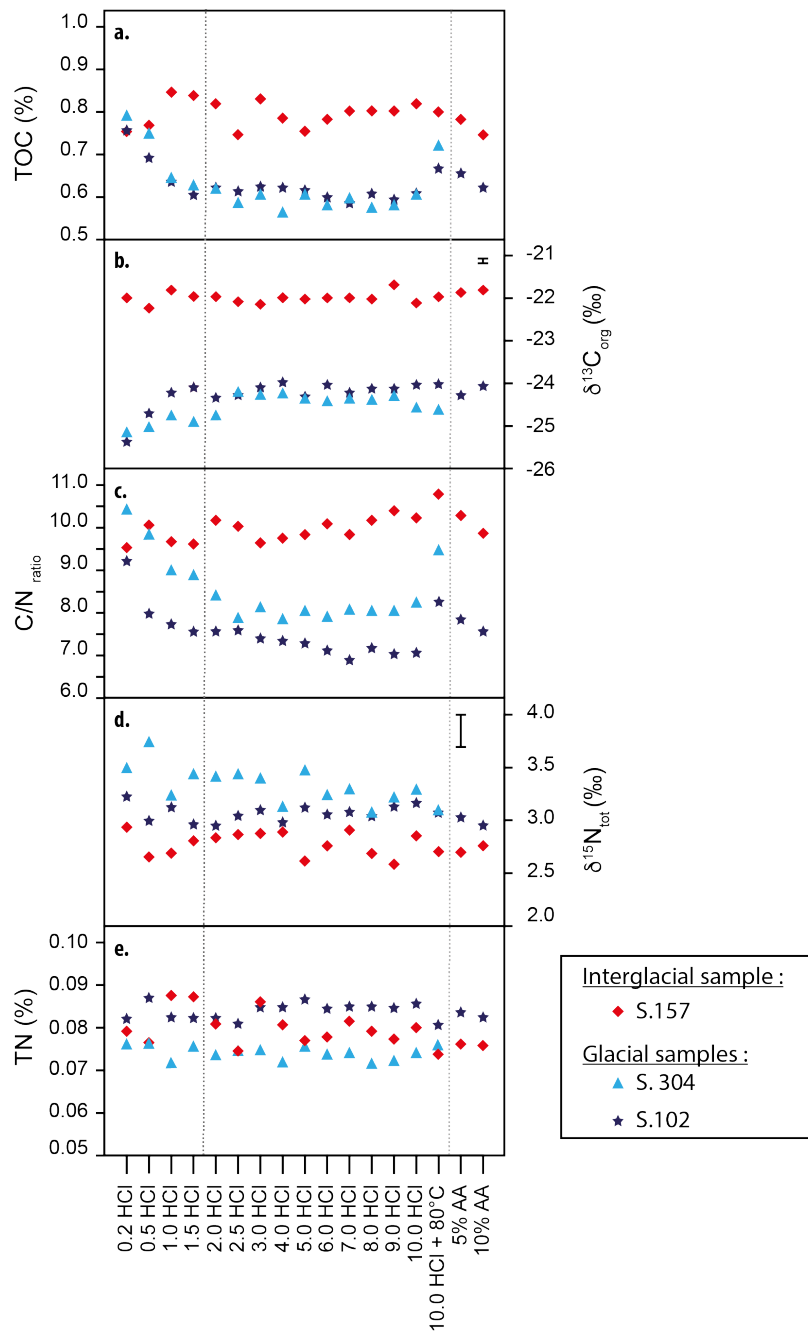


Figure 02

a. shows the percentage of total organic carbon (i.e.% TOC wt/wt); **b.** presents the organic carbon isotopic values preserved in our coastal samples (i.e. $\delta^{13}C_{org}$); **c.** C/N ratio of preserved organic matter in samples; **d.** $\delta^{15}N_{tot}$; **e.** Range of total nitrogen (i.e. %TN wt/wt). Symbol colors indicate various climatic context: red diamonds for interglacial times related to S.157 and light and dark blue symbols show glacial samples, S.304 and S.102, respectively. Data are presented as function of the acid type and strength using during the decarbonation step. Error bars obtained on isotopic measurements represent 1SD measured on certified material whereas for total organic carbon and total nitrogen the error bars are smaller than the dots size.

1
2
3
4
5
6
7
8
9
10
11
12
13
14
15
16
17
18
19
20
21
22
23
24
25
26
27
28
29
30
31
32
33
34
35
36
37
38
39
40
41
42
43
44
45
46
47
48
49
50
51
52
53
54
55
56
57
58
59
60

199 the climatic context. $\delta^{15}\text{N}_{\text{tot}}$ values obtained during this study show homogeneous
200 values with a global average of $3.0 \pm 0.1\%$, with no significant influence of the acid
201 strength on the isotopic ratio (Figure 2.d and 2.e). Therefore, TN and isotopic ratio
202 does not appear to be sensitive to the type of acid used.

203

204 **3.3. C/N ratios**

205 C/N ratio obtained on interglacial samples show an average of 10.0 ± 0.3
206 which is typical of marine particulate OM (i.e. broad term used for phytoplankton and
207 zooplankton OM; (23) and references therein).

208 C/N ratio obtained on glacial samples (i.e. S304 and S102) show an average
209 value of 8.0 ± 0.8 . The high variability observed, up to 30% in the two glacial samples
210 is due a decrease of the C/N ratios with increasing acid strength (from 10.5 to 7.5 for
211 S304 and from 9.5 to 7 for S102, Figure 2.c). For strength over 1.5N HCl, C/N ratios
212 do not show significant variations.

213

214 **4. Discussion**

215 Decarbonation is a necessary step to remove all carbonate (IC) phases from
216 samples before measuring content and isotopic composition of the OC pool in
217 sediments. In agreement with the data obtained in this study, no clear effect of the
218 acid strength is observed on TN and isotopic composition, (Figure 2.d and 2.e).
219 Therefore, no further consideration on these results will be addressed in this part of
220 the discussion. Below we discuss first the Glacial-Interglacial discrepancies of the
221 sediment which should have led to different acid attack response, then the presence
222 of a leachable pool of Organic Carbon.

223

224 **4.1. Glacial vs Interglacial samples geochemical response**

225 A clear distinction between glacial (i.e. S.102 and S.304) and interglacial (i.e.
226 S.157) samples is observed on Figure 2. Indeed, the carbon isotopic composition
227 and TOC of the interglacial sample do not seem to be affected by the pre-treatment
228 acidification; whereas glacial samples show a clear response to the acid strength
229 between 0.2 and 1.5N. This different geochemical response may reflect different
230 properties of the sediment including different sources and reactivities of the
231 sedimentary OM towards acid attack. Differences in the physical sediment properties
232 between glacial and interglacial sediments have already been highlighted in previous

1
2
3
4
5
6
7
8
9
10
11
12
13
14
15
16
17
18
19
20
21
22
23
24
25
26
27
28
29
30
31
32
33
34
35
36
37
38
39
40
41
42
43
44
45
46
47
48
49
50
51
52
53
54
55
56
57
58
59
60

233 studies of PRGL_1-4 (22). In the GoL shelf, glacial interglacial variations are
234 characterized by substantial glacio-eustatic movements inducing migration of the
235 coast line, and associated rivers (i.e. Rhône and Pyrenean rivers).

236 Lower sea level during glacial times induced a seaward migration of the coast
237 that brought the borehole location closer to the source of terrestrial materials (i.e.
238 rivers mouths). This proximal environment is characterized by greater inputs of fresh
239 terrestrial OM and deposition of low porosity silty-clay material. A higher proportion of
240 fresh terrestrial OM is buried into the sediment with limited degradation by oxic
241 respiration (22, 26).

242 In contrast, interglacial times are associated with higher temperature, higher
243 sea level and a disconnection of coastal river from our site location. This is supported
244 by an increase of $\delta^{13}\text{C}_{\text{org}}$, indicative of higher marine inputs. Coastal rivers
245 disconnection and high sea level is typically accompanied by lower sedimentation
246 rates together with an increase of the porosity due to high foraminifera abundance.
247 We propose that these changes increase oxygen diffusion depth into the sediment
248 which favoured aerobic respiration of the OM. Consequently, a lower proportion of
249 reactive OM remains within the sediment.

250 We thus propose that glacial samples S102 and S304 may have preserved a
251 higher proportion of OM including an acid leachable pool. This preservation may be
252 linked to both physical sediment properties and sedimentation rates, that influenced
253 early diagenesis processes. We highlight here that different samples with distinct
254 pools of OM react differently to the acid attack.

255 4.2. A weak HCl acid attack resistant pool of Carbon

256 For glacial samples S304 and S.102, the negative covariation observed
257 between TOC and $\delta^{13}\text{C}_{\text{org}}$ call for a loss of carbon with a different isotopic value. The
258 effect of the exposure to concentrated or diluted HCl on the TOC is clearly visible on
259 Figure 2.a and b, where TOC content shifted from 0.8 to 0.6%. Strong acids (above
260 1,5N HCl) allow a removal of at least 25% of OM compared to our lowest acid attack
261 (0.2N). It appears that the loss is stronger as the acid strength increase.

262 One hypothesis would be that the carbonate phases were not completely
263 dissolved or that another resistant carbonate phase was present as proposed by (13)
264 or (24). Indeed, it has been shown that some magnesium or iron carbonates, like
265 dolomite or siderite, can resist to a 25°C acid attack for hours (25). Interestingly, this
266

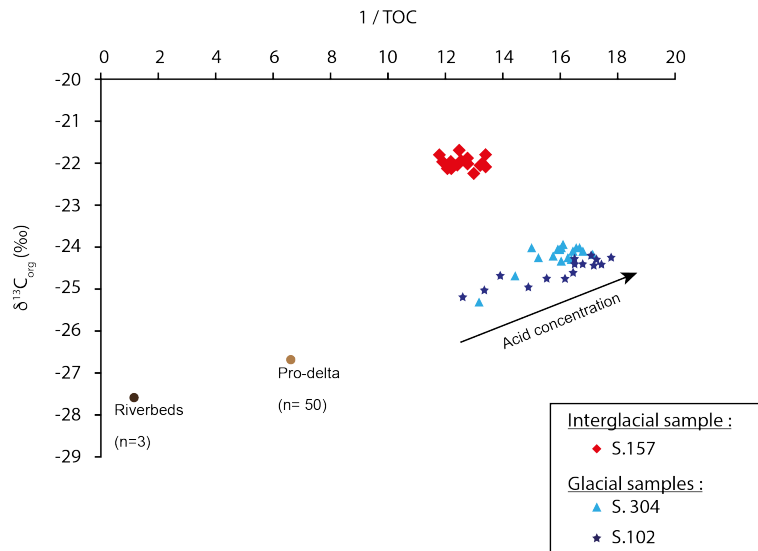


Figure 03 Linear mixing model showing a parental source between terrestrial derived riverbed / prodelta and our glacial samples (blues symbols). This clearly shows the influence of acid strength on preferential leaching of terrestrial organic carbon during decarbonation step. Red diamonds correspond to interglacial samples S.157; light and dark blue symbols show data obtained on glacial samples S.304 and S.102, respectively. Error bars are smaller than the dots size. Pro-delta values from Tesi et al., 2007; River bed data from Kim et al. 2006.

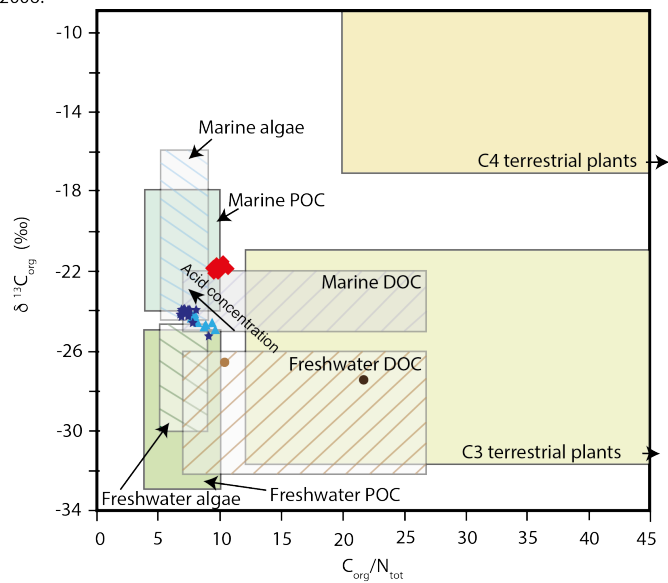


Figure 04 Bi-plot of $\delta^{13}C_{org}$ and C/N ratio currently used to determine the OM provenance. Error bars are smaller than the dots size. It clearly suggests a removal of terrestrial organic carbon when using concentrated acid during the decarbonation step. Typical $\delta^{13}C_{org}$ and C/N ranges for organic inputs to coastal environments are compiled from Lamb et al., 2006 and references therein. Pro-delta values from Tesi et al., 2007 (light brown dot); River bed data from Kim et al. 2006 (dark brown dot). Figure modified after Lamb et al., 2006

1
2
3
4
5
6
7
8
9
10
11
12
13
14
15
16
17
18
19
20
21
22
23
24
25
26
27
28
29
30
31
32
33
34
35
36
37
38
39
40
41
42
43
44
45
46
47
48
49
50
51
52
53
54
55
56
57
58
59
60

267 decrease in OM content is concomitant with increase in $\delta^{13}\text{C}_{\text{org}}$ values, (Figure 2.a
268 and 2.b). This suggest that the 25% pool of OM removed by strong acid attack is thus
269 enriched in ^{12}C with a $\delta^{13}\text{C}$ value lower than -25‰ (Figure 2.b). Such pool with low
270 $\delta^{13}\text{C}$ is incompatible with a remaining carbonate phase (26,27).

271 Moreover, the loss of isotopically light organic carbon seems proportional to the
272 strength of HCl between 0.2 to 1.5N. Above 1.5N, this leaching of isotopically light
273 OC seems complete and both isotopic and content values are stable.

274

275 **4.3. An isotopically light terrestrial organic matter leachable pool at** 276 **HCl strength above 1.5N**

277 In the GoL, glacial sediments are mostly composed of homogenous clastic
278 material with OM spots mainly exported from fresh and labile land OM, such as wood
279 and leaf fragments, which range from -32‰ to -21‰ (28). Therefore, the loss of
280 terrestrial labile fine organic materials during increased HCl strength could bias the
281 natural sedimentary mixing and explain the observed dataset.

282 In the GoL watershed and prodeltaic sedimentary accumulation, the TOC
283 content and the $\delta^{13}\text{C}_{\text{org}}$ of bulk OM from river beds have revealed values around -27
284 $\pm 1\text{‰}$ (1,2). To test our assumption of preferential leaching of terrestrial fresh OM, we
285 used a linear mixing extrapolation to confirm the removal of terrestrial OM (Figure 3).
286 Effectively in a $\delta^{13}\text{C}_{\text{org}}$ vs $1/\text{TOC}$ graphic (Figure 3) we can see that the obtained data
287 are aligned between (1) a terrestrial OC from the catchment area and (2) a stable mix
288 between marine primary production (and subsequent derived-products) and detrital
289 OM.

290 First, this trend confirms the main terrestrial origin of our samples.
291 Furthermore, a close examination of this figure allows us to observe the influence of
292 acid strength on the proportion of terrestrial organic carbon preserved in our glacial
293 samples. These results indicate that a small but isotopically important proportion of
294 terrestrial organic carbon is preferentially lost during decarbonation. In land-derived
295 sediments OM is composed of a vast pool of organic molecule that can be resistant
296 to weak acid conditions. For example in soils where pH can decrease strongly, humic
297 acid has been shown to be a significant component of the OC pool, which moreover
298 present low $\delta^{13}\text{C}_{\text{org}}$ values (1,29,30). In such context, we suggest a preferential
299 leaching of organic acid compounds during the decarbonation step. Nevertheless,

1
2
3
4
5
6
7
8
9
10
11
12
13
14
15
16
17
18
19
20
21
22
23
24
25
26
27
28
29
30
31
32
33
34
35
36
37
38
39
40
41
42
43
44
45
46
47
48
49
50
51
52
53
54
55
56
57
58
59
60

300 a careful investigation of the acid strength on the organic acid fraction is necessary to
301 confirm this hypothesis.

302

303 **4.4. Impact of acid attack on C/N ratios and interpretation.**

304 C/N ratios are indicators for OM source, when combined with $\delta^{13}\text{C}_{\text{org}}$ in a cross
305 plot, they are commonly used to distinguish terrestrial (C3 vs C4 land plants) and
306 aquatic (marine vs fresh water) sources (23,31). Figure 4 shows a classical bi-plot
307 used for paleo environment reconstruction. It clearly indicates procedural bias on
308 data that is equal in magnitude to the difference between terrestrial and marine
309 environment. We note that the bias in C/N ratio is concomitant with isotopic offset
310 reported in this study, highlighting the clear leaching of labile terrestrial OM
311 preserved in coastal marine sediments.

312

313

314 **5. Summary and conclusions**

315 We evaluated the acid strength effect on recent geological sediment samples
316 from a coastal environment by comparing different acid treatment methods (i.e. HCl
317 and AA) during the decarbonation step prior to TOC, TN, $\delta^{15}\text{N}$ and $\delta^{13}\text{C}_{\text{org}}$
318 measurements. We summarize the main findings in the following points:

319 1/ We identified that the TOC, TN, $\delta^{15}\text{N}$ and $\delta^{13}\text{C}_{\text{org}}$ values do not show
320 significant variability when using strong (>1.5N) HCl or AA treatment.

321 2/ Weak HCl acid attacks (<1.5N) in the Glacial samples shows systematically
322 higher TOC together with lower $\delta^{13}\text{C}_{\text{org}}$. Strong HCl acid attack and Acid acetic attack
323 remove a distinct pool of isotopically light OM which correspond to a 25% loss of the
324 TOC.

325 3/ This effect depends on the lithology and is only seen in samples containing
326 high terrestrial source organic matter. It does not affect the nitrogen content neither
327 isotopic nitrogen composition.

328 4/ Variations observed in TOC, $\delta^{13}\text{C}_{\text{org}}$ and C/N ratio after the different acid
329 pre-treatment protocols vary sufficiently to affect any interpretations of organic
330 carbon sources (Figure 4).

331

1
2
3
4
5
6
7
8
9
10
11
12
13
14
15
16
17
18
19
20
21
22
23
24
25
26
27
28
29
30
31
32
33
34
35
36
37
38
39
40
41
42
43
44
45
46
47
48
49
50
51
52
53
54
55
56
57
58
59
60

332 These results call for more precautions when using classic acid attack for
333 sediments. It is highly probable that this pool, which is leached by acetic acid and
334 hydrochloric acid up to 1.5N, is naturally removed during late diagenesis in old
335 sediments. This mean that for old rocks the main problem would be to remove
336 entirely the IC fraction and thus strong acid attack is recommended. However, for
337 modern sediments it is different. The presence of such pool could represent a major
338 problem for paleo environment interpretation. The weak strength acid attack
339 commonly used for modern sediments (23 and references within) may induce a large
340 bias. Variations in $\delta^{13}\text{C}_{\text{org}}$ values analysed on organic matter which experienced such
341 acid attack could represent different proportion of this weak acid leachable organic
342 pool over the total OM reservoir. It is thus essential to test different acid attack on the
343 main lithologies before any systematic down core study.

344
345

346 **Acknowledgements**

347 This work was supported by the "Laboratoire d'Excellence" LabexMER (ANR-
348 10-LABX-19) and co-funded by a grant from the French government under the
349 program "Investissements d'Avenir", and by a grant from the Regional Council of
350 Brittany. Additional founding came from Actions Marges Program (Mediterranean
351 Sea). The drilling operation was conducted within the European Commission Project
352 PROMESS (contract EVR1-CT-2002-40024). The European Promess Scientific
353 committee and colleagues at Ifremer are also thanked for previous contributions of
354 data acquisition, processing, interpretations and permitting to re-sample the
355 borehole.

356
357

358 **References:**

- 359 1. Tesi T, Miserocchi S, Goñi MA, Langone L. Source, transport and fate of
360 terrestrial organic carbon on the western Mediterranean Sea, Gulf of Lions,
361 France. *Marine Chemistry*. 2007;105:101–17.
- 362 2. Kim JH, Schouten S, Buscail R. Origin and distribution of terrestrial organic
363 matter in the NW Mediterranean (Gulf of Lions): Exploring the newly developed
364 BIT index. *Geochemistry, Geophysics, Geosystems*. 2006;7(11):1–20.
- 365 3. Cathalot C, Rabouille C, Pastor L, Deflandre B. Temporal variability of carbon
366 recycling in coastal sediments influenced by rivers: assessing the impact of

- 1
2
3 367 flood inputs in the Rhône River prodelta. *Biogeosciences*. 2010;7:1187–205.
4
5 368 4. Tesi T, Langone L, Goñi MA, Wheatcroft RA, Miserocchi S, Bertotti L. Early
6 369 diagenesis of recently deposited organic matter: A 9-yr time-series study of a
7 370 flood deposit. *Geochimica et Cosmochimica Acta*. 2012;83(C):19–36.
8
9 371 5. Aller RC. *Sedimentary Diagenesis, Depositional Environments, and Benthic*
10 372 *Fluxes*. 8 ed. Vol. 11, *The Oceans and Marine Geochemistry*. Elsevier Ltd;
11 373 2014. 42 p.
12
13 374 6. Meyers PA. Preservation of elemental and isotopic source identification of
14 375 sedimentary organic matter. *Chemical Geology*. 1994;114:289-.
15
16 376 7. Ader M, Sansjofre P, Halverson GP, Busigny V, Trindade RIF, Kunzmann M,
17 377 Nogueira A. Ocean redox structure across the Late Neoproterozoic
18 378 Oxygenation Event: A nitrogen isotope perspective. *Earth and Planetary*
19 379 *Science Letters*. Elsevier B.V; 2014 Jun 15;396(C):1–13.
20
21 380 8. Voss M, Dippner JW, Montoya JP. Nitrogen isotope patterns in the oxygen-
22 381 deficient waters of the Eastern Tropical North Pacific Ocean. *Deep Sea*
23 382 *Research Part I*. 2001;48:1905–21.
24
25 383 9. Möbius J, Lahajnar N, Emeis KC. Diagenetic control of nitrogen isotope ratios
26 384 in Holocene sapropels and recent sediments from the Eastern Mediterranean
27 385 Sea. *Biogeosciences*. 2010;7(11):3901–14.
28
29 386 10. Robinson RS, Kienast M. A review of nitrogen isotopic alteration in marine
30 387 sediments. *Paleoceanography*. 2012;27:1–13.
31
32 388 11. Ader M, Thomazo C, Sansjofre P, Busigny V. Interpretation of the nitrogen
33 389 isotopic composition of Precambrian sedimentary rocks: Assumptions and
34 390 perspectives. *Chemical Geology*. 2016;429:93–110.
35
36 391 12. Hayes JM. Factors controlling ^{13}C contents of sedimentary organic
37 392 compounds: principles and evidence. *Marine Geology*. 1993;113:111–25.
38
39 393 13. Brodie CR, Leng MJ, Casford J, Kendrick CP. Evidence for bias in C and N
40 394 concentrations and $\delta^{13}\text{C}$ composition of terrestrial and aquatic organic
41 395 materials due to pre-analysis acid preparation methods. *Chemical Geology*.
42 396 2011;282:67–83.
43
44 397 14. Brodie CR, Casford J, Lloyd JM, Leng MJ. Evidence for bias in C/N, $\delta^{13}\text{C}$
45 398 and $\delta^{15}\text{N}$ values of bulk organic matter, and on environmental interpretation,
46 399 from a lake sedimentary sequence by pre-analysis acid methods. *Quaternary*
47 400 *Science Reviews*. 2011;30.
48
49 401 15. Lorrain A, Savoye N, Chauvaud L, Paulet YM. Decarbonation and preservation
50 402 method for the analysis of organic C and N contents and stable isotope ratios
51 403 of low-carbonated suspended particulate material. *Analytica Chimica Acta*.
52 404 2003;491:125–33.
53
54 405 16. Schubert CJ, Nielsen B. Effects of decarbonation treatments on $\delta^{13}\text{C}$ values
55
56
57
58
59
60

- 1
2
3 406 in marine sediments. *Marine Chemistry*. 2000;72:55–9.
4
5 407 17. Ryba SA, Burgess RM. Effects of sample preparation on the measurement of
6 408 organic carbon, hydrogen, nitrogen, sulfur, and oxygen concentrations in
7 409 marine sediments. *Chemosphere*. 2002;48:139–47.
8
9 410 18. Froelich PN. Analysis of organic carbon in marine sediments. *Limnol*
10 411 *Oceanogr*. 1980;25(3):564–72.
11
12 412 19. Rabineau M, Berné S, Aslanian D, Olivet JL. Sedimentary sequences in the
13 413 Gulf of Lion: a record of 100,000 years climatic cycles. *Marine Petroleum*
14 414 *Geology*. 2005;22:775–804.
15
16 415 20. Jouet G, Berné S, Rabineau M, Bassetti MA, Bernier P. Shoreface migrations
17 416 at the shelf edge and sea-level changes around the Last Glacial Maximum
18 417 (Gulf of Lions, NW Mediterranean). *Marine Geology*. 2006 Sep 5;234:21–42.
19
20 418 21. Radakovitch O, Charmasson S, Arnaud M. 210 Pb and caesium accumulation
21 419 in the Rhône delta sediments. *Estuarine, Coastal and Shelf Sciences*.
22 420 1999;48:77–92.
23
24 421 22. Pasquier V, Sansjofre P, Rabineau M. Pyrite sulfur isotopes reveal glacial–
25 422 interglacial environmental changes. *PNAS*. 2017;117(23):5941–5945.
26
27 423 23. Lamb AL, Wilson GP, Leng MJ. A review of coastal palaeoclimate and relative
28 424 sea-level reconstructions using $\delta^{13}\text{C}$ and C/N ratios in organic material. *Earth*
29 425 *Science Reviews*. 2006 Mar;75:29–57.
30
31 426 24. Kolasinski J, Rogers K, Frouin P. Effects of acidification on carbon and
32 427 nitrogen stable isotopes of benthic macrofauna from a tropical coral reef. *Rapid*
33 428 *Communications in Mass Spectrometry*. 2008;22:2955–2960.
34
35 429 25. Lebeau O, Busigny V, Chaduteau C, Ader M. Organic matter removal for the
36 430 analysis of carbon and oxygen isotope compositions of siderite. *Chemical*
37 431 *Geology*. 2014;372:54–61.
38
39 432 26. Sierra FJ, Andersen N, Bassetti MA, Berné S. Phase relationship between sea
40 433 level and abrupt climate change. *Quaternary Science Reviews* [Internet].
41 434 2009;28:2867–2881.
42
43 435 27. Cortina A, Sierra FJ, Gonzalez-Mora B, Asioli A. Impact of climate and sea
44 436 level changes on the ventilation of intermediate water and benthic foraminifer
45 437 assemblages in the Gulf of Lions, off South France, during MIS 6 and 7.
46 438 *Palaeogeography, Palaeoclimatology, Palaeoecology*. 2011;309:215–28.
47
48 439 28. Khan NS, Vane CH, Horton BP. Stable carbon isotope and C/N geochemistry
49 440 of coastal wetland sediments as a sea-level indicator. *Handbook of Sea-Level*
50 441 *Research*. 2015;1:295–311.
51
52 442 29. Hood E, Williams MW, McKnight DM. Sources of dissolved organic matter
53 443 (DOM) in a Rocky Mountain stream using chemical fractionation and stable
54 444 isotopes. *Biogeochemistry*. 2005;74:231–55.
55
56
57
58
59
60

2.2.3. Elementar analyser. For the measure of the average isotopic composition of solid forms, around 30 mg and 400 μg of the decarbonated powder were loaded into tin capsules few hour prior the analyses for respectively C, N isotopes and S isotopes analyses. For sulfur isotopes measurement, few mg of vanadium penta-oxide (V_2O_5) were added to the sample into the tin capsule to ensure total combustion.

The capsules were loaded into an auto-sampler carousel(s) (31 positions: 20 samples + 1 blank capsule + 10 standards) for automatic analysis as shown in **Figure 26**. During analyses, samples were dropped into the oxidation furnace maintained at high temperature, and were combusted in presence of excess oxygen, during several seconds to assure complete combustion, see **Table 4** for precise analytical configuration.

EA configuration settings		
	C / N	S
O2 flow	240 mL/min - 8s	25 ml/min - 6 s
Oxydation oven	1020 °C	1005 °C
Reduction oven	650 °C	990 °C
GC column	67 °C	95 °C
He carrier	100 mL/min	100 mL/min

Table 4 EA configuration used during EA-IRMS sequences.

During organic carbon and nitrogen measurements, which is illustrated in **Figure 26**, flash combustion products (NO_x , CO_2 , H_2O) are carried into an oxidation reactor which is filled with chromium(III) and silver-plated cobalt oxide to ensure the complete oxidation of combustion gases. The produced gases are carried out using a Helium continuous flow to a reduce column filled with activated copper oxide. This column is heated at 600 °C, it removes excess of oxygen and reduce the residual NO_x to N_2 .

For sulfur isotopes measurements, flash combustion products are flown under the same He condition through an oxidation oven filled with copper oxide and electrolytic copper to complete the oxidation of SO_2 . Because flash combustion produces already reduced gases (i.e. SO_2) no reduction step is needed, then the reduction oven is filled with pure quartz which allows (i) $\delta^{18}\text{O}$ equilibration, and (ii) to reduce the analysis time.

In both case, prior to the mass spectrometer introduction, the remaining water vapor of the gas produced was removed by anhydrous $\text{Mg}(\text{ClO}_4)_2$ prior the separation step using a gas chromatography. Subsequent gases are introduced into mass spectrometer via a Conflo IV system (Thermo Scientific).

Total sulfur, nitrogen and organic carbon percentage (respectively TS, TN and TOC) were measured using the Thermal Conductivity Detector (TCD) of the Flash EA 2000, ThermoScientific. This detector looks at changes in the thermal conductivity of two gas flows, a pure carrier gas flow used as reference and carrier gas plus flash combustion products. This detector contains a filament that is heated electrically, when the sample pass over it, the power required to keep the filament at the same temperature is proportional to the ion concentration. Because TCD does not destroy the sample during the detection process (i.e. measuring the thermal conductivity difference), this type of detector is very useful for the determination of elemental compounds prior to mass spectrometry analyses.

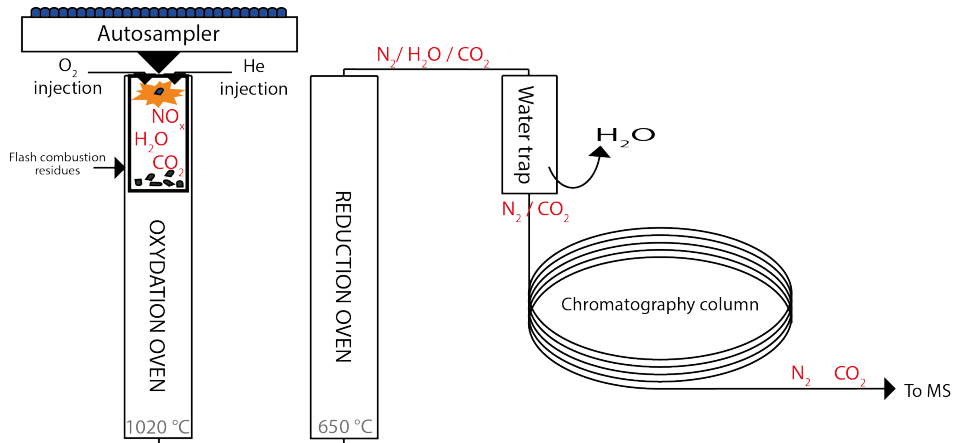


Figure 26

EA montage of organic carbon and nitrogen isotopes schematic.

2.3. Mass spectrometry

Mass spectrometry (MS) was developed in the early part of the 20th century (see Hoffman and Stoobant 2002) as a technique to separate chemical species using their mass-to-charge (m/z) ratios, and subsequently measure the concentration of ionic species in gas phase. In this section, we will focus on specialized Isotope Ratio Mass Spectrometry (IRMS) and Thermal Ionization Mass Spectrometry (TIMS) which have been mostly used during this PhD.

2.3.1. IRMS. IRMS measures the relative abundance of isotopes in a given sample, relative to a standard. In Earth Sciences, IRMS is mainly used for the analyses of stable isotope ratios, which typically vary as a result of mass-dependent isotopic fractionation (i.e. in opposition of decay-products of natural radioactive elements). Because samples are analyzed in gas-phase, we use Nier type mass spectrometers (see Figure 27).

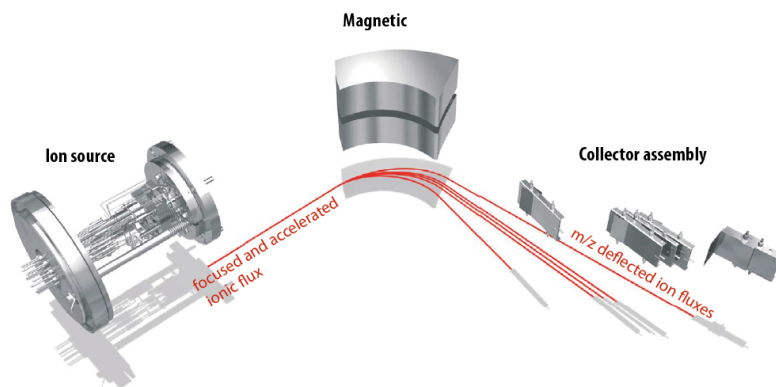


Figure 27

Nier type Mass Spectrometer schematic, modified after the DeltaV plus Operating Manual.

IRMS are composed of a few key parts:

- (i) A specific device which is used to extract and purify sample gas prior to analyses. During my PhD, I dominantly used an elemental analyzer (see detailed description in the previous paragraph II.2.2.3),
- (ii) An inlet to introduce the sample into the MS, with minimal loss of vacuum. Multiple inlet systems can be used to introduce a sample into the MS, in order to accommodate a wide variety of samples. However, most samples are injected as gas-phase,
- (iii) An electron ionization chamber, which is involved during the introduction of a gaseous sample into an ionization chamber, perpendicular to an accelerated electron beam (with electrons typically at 70 eV) formed by thermionic emission (**Figure 28**). As the accelerated electrons collide with the gas molecules, they knock out electrons residing in the outer electron shells, forming positive molecular ions,

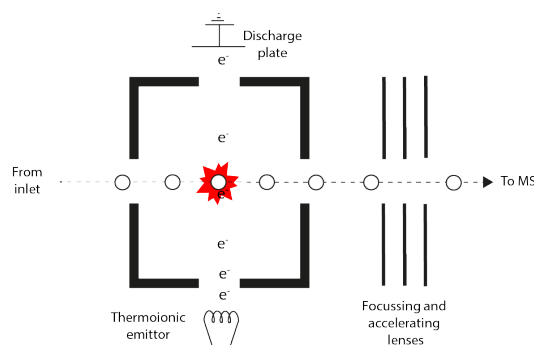


Figure 28

Diagram of an EI source (adapted from Hoffman and Stoobant 2002).

- (iv) A mass analyzer, which focuses and accelerates electron ionization products (i.e. positive molecular ion) to separate them based on m/z ratios (**Figure 27**). Positive ions are accelerated to approximately 3 keV and focused with electronic lenses to produce a stable and intense ionic flux at the magnetic sector entrance,
- (v) A deflection step using a magnetic sector dispersion, in which ions follow a circular trajectory with radius induced by a magnetic field (i.e. which vary in intensities for each isotopic systems). By constraining the radius, ion entering the magnetic field can be separated based on their m/z ratios. The relation between m/z and B is given in equation 7.

$$m/z = (r^2 \cdot B^2) / 2U \quad (7)$$

where r is the trajectory radius followed by ions into the magnetic field; B is the intensity of magnetic field; and U is a variable acceleration voltage.

- (vi) A detector using several Faraday cups used to detect ions. When a deflected ion hits the Faraday cup, its charge is neutralized by an electron jumping from the metal to the ion. Then, the ion flow is detected as an electric current which can be amplified and recorded. The more ions arriving, the greater the current.

IRMS determines relative abundance of $^{14}\text{N}^{14}\text{N}$ and $^{14}\text{N}^{15}\text{N}$ simultaneous on m/z 28 and m/z 29 and the isotope ratio of nitrogen gas relative to reference standards IAEA-SED-IVA and in-house standards. Carbon isotopes ratio was obtained with the same procedure measuring m/z 44, 45 and 46 referring to $^{12}\text{C}^{16}\text{O}^{16}\text{O}$, $^{12}\text{C}^{16}\text{O}^{18}\text{O}$ and $^{13}\text{C}^{16}\text{O}^{16}\text{O}$ respectively. During sulfur measurements, IRMS determine the relative abundance of $^{32}\text{S}^{16}\text{O}^{16}\text{O}$, $^{32}\text{S}^{16}\text{O}^{18}\text{O}$, $^{34}\text{S}^{16}\text{O}^{16}\text{O}$ and $^{34}\text{S}^{16}\text{O}^{18}\text{O}$ on mass m/z 64, 66 and 68.

In both case (i.e. coupled nitrogen/carbon and sulfur) the non-linearity response of the mass spectrometer, resulting from different signal intensities related to different isotopic measurements, was corrected. A second correction was applied to isotopically calibrate our measurements against international standards. The differences between measured and certified isotopic values are given in the **Table 5**:

EA-IRMS standards							
	n	Certified values			Measured values		
		$\delta^{13}\text{C}_{\text{org}}$	$\delta^{15}\text{N}$	$\delta^{34}\text{S}$	$\delta^{13}\text{C}_{\text{org}}$	$\delta^{15}\text{N}$	$\delta^{34}\text{S}$
		VPDB	VairN2		VPDB	VairN2	
SED-IVA	26	-26	4.5		-26.6	4.4	
Acetenalide	190	-27.1	0.97		-27.6	0.96	
CAP	17	-30.03	2.89		-29.9	3	
LIPG	53	-24.43	-0.16		-24.4	-0.03	
IAEA-S1	7			-0.3			-0.5
IAEA-S2	12			21.17			21.9
IAEA-S3	12			-32.55			-32.16

Table 5 Table of standards used for the isotopic calibration certified and house standard, and mean isotopic composition obtained during this PhD.

The effect of sample size and reproducibility were studied using several standards. In case of coupled nitrogen/carbon, each analytical sequence of 31 positions (i.e. corresponding to one auto-sampler carousel) shown the following order:

- 1 blank measurement
- 4 standards (Acetanilide / SED-IVA / CAP / LIPG)
- 6 samples
- 1 standard (Acetanilide)
- 6 samples
- 1 standard (Acetanilide)
- 6 samples
- 1 standard (Acetanilide)
- 2 samples replicates
- 3 standards (SED-IVA / CAP / LIPG)

In case of multiple carousels, the beginning, and ending, standard sequence was reduced to gain analytical times. The **Table 6** show the calculated reproducibility calculated for each sequence of coupled nitrogen/carbon measurements.

I used the same approach during sulfur isotopic measurement in St Louis. This time, the analytical sequences followed the next order:

- 1 blank measurement
- 3 house standards (BS / BaS / SZn)
- 3 certified standards (IAEA-S1 / IAEA-S2 / IAEA-S3)
- 17 samples
- 3 house standards (BS / BaS / SZn)
- 14 samples
- 4 replicates
- 2 international satandards (IAEA-S2 / IAEA-S3)
- 3 house standards (BS / BaS / SZn)

Reproducibility measured on sulfur standards are reported in **Table 7**. Rapidly, reproducibility range between 0.25 and 0.05 ‰, with an average of 0.17 ‰ 2σ .

	VP00-EA			VP01-EA			VP02-EA			VP03-EA		
	n	$\delta^{13}\text{C}_{\text{org}}$ 2 σ (‰)	$\delta^{15}\text{N}$ 2 σ (‰)	n	$\delta^{13}\text{C}_{\text{org}}$ 2 σ (‰)	$\delta^{15}\text{N}$ 2 σ (‰)	n	$\delta^{13}\text{C}_{\text{org}}$ 2 σ (‰)	$\delta^{15}\text{N}$ 2 σ (‰)	n	$\delta^{13}\text{C}_{\text{org}}$ 2 σ (‰)	$\delta^{15}\text{N}$ 2 σ (‰)
SED-IVA										4	0.05	0.04
Acetanilide	26	0.03	0.04	35	0.08	0.08	30	0.21	0.2	29	0.02	0.04
CAP												
LIPG	13	0.12	0.08	6	0.01	0.06	5	0.08	0.02	5	0.08	0.03

	VP04-EA			VP05-EA			VP06-EA			VP07-EA		
	n	$\delta^{13}\text{C}_{\text{org}}$ 2 σ (‰)	$\delta^{15}\text{N}$ 2 σ (‰)	n	$\delta^{13}\text{C}_{\text{org}}$ 2 σ (‰)	$\delta^{15}\text{N}$ 2 σ (‰)	n	$\delta^{13}\text{C}_{\text{org}}$ 2 σ (‰)	$\delta^{15}\text{N}$ 2 σ (‰)	n	$\delta^{13}\text{C}_{\text{org}}$ 2 σ (‰)	$\delta^{15}\text{N}$ 2 σ (‰)
SED-IVA	9	0.05	0.08	2	0.07	0.01	7	0.07	0.39	6	0.05	0.05
Acetanilide	48	0.08	0.06	16	0.05	0.07	37	0.07	0.08	28	0.09	0.06
CAP				3	0.08	0.08	8	0.07	0.07	6	0.07	0.09
LIPG	9	0.07	0.06	3	0.03	0.01	8	0.06	0.05	6	0.07	0.09

Table 6 Table of reproducibility on standards during each nitrogen/carbon analytical sequence obtain during his PhD.

	VP01-S		VP02-S		VP03-S	
	n	$\delta^{43}\text{S}_{\text{pyr}}$ 2 σ (‰)	n	$\delta^{43}\text{S}_{\text{pyr}}$ 2 σ (‰)	n	$\delta^{43}\text{S}_{\text{pyr}}$ 2 σ (‰)
BS	8	0.2	5	0.17	9	0.19
BaS	8	0.17	5	0.17	9	0.17
SZn	8	0.16	5	0.18	9	0.23
IAEA-S1	3	0.05	2	0.22	3	0.12
IAEA-S2	5	0.09	4	0.25	5	0.17
IAEA-S3	5	0.11	4	0.25	5	0.18

Table 7 Calculated reproducibility on Washington University house standards (BS / BaS / SZn) and certified standard (IAEA-S1 / IAEA-S2 / IAEA-S3).

During this PhD, a total of 1455 analyses were done with total independence on EA-IRMS in the Pole Spectrometry Ocean in Brest (PSO) using a coupled Delta V+ with a Flash EA2000 for carbon and nitrogen measurements (n= 1266); and with a Costech ECS 4010 at St Louis for sulfur acquisition (n= 189), Missouri, USA. I also learn how to do the maintenance of the EA (i.e. preparation of reactors and absorption filters), and participated to the Delta V+ ionic source maintenance (i.e. replacement of the thermo-ionic filament).

2.3.2. TIMS. Prior to TIMS measurement, all samples need to be purified to remove all elements not analyzed, and the Ca-matrix. This step is necessary to limit interference and make the ionization easier. This 'purification' step is describe below.

Samples preparation for Sr isotope measurements Sr separation was performed using 3 mL of the mother solution resulting of bulk carbonates digestion describe in **Figure 21**, see **Figure 21**. Nevertheless, when using this approach, user must be sure that the daughter solution contains at least 50 ng of Sr to ensure stable ionization after chemistry. The entire Sr extraction protocol was schematized on the **Figure 29**, and **Table 8**.

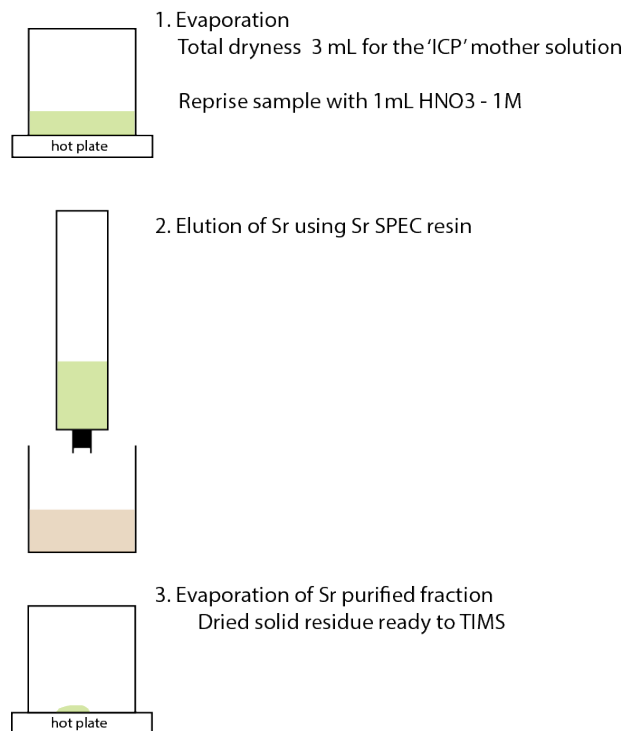


Figure 29

Sr purification protocol from Révillon et al. 2011.

I used an Eichrom[®] Sr SPEC resin for isolation of Sr from AA leached bulk samples. This resin is commonly used in geological, geochemical applications. HNO₃ acid ranging between 1 and 8 M are used for sample loading and matrix removal. The use of Sr SPEC resin allows a very good purity of Sr fraction, efficient Rb/Sr separation (Rb is one of the higher interfering element during the ionization step) and a good Sr recovery.

Elution profiles for Sr chemistry - Eichrom Sr resin		
Step	Acid	Quantity
Conditionning	HNO3 - 1M	3 mL
Sample loading	HNO3 - 1M	1mL
Sr sequestration	HNO3 - 1M	1mL
Rb elution (bin)	HNO3 - 8M	3mL
Sr elution (keep)	H2O - hot	2mL

Table 8 Sr elution step using Eichrom[®] Sr SPEC resin.

TRITON mass spectrometer Thermal Ionization Mass Spectrometer was used to measured Sr isotope composition using a Thermo Fisher TRITON, at the PSO, Brest. As for IRMS, TIMS are composed of three primary components:

- (i) Ion source (**Figure 30**), the region in which ions are produced, accelerated, and focused,
- (ii) Analyzer, the region in which the beam is separated based on mass/charge ratios,
- (iii) Collector, a region in which the ion beams are measured either sequentially (single collector) or simultaneously (multi-collector),
- (iv) The source part is very different from the EA-IRMS part. Indeed, this type of source uses high temperatures to volatilize and to ionize elements. This covers much of the periodic table, except the noble gases and light elements such as Hydrogen, Carbon, Nitrogen, Oxygen and Sulfur which are best analyzed as gases, using IRMS.

In our case the element of interest (i.e. Strontium) is deposited in a liquid form (after Sr separation from the carbonated matrix) as a dissolved compound in HNO₃ inorganic acid onto a filament made of refractory metal (i.e. Tungsten). Samples are loaded on the filament with an ionization enhancer (1 μ L of TaO₅). To fix the dissolved Sr on the filament a brief electric current flow through it until filament oxidation (for 4.6 A during approx. 15 s for Sr under neutral air atmosphere), this causes the volatilization of the element, and a small fraction is ionized. After loading, the filament is placed in the source of the MS with other filaments to be run in a MS sequence, see **Figure 30**.

In the MS the filament is raised to a high positive voltage under high vacuum environment (1.10^{-7} to $3.5.10^{-8}$ bar), this accelerates the positive ions away from the filament and determines their final energy. Resulting positive ions are directly accelerated using an electric field (10 kV). The ionic ray is focused using several electronical lenses before entering in the 'mass analyser', then in the 'detector system'. Both parts are permanently kept in ultra-high vacuum (3.19^{-9} bar). As for IRMS, the detector system is composed of Faraday cups which are used to detect ion crashes.

Each analysis is run during 10 blocks of 10 measurements (i.e. 100 measures per samples) during which a fractionation correction is automatically applied. This result of the fact that during the early emission lighter isotopes are preferentially ejected, then we bring back the measured ratio to the natural isotopic ratio measured in Earth. Then, the measured Sr ratio is corrected again a ratio of $^{87}\text{Sr}/^{86}\text{Sr} = 8.375202$.

Each TIMS sequence starts and ends with a standard measurement, for Sr isotopic ratio we use NBS987. This allows us to check any instrumental deviation or analytical error.

The average values obtained during NBS987 measurements is $^{87}\text{Sr}/^{86}\text{Sr} = 0.710240 \pm 0.000015$ (n= 29). This average value is slightly below the certified NBS987 values (0.710250) this explains why we daily corrected measured $^{87}\text{Sr}/^{86}\text{Sr}$ ratio, using a simple normalization to refer to the certified value.

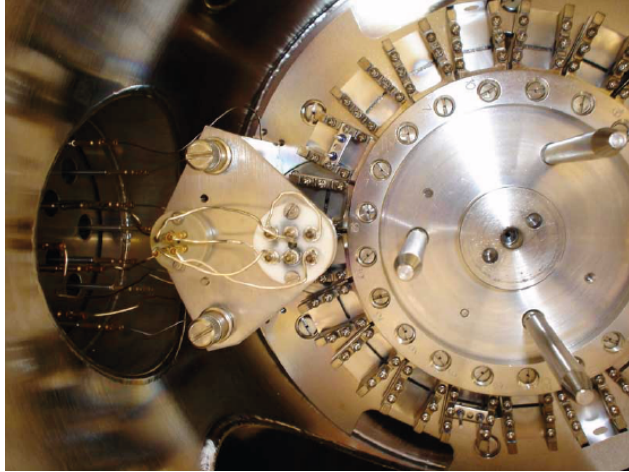


Figure 30
TMS TRITON ion source and samples magazine.

LITERATURE CITED

- Auffret, G., Zaragosi, S., Dennielou, B., Cortijo, E., 2002. Terrigenous fluxes at the Celtic margin during the last glacial cycle. *Marine Geology* 188 (1-2), 79–108.
- Barker, S., Knorr, G., Edwards, R. L., Parrenin, F., 2011. 800,000 years of abrupt climate variability. *Science* 334, 347–351.
- Beaudouin, C., Jouet, G., Suc, J.-P., Berné, S., Escarguel, G., Apr. 2007. Vegetation dynamics in southern France during the last 30kyBP in the light of marine palynology. *Quaternary Science Reviews* 26 (7-8), 1037–1054.
- Blum, J. D., Erel, Y., Aug. 1997. Rb-Sr isotope systematics of a granitic soil chronosequence: The importance of biotite weathering. *Geochimica et Cosmochimica Acta* 61 (15), 3193–3204.
- Burton, E. D., Sullivan, L. A., Bush, R. T., Johnston, S. G., 2008. A simple and inexpensive chromium-reducible sulfur method for acid-sulfate soils. *Applied Geochemistry* 23, 2759–2766.
- Cacho, I., Pelejero, C., Grimalt, J. O., Calafat, A., Canals, M., Jul. 1999. C37 alkenone measurements of sea surface temperature in the Gulf of Lions (NW Mediterranean). *Organic Geochemistry* 30 (7), 557–566.
- Canfield, D. E., Raiswell, R., Westrich, J. T., Reaves, C. M., 1986. The use of chromium reduction in the analysis of reduced inorganic sulfur in sediments and shales. *Chemical Geology* 54, 149–155.
- Cortina, A., Sierro, F. J., Flores, J. A., 2015. The response of SST to insolation and ice sheet variability from MIS 3 to MIS 11 in the northwestern Mediterranean Sea (Gulf of Lions). *Geophysical Research Letters* 42, 10366–10374.
- Eggins, S., De Deckker, P., Marshall, J., Jul. 2003. Mg/Ca variation in planktonic foraminifera tests: implications for reconstructing palaeo-seawater temperature and habitat migration. *Earth and Planetary Science Letters* 212 (3-4), 291–306.
- Eggins, S. M., Kinsley, L. P. J., Shelley, J. M. G., May 1998. Deposition and element fractionation processes during atmospheric pressure laser sampling for analysis by ICP-MS. *Applied Surface Science* 127-129, 278–286.
- Eglinton, G., Hamilton, R. J., Jun. 1967. Leaf Epicuticular Waxes. *Science* 156 (3780), 1322–1335.
- Frigola, J., Canals, M., Cacho, I., Moreno, A., Sierro, F. J., Flores, J. A., Berné, S., Jouet, G., Dennielou, B., Herrera, G., Pasqual, C., Grimalt, J. O., Galavazi, M., Schneider, R., 2012. A 500 kyr record of global sea-level oscillations in the Gulf of Lion, Mediterranean Sea: new insights into MIS 3 sea-level variability. *Climate of the Past* 8 (3), 1067–1077.
- Goldstein, S. L., O’Nions, R. K., Jul. 1981. Nd and Sr isotopic relationships in pelagic clays and ferromanganese deposits. *Nature* 292 (5821), 324–327.
- Grousset, F. E., Biscaye, P. E., Zindler, A., Prospero, J., Chester, R., Mar. 1988. Neodymium isotopes as tracers in marine sediments and aerosols: North Atlantic. *Earth and Planetary Science Letters* 87 (4), 367–378.
- Hodell, D., Crowhurst, S., Skinner, L., 2013. Response of Iberian Margin sediments to orbital and suborbital forcing over the past 420 ka. *Paleoceanography* 28 (1), 185–199.
- Hoffman, E., Stoobant, V., Feb. 2002. *Mass Spectrometry—Principles and Applications*. Wiley, Chichester, 2001, 2nd edition, 407 pp, ISBN 0-471-48565-9.
- Jeong, G. Y., Cheong, C.-S., Kim, J., Sep. 2006. Rb-Sr and K-Ar systems of biotite in surface environments regulated by weathering processes with implications for isotopic dating and hydrological cycles of Sr isotopes. *Geochimica et Cosmochimica Acta* 70 (18), 4734–4749.
- Margari, V., Skinner, L. C., Hodell, D. A., Martrat, B., 2014. Land-ocean changes on orbital and millennial time scales and the penultimate glaciation. *Geology* 42 (3), 183–186.
- Martinson, D. G., Pisias, N. G., Hays, J. D., Imbrie, J., Moore, T. C., Shackleton, N. J., Jan. 1987. Age Dating and the Orbital Theory of the Ice Ages: Development of a High-Resolution 0 to 300,000-Year Chronostratigraphy. *Quaternary Research* 27 (01), 1–29.
- McNichol, A. P., Jull, A. J. T., Burr, G. S., Jul. 2016. Converting AMS Data to Radiocarbon Values: Considerations and Conventions. *Radiocarbon* 43 (2A), 313–320.
- Pasquier, V., Sansjofre, P., Rabineau, M., Houghton, J., Fike, D. A., 2017. Pyrite sulfur isotopes reveal glacial–interglacial environmental changes. *Proceedings of the National Academy of Sciences of the United States of America* 114 (23), 5941–5945.
- Railsback, L. B., Gibbard, P. L., Head, M. J., 2015. An optimized scheme of lettered marine isotope substages for the last 1.0 million years, and the climatostratigraphic nature of isotope stages and substages. *Quaternary Science Reviews* 111, 94–106.

- Rasmussen, S. O., Andersen, K. K., 2006. A new Greenland ice core chronology for the last glacial termination. *Journal of Geological Research* 111, 1–16.
- Reimer, P. J., Bard, E., Bayliss, A., Beck, J. W., Blackwell, P. G., 2013. IntCal13 and Marine13 radiocarbon age calibration curves 0–50,000 years cal BP. *Radiocarbon* 55 (4), 1869–1887.
- Réveillon, S., Jouet, G., Bayon, G., 2011. The provenance of sediments in the Gulf of Lions, western Mediterranean Sea. *Geochemistry, Geophysics, Geosystems* 12 (8), 1–20.
- Rongemaille, E., Bayon, G., Pierre, C., Bollinger, C., Chu, N. C., Fouquet, Y., Riboulot, V., Voisset, M., Jul. 2011. *Chemical Geology*. *Chemical Geology* 286 (3-4), 196–206.
- Siani, G., Paterne, M., Michel, E., Sulpizio, R., Arnold, M., Haddad, G., Nov. 2001. Mediterranean Sea Surface Radiocarbon Reservoir Age Changes Since the Last Glacial Maximum. *Science* 294 (5548), 1917–1920.
- Sierro, F. J., Andersen, N., Bassetti, M. A., Berné, S., 2009. Phase relationship between sea level and abrupt climate change. *Quaternary Science Reviews* 28, 2867–2881.
- Svensson, A., Andersen, K. K., Bigler, M., 2008. A 60 000 year Greenland stratigraphic ice core chronology. *Climate of the Past* 4, 47–57.
URL <https://hal-insu.archives-ouvertes.fr/docs/00/33/07/68/PDF/cp-4-47-2008.pdf>
- Toucanne, S., Minto'o, C., Fontanier, C., 2015. Tracking rainfall in the northern Mediterranean borderlands during sapropel deposition. *Quaternary Science Reviews* 129, 178–195.
- Villanueva, J., Pelejero, C., Grimalt, J. O., Jan. 1997. Clean-up procedures for the unbiased estimation of C37 alkenone sea surface temperatures and terrigenous n-alkane inputs in paleoceanography. *Journal of Chromatography A* 757 (1-2), 145–151.
- White, W. M., Dupré, B., Vidal, P., Sep. 1985. Isotope and trace element geochemistry of sediments from the Barbados Ridge-Demerara Plain region, Atlantic Ocean. *Geochimica et Cosmochimica Acta* 49 (9), 1875–1886.

Increase runoff in North Mediterranean borderland during periodic deposition of anoxic events (sapropels): The emerging role of the North Atlantic climate.

Augmentation des débits fluviaux le long de la bordure Nord Méditerranée pendant les dépôts anoxiques (sapropèles): Le rôle émergeant du climat Nord Atlantique.

Abstract

Le chapitre III se focalise sur l'un des exemples principaux d'interaction entre climat et sédimentation : les niveaux sapropéliques Méditerranéens. Après avoir donné les principales caractéristiques climatiques et océanographiques, nous expliquerons ce que sont les sapropèles.

Depuis de nombreuses années, la corrélation entre les changements d'insolation, la mousson Africaine et les dépôts sapropéliques a été documentée. Cependant, durant la dernière décennie, de nombreuses études attestent de la présence de fortes pluies sur la bordure Nord du bassin Méditerranéen. En utilisant les variations de compositions isotopique en carbone ($\delta^{13}\text{C}$) et azote ($\delta^{15}\text{N}$) de la matière organique préservées dans les sédiments du Golfe du Lion, nous avons mis en évidence de fortes périodes de décharges fluviales. Et proposons que ces dernières résultent de l'intensification du passage des perturbations Nord Atlantique en Méditerranée lors des périodes de NAO négatives.

Cette étroite relation entre le climat Atlantique et Méditerranéen apporte de nouvelles contraintes spatiales, et hydrologiques sur les conditions qui ont amenées au dépôt des niveaux sapropéliques.

Contents

1	Modern Mediterranean state	92
1.1	Climate	92
1.2	Oceanic circulation	94
2	What are 'Sapropels'	94
2.1	Appearance and duration	96
2.2	Sapropel formation: Anoxia and/or Productivity.....	98
2.3	The emergence of a North Borderland freshwater contribution to sapropel formation	100
2.4	Mediterranean climate response to North Atlantic climate variability	102
3	New evidences of enhanced rainfall activity in the Gulf of Lion.....	104
4	Implication for sapropel history	118

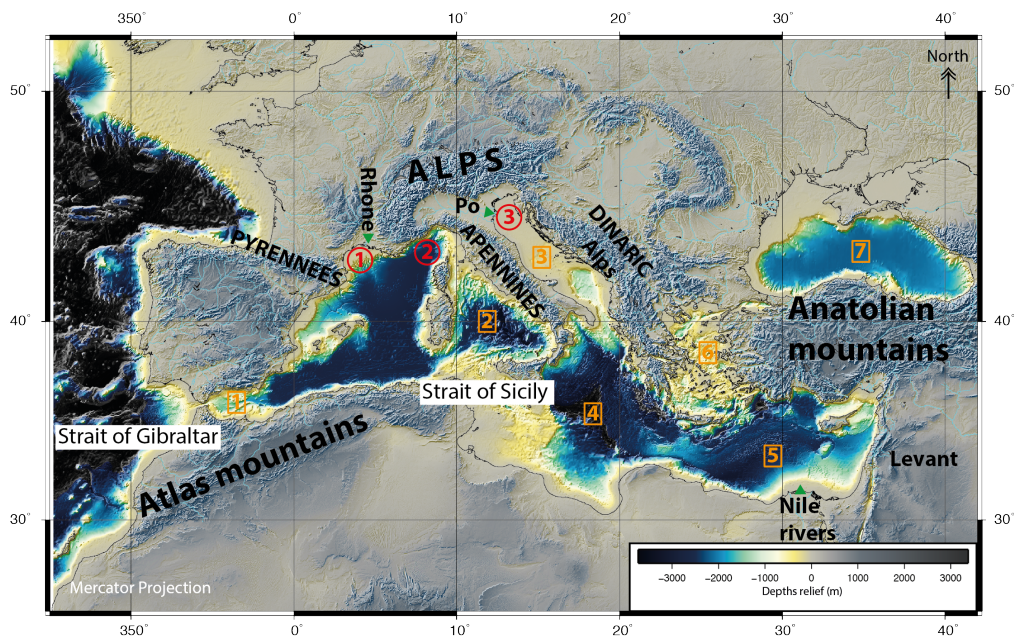
List of Figures

31	Topographic map of the Mediterranean Sea showing the general location between the African and the Eurasian continent. Bathymetrical depth coming from Gebco highlight the sea-water connection between the Mediterranean and the Atlantic basins via the Strait of Gibraltar and the two Mediterranean sub-basins. Modified after Leroux (2012).	92
32	Key characteristics of the Mediterranean hydrological features. (A) Winter sea surface temperature and schematic surface circulation pattern (data from Levitus et al. 2013 and Pinardi et al. 2015). (B) Annual sea surface salinity and schematic circulation of Levantine Intermediate Water (data from: JI et al. 2013 and Pinardi et al. 2015). Modified after Rohling et al. 2015.	95
33	Vertical distribution of Mediterranean Sea water masses. Schematic showing the eastward inflow of Atlantic water into the Western Mediterranean basin via the Strait of Gibraltar and the subsequent generation of Levantine Intermediate Water (LIW) in the Eastern part of the Mediterranean Sea. LIW flows eastward toward the entire basin and return to the global oceanic circulation at the Strait of Gibraltar. Each Mediterranean basin have its own deep-water cell, we note that the East cell is closed, whereas the Western one flow out of the Mediterranean Sea. From: https://www.grida.no/resources/5885	96
34	(A) Sapropels (dark coloured interval) recovering during the ODP leg 160 at site 967 (Erastosthenes seamount, Eastern Mediterranean Sea). Core pictures show well marked black intervals defined as sapropels (hypoxic to anoxic conditions) which are interbed by beige sediments (oxygenated conditions). Note that bioturbation is evident in most sapropels. From IODP leg 160 initial Results. (B) Sapropels and/or Organic Rich Layers recovering during the ODP leg 161 at 975 site (South Balearic margin, Western Mediterranean Sea). From IODP leg 161 initial Results. Core pictures show darker intervals with bioturbations.	97
35	$\delta^{18}\text{O}$ of modern precipitation close to North Italy from GNIP-IAEA database. Upper graph shows the monthly mean vs temperature for 411 months. Lower case highlights the 'amount' relationship between monthly $\delta^{18}\text{O}_p$ and monthly mean precipitation. The dashes lines correspond to 95% confidence level from the regressive slope.	101
36	Correlation between the NAO index and winter rainfall with location of sea level pressure over North Atlantic and main direction of westerlies flows during negative- and positive- NAO (grey circle and black arrows). NAO-rainfall belt is located using a color ramp associated with the state of the NAO. Blue to purple colours indicate negative NAO spatial repartition of rainbelt, which are mainly located over the north Mediterranean borderland. Potential movements of SLP centers toward a positive- NAO is schematically represented with yellow and red arrows. A southward shift of Icelandic low/northward shift of Azores high (i.e. positive NAO) induce to a strong angle modulation of the NAO rain belt leading to decrease precipitation over North Mediterranean Borderland. Adapted from Wassenburg et al. 2013.	103

1. Modern Mediterranean state

1.1. Climate

The Mediterranean Sea is located at a geographical transition between the European and the African continents. It lies between 30° and 46°N, and 5°W to 38°E. The entire coastline is very irregular and characterized by a complex topography (Figure III.31) which created artificial gulfs, sea, straits and channels. The topographic reliefs, land masses and bathymetry anomalies induce the division of the whole Sea into 2 main basins: (i) The Western basin is located between the Gulf of Gibraltar and the Strait of Sicily; and (ii) the Eastern basin from Sicily to the Syrian coast.



Geographic element in the map:

Gulfs (denoted with red labellings and circles)

- ① Gulf of Lion
- ② Gulf of Genoa
- ③ Gulf of Venice

Seas and basins (orange labellings and boxes)

- ① Alboran sea
- ② Tyrrhenian sea
- ③ Adriatic sea
- ④ Ionian sea
- ⑤ Levantine basin
- ⑥ Aegean sea
- ⑦ Black sea

Figure 31

Topographic map of the Mediterranean Sea showing the general location between the African and the Eurasian continent. Bathymetrical depth coming from Gebco highlight the sea-water connection between the Mediterranean and the Atlantic basins via the Strait of Gibraltar and the two Mediterranean sub-basins. Modified after Leroux (2012).

Climatologically, the Mediterranean Sea is located on the transition between the temperate westerlies flowing over the entire Europe and the African subtropical high pressures (Lolis et al. 2002). The Mediterranean basin is characterized by mild and wet winters and warm and dry summers. These climatic characteristics define the typical 'Mediterranean climate', and a large variety of climates arising from the complex land-ocean interactions

(Trigo et al. 2002). In summer, a northward displacement of this transition causes droughts over most of the Mediterranean area, especially in the East / South-East sector. During winters, the southward migration of the transition exposes the North borderland to the temperate westerlies, with associated North Atlantic depressions (Trigo et al. 2002; Lolis et al. 2002). Western Mediterranean basin weather is influenced by Atlantic depressions, which occasionally enter into the Eastern Mediterranean area, causing characteristic winter precipitations. The Mediterranean Seas show a high thermal capacity water masses, which reacted with the overlying air masses in various and complex way due to the topography interactions. Therefore, the Mediterranean basin affects the atmospheric circulation, generating the main area of cyclogenesis and modifying the depressions' trajectories (Trigo et al. 2000, 2002).

After the Gulf of Genoa and the Ligurian Sea, i.e. Western basin, other regions are known to strongly generate depressions which move eastward into the Eastern basin. Along their way, such depressions also cause winter precipitation but contrary to Atlantic depressions their dominant source-moisture comes from the Mediterranean Sea itself. Such Mediterranean origin can be traced using oxygen and hydrogen stable isotopes due to a specific evaporation process into low-humidity air masses (i.e. specific Mediterranean mixing line see paragraph IV.3 for further explanations; Matthews et al. 2000; Piccini et al. 2008). Geological archives, i.e. Levant speleothems, show that such precipitations controlled the East Mediterranean rainfall availability over glacial interglacial cycles (Bar-Matthews et al. 2003; Rohling et al. 2013; McGarry et al. 2004).

Polar air masses are channeled over Europe toward the Mediterranean Sea through valleys that cross the mountain belts of the Northern borderland. Especially during winter, strong cold and dry air flows affect the Gulf of Lion (i.e. Mistral and Tramontane), the Adriatic Sea (i.e. Bora) and the Aegean Sea (i.e. Vardar), where they induce a cooling of sea surface temperature and an enhancement of the evaporation. During winter, Atlantic westerlies flow into Western and Eastern Mediterranean Seas due to favorable atmospheric circulation, i.e. extremely high Low pressure over the Eastern Mediterranean and Northward position of the Azores High or Westward extension of the Siberian High. The most important controlling factor regarding the westerlies is the atmospheric configuration over the North Atlantic (i.e. position and extension of atmospheric centers). Europe's cold climate and fresh water fluxes over the North Mediterranean borderland are associated with extremes positive sea-level pressures between the Icelandic-Low and Azores-High, which define the North Atlantic Oscillation (NAO, Lionello et al. 2006; Tsimplis and Josey 2001; Mariotti and Arkin 2007). Nevertheless, other atmospheric modes have been used to explain the Mediterranean climate where the NAO show little impact (Josey et al. 2011; Martin-Vide and Lopez-Bustins 2006; Lopez-Bustins et al. 2008).

The main mode of climatic variability in the Mediterranean is the so-called Mediterranean Oscillation (MO) which is defined by a west-east pressure see-saw happening at the sea surface and at 500 hPa during winter and springs (Lolis et al. 2002). Several studies have highlighted a statistical correlation between the MO and the NAO, where low NAO induce high rainfall availability over Western Mediterranean (Lolis et al. 2002; Maheras et al., 2002), while the relationship with the NAO is less clear and debated on the Eastern Mediterranean climate (Ziv et al. 2006; Dünkeloh and Jacobeit 2003; Lamy et al. 2006).

The overall Mediterranean excess of evaporation over freshwater inputs is an admitted characteristic of the Mediterranean basin. North areas are characterized by huge freshwater inputs from coastal rivers, therefore they show relatively low excess of evaporation (i.e. which is define as: $X = \text{Evaporation} - \text{Precipitation} - \text{Runoff}$), whereas the southern regions of the Eastern basin show high X values therefore a strong west-east salinity gradient is observed within the overall Mediterranean basin (from 35 to 41 PSU see **Figure 32**, Bethoux

and Gentili 1999; Fichaut et al. 2003; Béranger et al. 2004). This sea surface salinity (SSS) gradient is mainly caused by an excess of evaporation toward the East, therefore a rise of sea surface temperature (SST) is also observed (Levitus et al. 2013; Pinardi et al. 2015).

1.2. Oceanic circulation

The Mediterranean Sea oceanic circulation have been accessed through a huge series of observation programs and modelling studies in the last decades (POEM, PRIMO, WMCE, EU/MAST/MTP part I and II, see Millot 1999 and reference therein for a throughout review). The main features of the basin-scale circulation are three major thermohaline cells. But it is first necessary to mention the prominent role of the Strait of Gibraltar which allows the eastward inflow of Atlantic Water in surface layer, and the outflowing return of Levantine Intermediate Water (LIW) and sea-water masses below (**Figure III.32**; Hernández-Molina and Stow 2014; Rohling et al. 2014). The two other convective cells are located in the Eastern and Western Mediterranean basins. Those two thermohaline cells are driven by local processes allowing the formation of dense water masses, which dive on the slope and spread in the deepest layers prior to return into the Atlantic basins. Eastern Mediterranean Deep Water (EMDW) is formed in Adriatic and Aegean Seas, whereas the Western Mediterranean Deep Water (WMDW) is created in the north-west sector, notably in the Gulf of Lion. They resulted from long term sea-air interactions allowing intense sea surface cooling (i.e. induced by northward winds) and evaporation over small areas. However, we note that the two deep water cells are separated, therefore the Eastern cells is a closed cell.

During winters, intense evaporation (induced by strong wind) in the Easternmost part of the Mediterranean Sea, i.e. the Levantine basin, leads to low SST and high salinities, which favor the formation of the Levantine Intermediate Water (LIW). LIW flows westward from its source of origin and mixes with WMDW prior to exiting the Western Mediterranean basin through Gibraltar. A schematic of the vertical sea water masses distribution is show in the **Figure III.33**, where hydrological characteristics are given (Zavatorielli and Mellor 1995).

The sub-surface Mediterranean outflowing through the Gibraltar Strait is characterized by a temperature around 13 °C and salinity of 38.4 psu, while the surface inflow has a temperature of 15 - 16 °C and 36.2 salinity (**Figure III.33**). This clearly highlight the fact that the Mediterranean basin acts as an evaporating and cooling basin (Garrett 1996), resulting in dense waters flowing out. These two layers structure creates an hydraulic control of the Atlantic inflow into Mediterranean Sea, but also controls the outflow of WMDW due to the process of Bernoulli aspiration or suction (Kinder and Parrilla 1987; Stommel et al. 1973). Such effect was quantified by several authors (Kinder and Parrilla 1987; Bryden and Kinder 1991; Garrett 1996; Béranger et al. 2005) as a flux of 0.7 to 1.0 Sv and a mean velocity of approximately 1 m.s⁻¹. We note that small changes of those two components can have strong consequences on the Mediterranean deep-water circulation, especially into the Western basin.

2. What are 'Sapropels'

Over the geological times, organic-carbon rich sediments were deposited and/or preserved over the world and within a wide range of climatic and environmental conditions. Organic rich deposits are quite common within marine sedimentary sequences. One of the most representative ones is the black shales deposited during Carboniferous times, and the Plio-Pleistocene Sapropels (S). Due to their exceptional preservation and spatial extent sapropels are extensively studying, even if some extents still remain unsolved and are prone

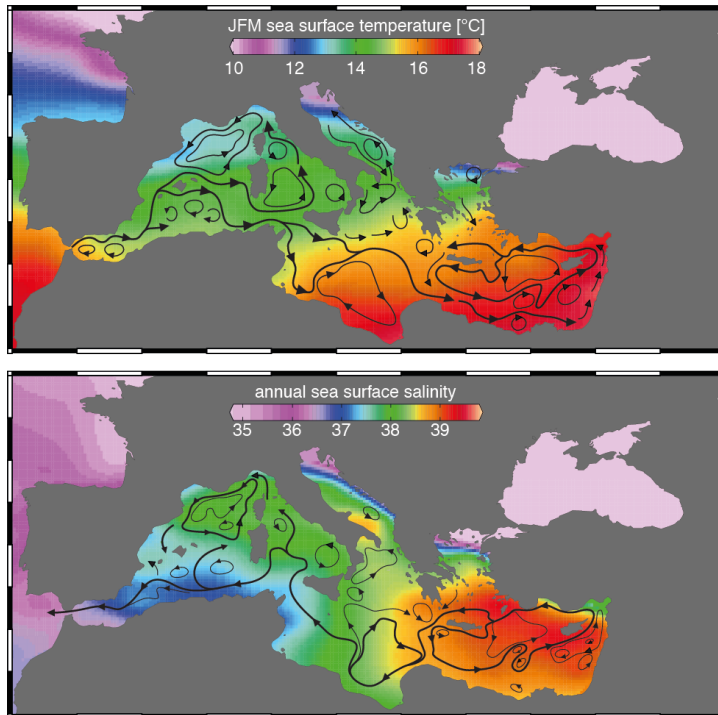


Figure 32

Key characteristics of the Mediterranean hydrological features. **(A)** Winter sea surface temperature and schematic surface circulation pattern (data from Levitus et al. 2013 and Pinardi et al. 2015). **(B)** Annual sea surface salinity and schematic circulation of Levantine Intermediate Water (data from: Ji et al. 2013 and Pinardi et al. 2015). Modified after Rohling et al. 2015.

to passionate debates in the scientific community.

The word sapropel was introduced in the literature by Potonié (1904) to describe dark sediments containing decomposing organisms deposited under stagnant water. The word itself comes from German translation of the words 'Fulniss' and 'Schlamm' into ancient Greek (sapro and pelos which mean putrefaction and mud respectively). Sapropelic layers were first discovered over the 40s by Olausson, 1947 and Kullenberg 1952.

Since then, advances in coring systems and the Ocean Drilling Program (ODP) have allowed scientists to better understand their origin, which is still extremely debated. However, sapropel appears to be a basin wide phenomenon, even if sedimentary sequences do not necessarily contain the complete chronological/stratigraphical history. Such discrepancies result from re-deposition and/or post-deposition geochemical alteration or sedimentary history (i.e. sub-aerial exposure, bioturbation, etc).

Sedimentological and geochemical studies revealed that they were deposited under hypoxic or anoxic conditions, making them sensitive to major changes in climate or water circulation conditions. Other mechanisms were proposed to explain sapropel layers, such as an increase in the organic matter accumulation related to enhance primary productivity, even if such phenomenon is not common at a basin scale. In the last past decades, long coring and ODP projects (Leg 161 and 162, Lourens et al. 1996) allowed the establishment of a strong link between sapropel and astronomical forcing (Hilgen 1991; Lourens et al. 1996; Hilgen et al. 1997). Indeed, land and ocean sapropel deposits reveal that precession (i.e. through its role on both the latitudinal migration of the Inter Tropical Convergence Zone (ITCZ),

ITCZ: is a belt of low pressure which circles the Earth generally near the equator where the trade winds of the Northern and Southern Hemispheres come together. ITCZ exhibits a strong seasonal dependence so-called monsoon. Monsoon times are generally characterized by heavy rainfall.

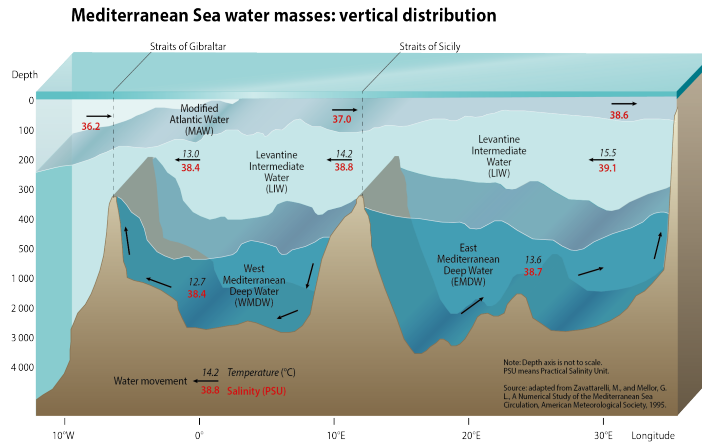


Figure 33

Vertical distribution of Mediterranean Sea water masses. Schematic showing the eastward inflow of Atlantic water into the Western Mediterranean basin via the Strait of Gibraltar and the subsequent generation of Levantine Intermediate Water (LIW) in the Eastern part of the Mediterranean Sea. LIW flows eastward toward the entire basin and return to the global oceanic circulation at the Strait of Gibraltar. Each Mediterranean basin have its own deep-water cell, we note that the East cell is closed, whereas the Western one flow out of the Mediterranean Sea. From: <https://www.grida.no/resources/5885>

the African monsoon variability and the associated runoff from North Africa) has been the pacemaker of their deposition in the Mediterranean Sea (Lourens et al. 1992; Cramp and O’Sullivan 1999; Tzedakis 2007; Tzedakis et al. 2009; Rohling et al. 2015).

Here, we review our current knowledge on Mediterranean sapropel layers and our understanding of their formation because they provide important information for paleo-climatic and paleo-environmental reconstructions, and add the emerging idea of the implications of the Western basin during sapropel deposition.

2.1. Appearance and duration

Sapropels are deposited in hypoxic or anoxic conditions, which allow the preservation of organic matter within the sediment. In marine section, they are easily recognizable as dark grey to olive green and black intervals (see Fig.IV.4; Kullenberg, 1952; Olausson, 1961; Cita et al. 1977; Calvert 1983; MURAT and GOT 1987; Cramp and O’Sullivan 1999; Rohling et al. 2015; Rohling and Hilgen, 1991; and references herein). When fresh, sapropel contains elevated organic carbon concentration (C_{org}) relative to surrounding sediments (Kidd et al., 1978; Emeis et al. 1998). In the first definition of Kidd (1978) true sapropels are composed of C_{org} concentration up to 2 wt%. Later, the term sapropel was used for sediments containing lower C_{org} values due to evidence of post deposition alteration and because preserved C_{org} is strongly dependent of the sedimentation rate (Cramp and O’Sullivan 1999; Murat and Got 2000). The highest level of C_{org} preservation have been describe in the Eastern Mediterranean basin, whereas in the Western basin only few locations, i.e. the Tyrrhenian Sea and the Balearic basin, yielded the deposition of sapropel. In the Western basin, their existence and geographical localization is less understood and authors used the term Organic Rich Layers (ORL) firstly define by Comas et al. (1997). Indeed, ORL show low C_{org} content, up to at most 3% (Murat 1999). Murat (1999) also highlighted a good correlation between Eastern and Western Mediterranean sapropelic events, even if some discrepancies

occurred due to specific oceanographic Western Mediterranean processes (i.e. water masses fronts, wind induced gyres).

Sapropelic layers often show sub-millimeter to millimeter-scale internal laminated structure, when the sediments do not present bioturbation traces (Fig. IV.4). Such laminations may represent the original sediment structure. In most of the cases laminations appeared with the total disappearance of benthic foraminifera, which suggests continuous anoxic condition at the sea floor (Nijenhuis et al. 1996; Rohling et al. 1997; Jorissen 1999; Mercone et al. 2001; Casford et al. 2003; Schmiedl et al. 2003, 2010). High resolution studies of those laminations highlighted the fact they should have resulted in annual depositions, or 'varves' (Pearce et al. 1998; Kemp et al. 2000), or complex interaction between productivity/terrestrial inputs and redox condition (Moller et al. 2012).

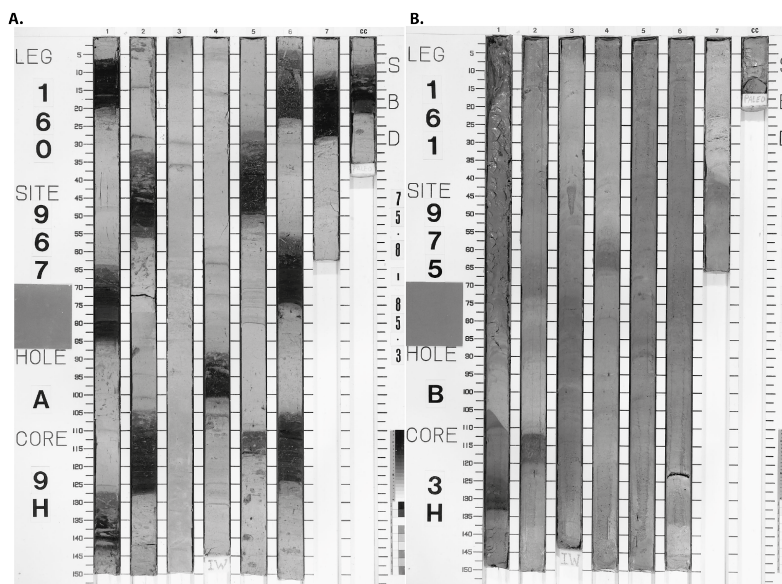


Figure 34

(A) Sapropels (dark coloured interval) recovering during the ODP leg 160 at site 967 (Erastosthenes seamount, Eastern Mediterranean Sea). Core pictures show well marked black intervals defined as sapropels (hypoxic to anoxic conditions) which are interbed by beige sediments (oxygenated conditions). Note that bioturbation is evident in most sapropels. From IODP leg 160 initial Results. (B) Sapropels and/or Organic Rich Layers recovering during the ODP leg 161 at 975 site (South Balearic margin, Western Mediterranean Sea). From IODP leg 161 initial Results. Core pictures show darker intervals with bioturbations.

The conventional identification scheme for Late Pleistocene sapropels is based on the use of astronomical time scales, as introduced by Hilgen (1991). The correlation of Mediterranean sapropels to summer insolation forms the basis of the astronomically tuned timescale for late Neogene (Rossignol-Strick 1983; Hilgen et al. 1993; Lourens et al. 1996; Emeis et al., 2000a). As the result, a time lag of 3,000 years between sapropel deposition and precession minimum has been reported (Lourens et al. 1996). This time lag is derived from radiocarbon ages of the mid-point of the youngest sapropel which occurred at 8,500 years, whereas the insolation maxima occurred at 11,500 years. Recently, Ziegler and colleagues (2010) demonstrated the cause of this time lag as a consequence of a strong negative feedback of North Atlantic cold events (i.e. AMOC slowdown) on the strength of the monsoon. The sapropel numbering related to downward counted sequential number of the orbital insolation maximum that they are associated with, i.e. i-numbers, is widely accepted as a

standard of Mediterranean sapropel stratigraphy.

2.2. Sapropel formation: Anoxia and/or Productivity

There is a continuous and unsolved debate concerning the origin of sapropel. On one side, peoples proposed that the anoxia was the main controlling factor for the preservation of organic carbon, whereas on the other side the main mechanism involve is an increase of primary productivity, and thus an increase of organic carbon flux at the sea floor. However, it should be noted that those two mechanisms are not mutually exclusive. Indeed, increase primary productivity will inherently lead to a decrease of the oxygen availability in deep parts of the basin. It should be also noted that most of the literature has concentrated on the last sapropels mechanisms of formation, and especially on S1 and S5 (see Rohling et al. 2015 for a complete discussion). However, those two sapropels were deposited under Interglacial conditions and should not be considered representative of the entire story.

2.2.1. Anoxia. In marine environment, anoxia is reached when dissolved oxygen concentration is lower than 0.2 ml O₂/l H₂O (Tribovillard et al. 2006). As oxygen is depleted, in sea water and/or sediment, redox reactions proceed with the use of alternative electron acceptor (i.e. in the following order O₂ /NO₃²⁻ / Fe²⁺ / Mn⁴⁺ / SO₄²⁻ / CO₂). Such conditions decrease the organic matter degradation within the sea water column, and therefore increase preservation of the later. Moreover, when anoxic condition is reached macro-benthic fauna is reduced as long as it is not muted. This process will increase the organic carbon flux at the sea floor.

An easy way to enhance/generate anoxia in marine environment is to inject large-scale fresh water which creates a low salinity surface or lens. The presence of such fresh-water surface layer induces a strong stratification of the water column and a slowing or stopping of deep water circulation. Moreover, once stratified the ocean oxygen concentration reaches a minimum due to limited exchanges at the ocean-atmosphere boundary. During Mediterranean sapropel formation, the presence of a fresh water lens is supported by the ubiquitous appearance within planktonic foraminifera assemblage of low-salinity taxa (Vergnaud-Grazzini et al. 1977; Thunell and Williams 1983; Kallel et al. 1997b,a, 2000; Emeis et al. 2003; Rohling and Rijk 1999b,a; Rohling et al. 2002, 2004; Marino et al. 2009; Boussetta et al. 2012; Fontugue et al., 1994). Multi-proxy based studies also confirm that times of sapropel deposition were characterized by high freshwater flooding, high runoff into the basin (Lourens et al., 2001; Larrasoana et al. 2003; Osborne et al. 2008, 2010; Revel et al. 2010; Zhao et al. 2012; Weldeab et al. 2014; Toucanne et al. 2015). Two theories have been proposed to explain the increase in fresh water, the first one is the influx of meltwater during deglaciation times, and the other concerns an increase of monsoon-derived freshwater.

The idea that change in buoyancy sea surface sea water could be related to influx of meltwater is principally based on the fact that most sapropel layers (i.e. except S2, S6) were deposited during climatic warming (Kullenberg, 1952; Olausson, 1961; Ryan, 1972). The mechanism is simple, during sapropel deposition an increase in temperature induces the melting of the North Mediterranean ice-cap and therefore increases runoff into the Mediterranean basin. Melt-water injections were high enough to enhanced stratification and stop vertical mixing, the resulting bottom water became stagnant and anoxic. Latter, Rohling and collaborators (Rohling et al. 1991a,b; Rohling and Bryden, 1994; Rohling, 1994) based on salinity model calculation shown that sea level rise can induce such stagnation of Mediterranean sea water, but act as a preconditioning of the Mediterranean Sea by lowering sea surface salinity. This was confirmed by several studies using a wide variety of proxies and physical modeling of the such effect on Gibraltar Bernoulli suction of deep-

water (Rogerson et al. 2008; Grimm et al. 2015; Grant et al. 2016).

Intensification of North Hemisphere monsoon precipitation over North Africa is generally view as the major source of extra-freshwater into the Eastern Mediterranean basin. The extra amount of freshwater has long been attributed to monsoon precipitation in response to episodic northward shifts of the ITCZ (Rossignol-Strick et al., 1982). Such shifts were associated with minima in precession cycle, which caused the summer monsoon rain belt to intensify and migrate north over the North Africa river catchments (i.e. Nile river and paleo Wadi system; Rossignol-Strick 1983; Rossignol-Strick et al. 1982; Rossignol-Strick 1985; Rohling et al. 2002, 2004, 2015; Rohling and Rijk 1999b; Larrasoana et al. 2003; Marino et al. 2009; Osborne et al. 2008, 2010; Revel et al. 2010; Zhao et al. 2012; Kutzbach et al. 2014; Bosmans et al. 2015; Scrivner et al. 2004). For example, during the last Northern Hemisphere summer insolation maxima, which was reached at ~ 11 ka (Berger and Loutre, 1991), several geochemical evidences of increased influx of monsoon freshwater (low $\delta^{18}\text{O}$, high dissolved Ba) have been observed within the Mediterranean basin between ~ 10.8 to ~ 9.7 ka (e.g. Marino et al. 2009; Weldeab et al. 2014). Such evidence of Ba-enriched water provides a spatially integrated measure of hydro-climate changes of Nile basin (increase in Blue Nile and decrease in White Nile sediments; Box et al. 2011; Costa et al. 2014) and resulting variations of Nile river discharges (Revel et al. 2010; Weldeab et al. 2014). African monsoon had other influence on the Mediterranean, in addition to Nile river runoff intensification, such as the reduction of the Sahara Desert by the northward extension of the ITCZ associated rain-belt (Larrasoana et al. 2003). Northward ITCZ also influences the atmospheric circulation over the North Africa due to enhanced moisture advection from the Atlantic Ocean (Bosmans et al. 2015; Zielhofer et al. 2017). Runoff associated to the monsoon front not only reached the Mediterranean via the Nile river, but also used a network of (now buried) fossil rivers channels that extend across the desert to the Mediterranean coast (Osborne et al. 2008). These fossil systems were active during maxima insolation wet periods when the monsoon front penetrated sufficiently northward ($\sim 21^\circ\text{N}$; Rohling et al. 2002, 2012) to cause extra fresh-water into the Gulf of Sirte (Osborne et al. 2010).

2.2.2. Productivity. An alternative to water column anoxia is that sapropel formed as the consequence of higher settling fluxes of organic matter caused by enhanced primary production related to the increased runoff (which involve a rise of inputs of organic matter rather than a decrease in the rate of degradation; Schrader and Matherne 1981; Fontugne et al. 1989; Calvert et al. 1992; Sachs and Repeta 1999; Struck et al. 2001; Higgins et al. 2010; Möbius et al. 2010; Thunell and Williams, 1983). This scenario is based on geochemical evidences showing a minor terrestrial origin of organic matter (i.e. also supported by lipid analyses; Smith et al. 1986; Haven et al. 1987), and on the fact that there is no isotopic gradient between cores at variable distance from the Nile river (i.e. principal supplier of terrestrial material; Calvert et al. 1992). Moreover, sedimentary nitrogen isotopes ($\delta^{15}\text{N}$) show strong shifts to low values which were interpreted as the result of different isotopic fractionation during nitrate uptake under nitrate-rich and nutrient-poor conditions. In such context, the low $\delta^{15}\text{N}$ was used to identify incomplete utilization of dissolved nitrate due to enhance near-surface nutrient concentration (Calvert et al. 1992). High nutrient utilization implies high nutrient concentration, which in turn implies high primary production. Therefore, induce high settlement of organic material at the sea-floor, as observed during sapropel times. High organic carbon concentration at the sea-floor would have caused a decrease in oxygen in deep water cells, which is consistent with low oxygen level in deep basin. Authors changed their interpretation and argued for a high abundance of diazotrophic phytoplankton during sapropel deposition because atmospheric fixation of nitrogen would also cause a shift toward low $\delta^{15}\text{N}$ (Hood et al.

The Blue Nile: is a river originating at lake Tana in Ethiopia. This appellation refers to the the easternmost part of Nile. The Blue Nile is so-called because floods during the summer monsoon erode a vast amount of fertile soil from the Ethiopian Highlands and carry it downstream as silt, turning the water dark brown or almost black.

The White Nile: is the second river that form the actual Nile. It called the white Nile because of this whitish-grey color. It take his source in the Victoria lake (boundary of Kenya, Uganda and Tanzania) Both rivers does not records the same rainfall season, i.e. Blue Nile records a summer signal while the Blue Nile show high runoff during winter. Seasonal runoff characteristics are combine with strong geochemical difference in source tracers are used to reconstruct Nile fluctuation to ITCZ motion over times.

2000). This second option is supported by several studies (Bouloubassi et al. 1999; Hood et al. 2000; Corselli et al. 2002; Sancetta 1994; Moller et al. 2012) and consistent with the development of deep chlorophyll maximum, stratified surface waters and sub-surface algal community (mat-forming diatoms with diazotrophic symbionts).

Overall, it appears that an increase in the algal production rates during sapropel formation may have contributed to the increase in the C_{org} flux and diluted the clastic components preserved in sediment. Nevertheless, it is hard to imagine that an increase in productivity could have induced such a long and cyclic deposition of organic rich sediments at an entire basin scale. Redox-sensible elements in sapropels and sulfur isotopes suggest that the depositional environment was anoxic to anoxic-sulphidic (Calvert 1983; Nijenhuis et al. 1996, 1999; Passier et al. 1999b,a; Nijenhuis and de Lange 2000; Mercone et al. 2001). In addition, there is a wide amount of evidences (geochemical, environmental magnetic, clay mineralogy) from various places around the Mediterranean basin that strongly support the high runoff into the basin during sapropel deposition. For example, enhanced runoff of both Nile river (Rossignol-Strick 1983, 1985; Scrivner et al. 2004; Ducassou et al. 2009; Revel et al. 2010) and central Saharan watershed (Rohling et al. 2002; Larrasoana et al. 2003; Osborne et al. 2008; Coulthard et al. 2013), or significant decrease of salinity has been reported in the Tyrrhenian sea; Adriatic sea and Corsica Trough (Kallel et al. 2000; Toucanne et al. 2015; Piva et al., 2008; Dixit et al., in review). Moreover, and in agreement with increase runoff, many evidences of wetter conditions has been reported from the entire Mediterranean borderland, i.e. from the Levant to the Alps (Israel caves: Bar-Matthews et al. 2003; Greece pollen records: Milner et al. 2012; Tzedakis 2007; Italian caves and land cores: Zanchetta et al. 2007; Magny and Nebout 2013; Regattieri et al. 2014, 2015; Bard et al. 2002; Marocco land cores: Zielhofer et al. 2017; Wassenburg et al. 2013).

2.3. The emergence of a North Borderland freshwater contribution to sapropel formation

Recent advances in paleo-hydrology and paleo-climate reconstruction during sapropel deposition have shown interesting evidences of additional source of enhanced rainfall around the Northern Borderland of the Eastern Mediterranean (Aegean Sea: Kotthoff et al. 2008, Turkey: Gktrk et al. 2011, Red Sea: Arz et al. 2003). Similar results have been obtained based on the high abundance of tree taxa and low abundance of steppe elements in northeast Greece and Tenaghi Phillippon peatland (Tzedakis 2007; Milner et al. 2012). Such palynological assemblages have been first interpreted as the result of increase summer rainfall/moisture availability (Rossignol-Strick 1987; Rohling and Hilgen 1991; Tzedakis 1993; Rossignol-Strick 1999; Rossignol-Strick and Paterne 1999). Later, Tzedakis (2007) demonstrate that such amount of precipitation ($800 - 1200 \text{ mm.yr}^{-1}$) can only occurred during winter times. Since that time other palynological studies around the Mediterranean Sea have reported important increase in winter precipitation ($\sim 50\%$ during S1 in the Aegean Sea, Kotthoff et al. 2008) over the entire Eastern Mediterranean Borderland. These finding seriously challenge the idea of restricted monsoon precipitation over the North Africa as the only actors in sapropel deposition origin (Section 2).

Further insight of increase precipitation during sapropel deposition over the North Mediterranean Borderland have also been reported in the Western basin, up to 40°N using a set of speleothems isotopic studies (Bar-Matthews et al. 2003, 1999; Matthews et al. 2000; Bard et al. 2002; Zanchetta et al. 2007; Regattieri et al. 2012, 2014, 2016; Spotl et al. 2010), lake archives (Regattieri et al. 2014, 2015, 2017a) and marine sequences (Ariztegui et al. 2000; Kallel et al. 2000; Toucanne et al. 2015).

Caves and lake isotopes records from the Alps mountain rim show anomalously low oxygen

isotopes values during the deposition of S1. Speleothems data from Corchia cave (Tuscany, North Italy) provide the most precise terrestrial chronology and precisely highlight several intervals of low $\delta^{18}\text{O}$ values over the last 200 ka (Regattieri et al. 2012, 2014, 2016; Bard et al. 2002; Zanchetta et al. 2007). The origin of oxygen isotopes variability recorded in precipitation can be studied in the Mediterranean Sea using data from the Global Network in Precipitation of the International Atomic Energy Agency (GNIP-IAEA; see Bard et al. 2002 for a full description). **Figure III.35** shows the $\delta^{18}\text{O}$ of monthly precipitation (17 years) plotted against atmospheric temperature. The plot is characterized by a degree of scatter, which is typical of monthly data for mid and low latitude. However, the data clearly define a slope on the order of $0.2 \text{‰}/^\circ\text{C}$. We can also identify a clear anti-correlation between the amount of precipitation and the $\delta^{18}\text{O}$ of precipitation. This behavior is usually known as the 'amount' effect (Dansgaard 1964; Mazor et al. 1991). In the case of study of the **Figure III.35**, the slope of this effect is approximately of -2‰ per 100 mm/months.

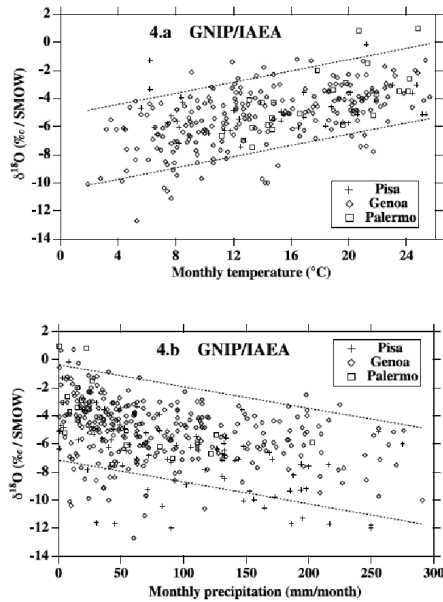


Figure 35

$\delta^{18}\text{O}$ of modern precipitation close to North Italy from GNIP-IAEA database. Upper graph shows the monthly mean vs temperature for 411 months. Lower case highlights the 'amount' relationship between monthly $\delta^{18}\text{O}_p$ and monthly mean precipitation. The dashes lines correspond to 95% confidence level from the regressive slope.

Using this approach, numerical modelling of past precipitation and the oxygen isotopic conservation between precipitation and calcium carbonate (i.e. speleothems material), Bard et al. (2002) show that low $\delta^{18}\text{O}_{\text{speleothem}}$ values correspond to wetter condition. Those wetter phases are shown to correspond chronologically to the deposition of sapropels over the last 200 ka (Bard et al. 2002; Regattieri et al. 2012, 2014, 2016). This 'amount' isotopic signal can be traced up to the North rim of the Alps during S1, albeit decreasing in amplitude toward the North (Spotl et al. 2010). This suggest that freshwater runoff during sapropels are not restricted to the Eastern Mediterranean (i.e. Nile river and Central Saharan watershed), but was rather widespread over the entire Mediterranean basin due to increased rainfall (Bard et al. 2002; Kallel et al. 2000; Piva et al. 2008; Toucanne et al. 2015).

Mediterranean lake level and associated carbonate isotopic records also suggest wetter

condition (or even the wettest; high lake level associated with low $\delta^{18}\text{O}$ values in carbonates) during the first half of the Holocene which correspond to the deposition of S1 (Roberts et al. 2008). This regional pattern is also observable in central and southern Italian lake level during S1 and S5 (Giraudi et al. 2011; Regattieri et al. 2015, 2017a). Nevertheless, the use of lake data does not give straightforward information because it is dependent on a complex interaction of changes in precipitation and evaporation, and it is strongly sensitive to local processes (i.e. especially high-altitude lake such as Alpine lakes). For example, for the same climatic event (i.e. cooling at 8.2 ka) several hydrological responses have been described in Western Alps rim lakes (Magny et al. 2003). Nevertheless, during the deposition times of S1 mid-European lakes (i.e. close to the Rhone river) show low lake level (Magny 2004) whereas speleothems data seem to indicate wetter condition with a Mediterranean origin (Spotl et al. 2010). Therefore, we can speculate that lake level during S1 was more influenced by evaporation or local processes. If it is the case, the discrepancies observed between lake level and stable isotopes should not exist.

Several hypotheses have been postulated in order to explain such wetter condition over the entire Mediterranean Sea during periods of high-amplitude precession minima/insolation maxima. One is related to penetration of direct precipitation from the African and/or Indian monsoon system into the Mediterranean basin (Goodfriend 1991; Arz et al. 2003; Vaks et al. 2003, 2007, 2010). If this scenario occurred in the past, it would have led to an increase in precipitation during late summer which seems not consistent with the seasonality deduced from palynological studies (Tzedakis 2007). The second scenario introduced by Rohling and Hilgen (1991) is widely documented and might be related to increased winter depression activity over the Mediterranean borderland. Based on actual meteorological observation in the Mediterranean basin, increased winter-time penetration of Atlantic depression (i.e. NAO) into the Western basin lead to strong increase in the cyclogenesis which enhance the winter precipitation over the Nord Mediterranean borderland. Recent numerical modeling focusing on sapropel deposition times supports this assumption (Bosmans et al. 2015; Kutzbach et al. 2014). This suggest strong atmospheric feedback between ITCZ motion, NAO and Mediterranean cyclogenesis. However, relatively few studies based on long records address this question in the Western Mediterranean basin.

2.4. Mediterranean climate response to North Atlantic climate variability

The above paragraph highlights a direct relationship between North Mediterranean borderland rainfall activity and the precession forcing. Using the well-established link between precession forcing and low-latitude climate (Hilgen 1991; Rossignol-Strick 1985; Tzedakis 2000), we can hypothesize a strong communication between Mediterranean cyclogenesis and the monsoon activity (i.e. ITCZ, low latitude climate). In a recent study, Trigo et al. (2002) highlighted that Mediterranean cyclones are mainly formed in three different areas in winter, the gulf of Genoa, the Aegean Sea and the Black Sea, and are triggered by the penetration of atmospheric North Atlantic systems, which are channelized by the orographic highs over the North Mediterranean coast. Therefore, identifying the present mechanism which translates large-scale Atlantic atmospheric perturbations (i.e. Mediterranean storm track) into the Mediterranean Sea seems to be useful for the comprehension of past Mediterranean rainfall regime changes.

Because the Western Mediterranean Sea, and by extension Western cyclogenetic area, experience a strong influence of the North Atlantic atmospheric variability, there is also an immediate link between Mediterranean storm track and the NAO pattern. Modern observation and modelling experiences have shown that it is the variation in the mode of NAO, define as the difference in pressure between the Icelandic low and the Azores high (see **Figure III.36**; Walker and Bliss 1932; Bjerknes 1964; Wallace and Gutzler 1981), which is the primary control over the relative positioning of westerlies wind tracks and the

propagation of Atlantic storms into Mediterranean (Lamy et al. 2006; Magny et al. 2006; Roberts et al. 2011). Climate variability is usually characterized in terms of 'anomalies', where an anomaly is the difference between an instantaneous state and the mean state (computed over many years of observation; Wallace et al. 1993). Large changes in the mean distribution of sea-level pressure over the North Atlantic have been observed and used to define the NAO anomaly (Bjerknes 1964). Over the North Atlantic Ocean, the Azores high (i.e. anticyclone) migrates northward and then dominates nearly all the North Atlantic during summer (positive NAO), see **Figure III.36**. It then weakens and moves equatorward (i.e. southward) during winter, when the high-latitude Iceland low predominates (negative NAO, Hurrell 1995). Because of air-flow around atmospheric pressure centers (i.e. counterclockwise around low pressure and clockwise around high pressure in the NH), the main wind flows westward (i.e. westerlies) across the Est and have strong effects on the European climate, see **Figure III.36**.

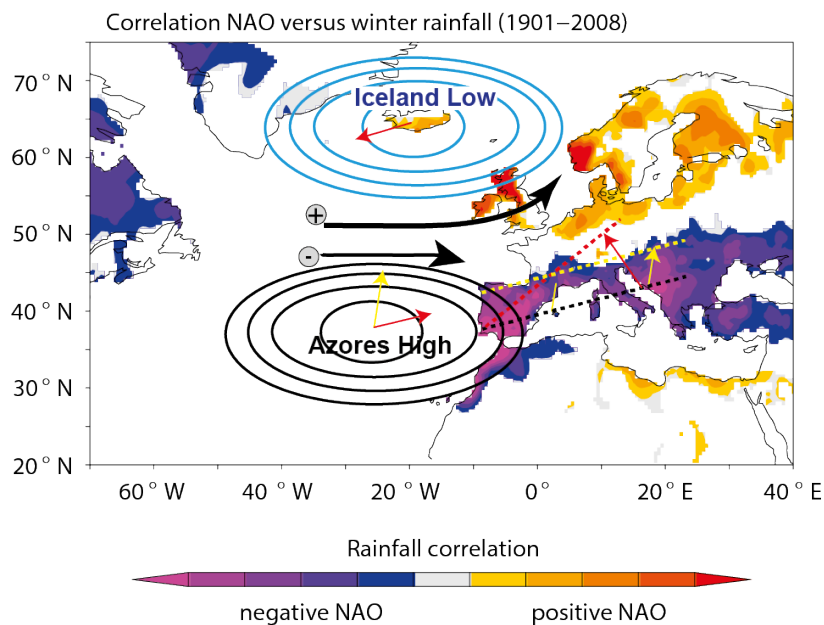


Figure 36

Correlation between the NAO index and winter rainfall with location of sea level pressure over North Atlantic and main direction of westerlies flows during negative- and positive- NAO (grey circle and black arrows). NAO-rainfall belt is located using a color ramp associated with the state of the NAO. Blue to purple colours indicate negative NAO spatial repartition of rainbelt, which are mainly located over the north Mediterranean borderland. Potential movements of SLP centers toward a positive- NAO is schematically represented with yellow and red arrows. A southward shift of Icelandic low/northward shift of Azores high (i.e. positive NAO) induce to a strong angle modulation of the NAO rain belt leading to decrease precipitation over North Mediterranean Borderland. Adapted from Wassenburg et al. 2013.

Under negative NAO (NAO-), Atlantic westerlies weaken and shifts southward reversing the pattern (**Figure III.36**). Indeed, it would result in a change of atmospheric circulation toward a more sub-meridional area, weakening the westerlies and enhancing the passage of Atlantic storms over Western Mediterranean. The rise of Atlantic storm passage toward the Mediterranean lead to (i) increase available moisture into the Western Mediterranean, and (ii) enhance winter rainfall associated with the Mediterranean cyclogenesis (Trigo et al. 2000). Traditionally, positive NAO (NAO+) conditions induce winter storm track asso-

ciated with westerlies that shift northward, leading to wetter and warmer condition over North Europe and drier condition over southern Europe (Goodess and Jones 2002; Rodó et al. 1997; Sáenz et al. 2001; Wanner et al. 2001), see **Figure III.36**.

Those variations have been observed from inter-annual to longer timescale due to the relatively stable position of the Atlantic westerlies Jet through time (Trigo et al. 2000; Zielhofer et al. 2017; Zhao et al. 2012; Wassenburg et al. 2013; Fletcher et al. 2013; Smith et al. 2016; Zielhofer et al. 2017).

Moreover, during sapropel deposition the northward position of the ITCZ has favoured warming and moisture availability/accumulation above the Atlantic subtropical zone (Margari et al. 2014; Marino et al. 2015). Because the strength of the NAO is related to the sub-tropical sea water surface (Visbeck 2002; Knight et al. 2006), we can also hypothesise that a higher proportion of Atlantic moisture can penetrate into the Western Mediterranean basin. North Mediterranean mountains (French and Apuan Alps) are known to present a strong land-ocean thermal gradient which enhance moisture condensation (i.e. cyclogenesis region, Trigo et al. 2002), catching a Mediterranean origin before flowing eastward over the North Mediterranean borderland (i.e. until Jordan and Israel region; Black 2012).

Despite pioneering works (Rohling and Hilgen 1991) and recent paleo-environmental studies (Bard et al. 2002; Zanchetta et al. 2007; Regattieri et al. 2012, 2014, 2016; Toucanne et al. 2015) in the Western basin, the idea of a North Atlantic influence on Mediterranean rainfall need to be tested in order to establish a clear coupling at a regional scale. For example, Toucanne et al. (2015), using marine sediment, provided the first evidence for enhanced rainfall in Western Mediterranean during warm intervals of interglacial periods over the last 500 kyr. Comparison of pluvial proxies on the eastern Corsican margin with pollen sequences and speleothems from the entire Mediterranean reveals the regional character of such rain events. Toucanne and collaborators (2015), following the idea of Rohling and Hilgen (1991), interpreted these pluvial events as the result of intensification of Mediterranean storm track in autumn/winter. Beside highlighting a strong coupling between Western and Eastern Mediterranean basins, those results provide information of enhanced cyclogenesis in the Gulf of Genoa, which is located few kilometers westward from the Corsican margin. Thus, high flux of fresh water, nutrient and continental organic matter entered into the Mediterranean basin from the North African coast during spring/summer but also from the North Mediterranean Borderland in autumn/winter. This Northern contribution of fresh water during sapropel events have been underestimated during the last decades of sapropel studies. However, during the last decade the North borderland contribution has been estimated as equally or more important than the increase in Nile discharges (Meijer and Tuenter 2007; Bosmans et al. 2015). Recent modelling supports the North Atlantic origin of such autumn/winter rainfall (Bosmans et al. 2015) which is also supported by modern atmospheric observation of extreme events over the North Mediterranean Borderland (Gat and Carmi 1970; Reale et al. 2001; Sodemann and Zubler 2010) and changes of moisture sources in Italian speleothems during sapropel deposition (Bard et al. 2002; Drysdale et al. 2005; Zanchetta et al. 2007; Regattieri et al. 2012, 2014, 2016).

3. New evidences of enhanced rainfall activity in the Gulf of Lion

Organic matter isotopes reveals enhanced rainfall activity in North-Western Mediterranean borderland during warm substages of the last 200 kyr.

Pasquier Virgil^a, Toucanne Samuel^b, SansJofre Pierre^a, Dixit Yama^b, Revillon Sidonie^c, Rabineau Marina^a

^aUMR 6538 'Laboratoire Geosciences Ocean', Institut Universitaire Europeen de la Mer, Place Nicolas Copernic, 29280 Plouzane, France

^bIFREMER, Laboratoire Geodynamique et enregistrements sedimentaires, BP70, 29280 Plouzane, France

^cSEDISOR, Institut Universitaire Europeen de la Mer, Place Nicolas Copernic, 29280 Plouzane, France

Abstract

In this study we examined the nature and the timing of preserved organic matter in borehole PRGL1-4 from North-western Mediterranean Sea, a transitional zone between North Atlantic rainfall and North African monsoon system. In the Gulf of Lion, episodes of high river inputs of organic matter occurred during warm substages of the last 200 kyr. They resulted from regional rainfall increase under the influence of NAO-negative-like conditions, which are known to enhance the frequency of North Atlantic lows in the Western Mediterranean. The long term evolution of rainfall activity confirm the precession modulation of eccentricity on Mediterranean climate, but also reveal constant NAO atmospheric circulation over Europe. Changes in the NAO atmospheric circulation is associated with changes in atmospheric moisture over southern Europe and the Mediterranean. During NAO-negative conditions wetter conditions are observed over the Gulf of Lion watershed whereas Northern Europe experience drier conditions, and vice versa during NAO-positive conditions. Beside highlighting enhanced river discharges due to high rainfall over the North-Western Mediterranean borderland, we assume that PRGL1-4 provides a new valuable record for regional NAO reconstruction in the Western Mediterranean basin.

Keywords: Mediterranean, Rainfall, North Atlantic Oscillation, Organic matter, North Mediterranean borderland, Mediterranean storm track

1. Introduction

The Mediterranean Sea occupies a critical transitional location between polar and subtropical air-masses at the polar front jet-stream. As a result, the Mediterranean climate (i.e. hydrology), is controlled by both Atlantic influence (i.e. driving the wintertime Mediterranean storm track) and latitudinal migrations of the Inter-Tropical Convergence Zone (ITCZ). Climate variations in the Mediterranean depend on these two climatic components (e.g. Rohling et al. 2015 for a thorough review), and a exhaustive understanding of these variations is required to establish climate models for the region (Bosmans et al. 2015; Kutzbach et al. 2014), (Bosmans et al., 2015; Kutzbach et al., 2014), and evaluate modern hydrological system and its contributions to climate change.

At a global scale, the quaternary climate is controlled by Earth's orbital parameters (i.e. Eccentricity, Obliquity and Precession) which control the insolation intensity on the Earth surface. Intercomparison between marine and terrestrial records have highlighted the im-

portance of precession on the Mediterranean climate variations (Rossignol-Strick 1983; Siero et al. 2000). This precessional imprint results from the African monsoon variability and its capacity to enhance the freshwater discharge into the Eastern Mediterranean Sea during summertimes (through the Nile River and Wadi systems; Rohling et al. 2002) when the ITCZ reaches its northern position (see Fig.1 for ITCZ position; Revel et al. 2010; Rossignol-Strick 1983, 1985). This pattern reaches a maxima during precession minima when the summer insolation peaks (maxima; i.e. interglacials) induces a strong thermal gradient between land and sea and intensify the monsoon circulation. The resulting phenomena is the sapropel (S) deposition in the deep Mediterranean, i.e. dark layers deposited under stratified conditions containing a high amount of organic materials (Rohling et al. 2015 for a thorough review). Sapropels have long been attributed to this low latitude phenomena (i.e. ITCZ shifts). However, recent understanding of North-Eastern Mediterranean paleo-hydrology variations have showed increased precipita-

tion over the entire Eastern Mediterranean region during sapropel deposition (Soreq cave speleothem, [Bar-Matthews et al. 2003](#)). This is supported by many records of increased rainfall with Mediterranean signature during the last insolation maxima centred around 8 ka (S1 deposition; [Arz et al. 2003](#)), and evidence of available water in Greece peat land) during S5 deposition (125 ka; [Tzedakis 2007](#)). The evidence of pluvial periods in North-Eastern borderland call into question the northward influence of African monsoon during insolation maxima.

Recent studies from continental and marine records from the Western Mediterranean region also highlighted the intensification of hydrological activity during S1 (i.e. 6.5 to 10.2 ka according to [Ziegler et al. 2010b](#) chronology) around the Italian Peninsula ([Ariztegui et al. 2000](#); [Magny and Nebout 2013](#); [Zanchetta et al. 2007](#)), but also during each insolation maxima over the last half million years ([Kallel et al. 2000](#); [Toucanne et al. 2015](#)). These findings seriously challenge the idea of restricted river runoff from Eastern Mediterranean basin during sapropel episodes, and suggest a wide increase in rainfall over the Mediterranean ([Bard et al. 2002](#); [Kallel et al. 1997, 2000](#)) with a strong Northern borderland contribution (From Corsica to Turkey; [Rohling and Hilgen 1991](#); [Toucanne et al. 2015](#)).

Here, we investigated the processes involving the export, dilution and preservation of land-derived particulates into the Gulf of Lion (GoL), South East France, over the last 200 kyr. The GoL is a climate-sensitive margin, and is prone to recording high resolution climate changes (including sea-level; [Cortina et al. 2015](#); [Rabineau et al. 2006](#); [Sierro et al. 2009](#) among others) due to the combination of high sediment inputs and high subsidence rates favorable for sediment - accumulations ([Rabineau et al. 2006, 2014](#)). By focusing on $\delta^{13}\text{C}_{\text{org}}$, $\delta^{15}\text{N}_{\text{tot}}$, Total Organic Carbon (TOC) and Total Nitrogen (TN), we trace the origin of the organic matter (i.e. terrestrial vs marine) and then track the paleohydrology of the Pyrenean-Languedocian and Western Alps (drained by the Rhne river) catchement area contributions to the Western Mediterranean Sea. In the GoL watershed region, moisture level changes are triggered by complex interactions between several ocean sources and atmospheric circulation modes, that may generate mingled signatures for glacial and interglacial reconstructions of past precipitation. Moreover, reconstructions of past variabilities may also be attributed to the solar cycles, ice sheet forcing, changes in the Atlantic oceanic circulation (Atlantic Meridional Overturning Circulation) or atmospheric circulation (e.g. North Atlantic Oscillation; NAO). Variabilities within each of

these parameters and their associated hydrologic and atmospheric changes impacted climate changes over the Mediterranean Sea, North-West Europe, Greenland and Asia over different time scales ([Hurrell 1995](#); [Mariotti et al. 2002](#); [Mariotti and Arkin 2007](#); [Serreze et al. 1997](#); [Ziegler et al. 2010a](#)). This work is ultimately valuable for extending our understanding of past climate mechanisms leading to enhanced precipitation over the Northern Mediterranean borderlands during insolation maxima.

2. Geological Setting, material and methods

2.1. PRGL 1-4 drill-core: a high-resolution record for GoL shelf history

Located in North-Western Mediterranean basin, the GoL is characterised by a wide continental shelf (70 km), that was sub-aerially exposed during Quaternary glacial times ([Jouet et al. 2006](#); [Rabineau et al. 2005, 2006](#)). The shelf morphology has been studied in detail over the last decade, highlighting some morphological features providing indicators of paleo-connection between fluvial systems and submarine canyons (e.g. [Bassetti et al. 2008](#); [Baztan et al. 2005](#); [Mauffrey et al. 2015](#); [Rabineau et al. 2005, 2006](#)).

Spatial and temporal distribution of sediment in the studied area are mostly governed by eustatic changes. Seismic investigations and dated sediment cores allowed a detailed reconstruction of sedimentary accumulation since the Messinian (ca. 6 Myr; [Bassetti et al. 2008](#); [Berné and Gorini 2005](#); [Jouet et al. 2006](#); [Rabineau et al. 1998, 2005, 2006](#); [Tesson et al. 1990](#); [Lofi et al. 2003](#); [Leroux et al. 2017](#) among others), which is described as a superposition of 100 kyr seismic sequences separated by major discontinuities formed in response to glacio-eustatic sea level changes. In the GoL, seaward migration of the shoreline close to our study site ($\sim 90/100$ mbsf, [Rabineau et al. 2006](#)) induced high to very high sedimentation rates during glacial times (average of 1 to 2 $\text{m}\cdot\text{ka}^{-1}$).

The present study is based on borehole PRGL 1-4 (42.690N; 3.838E), a 300m continuous record drilled on the upper slope (298 metres water depth) of the GoL, on the interfluvium of the Bourcart and Hérault canyons ([Figure 1](#)). Borehole PRGL 1-4 was drilled with the framework of the European Union project PROMESS1 (<http://www.pangaea.de/Projects/PROMESS1/>).

2.1.1. Organic matter specific compounds: Carbon and Nitrogen isotopes and quantification

Sedimentary organic matter (OM) in marine environment is typically composed of a mixture of in-situ ma-

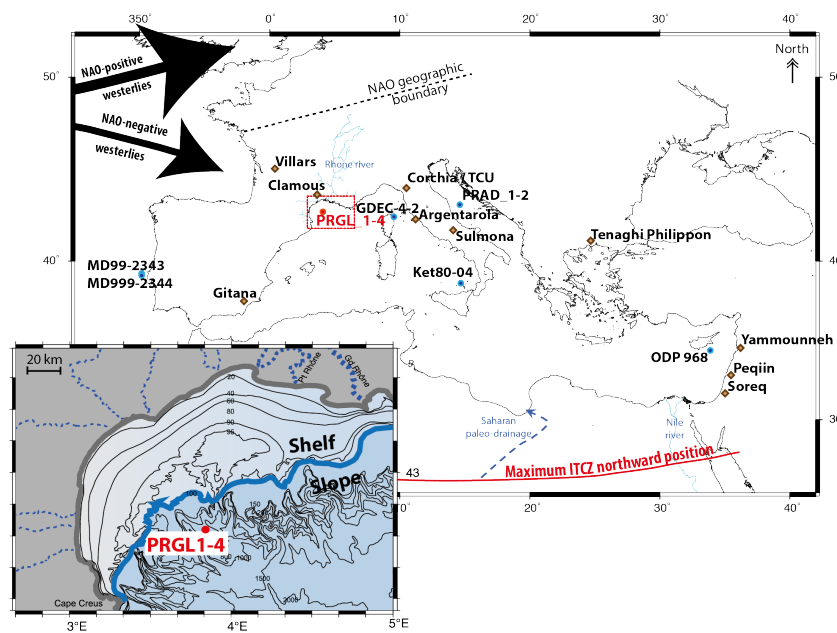


Figure 1: (A) Location of the main sites mentioned in the text, including our study site PRGL1-4, red circle, brown and blue circles (with associated name) represent continental and marine records. The red line over North Africa show the maximum northward displacement of the ITCZ over the last millions years from (Tuenter et al. 2003). Course of the Central Saharan rivers according to (Coulthard et al. 2013). The general trajectory of the atmospheric westerlies is show for NAO-positive and NAO-negative states according to the present day observation. (B) Gulf of Lion shelf morphology, red circle corresponds to our study site PRGL1-4, blue line correspond to the LGM coastline position.

rine particulates and land exported particulates. Autochthonous grains are derived from land erosion, land plant detritus and old marine deposits which has been already degraded to various degrees. The present day spatial composition of OM in the GoL have already been studied in detail (Cathalot et al. 2010; Kim et al. 2006; Tesi et al. 2007) showing that origin and spatial distribution of OM are strongly impacted by rivers mouth accumulations. Rivers pro-delta are characterized by a very low $\delta^{13}\text{C}_{\text{org}}$ values ($\sim -25\text{‰}$) and high sedimentation rates (20 cm years^{-1} , Radakovitch et al. 1999), contrasting with the open ocean production (primary producers and derived outcomes) which is characterized by heavier values around -22‰ at the shelf break. According to the shelf distribution, organic carbon isotopes ($\delta^{13}\text{C}_{\text{org}}$) preserved in sediments can be interpreted as reflecting the relative proportion of terrestrial carbon organic particulates and marine production (i.e. seaward dilution), then can be used as an indicator of the terrigenous flux into the basin (Meyers 1994).

2.2. Samples pre-analyses treatment and analytical method

Once the borehole had been subsampled, sediments were freeze-dried prior to any treatment. A well-known portion of dried samples ($1.5 \pm 0.1\text{g}$) was grounded in agate mortar, and transferred to pre-cleaned 15 mL centrifuge tubes. Prior to elemental and isotopic analyses carbonate fraction was removed by dissolution in excess 2N HCl for 24 hours at room temperature (Pasquier et al., In prep). During digestion centrifuge tubes were placed in ultrasonic bath to increase the mechanical separation of clay and calcium carbonates. After digestion, residues were washed three times with distilled water, centrifuged and dried at 50°C . Few hours before analyses samples were weighed using tin capsules.

All analyses were performed using an elemental analyser (EA, Flash 2000 - Thermo Scientific) coupled to an isotope ratio mass spectrometer (Delta V plus, Thermo Scientific EA-IRMS) at the Ple de Spectromtrie Ocan (PSO, Brest, France). The principles of EA-IRMS are described in detail in Preston and Owens 1983. Samples were loaded into an auto-sampler for automatic analysis. During analyses, samples were dropped into the oxidation furnace maintained at temperature of 1020C , and were combusted in presence of excess oxygen (240 ml/min) for 8s. Flash combustion products were carried with a Helium flow (100 ml/min) prior to entering into the mass spectrometer via a ConFlo IV system (Thermo Scientific).

$\delta^{15}\text{N}$ and $\delta^{13}\text{C}_{\text{org}}$ are given as the per mil deviation from the N-isotopes of atmospheric N_2 , and per mil de-

viation from the PDB standard. Routine replicate measurements shows internal reproductivity less than 0.1‰ (2σ) for standards and 0.6‰ (2σ) for samples; and 0.1‰ (2σ) for standards and 0.3‰ (2σ) for samples respectively for nitrogen and carbon.

2.2.1. Chronology

The chronostratigraphical framework of PRGL 1-4 is based on $\delta^{18}\text{O}$ measurements (slightly modified from Sierro et al., 2009), which show distinct end-members characterizing interglacials (light oxygen isotopes ratios) and glacials (heavy $\delta^{18}\text{O}$); (Figure 2). Our age model is based on the close similarities between PRGL1-4 planktonic *G. bulloides* $\delta^{18}\text{O}$ and the NGRIP ice core isotopes from Greenland for the last 60 ka (GICC05 chronology, (Rasmussen and Andersen, 2006; Svensson et al., 2008)), and the synthetic Greenland record (GLT-syn using GICC05/NALPSSpeleo age) reported in (Barker et al., 2011) from 60 to 200 ka (Figure 2; Table 1). Such a synchronization was previously used to produce accurate chronologies in Iberian and Corsican margins (Hodell et al. 2013; Margari et al. 2014; Toucanne et al. 2015), and allow us to use the absolute 'Speleo-Age' chronology based on Uranium-Thorium isotopic system during the entire study interval (60-200 ka). Sedimentation rates for PRGL 1-4 ranges between 14 and 230 cm.ka^{-1} , respectively during interglacials and glacials, with an average of 0.7 m.ka^{-1} over the entire studied interval. Such marine accumulation rate discrepancy resulted from the landward/seaward of coastal rivers prodelta on the GoL shelf, which induced a prodeltaic sedimentation during glacials (i.e. low sea level) at PRGL 1-4 contrasting with an open marine regime during interglacials (i.e. high sea level).

Because isotopes substages labelling to identify intervals of glacio-climatic events have been subject to debate over the last decade, in this study we use the scheme of marine stage published in detail in Railsback et al. 2015.

3. Results

3.1. General interpretation of proxies ($\delta^{13}\text{C}_{\text{org}}$ / $\delta^{15}\text{N}_{\text{tot}}$)

The results of organic proxies ($\delta^{13}\text{C}_{\text{org}}$, $\delta^{15}\text{N}_{\text{tot}}$, TOC and TN) are shown in Figure 3 parallel to oxygen isotopes of planktonic *G. bulloides* species from the same core (Sierro et al. 2009; Figure 3.A.) and the reconstructed sea level from the Red Sea (Figure 3.B.; Grant et al. 2014). The $\delta^{13}\text{C}_{\text{org}}$ values range from -25.4‰ to -21.6‰ with an average of -24.1‰ . The lightest values in $\delta^{13}\text{C}_{\text{org}}$ are observed during glacial times, especially during glacial maxima (i.e. heavy $\delta^{18}\text{O}$ values,

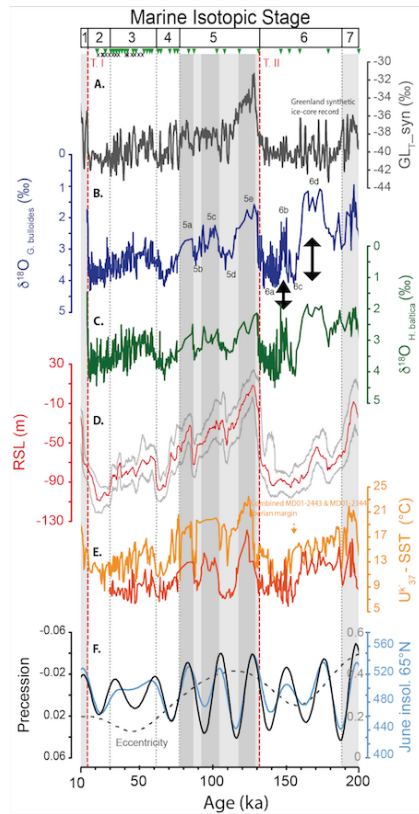


Figure 2: (A) Greenland synthetic $\delta^{18}\text{O}$ record (GLT-syn; (Barker et al. 2011); (B) $\delta^{18}\text{O}$ of planktonic species [*G. bulloides*] (Sierro et al. 2009); (C) $\delta^{18}\text{O}$ of benthic species [*H. baltica*] from PRGL1-4 site (Sierro et al. 2009); (D) Red Sea sea level record (core KL09, red curve, grey line corresponds to with maximum probability 95%, (Grant et al., 2014)); (E) Uk'37-SST of combined record of core MD01-2444 and MD01-2443 (Iberian margin) yellow line (Martrat et al. 2007) and C37_{alkenones}-SST from PRGL1-4 orange line (Cortina et al. 2015); (F) June insolation for 65°N (blue line) with precession (black line) and eccentricity of Earth orbit (dashed grey line; (Laskar et al. 2004). Black arrows highlight the unexpected low $\delta^{18}\text{O}$ during MIS6 warm substages; Top black crosses indicate C^{14} dating and green triangles indicate position of tie-points (see Table 1). Grey bands indicate interglacial conditions s.l, dark grey bands indicate interglacial warm-periods. Termination (T), according to (Barker et al. 2011). Scheme of marine stage according to (Raisback et al. 2015).

Stratigraphic Event	NorthGRIP Age (ka BP)	GLT-syn	
		GICC05/NALP/Speden Age (ka BP)	PRGL1-4 - depth (mbs)
Top PRGL1-4	14.16		0
Onset GI-1/T.I	14.8		0.25
Onset GI-2	23.2		19.8
Onset GI-3	27.7		27.99
Onset GI-4	28.63		29.6
End GI-4	31.49		33
Onset GI-5	32.14		33.55
Onset GI-6	33.57		34.32
Onset GI-7	35.72		35.69
Onset GI-8	38.83		37
Onset GI-9	40.1		38.3
Onset GI-10	41.05		40.08
Onset GI-11	43.02		41.86
Onset GI-12	46.1		44.79
Onset GI-13	48.35		46.66
Onset GI-14	54.06		49.44
Onset GI-15	55.88		50.71
Onset GI-16	57.95		52.24
Onset GI-17	59.09		53.89
End GI-18		62.95	56.63
Onset GI-18		64.2	58.95
Onset GI-19		71.95	63.83
Onset GI-20		75.74	64.99
End GI-20		75.88	65.13
Onset GI-21 / MIS5.1		86.46	65.52
MIS5.3-MIS5.2 transition		89.82	66.8
Onset GI-22		103.66	68.7
Onset MIS5.3 / GI-23		106.92	70.2
Onset MIS5.4		116.29	71.6
Onset MIS5.5 / T.III		131	72.4
MIS6.3-MIS6.2 transition		146.51	93.8
Onset MIS6.3		151.01	105.45
Onset 6c1		160	110.8
Onset MIS6.5		178	115.27
Onset MIS7.1		199	125.18
Onset MIS7.2		201.17	125.46
Onset MIS7.3		217	125.75
Onset MIS7.5 / T.III		243	127.6
Onset MIS8.3		264.3	139.19
MIS8.4-MIS8.3 transition		280.5	155.5
Onset MIS8.5		291.5	158.55
MIS9.3-MIS9.2 transition		321	160.91
Onset MIS9.3 / T.IV		336	161.7
End MIS10		351	179.9
MIS11 / MIS10 transition		396.5	198.4
Mid-MIS11.2		413	199.38
Mid-MIS11.3		423	212.37
Onset MIS11.3 / T.V		431	223.25
Mid-MIS12		460.5	242.31
MIS13.2-MIS13.1 transition		495.5	290.7
MIS13.3-MIS13.2 transition		520.5	296.3
Base PRGL1-4		536	304.5

Table 1: Chronological framework for PRGL1-4. 0-60 ka age of isotope events from North-GRIP ice core (Rasmussen and Andersen, 2006; Svensson et al., 2008) and 60-500 ka from the synthetic Ice Greenland record of (Barker et al. 2011) (GLT-syn). GI refer to Greenland Interstadial, MIS is Marine Isotope Stage and T correspond to Termination. Scheme of marine stage according to (Raisback et al. 2015).

MIS 2, MIS 6.a). $\delta^{15}\text{N}_{\text{tot}}$ is characterized by values comprised between 2.3 ‰ and 4.0 ‰, with an average of 3.1 ‰, with strong depletion (up to 1 ‰) associated with glacial maxima. During these intervals, values drop below 3 ‰ suggesting sub-oxic/anoxic environments in modern ocean, i.e. oxygen minimum environments (OMZ, Ader et al. 2014). At site PRGL1-4 this is supported by the occurrence of *Brizalina dilatata* benthic species (Cortina et al. 2011). Sediment deposited at PRGL1-4 site are poor in organic matter (0.6% of mean TOC and 0.08% of mean TN) and no clear relationship is observed between the organic content (OC) and climate changes and/or sea-level (Figure 3.E and F). This is unexpected considering significant sedimentary input from the Rhone and the seaward

migrations of coastal rivers (i.e. including the Rhone) during glacial lowstands (Rabineau et al. 2006). High bacterial activity, and the use of organic carbon as electron donor by sulfate reducing bacteria could explain this observation (Pasquier et al. 2017). Interestingly the organic carbon isotopes show significant fluctuations in phase with global climate changes, suggesting that $\delta^{13}\text{C}_{\text{org}}$ at PRGL 1-4 is climatic sensitive. We show hereafter that these changes can improve our understanding of paleo-hydrological changes in the North-western Mediterranean Sea over the last 200 kyr.

3.2. Detailed signals recorded in organic matter isotopes ($\delta^{13}\text{C}_{\text{org}} / \delta^{15}\text{N}_{\text{tot}}$)

3.2.1. Last Glacial Period (MIS2/4)

During the last glacial period (i.e MIS2/4, 15-85 ka), large ice accumulation in the North Hemisphere (NH) induced dry conditions [i.e. especially in the Alps where continental water is turned into ice associated with a low vegetation (Beaudouin et al. 2007; Bonneau et al. 2014; Tzedakis et al. 2006)] and sea level drop substantially as supported by the benthic foraminifera $\delta^{18}\text{O}$ (drop of 4 - 5 ‰) at our site (Figure 3). For this period, $\delta^{13}\text{C}_{\text{org}}$ fluctuations are consistent with both benthic and planktic foraminifera $\delta^{18}\text{O}$ profiles, and sea level variation. $\delta^{13}\text{C}_{\text{org}}$ characterizing pro-deltaic values (-24.7 ‰) are observed at the end of the last glacial (i.e. 18-24 ka) following a continuous drop since 50 ka. This is supported by the positive trend ($R^2=0.55$) observed between sea level and $\delta^{13}\text{C}_{\text{org}}$ (Figure 4). This lowering trend is interpreted as reflecting higher proportion/preservation of land-derived particulates at our site through time in response to sea level fall. Therefore, we propose that the organic carbon isotopic composition at PRGL1-4 is controlled by glacio-eustatic changes.

3.2.2. Warm substages of the Last interglacial (MIS5)

During MIS5 (~ 78-130 ka), our results show heavier $\delta^{13}\text{C}_{\text{org}}$ (up to 22 ‰), indicative of increased marine influences in comparison to glacial intervals. Specifically, three $\delta^{13}\text{C}_{\text{org}}$ peaks occurred during interglacial warm substages (MIS5e,c,a) and associated sea level highstands. Such values are consistent with decreasing seaward sediment transfers and landward migration of coastal rivermouths in the Northwestern Mediterranean Sea (Rabineau et al. 2006). Subsequent climate cooling (MIS5d and b) show the inverse pattern (increase inputs and seaward migration of coastal rivermouths) as recorded by significant decrease of the $\delta^{13}\text{C}_{\text{org}}$ (Figure 3). This pattern is consistent with that described for the last glacial.

Surprisingly, the interglacial warm substages show an unexpected trend compared to sea-level variation. The highest sea-level condition described during the MIS5e (Grant et al. 2014) do not correspond to the most marine signature in $\delta^{13}\text{C}_{\text{org}}$ at PRGL 1-4 site (Figure 3.C). This signature is observed later, during MIS5a warm substage, when the sea-level was about 40 m lower in comparison (Grant et al. 2014). This is nicely illustrated by the strong inverse relationship ($R^2= 0.73$) recorded during MIS5 warm substages between sea-level and $\delta^{13}\text{C}_{\text{org}}$ (Figure 4). As a result, we conclude that the impact of the sea-level on the $\delta^{13}\text{C}_{\text{org}}$ signature described above is overwhelmed by an additional forcing. We suggest that sediments during MIS5 warm substages have preserved important proportion of terrestrial land-derived organic carbon particulates (low $\delta^{13}\text{C}_{\text{org}}$) due to high river runoff. The gradual decrease in $\delta^{13}\text{C}_{\text{org}}$ in the course of the MIS5 warm substages likely indicate a gradual reduction of riverine delivery through the last Interglacial, with the highest runoff during MIS5e. A detailed observation of the MIS5 warm substages $\delta^{13}\text{C}_{\text{org}}$ record (i.e. increasing $\delta^{13}\text{C}_{\text{org}}$ values throughout the substage, e.g. MIS5e,c) suggest enhanced riverine inputs at the onset of the intervals (highlighted with red arrows on the Figure 5.C). Peaks in coastal river runoff during these intervals have also been highlighted by Toucanne et al. 2015 off the Corsican island, with concomitant high amount of OM arrival at the continental slope, (Figure 5.E). At PRGL1-4 site, the organic matter is not well preserved during MIS5e and c (see discussion above) but attendant $\delta^{15}\text{N}$ lows suggest high nutrient content and possible past local dysoxia to anoxia (i.e. OMZ development; $\delta^{15}\text{N} < 3\text{‰}$). Indeed, in present day OMZs, when nitrate (NO_3^-) consumption does not reach completion, a net ^{15}N -enrichment of the residual NO_3^- pool is observed (Voss et al. 2001). In those environments, the water column produces low $\delta^{15}\text{N}$ organic matter as we observe during the MIS5 warm substages ($\delta^{15}\text{N}$ around 3-2.5 ‰) where $\delta^{15}\text{N}$ reached similar values than those observed during glacial maxima (i.e. MIS2 and MIS6a). All the above results suggest enhanced riverine inputs in the GoL and surrounding regions (including Corsica) during the warm substages of MIS5. This temporal decrease of riverine inputs during warm periods (i.e. $\delta^{13}\text{C}_{\text{org}}$ MIS5e > MIS5c > MIS5a) could reveal a possible forcing of the decreasing eccentricity through time, where more intense pluvial periods correspond to maximum of eccentricity (Figure 2).

3.2.3. Warm substages of the MIS6

The detailed observation of our proxies for MIS 6 reveals, based on the above consideration, enhanced river-

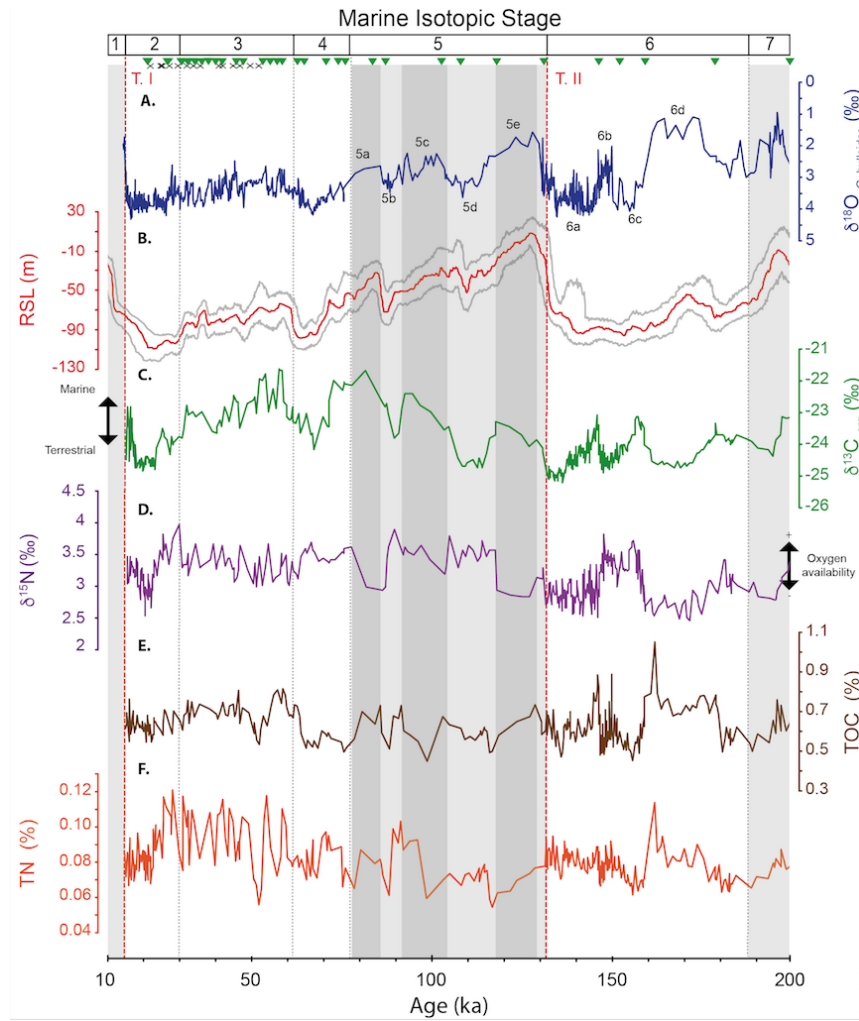


Figure 3: (A) $\delta^{18}\text{O}$ of planktonic species [*G. bullodes*] from PRGL1-4 (Sierra et al. 2009); (B) Red Sea sea level record (coreKL09, red curve, grey line corresponds to with maximum probability 95%, (Grant et al. 2014); (C) $\delta^{13}\text{C}_{\text{org}}$ of PRGL1-4, this study; (D) $\delta^{15}\text{N}_{\text{tot}}$ of PRGL1-4, this study; (E) % of Total Organic Carbon (TOC), this study; (F) % Total Nitrogen (TN). Top black crosses indicate C^{14} dating and green triangles indicate position of tie-points (see Table 1). Grey bands indicate interglacial conditions s.l, dark grey bands indicate interglacial warm-periods. Termination (T) according to (Barker et al. 2011). Scheme of marine stage according to (Railsback et al. 2015).

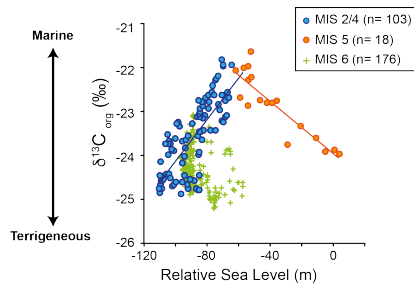


Figure 4: $\delta^{13}\text{C}_{\text{org}}$ versus Relative Sea Level reconstruction in Red Sea (Grant et al. 2014). Blue circles correspond to MIS2/4 values ($n=103$), orange diamond to warm substages of MIS5 ($n=18$) and green crosses to MIS6 ($n=176$)

ine inputs during MIS6 warm substages as well, i.e. MIS6d and b as revealed by low $\delta^{13}\text{C}_{\text{org}}$, low $\delta^{15}\text{N}$, high TOC; see **Figure 3.A.B.C.D.** Depleted planktic $\delta^{18}\text{O}$ values during these intervals corroborate our interpretation (black narrows on **Figure 2.B and C**). It is interesting to note that evidence for riverine inputs are not found in the PRGL1-4 record during MIS2/4 suggesting possible different mechanisms during the last two glacial periods.

4. Discussion

4.1. Regional significance

Specific episodes of enhanced preservation/proportion of land-derived material during the warm intervals of both MIS5 and MIS6 agree with high rainfall intervals recorded in speleothems in Spain (i.e. Gitana cave; Fig.5.b; Hodge et al. (2008)), southern France (i.e. Villars and Clamous caves speleothems growth phases Plagnes et al. 2002; Wainer et al. 2013) and in the Levant (i.e. Corchia, Tana Che Urla, Yammounneh, Pequin and Soreq caves; Fig.5.f and h; Ayalon et al. 2002; Bar-Matthews et al. 2003; Drysdale et al. 2005; Regattieri et al. 2014). These records revealed the regional character of the pluvial events, recorded as well in the GoL (Fig. 5). Recently, Regattieri et al. (2015) found wetter conditions in central Italy during the first half of the MIS5e, by using oxygen isotopic composition of the Sulmona paleo-lake carbonates (Fig.5.f). Similarly, Bard et al. (2002) revealed such pluvial conditions in the western Mediterranean basin during MIS6d, ca. 175 ka (Fig.5.f). These events are coeval with high runoff from North African river

systems, including the Nile River, and the sapropel deposition (Fig.5.g; Bard et al. 2002; Revel et al. 2010; Rohling et al. 2002; Ziegler et al. 2010b). If North African river runoff variability depends on the monsoon system and associated latitudinal ITCZ fluctuations (up to 25N, Rohling et al. 2002; Tuenter et al. 2003; see Fig.5.i), the GoL river runoff (43N) is controlled by the North Atlantic system and associated autumn/winter cyclogenesis activity (Moreno et al. 2005; Reale et al. 2001; Spotl et al. 2010; Struglia et al. 2004; Trigo et al. 2002). In agreement with previous studies (e.g. Bard et al. 2002; Milner et al. 2012; Rohling and Hilgen 1991; Toucanne et al. 2015), this suggests that rainfall in the Northern Mediterranean borderland and by extension the North Atlantic component may have been a primary source, in addition to the North African river systems, for sapropel formation through freshwater and organic matter inputs. Although this hypothesis is still debated (see Rohling et al. 2015 for a through discussion), the synchronicity between GoL runoff intervals and North African monsoon peaks highlights a close coupling between mid- and low-latitude climate systems as discussed in the following sections.

4.2. 1.1. High- low latitude coupling

Understanding the modern climatology over the North Atlantic, the Mediterranean and North Africa is necessary to explore the forcing for the synchronicity observed between GoL runoff intervals and North African monsoon peaks. Owing to its key location between the North Atlantic and Eastern Mediterranean, the modern GoL climate is under the influence of complex interactions resulting from North Atlantic atmospheric depressions and intra-basin climate variability (i.e. also called Mediterranean Oscillation, MO; Hurrell 1995; Martin-Vide and Lopez-Bustins 2006; Lopez-Bustins et al. 2008). North Atlantic Oscillation (NAO) is the dominant atmospheric process in the North Atlantic sector, including Western Mediterranean (Hurrell 1995; Trigo et al. 2002). Fluctuation of the NAO strongly affects the intensity of zonal flows over the North Atlantic (i.e. westerlies), the position of storm tracks and subsequent precipitation across Europe and the Mediterranean basin (Hurrell and Van Loon 1997; López-Moreno et al. 2011). NAO negative phases show a weakening of the Atlantic sea level pressure, which contributes to reduced westerly intensities and trajectories and enhancing penetration of warm and moist Atlantic air masses toward south-west Europe. Under such an atmospheric pattern, Southern Europe, the Iberian Peninsula and Northern Africa

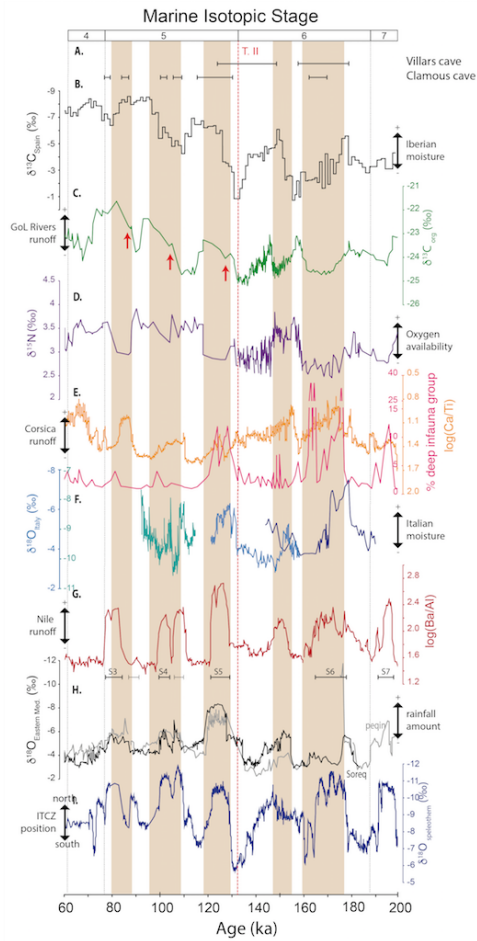


Figure 5: (A) Chronology of speleothem growth periods from Villars and Clamouse caves, they indicate humid period in South France (respectively (Plagnes et al. 2002); Wainer et al. 2011)); (B) $\delta^{13}\text{C}$ record at Gitana cave (Spain); (Hodge et al. 2008); (C) $\delta^{13}\text{C}_{\text{org}}$ of PRGL1-4, this study, Red arrows show the gradual increase of precipitation during MIS5 warm substages.; (D) $\delta^{15}\text{N}_{\text{tot}}$ of PRGL1-4, this study; (E) Abundance of benthic foraminifera deep-infauna group (pink line) and XRF Ti/Ca from Corsica borehole GDEC4 (orange line in log scale, (Toucanne et al. 2015); (F) $\delta^{18}\text{O}$ record from Tana Che urla (centrale Italy, light blue line; (Regattieri et al. 2014), Argentarola (Tyrrhenian coast of Italy, dark blue line, (Bard et al. 2002), Sulmona basin (aqua curve, (Regattieri et al. 2015); (G) XRF Ba/Al (log scale, ODP968 - south Cyprus, (Ziegler et al. 2010b)) and sapropel chronology (speleothem age-scale) according to (Ziegler et al. 2010b); (H) $\delta^{18}\text{O}$ record of Soreq (Central Israel, black line; (Bar-Matthews et al. 2003), Pepiin (north Israel; grey line (Bar-Matthews et al. 2003); (I) $\delta^{18}\text{O}$ from Sanbao / Hulu cave (Asia, (Wang et al. 2008). Brown bands indicate pluvial periods. Termination (T.) according to (Barker et al. 2011). Scheme of marine stage according to (Railsback et al. 2015).

experience anomalous cyclonic circulation which enhances precipitation, especially over North borderland mountains (López-Moreno et al. 2011; López-Moreno and Vicente-Serrano 2008). Our findings corroborate with recent PMIP3 model simulations for the early-mid Holocene that reveal enhanced southwesterly flowing moisture from the North Atlantic causing high precipitation during winters in the Mediterranean (Dixit et al. 2017). Besides the NAO, others atmospheric patterns also influence the Mediterranean climate. The Mediterranean itself is a source of moisture and subsequent eastward transport, by atmospheric advection toward the Eastern Mediterranean low pressure (i.e. Mediterranean Oscillation), implying a more complex situation especially in the Eastern Mediterranean sea where the role of NAO is weaker (Price et al. (1998)). On a wider scale, some studies also revealed close relationship between NAO and low latitude hydroclimate processes (North Africa, North Indian Ocean; e.g. Bader and Latif 2003; Moulin et al. 1997). In this context, and because of the buffer location of the GoL between the high and low latitudes, the forcing for the observed variability at PRGL1-4 over the last 200 kyr is difficult to constrain. Nevertheless, we propose that our records likely highlight low frequency NAO variability at orbital timescale, in agreement with modern relationship between river discharges and NAO forcing in western Mediterranean Sea (Struglia et al. 2004). We also suggest that NAO-negative-like phases occurred during warm substages (MIS5.a,c,e and MIS6.b and d), likewise NAO-positive-like conditions occurred during cold substages of the last 200 ka (MIS5.b and d and MIS6.a and c).

The latter pattern is supported by the modern variability of NAO rainfall pathways over Europe, considering that the European Alps present the main geographic boundary between the NAO-negative (i.e. south Alps and Mediterranean including the Rhone watershed) and NAO-positive mode (i.e. North Alps and North Europe; Hurrell 1995; Hurrell and Deser 2009). Moreover, this indicates the importance of the geographic boundary over the last two climatic cycles thereby explaining the record of well-defined wet (negative-NAO-like conditions) and dry (positive-NAO-like conditions) intervals around the GoL (vicinity of PRGL1-4 site) at an orbital timescale. The Rhone river is by far the main source of sediments in the GoL. Despite its relative low resolution, records obtained in PRGL1-4 borehole give for the first time a valuable, continuous long-term records of NAO variabilities over the Rhone watershed, which is complementary to lacustrine records widely used for NAO reconstructions despite their potential local signif-

icance (eg. Wilhelm et al. 2012).

5. Conclusion

In this study, we tackled an innovative approach using bulk isotope measurements to determine the nature of the organic matter preserved in the Gulf of Lion sediments, with the aim to better assess variations of rivers inputs during the Past 200 kyr. Our investigation reveals periods of high land-derived organic matter proportion/preservation indicative of high coastal rivers activities. Our findings point towards a high terrigenous flux in response to high precipitation level over the GoL watershed (mainly Rhône river influx). Comparison of PRGL1-4 proxies of high riverine inputs with regional records highlight the regional character of such wetter conditions well-preserved in PRGL1-4 sediment during the warm substages of the last 200 ka (i.e. MIS5.a,c,e and MIS6.b and d). Long-term variations in rainfall activity confirm the precessional component of the Mediterranean climate but also the impact of eccentricity modulation of precession on Mediterranean rainfall activity. Regarding the modern atmospheric forcing that impacts the GoL rivers discharges, we propose that a NAO-like forcing may explain the high rainfall activity periods recorded at PRGL1-4. During the warm substages, NAO-negative-like phases enhanced penetration of Atlantic depression into Western Mediterranean allowing increased river discharges due to high rainfall regimes over the North Mediterranean borderland. Repetition of this scheme through the last 200 kyr likely indicate the perpetuation of NAO atmospheric circulation, and rainbelt pathway over Europe (i.e. wetter conditions over South Europe and North Mediterranean borderland during NAO-negative mode). Thus, we assume that PRGL1-4 organic matter isotopic investigation brings a new and valuable record for regional NAO reconstruction in Western Mediterranean region.

Considering the fact that our reconstructed rainfall phases may have been synchronous with intense Nile river discharges and sapropels deposition (i.e. northward ITCZ position), our data suggest a strong atmospheric coupling between Mid- and Low- latitudes (i.e. ITCZ motion) and thus needs to be studied carefully for a better understanding of the Mediterranean climate.

6. Acknowledgments

The authors are warmly acknowledge O. Lebeau for assistance on the EA-IRMS in Brest; E. Regattieri, D. Genty that kindly provided data respec-

tively from Italian continental records and an European speleothems database; JP Suc; A. Cortina, F. Sierro for helpful discussions at various step of this work. S. Barker for providing us the most updated age model related to the Greenland synthetic $\delta^{18}\text{O}$ record GL_T-syn This work was supported by the "Laboratoire d'Excellence" LabexMER (ANR-10-LABX-19) and co-funded by a grant from the French government under the program "Investissements d'Avenir", and by a grant from the Regional Council of Brittany. The European Promess shipboard party and colleagues at Ifremer are also thanked for previous contributions of data acquisition and processing. All data reported in this study are available at PROMESS pangea website (<http://www.pangea.de/?q=PROMESS1>).

7. References

- Ader, M., Sansjofre, P., Halverson, G. P., Busigny, V., Trindade, R. I. F., Kunzmann, M., Nogueira, A. C. R., Jun, 2014. Ocean redox structure across the Late Neoproterozoic Oxygenation Event: A nitrogen isotope perspective. *Earth and Planetary Science Letters* 396 (C), 1–13.
- Ariztegui, D., Asioli, A., Lowe, J. J., Trincardi, F., 2000. Palaeoclimate and the formation of sapropel S1: inferences from Late Quaternary lacustrine and marine sequences in the central Mediterranean region. *Palaeogeography, Paleoclimatology, Paleoecology* 158 (3-4), 215–240.
- Arz, H. W., Lamy, F., Pätzold, J., Müller, P. J., Prins, M., 2003. Mediterranean moisture source for an early-Holocene humid period in the northern Red Sea. *Science* 300, 118–121.
- Ayalon, A., Bar-Matthews, M., Kaufman, A., 2002. Climatic conditions during marine oxygen isotope stage 6 in the eastern Mediterranean region from the isotopic composition of speleothems of Soreq Cave, Israel. *Geology* 30 (4), 303.
- Bader, J., Latif, M., Nov, 2003. The impact of decadal-scale Indian Ocean sea surface temperature anomalies on Sahelian rainfall and the North Atlantic Oscillation. *Geophysical Research Letters* 30 (22), 602–4.
- Bar-Matthews, M., Ayalon, A., Gilmour, M., 2003. Sea–land oxygen isotopic relationships from planktonic foraminifera and speleothems in the Eastern Mediterranean region and their implication for paleorainfall. *Geochimica et Cosmochimica Acta* 67 (17), 3181–3199.
- Bard, E., Delaygue, G., Rostek, F., Antonioli, F., 2002. Hydrological conditions over the western Mediterranean basin during the deposition of the cold Sapropel 6 (ca. 175 kyr BP). *Earth and Planetary Science Letters* 202, 481–494.
- Barker, S., Knorr, G., Edwards, R. L., Parrenin, F., 2011. 800,000 years of abrupt climate variability. *Science* 334, 347–351.
- Bassetti, M. A., Berné, S., Jouet, G., Taviani, M., 2008. The 100-ka and rapid sea level changes recorded by prograding shelf sand bodies in the Gulf of Lions (western Mediterranean Sea). *Geochemistry, Geophysics, Geosystems* 9 (11), 1–27.
- Baztan, J., Berné, S., Olivet, J. L., Rabineau, M., 2005. Axial incision: the key to understand submarine canyon evolution (in the western Gulf of Lion). *Marine and Petroleum Geology* 22, 805–826.
- Beaudouin, C., Suc, J.-P., Escarguel, G., Arnaud, M., Charmasson, S., Mar, 2007. The significance of pollen signal in present-day marine terrigenous sediments: The example of the Gulf of Lions (western Mediterranean Sea). *Geobios* 40 (2), 159–172.
- Berné, S., Gorini, C., Jun, 2005. The Gulf of Lions: An overview of recent studies within the French 'Margins' programme. *Marine and Petroleum Geology* 22 (6-7), 691–693.
- Bonneau, L., Jorry, S. J., Toucanne, S., Silva Jacinto, R., Emmanuel, L., Nov, 2014. Millennial-Scale Response of a Western Mediterranean River to Late Quaternary Climate Changes: A View from the Deep Sea. *The Journal of Geology* 122 (6), 687–703.
- Bosmans, J. H. C., Drijfhout, S. S., Tuenter, E., Hilgen, F. J., Lourens, L. J., Jan 2015. Response of the north african summer monsoon to precession and obliquity forcings in the ec-earth gem. *Climate Dynamics* 44 (1), 279–297.
- Cathalot, C., Rabouille, C., Pastor, L., Deflandre, B., 2010. Temporal variability of carbon recycling in coastal sediments influenced by rivers: assessing the impact of flood inputs in the Rhône River prodelta. *Biogeosciences* 7, 1187–1205.
- Cortina, A., Sierro, F. J., Flores, J. A., 2015. The response of SST to insolation and ice sheet variability from MIS 3 to MIS 11 in the northwestern Mediterranean Sea (Gulf of Lions). *Geophysical Research Letters* 42, 10366–10374.
- Cortina, A., Sierro, F. J., Gonzalez-Mora, B., Asioli, A., 2011. Impact of climate and sea level changes on the ventilation of intermediate water and benthic foraminifer assemblages in the Gulf of Lions, off South France, during MIS 6 and 7. *Palaeogeography, Paleoclimatology, Paleoecology* 309, 215–228.
- Coulthard, T. J., Ramirez, J. A., Barton, N., Rogerson, M., Brücher, T., Sep. 2013. Were Rivers Flowing across the Sahara During the Last Interglacial? Implications for Human Migration through Africa. *PLoS ONE* 8 (9), e74834.
- Dixit, Y., Toucanne, S., Tripathi, A., Lora, J., Fontanier, C., Pasquier, V., Bonnin, L., Jouet, G., 2017. Eccentricity forcing on the precession-derived Mediterranean rainfall during the past interglacials. In preparation.
- Drysdale, R. N., Zanchetta, G., Hellstrom, J. C., 2005. Stalagmite evidence for the onset of the Last Interglacial in southern Europe at 129±1 ka. *Geophysical Research Letters*.
- Grant, K. M., Rohling, E. J., Ramsey, C. B., Cheng, H., 2014. Sea-level variability over five glacial cycles. *Nature Communications* 5.
- Hodell, D., Crowhurst, S., Skinner, L., 2013. Response of Iberian Margin sediments to orbital and suborbital forcing over the past 420 ka. *Paleoceanography* 28 (1), 185–199.
- Hodge, E. J., Richards, D. A., Smart, P. L., Andreo, B., 2008. Effective precipitation in southern Spain (266 to 46 ka) based on a speleothem stable carbon isotope record. *Quaternary Research* 69, 447–457.
- Hurrell, J. W., Aug, 1995. Decadal Trends in the North Atlantic Oscillation: Regional Temperatures and Precipitation. *Science* 269 (5224), 676–679.
- Hurrell, J. W., Deser, C., 2009. North Atlantic climate variability: the role of the North Atlantic Oscillation. *Journal of Marine Systems* 78, 28–41.
- Hurrell, J. W., Van Loon, H., 1997. Decadal variations in climate associated with the North Atlantic Oscillation. *Climatic Change* 36, 301–326.
- Jouet, G., Berné, S., Rabineau, M., Bassetti, M. A., Bernier, P., Sep. 2006. Shoreface migrations at the shelf edge and sea-level changes around the Last Glacial Maximum (Gulf of Lions, NW Mediterranean). *Marine Geology* 234, 21–42.
- Kallel, N., Duplessy, J. C., Labeyrie, L., Fontugne, M., 2000. Mediterranean pluvial periods and sapropel formation over the last 200 000 years. *Palaeogeography, Paleoclimatology, Paleoecology* 157 (1-2), 45–58.
- Kallel, N., Paterne, M., Duplessy, J. C., 1997. Enhanced rainfall in the Mediterranean region during the last sapropel event. *Oceanologica acta* 20 (5), 697–712.

- Kim, J. H., Schouten, S., Buscail, R., 2006. Origin and distribution of terrestrial organic matter in the NW Mediterranean (Gulf of Lions): Exploring the newly developed BIT index. *Geochemistry, Geophysics, Geosystems* 7 (11), 1–20.
- Kutzbach, J. E., Chen, G., Cheng, H., Edwards, R. L., Liu, Z., Feb 2014. Potential role of winter rainfall in explaining increased moisture in the mediterranean and middle east during periods of maximum orbitally-forced insolation seasonality. *Climate Dynamics* 42 (3), 1079–1095.
- Laskar, J., Robutel, P., Joutel, F., Gastineau, M., Correia, A. C. M., Levrard, B., Dec. 2004. A long-term numerical solution for the insolation quantities of the Earth. *Astronomy & Astrophysics* 428 (1), 261–285.
- Leroux, E., Rabineau, M., Aslanian, D., Gorini, C., 2017. High-resolution evolution of terrigenous sediment yields in the Provence Basin during the last 6 Ma: relation with climate and tectonics. *Basin Research*, 1–35.
- Lofi, J., Rabineau, M., Gorini, C., Berne, S., Clauzon, G., De Clarens, P., Dos Reis, A. T., Mountain, G. S., Ryan, W. B., Steckler, M. S., et al., 2003. Plioquaternary prograding clinoform wedges of the western gulf of lion continental margin (nw mediterranean) after the messinian salinity crisis. *Marine Geology* 198 (3), 289–317.
- Lopez-Bustins, J.-A., Martin-Vide, J., Sanchez-Lorenzo, A., Sep. 2008. Iberia winter rainfall trends based upon changes in teleconnection and circulation patterns. *Global and Planetary Change* 63 (2-3), 171–176.
- López-Moreno, J. I., Vicente-Serrano, S. M., 2008. Positive and negative phases of the wintertime North Atlantic Oscillation and drought occurrence over Europe: a multitemporal-scale approach. *Journal of Climate* 21, 1220–1243.
- López-Moreno, J. I., Vicente-Serrano, S. M., Morán-Tejeda, E., Lorenzo-Lacruz, J., Kenawy, A., Beniston, M., May 2011. Effects of the North Atlantic Oscillation (NAO) on combined temperature and precipitation winter modes in the Mediterranean mountains: Observed relationships and projections for the 21st century. *Global and Planetary Change* 77 (1-2), 62–76.
- Magny, M., Nebout, N. C., 2013. Holocene changes in environment and climate in the central Mediterranean as reflected by lake and marine records. Preface. *Climate of the Past* 9, 1447–1454.
- Margari, V., Skinner, L. C., Hodell, D. A., Martrat, B., 2014. Land-ocean changes on orbital and millennial time scales and the penultimate glaciation. *Geology* 42 (3), 183–186.
- Mariotti, A., Arkin, P., 2007. The North Atlantic Oscillation and oceanic precipitation variability. *Climate Dynamics* 51, 28–35.
- Mariotti, A., Zeng, N., Lau, K. M., 2002. Euro-Mediterranean rainfall and ENSO—a seasonally varying relationship. *Geophysical Research Letters* 29 (12), 59–63.
- Martin-Vide, J., Lopez-Bustins, J.-A., 2006. The Western Mediterranean Oscillation and rainfall in the Iberian Peninsula. *International Journal of Climatology* 26 (11), 1455–1475.
- Martrat, B., Grimalt, J. O., Shackleton, N. J., de Abreu, L., 2007. Four climate cycles of recurring deep and surface water destabilizations on the Iberian margin. *Science* 317 (502), 502–507.
- Mauffrey, M. A., Berné, S., Jouet, G., Giresse, P., Gaudin, M., 2015. Sea-level control on the connection between shelf-edge deltas and the Bourcart canyon head (western Mediterranean) during the last glacial/interglacial cycle. *Marine Geology* 370, 1–19.
- Meyers, P. A., 1994. Preservation of elemental and isotopic source identification of sedimentary organic matter. *Chemical Geology* 114, 289–302.
- Milner, A. M., Collier, R. E. L., Roucoux, K. H., Müller, U. C., Pross, J., Kalaitzidis, S., Christanis, K., Tzedakis, P. C., Sep. 2012. Enhanced seasonality of precipitation in the Mediterranean during the early part of the Last Interglacial. *Geology* 40 (10), 919–922.
- Moreno, A., Cacho, I., Canals, M., Grimalt, J. O., Sanchez Goñi, M. F., Shackleton, N., Sierro, F. J., Aug. 2005. Links between marine and atmospheric processes oscillating on a millennial time-scale. A multi-proxy study of the last 50,000yr from the Alboran Sea (Western Mediterranean Sea). *Quaternary Science Reviews* 24 (14-15), 1623–1636.
- Moulin, C., Lambert, C. E., Dulac, F., Dayan, U., 1997. Control of atmospheric export of dust from North Africa by the North Atlantic Oscillation. *Nature* 387, 691–694.
- Pasquier, V., Sansjofre, P., Rabineau, M., Houghton, J., Fike, D. A., 2017. Pyrite sulfur isotopes reveal glacial– interglacial environmental changes. In: *Proceedings of the National Academy of Sciences of the United States of America*. pp. 5941–5945.
- Plagnes, V., Causse, C., Genty, D., Paterne, M., 2002. A discontinuous climatic record from 187 to 74 ka from a speleothem of the Clamouse Cave (south of France). *Earth and Planetary Science Letters* 201 (1), 87–103.
- Preston, T., Owens, N., 1983. Interfacing an automatic elemental analyser with an isotope ratio mass spectrometer: the potential for fully automated total nitrogen and nitrogen-15 analysis. *Analyst* 108, 971–977.
- Price, C., Stone, L., Huppert, A., 1998. A possible link between El Niño and precipitation in Israel. *Geophysical Research Letters* 25 (21), 3963–3966.
- Rabineau, M., Berné, S., Aslanian, D., Olivet, J. L., 2005. Sedimentary sequences in the Gulf of Lion: a record of 100,000 years climatic cycles. *Marine Petroleum Geology* 22, 775–804.
- Rabineau, M., Berné, S., Ledrezen, E., Lericolais, G., 1998. 3D architecture of lowstand and transgressive Quaternary sand bodies on the outer shelf of the Gulf of Lion, France. *Marine and Petroleum Geology*.
- Rabineau, M., Berné, S., Olivet, J. L., Aslanian, D., 2006. Paleo sea levels reconsidered from direct observation of paleoshoreline position during Glacial Maxima (for the last 500,000 yr). *Earth and Planetary Science Letters* 252, 119–137.
- Rabineau, M., Leroux, E., Aslanian, D., Bache, F., Gorini, C., Moulin, M., Molliex, S., Droz, L., dos Reis, A. T., Rubino, J. L., Guillocheau, F., Olivet, J. L., Feb. 2014. Quantifying subsidence and isostatic readjustment using sedimentary paleomarkers, example from the Gulf of Lion. *Earth and Planetary Science Letters* 388 (C), 353–366.
- Radakovitch, O., Charmasson, S., Arnaud, M., 1999. 210 Pb and caesium accumulation in the Rhône delta sediments. *Estuarine, Coastal and Shelf Sciences* 48, 77–92.
- Railsback, L. B., Gibbard, P. L., Head, M. J., 2015. An optimized scheme of lettered marine isotope substages for the last 1.0 million years, and the climatostratigraphic nature of isotope stages and substages. *Quaternary Science Reviews* 111, 94–106.
- Rasmussen, S. O., Andersen, K. K., 2006. A new Greenland ice core chronology for the last glacial termination. *Journal of Geological Research* 111, 1–16.
- Reale, O., Feudale, L., Turato, B., 2001. Evaporative moisture sources during a sequence of floods in the Mediterranean region. *Geophysical Research Letters* 28 (10), 2085–2088.
- Regattieri, E., Giaccio, B., Zanchetta, G., 2015. Hydrological variability over the Apennines during the Early Last Glacial precession minimum, as revealed by a stable isotope record from Sulmona basin. *Central Journal of Quaternary Science* 30 (1), 19–31.
- Regattieri, E., Zanchetta, G., Drysdale, R. N., Isola, I., 2014. A continuous stable isotope record from the penultimate glacial maximum to the Last Interglacial (159–121ka) from Tana Che Urla Cave (Apuan Alps, central Italy). *Quaternary Research* 82 (4), 1–12.
- Revel, M., Ducassou, E., Grousset, F., Bernasconi, S., Migeon, S., Revillon, S., Masclé, J., Murat, A., Zaragosi, S., Bosch, D., 2010. 100,000 years of african monsoon variability recorded in sedi-

- ments of the Nile margin. *Quaternary Science Reviews* 29 (11), 1342–1362.
- Rohling, E. J., Cane, T. R., Cooke, S., Sprovieri, M., 2002. African monsoon variability during the previous interglacial maximum. *Earth and Planetary Science Letters* 202 (1), 61–75.
- Rohling, E. J., Hilgen, F. J., 1991. The eastern Mediterranean climate at times of sapropel formation: a review. *Geologie en Mijnbouw* 70, 253–264.
- Rohling, E. J., Marino, G., Grant, K. M., 2015. Mediterranean climate and oceanography, and the periodic development of anoxic events (sapropels). *Earth Science Reviews* 143, 62–97.
- Rossignol-Strick, M., 1983. African monsoons, an immediate climate response to orbital insolation. *Nature* 304 (5921), 46–49.
- Rossignol-Strick, M., 1985. Mediterranean Quaternary sapropels, an immediate response of the African monsoon to variation of insolation. *Palaeogeography, Paleoclimatology, Paleocology* 49 (3–4), 237–263.
- Serreze, M. C., Carse, F., Barry, R. G., 1997. Icelandic low cyclone activity: Climatological features, linkages with the NAO, and relationships with recent changes in the Northern Hemisphere circulation. *Journal of Climate* 10 (3), 453–464.
- Sierro, F. J., Andersen, N., Bassetti, M. A., Berné, S., 2009. Phase relationship between sea level and abrupt climate change. *Quaternary Science Reviews* 28, 2867–2881.
- Sierro, F. J., Ledesma, S., Flores, J. A., Torrescusa, S., 2000. Sonic and gamma-ray astrochronology: cycle to cycle calibration of Atlantic climatic records to Mediterranean sapropels and astronomical oscillations. *Geology* 28 (8), 695.
- Spotl, C., Nicolussi, K., Patzelt, G., Boch, R., 2010. Humid climate during deposition of sapropel 1 in the Mediterranean Sea: Assessing the influence on the Alps. *Global and Planetary Change* 71, 242–248.
- Struglia, M. V., Mariotti, A., Filograsso, A., 2004. River discharge into the Mediterranean Sea: climatology and aspects of the observed variability. *Journal of Climate* 17, 4740–4751.
- Svensson, A., Andersen, K. K., Bigler, M., 2008. A 60 000 year Greenland stratigraphic ice core chronology. *Climate of the Past* 4, 47–57.
- Tesi, T., Miserocchi, S., Goñi, M. A., Langone, L., 2007. Source, transport and fate of terrestrial organic carbon on the western Mediterranean Sea, Gulf of Lions, France. *Marine Chemistry* 105, 101–117.
- Tesson, M., Gensous, B., Allen, G. P., Ravenne, C., 1990. Late Quaternary deltaic lowstand wedges on the Rhône continental shelf, France. *Marine Geology* 91 (4), 325–332.
- Toucanne, S., Minto'o, C., Fontanier, C., 2015. Tracking rainfall in the northern Mediterranean borderlands during sapropel deposition. *Quaternary Science Reviews* 129, 178–195.
- Trigo, I. F., Bigg, G. R., Davies, T. D., 2002. Climatology of cyclogenesis mechanisms in the Mediterranean. *Monthly Weather Review*, 549–569.
- Tuenter, E., Weber, S. L., Hilgen, F. J., Lourens, L. J., May 2003. The response of the African summer monsoon to remote and local forcing due to precession and obliquity. *Global and Planetary Change* 36 (4), 219–235.
- Tzedakis, P. C., 2007. Seven ambiguities in the Mediterranean palaeoenvironmental narrative. *Quaternary Science Reviews* 26, 2042–2066.
- Tzedakis, P. C., Hooghiemstra, H., Pälike, H., 2006. The last 1.35 million years at Tenaghi Philippon: revised chronostratigraphy and long-term vegetation trends. *Quaternary Science Reviews* 25, 3416–3430.
- Voss, M., Dippner, J. W., Montoya, J. P., 2001. Nitrogen isotope patterns in the oxygen-deficient waters of the Eastern Tropical North Pacific Ocean. *Deep Sea Research Part I* 48, 1905–1921.
- Wainer, K., Genty, D., Blamart, D., Bar-Matthews, M., Quinif, Y., Plagnes, V., Apr. 2013. Millennial climatic instability during penultimate glacial period recorded in a south-western France speleothem. *Palaeogeography, Paleoclimatology, Paleocology* 376 (C), 122–131.
- Wainer, K., Genty, D., Blamart, D., Daëron, M., 2011. Speleothem record of the last 180 ka in Villars cave (SW France): Investigation of a large δ 18 O shift between MIS6 and MIS5. *Quaternary Science Reviews* 30, 130–146.
- Wang, Y., Cheng, H., Edwards, R. L., Kong, X., Shao, X., 2008. Millennial-and orbital-scale changes in the East Asian monsoon over the past 224,000 years. *Nature* 451, 1090–1093.
- Wilhelm, B., Arnaud, F., Sabatier, P., Crouzet, C., 2012. 1400 years of extreme precipitation patterns over the Mediterranean French Alps and possible forcing mechanisms. *Quaternary ...* 78 (01), 1–12.
- Zanchetta, G., Drysdale, R. N., Hellstrom, J. C., 2007. Enhanced rainfall in the Western Mediterranean during deposition of sapropel S1: stalagmite evidence from Corchia cave (Central Italy). *Quaternary Science Reviews* 26, 279–286.
- Ziegler, M., Lourens, L. J., Tuenter, E., Hilgen, F., Reichert, G.-J., Weber, N., Sep. 2010a. Precession phasing offset between Indian summer monsoon and Arabian Sea productivity linked to changes in Atlantic overturning circulation. *Paleoceanography* 25 (3), 732–16.
- Ziegler, M., Tuenter, E., Lourens, L. J., 2010b. The precession phase of the boreal summer monsoon as viewed from the eastern Mediterranean (ODP Site 968). *Quaternary Science Reviews* 29, 1481–1490.

4. Implication for sapropel history

As we already discuss earlier, the origin of sapropel, and more precisely the source for freshwater, nutrient and continental organic matter inputs has long been debated (Rohling et al. 2015). Since the 1970's the idea of high runoff resulting from (i) ice-sheet and regional ice-cap (i.e. Ryan and Cita 1977) and/or (ii) high summer monsoon precipitations through the southern Mediterranean borderland (i.e. Rossignol-Strick 1983, 1985) have been inferred to be the pacemaker of sapropel deposition. Few years later, Rohling and Hilgen (1991) first recognized significant precipitation over the north-Mediterranean borderland, then several works point out high rivers activities during S1 over the north Eastern Mediterranean borderland (Tzedakis 2007; Casford et al. 2003 among others). All those evidences for high rainfall regime over the entire eastern Mediterranean basin were later confirmed by the Mediterranean origin of rainfall in Levant cave speleothems over the last 250 kyr (Bar-Matthews et al. 2003).

At this point, the western part of the Mediterranean Sea was not considered as a potential actor in Sapropel history. Although, first evidences of enhanced precipitation over the north western Mediterranean borderland was revealed during S1 (Ariztegui et al. 2000; Magny et al. 2003; Zanchetta et al. 2007), S4 (Regattieri et al. 2015, 2017b), S5 (Drysdale et al. 2005; Kallel et al. 2000), S6 (Bard et al. 2002), S7 (Kallel et al. 2000), S8 and S9 (Toucanne et al. 2015). Such findings suggested that the increase precipitation was not restricted to the eastern basin.

The correlation of PRGL 1-4 South France high rainfall activity with a wide variety of discontinuous records for high rainfall activity combine with the long records from Corsica confirmed strong cyclogenesis activity over the North Mediterranean borderland during sapropel deposition. Taking advantage of the location of PRGL 1-4 (i.e. off of the Mediterranean cyclogenetic region), we proposed that warm substages of the last 200 kyr are related to enhanced penetration of North Atlantic lows in the Mediterranean Sea (i.e. Reale et al. 2001; Rohling and Hilgen 1991; Toucanne et al. 2015). This provides an additional constraint on the role of the mid-latitude climate on the forcing leading to sapropel deposition, and confirm modelling results (Bosmans et al. 2015; Dixit et al., in review). First by increasing the amount of organic carbon reaching the sediment interface through high runoff, which in the case of the Gulf of Lion enhanced the primary production and therefore the marine settling flux as proposed by Rohling and Hilgen (1991) and Toucanne et al. (2015). Secondly, increase runoff in the Western basin, especially in the Gulf of Lion where deep waters are formed, should have strong implications in the hydrological changes necessary to disrupt the entire basin circulation. As a consequence, western Mediterranean runoff should be considered as freshwater suppliers, as the Nile and Wady system rivers (Scrivner et al. 2004; Meijer and Tuenter 2007; Toucanne et al. 2015) during warm interval of the last 200 kyr, and therefore as a possible forcing on sapropel deposition.

LITERATURE CITED

- Ariztegui, D., Asioli, A., Lowe, J. J., Trincardi, F., 2000. Palaeoclimate and the formation of sapropel S1: inferences from Late Quaternary lacustrine and marine sequences in the central Mediterranean region. *Palaeogeography, Paleoclimatology, Paleoecology* 158 (3-4), 215–240.
- Arz, H. W., Lamy, F., Pätzold, J., Müller, P. J., Prins, M., 2003. Mediterranean moisture source for an early-Holocene humid period in the northern Red Sea. *Science* 300, 118–121.
- Bar-Matthews, M., Ayalon, A., Gilmour, M., 2003. Sea–land oxygen isotopic relationships from planktonic foraminifera and speleothems in the Eastern Mediterranean region and their implication for paleorainfall during interglacial intervals. *Geochimica et Cosmochimica Acta* 67 (17), 3181–3199.
- Bar-Matthews, M., Ayalon, A., Kaufman, A., Wasserburg, G. J., 1999. The eastern mediterranean paleoclimate as a reflection of regional events: Soreq cave, israel. *Earth and Planetary Science Letters* 166 (1), 85 – 95.
- Bard, E., Delaygue, G., Rostek, F., Antonioli, F., 2002. Hydrological conditions over the western Mediterranean basin during the deposition of the cold Sapropel 6 (ca. 175 kyr BP). *Earth and Planetary Science Letters* 202, 481–494.
- Béranger, K., Mortier, L., Crépon, M., 2005. Seasonal variability of water transport through the straits of gibraltar, sicily and corsica, derived from a high-resolution model of the mediterranean circulation. *Progress in Oceanography*.
- Béranger, K., Mortier, L., Gasparini, G.-P., Gervasio, L., Astraldi, M., Crépon, M., 2004. The dynamics of the sicily strait: a comprehensive study from observations and models. *Deep Sea Research Part II: Topical Studies in Oceanography* 51 (4), 411–440.
- Bethoux, J. P., Gentili, B., 1999. Functioning of the Mediterranean Sea: past and present changes related to freshwater input and climate changes. *Journal of Marine Systems* 20, 33–47.
- Bjerknes, J., 1964. Atlantic air-sea interaction. *Advances in geophysics* 10, 1–82.
- Black, E., 2012. The influence of the north atlantic oscillation and european circulation regimes on the daily to interannual variability of winter precipitation in israel. *International Journal of Climatology* 32 (11), 1654–1664.
- Bosmans, J. H. C., Drijfhout, S. S., Tuentner, E., Hilgen, F. J., Lourens, L. J., Jan 2015. Response of the north african summer monsoon to precession and obliquity forcings in the ec-earth gcm. *Climate Dynamics* 44 (1), 279–297.
- Bouloubassi, I., Rullkötter, J., Meyers, P. A., 1999. Origin and transformation of organic matter in pliocenepleistocene mediterranean sapropels: organic geochemical evidence reviewed. *Marine Geology* 153 (1), 177 – 197.
- Boussetta, S., Kallel, N., Bassinot, F., Labeyrie, L., Duplessy, J.-C., Caillon, N., Dewilde, F., Rebaubier, H., May 2012. Mg/Ca-paleothermometry in the western Mediterranean Sea on planktonic foraminifer species *Globigerina bulloides*: Constraints and implications . *Compte Rendus Geosciences* 344 (5), 267–276.
- Box, M. R., Krom, M. D., Cliff, R. A., Bar-Matthews, M., Almogi-Labin, A., Ayalon, A., Paterno, M., Feb. 2011. Response of the Nile and its catchment to millennial-scale climatic change since the LGM from Sr isotopes and major elements of East Mediterranean sediments. *Quaternary Science Reviews* 30 (3-4), 431–442.
- Bryden, H. L., Kinder, T. H., 1991. Steady two-layer exchange through the strait of gibraltar. *Deep Sea Research Part A. Oceanographic Research Papers* 38 (Supplement 1), S445 – S463.
- Calvert, S., 1983. Geochemistry of pleistocene sapropels and associated sediments from the eastern mediterranean. *Oceanologica Acta* 6 (3), 255–267.
- Calvert, S. E., Nielsen, B., Fontugne, M. R., 1992. Evidence from nitrogen isotope ratios for enhanced productivity during formation of eastern Mediterranean sapropels. *Nature* 359, 223–225.
- Casford, J., Rohling, E., Abu-Zied, R., Fontanier, C., Jorissen, F., Leng, M., Schmiedl, G., Thomson, J., 2003. A dynamic concept for eastern mediterranean circulation and oxygenation during sapropel formation. *Palaeogeography, Palaeoclimatology, Palaeoecology* 190 (Supplement C), 103 – 119.
- Cita, M. B., Vergnaud-Grazzini, C., Robert, C., Chamley, H., Ciaranfi, N., d’Onofrio, S., 1977. Paleoclimatic record of a long deep sea core from the eastern mediterranean. *Quaternary Research* 8 (2), 205235.
- Comas, M., Zahn, R., Klaus, A., 1997. Proceedings, initial reports, ocean drilling program, leg 161,

- mediterranean sea ii, the western mediterranean. *Oceanographic Literature Review* 2 (44), 98.
- Corselli, C., Principato, M. S., Maffioli, P., Crudeli, D., 2002. Changes in planktonic assemblages during sapropel s5 deposition: Evidence from urania basin area, eastern mediterranean. *Paleoceanography* 17 (3), 1–1–1–30.
- Costa, K., Russell, J., Konecky, B., Lamb, H., Jan. 2014. *Quaternary Science Reviews*. *Quaternary Science Reviews* 83 (C), 58–67.
- Coulthard, T. J., Ramirez, J. A., Barton, N., Rogerson, M., Brücher, T., Sep. 2013. Were Rivers Flowing across the Sahara During the Last Interglacial? Implications for Human Migration through Africa. *PLoS ONE* 8 (9), e74834.
- Cramp, A., O’Sullivan, G., 1999. Neogene sapropels in the mediterranean: a review. *Marine Geology* 153 (1), 11 – 28.
- Dansgaard, W., 1964. Stable isotopes in precipitation. *Tellus* 16 (4), 436–468.
- Drysdale, R. N., Zanchetta, G., Hellstrom, J. C., 2005. Stalagmite evidence for the onset of the Last Interglacial in southern Europe at 129±1 ka. *Geophysical Research Letters*.
- Ducassou, E., Migeon, S., Mulder, T., Murat, A., Capotondi, L., Bernasconi, S. M., Mascle, J., 2009. Evolution of the Nile deep-sea turbidite system during the late quaternary: influence of climate change on fan sedimentation. *Sedimentology* 56 (7), 2061–2090.
- Düneloh, A., Jacobeit, J., Dec. 2003. Circulation dynamics of Mediterranean precipitation variability 1948–98. *International Journal of Climatology* 23 (15), 1843–1866.
- Emeis, K. C., Martin, H. M., sakamoto, T., Doose, H., Erlenkeuser, H., Howells, M. W., Krom, M. D., Paterne, M., 1998. Stable isotope and alkenone temperature records of sapropels from sites 964 and 967: Constraining the physical environment of sapropel formation in the eastern mediterranean sea. *Proceedings of Ocean Drillings Program, Scientific results* 160, 1–23.
- Emeis, K.-C., Schulz, H., Struck, U., Rossignol-Strick, M., Erlenkeuser, H., Howell, M. W., Kroon, D., Mackensen, A., Ishizuka, S., Oba, T., Sakamoto, T., Koizumi, I., 2003. Eastern mediterranean surface water temperatures and $\delta^{18}O$ composition during deposition of sapropels in the late quaternary. *Paleoceanography* 18 (1), n/a–n/a.
- Fichaut, M., Garcia, M., Giorgetti, A., Iona, A., Kuznetsov, A., Rixen, M., Group, M., 2003. Medar/medatlas 2002: A mediterranean and black sea database for operational oceanography. In: Dahlin, H., Flemming, N., Nittis, K., Petersson, S. (Eds.), *Building the European Capacity in Operational Oceanography*. Vol. 69 of Elsevier Oceanography Series. Elsevier, pp. 645 – 648.
- Fletcher, W. J., Debret, M., Goñi, M. F. S., 2013. Mid-holocene emergence of a low-frequency millennial oscillation in western mediterranean climate: Implications for past dynamics of the north atlantic atmospheric westerlies. *The Holocene* 23 (2), 153–166.
- Fontugne, M. R., Paterne, M., Calvert, S. E., Murat, A., Guichard, F., Arnold, M., 1989. Adriatic deep water formation during the holocene: Implication for the reoxygenation of the deep eastern mediterranean sea. *Paleoceanography* 4 (2), 199–206.
- Garrett, C., 1996. The role of the strait of gibraltar in the evolution of mediterranean water, properties and circulation. *Bulletin Institut Oceanographic Monaco Numero Special*, 1–20.
- Gat, J., Carmi, I., 1970. Evolution of the isotopic composition of atmospheric waters in the mediterranean sea area. *Journal of Geophysical Research* 75 (15), 3039–3048.
- Giraudi, C., Magny, M., Zanchetta, G., Drysdale, R., 2011. The holocene climatic evolution of mediterranean italy: A review of the continental geological data. *The Holocene* 21 (1), 105–115.
- Goodess, C., Jones, P., 2002. Links between circulation and changes in the characteristics of iberian rainfall. *International Journal of Climatology* 22 (13), 1593–1615.
- Goodfriend, G. A., 1991. Holocene trends in $\delta^{18}O$ in land snail shells from the negev desert and their implications for changes in rainfall source areas. *Quaternary Research* 35 (3-Part1), 417–426.
- Grant, K. M., Grimm, R., Mikolajewicz, U., Marino, G., 2016. The timing of Mediterranean sapropel deposition relative to insolation, sea-level and African monsoon changes. *Quaternary Science Reviews* 140, 125–141.
- Grimm, R., Maier-Reimer, E., Mikolajewicz, U., Schmiedl, G., Müller-Navarra, K., Adloff, F., Grant, K. M., Ziegler, M., Lourens, L. J., Emeis, K.-C., Jun. 2015. Late glacial initiation of Holocene eastern Mediterranean sapropel formation. *Nature Communications* 6, 7099.
- Gktrk, O., Fleitmann, D., Badertscher, S., Cheng, H., Edwards, R., Leuenberger, M., Fankhauser, A., Tysz, O., Kramers, J., 2011. Climate on the southern black sea coast during the holocene: implications from the sofular cave record. *Quaternary Science Reviews* 30 (19), 2433 – 2445.
- Haven, H., Baas, M., Kroot, M., de Leeuw, J., Schenck, P., Ebbing, J., 1987. Late quaternary

- mediterranean sapropels. iii: Assessment of source of input and palaeotemperature as derived from biological markers. *Geochimica et Cosmochimica Acta* 51 (4), 803 – 810.
- Hernández-Molina, F. J., Stow, D., 2014. Onset of Mediterranean outflow into the North Atlantic. *Science* 344 (6189), 1244–1250.
- Higgins, M. B., Robinson, R. S., Carter, S. J., Pearson, A., 2010. Evidence from chlorin nitrogen isotopes for alternating nutrient regimes in the eastern mediterranean sea. *Earth and Planetary Science Letters* 290 (12), 102 – 107.
- Hilgen, F., 1991. Astronomical calibration of gauss to matuyama sapropels in the mediterranean and implication for the geomagnetic polarity time scale. *Earth and Planetary Science Letters* 104 (2), 226 – 244.
- Hilgen, F. J., Krijgsman, W., Langereis, C. G., Lourens, L. J., 1997. Breakthrough made in dating of the geological record. *Eos, Transactions American Geophysical Union* 78 (28), 285–289.
- Hilgen, F. J., Lourens, L. J., Berger, A., Loutre, M. F., 1993. Evaluation of the astronomically calibrated time scale for the late pliocene and earliest pleistocene. *Paleoceanography* 8 (5), 549–565.
- Hood, R. R., Michaels, A. F., Capone, D. G., 2000. Answers sought to the enigma of marine nitrogen fixation. *Eos, Transactions American Geophysical Union* 81 (13), 133–139.
- Hurrell, J. W., Aug. 1995. Decadal Trends in the North Atlantic Oscillation: Regional Temperatures and Precipitation. *Science* 269 (5224), 676–679.
- Ji, A., OK, B., TP, B., HE, G., AI, G., RA, L., AV, M., Seidov, D., Smolyar, I., et al., 2013. The world ocean database 2009. volume2: Salinity. *Data Science Journal* 12, WDS229–WDS234.
- Jorissen, F. J., 1999. Benthic foraminiferal successions across late quaternary mediterranean sapropels. *Marine Geology* 153 (1), 91 – 101.
- Josey, S. A., Somot, S., Tsimplis, M., Feb. 2011. Impacts of atmospheric modes of variability on Mediterranean Sea surface heat exchange. *Journal of Geophysical Research* 116 (C2), 170–15.
- Kallel, N., Duplessy, J. C., Labeyrie, L., Fontugne, M., 2000. Mediterranean pluvial periods and sapropel formation over the last 200 000 years. *Palaeogeography, Paleoclimatology, Paleoecology* 157 (1-2), 45–58.
- Kallel, N., Paterne, M., Duplessy, J. C., 1997a. Enhanced rainfall in the Mediterranean region during the last sapropel event. *Oceanologica acta* 20 (5), 697–712.
- Kallel, N., Paterne, M., Labeyrie, L., Duplessy, J.-C., Arnold, M., 1997b. Temperature and salinity records of the tyrrhenian sea during the last 18,000 years. *Palaeogeography, Palaeoclimatology, Paleoecology* 135 (1), 97 – 108.
- Kemp, A. E., Pike, J., Pearce, R. B., Lange, C. B., 2000. The fall dump a new perspective on the role of a shade flora in the annual cycle of diatom production and export flux. *Deep Sea Research Part II: Topical Studies in Oceanography* 47 (9), 2129 – 2154.
- Kidd, R. B., 1978. Stratigraphy of eastern mediterranean sapropel sequences recovered during leg 42a and their paleoenvironmental significance. *Initial Report of Deep Sea Drilling Project* 42, 421–443.
- Kinder, T. H., Parrilla, G., 1987. Yes, some of the mediterranean outflow does come from great depth. *Journal of Geophysical Research: Oceans* 92 (C3), 2901–2906.
- Knight, J. R., Folland, C. K., Scaife, A. A., 2006. Climate impacts of the atlantic multidecadal oscillation. *Geophysical Research Letters* 33 (17).
- Kotthoff, U., Mller, U. C., Pross, J., Schmiedl, G., Lawson, I. T., van de Schootbrugge, B., Schulz, H., 2008. Lateglacial and holocene vegetation dynamics in the aegean region: an integrated view based on pollen flora from marine and terrestrial archives. *The Holocene* 18 (7), 1019–1032.
- Kutzbach, J. E., Chen, G., Cheng, H., Edwards, R. L., Liu, Z., Feb 2014. Potential role of winter rainfall in explaining increased moisture in the mediterranean and middle east during periods of maximum orbitally-forced insolation seasonality. *Climate Dynamics* 42 (3), 1079–1095.
- Lamy, F., Arz, H. W., Bond, G. C., Bahr, A., 2006. Multicentennial-scale hydrological changes in the Black Sea and northern Red Sea during the Holocene and the Arctic/North Atlantic Oscillation. *Paleoceanography* 21, 1–11.
- Larrasoana, J. C., Roberts, A. P., Rohling, E. J., Winkhofer, M., Wehausen, R., Dec 2003. Three million years of monsoon variability over the northern sahara. *Climate Dynamics* 21 (7), 689–698.
- Leroux, E., May 2012. Quantification of sediment fluxes and subsidence on the Gulf of lion margin. Theses, Université de Bretagne occidentale - Brest.
- Levitus, S., Ji, A., OK, B., TP, B., HE, G., AI, G., RA, L., AV, M., Seidov, D., Smolyar, I., et al.,

2013. The world ocean database. *Data Science Journal* 12, WDS229–WDS234.
- Lionello, P., Malanotte-Rizzoli, P., Boscolo, R., 2006. The Mediterranean climate: an overview of the main characteristics and issues. *Mediterranean* 4, 1–26.
- Lolis, C. J., Bartzokas, A., Katsoulis, B. D., 2002. Spatial and temporal 850 hPa air temperature and sea-surface temperature covariances in the Mediterranean region and their connection to atmospheric circulation. *International Journal of Climatology* 22 (6), 663–676.
- Lopez-Bustins, J.-A., Martin-Vide, J., Sanchez-Lorenzo, A., Sep. 2008. Iberia winter rainfall trends based upon changes in teleconnection and circulation patterns. *Global and Planetary Change* 63 (2-3), 171–176.
- Lourens, L., Hilgen, F., Gudjonsson, L., Zachariasse, W., 1992. Late pliocene to early pleistocene astronomically forced sea surface productivity and temperature variations in the mediterranean. *Marine Micropaleontology* 19 (1-2), 49–78.
- Lourens, L. J., Antonarakou, A., Hilgen, F. J., Van Hoof, A. A. M., Vergnaud-Grazzini, C., Zachariasse, W. J., 1996. Evaluation of the plio-pleistocene astronomical timescale. *Paleoceanography* 11 (4), 391–413.
- Magny, M., 2004. Holocene climate variability as reflected by mid-european lake-level fluctuations and its probable impact on prehistoric human settlements. *Quaternary international* 113 (1), 65–79.
- Magny, M., Bégeot, C., Guiot, J., Peyron, O., 2003. Contrasting patterns of hydrological changes in europe in response to holocene climate cooling phases. *quaternary science reviews* 22 (15), 1589–1596.
- Magny, M., de Beaulieu, J.-L., Drescher-Schneider, R., Vanni re, B., Walter-Simonnet, A.-V., Millet, L., Bossuet, G., Peyron, O., 2006. Climatic oscillations in central italy during the last glacial–holocene transition: the record from lake accessa. *Journal of Quaternary Science* 21 (4), 311–320.
- Magny, M., Nebout, N. C., 2013. Holocene changes in environment and climate in the central Mediterranean as reflected by lake and marine records. Preface. *Climate of the Past* 9, 1447–1454.
- Margari, V., Skinner, L. C., Hodell, D. A., Martrat, B., 2014. Land-ocean changes on orbital and millennial time scales and the penultimate glaciation. *Geology* 42 (3), 183–186.
- Marino, G., Rohling, E., Rodr guez-Sanz, L., Grant, K., Heslop, D., Roberts, A., Stanford, J., Yu, J., 2015. Bipolar seesaw control on last interglacial sea level. *Nature* 522 (7555), 197.
- Marino, G., Rohling, E. J., Sangiorgi, F., Hayes, A., Casford, J. L., Lotter, A. F., Kucera, M., Brinkhuis, H., 2009. Early and middle holocene in the aegean sea: interplay between high and low latitude climate variability. *Quaternary Science Reviews* 28 (27), 3246 – 3262.
- Mariotti, A., Arkin, P., 2007. The North Atlantic Oscillation and oceanic precipitation variability. *Climate Dynamics* 51, 28–35.
- Martin-Vide, J., Lopez-Bustins, J.-A., 2006. The Western Mediterranean Oscillation and rainfall in the Iberian Peninsula. *International Journal of Climatology* 26 (11), 1455–1475.
- Matthews, A., Ayalon, A., Bar-Matthews, M., May 2000. D/H ratios of fluid inclusions of Soreq cave (Israel) speleothems as a guide to the Eastern Mediterranean Meteoric Line relationships in the last 120 ky. *Chemical Geology* 166 (3-4), 183–191.
- Mazor, E., et al., 1991. Chemical and isotopic groundwater hydrology: the applied approach. No. Ed. 2. Marcel Dekker Inc.
- McGarry, S., Bar-Matthews, M., Matthews, A., Vaks, A., Schilman, B., Ayalon, A., Apr. 2004. Constraints on hydrological and paleotemperature variations in the Eastern Mediterranean region in the last 140ka given by the δD values of speleothem fluid inclusions. *Quaternary Science Reviews* 23 (7-8), 919–934.
- Meijer, P. T., Tuenter, E., 2007. The effect of precession-induced changes in the mediterranean freshwater budget on circulation at shallow and intermediate depth. *Journal of Marine Systems* 68 (3), 349–365.
- Mercone, D., Thomson, J., Abu-Zied, R., Croudace, I., Rohling, E., 2001. High-resolution geochemical and micropalaeontological profiling of the most recent eastern mediterranean sapropel. *Marine Geology* 177 (1), 25 – 44.
- Millot, C., 1999. Circulation in the western Mediterranean Sea. *Journal of Marine Systems* 20, 423–442.
- Milner, A. M., Collier, R. E. L., Roucoux, K. H., M ller, U. C., Pross, J., Kalaitzidis, S., Christanis, K., Tzedakis, P. C., Sep. 2012. Enhanced seasonality of precipitation in the Mediterranean during

- the early part of the Last Interglacial. *Geology* 40 (10), 919–922.
- Möbius, J., Lahajnar, N., Emeis, K.-C., 2010. Diagenetic control of nitrogen isotope ratios in holocene sapropels and recent sediments from the eastern mediterranean sea. *Biogeosciences* 7 (11), 3901–3914.
- Moller, T., Schulz, H., Hamann, Y., Dellwig, O., Kucera, M., 2012. Sedimentology and geochemistry of an exceptionally preserved last interglacial sapropel s5 in the levantine basin (mediterranean sea). *Marine Geology* 291 (Supplement C), 34 – 48.
- Murat, A., 1999. 41. Pliocene–Pleistocene occurrence of sapropels in the western Mediterranean Sea and their relation to eastern Mediterranean sapropels. *Proceedings of the Ocean Drilling Program Scientific . . .*
- MURAT, A., GOT, H., 1987. Middle and late quaternary depositional sequences and cycles in the eastern mediterranean. *Sedimentology* 34 (5), 885–899.
- Murat, A., Got, H., 2000. Organic carbon variations of the eastern mediterranean holocene sapropel: a key for understanding formation processes. *Palaeogeography, Palaeoclimatology, Palaeoecology* 158 (3), 241 – 257.
- Nijenhuis, I., Bosch, H.-J., Damst, J. S., Brumsack, H.-J., Lange, G. D., 1999. Organic matter and trace element rich sapropels and black shales: a geochemical comparison. *Earth and Planetary Science Letters* 169 (34), 277 – 290.
- Nijenhuis, I. A., de Lange, G., 2000. Geochemical constraints on pliocene sapropel formation in the eastern mediterranean. *Marine Geology* 163 (14), 41 – 63.
- Nijenhuis, I. A., Schenau, S. J., Van der Weijden, C. H., Hilgen, F. J., Lourens, L. J., Zachariasse, W. J., 1996. On the origin of upper miocene sapropelites: A case study from the faneromeni section, crete (greece). *Paleoceanography* 11 (5), 633–645.
- Osborne, A., Marino, G., Vance, D., Rohling, E., 2010. Eastern mediterranean surface water nd during eemian sapropel s5: monitoring northerly (mid-latitude) versus southerly (sub-tropical) freshwater contributions. *Quaternary Science Reviews* 29 (1920), 2473 – 2483, special Theme: Case Studies of Neodymium Isotopes in Paleoceanography.
- Osborne, A. H., Vance, D., Rohling, E. J., Barton, N., Rogerson, M., Fello, N., 2008. A humid corridor across the sahara for the migration of early modern humans out of africa 120,000 years ago. *Proceedings of the National Academy of Sciences* 105 (43), 16444–16447.
- Passier, H. F., Bosch, H.-J., Nijenhuis, I. A., Lourens, L. J., Böttcher, M. E., Leenders, A., Damsté, J. S. S., de Lange, G. J., Leeuw, J. W., Jan. 1999a. Sulphidic Mediterranean surface waters during Pliocene sapropel formation. *Nature* 397 (6715), 146–149.
- Passier, H. F., Middelburg, J. J., de Lange, G. J., Bttcher, M. E., 1999b. Modes of sapropel formation in the eastern mediterranean: some constraints based on pyrite properties. *Marine Geology* 153 (14), 199 – 219.
- Pearce, R. B., Kemp, A. E., Koizumi, I., Pike, J., Cramp, A., Rowland, S., 1998. A lamina-scale, sem-based study of a late quaternary diatom-ooze sapropel from the mediterranean ridge, site 971. In: *Proceedings of the Ocean Drilling Program. Scientific results. Vol. 160. Ocean Drilling Program*, pp. 349–363.
- Piccini, L., Zanchetta, G., Drysdale, R. N., Hellstrom, J., Isola, I., Fallick, A. E., Leone, G., Doveri, M., Mussi, M., Mantelli, F., Molli, G., Lotti, L., Roncioni, A., Regattieri, E., Meccheri, M., Vaselli, L., Nov. 2008. The environmental features of the Monte Corchia cave system (Apuan Alps, central Italy) and their effects on speleothem growth. *International Journal of Speleology* 37 (3), 153–172.
- Pinardi, N., Zavatarelli, M., Adani, M., Coppini, G., Fratianni, C., Oddo, P., Simoncelli, S., Tonani, M., Lyubartsev, V., Dobricic, S., et al., 2015. Mediterranean sea large-scale low-frequency ocean variability and water mass formation rates from 1987 to 2007: A retrospective analysis. *Progress in Oceanography* 132, 318 – 332, *oceanography of the Arctic and North Atlantic Basins*.
- Piva, A., Asoli, A., Schneider, R. R., Trincardi, F., Andersen, N., Colmenero-Hidalgo, E., Denielou, B., Flores, J.-A., Vigliotti, L., 2008. Climatic cycles as expressed in sediments of the promess1 borehole prad1-2, central adriatic, for the last 370 ka: 1. integrated stratigraphy. *Geochemistry, Geophysics, Geosystems* 9 (1), n/a–n/a.
- Potonié, H., 1904. Über faulschlamm-(sapropel)-gesteine. *Sitz. Gesell. nat. F. Berlin*, 243–245.
- Reale, O., Feudale, L., Turato, B., 2001. Evaporative moisture sources during a sequence of floods in the Mediterranean region. *Geophysical Research Letters* 28 (10), 2085–2088.
- Regattieri, E., Giaccio, B., Nomade, S., Francke, A., Vogel, H., Drysdale, R. N., Perchiazzi, N.,

- Wagner, B., Gemelli, M., Mazzini, I., Boschi, C., Galli, P., Peronace, E., 2017a. A last interglacial record of environmental changes from the sulmona basin (central italy). *Palaeogeography, Palaeoclimatology, Palaeoecology* 472 (Supplement C), 51 – 66.
- Regattieri, E., Giaccio, B., Nomade, S., Francke, A., Vogel, H., Drysdale, R. N., Perchiazzi, N., Wagner, B., Gemelli, M., Mazzini, I., et al., 2017b. A last interglacial record of environmental changes from the sulmona basin (central italy). *Palaeogeography, Palaeoclimatology, Palaeoecology* 472, 51–66.
- Regattieri, E., Giaccio, B., Zanchetta, G., 2015. Hydrological variability over the Apennines during the Early Last Glacial precession minimum, as revealed by a stable isotope record from Sulmona basin, Central *Journal of Quaternary Science* 30 (1), 19–31.
- Regattieri, E., Isola, I., Zanchetta, G., 2012. Stratigraphy, petrography and chronology of speleothem concretion at Tana Che Urla (Lucca, Italy): paleoclimatic implications. *Geografia Fisica e Dinamica Quaternaria* 32, 141–152.
- Regattieri, E., Zanchetta, G., Drysdale, R. N., Isola, I., 2014. A continuous stable isotope record from the penultimate glacial maximum to the Last Interglacial (159–121ka) from Tana Che Urla Cave (Apuan Alps, central Italy). *Quaternary Research* 82 (4), 1–12.
- Regattieri, E., Zanchetta, G., N. Drysdale, R., Isola, I., Woodhead, J. D., Hellstrom, J. C., Giaccio, B., Greig, A., Banerjee, I., Dotsika, E., 2016. Environmental variability between the penultimate deglaciation and the mid eemian: Insights from tana che urla (central italy) speleothem trace element record. *Quaternary Science Reviews* 152 (Supplement C), 80 – 92.
- Revel, M., Ducassou, E., Grousset, F., Bernasconi, S., Migeon, S., Revillon, S., Mascle, J., Murat, A., Zaragosi, S., Bosch, D., 2010. 100,000 years of african monsoon variability recorded in sediments of the Nile margin. *Quaternary Science Reviews* 29 (11), 1342 – 1362.
- Roberts, N., Brayshaw, D., Kuzucuolu, C., Perez, R., Sadori, L., 2011. The mid-holocene climatic transition in the mediterranean: Causes and consequences. *The Holocene* 21 (1), 3–13.
- Roberts, N., Jones, M., Benkaddour, A., Eastwood, W. J., Filippi, M. L., Frogley, M. R., Lamb, H. F., Leng, M. J., Reed, M. J., Stein, M., Stevens, L., Valero-Garcés, B., Zanchetta, G., 2008. Stable isotope records of late quaternary climate and hydrology from mediterranean lakes: the isomed synthesis. *Quaternary Science Reviews* 27 (25), 2426 – 2441.
- Rodó, X., Baert, E., Comin, F., 1997. Variations in seasonal rainfall in southern Europe during the present century: relationships with the north atlantic oscillation and the El Niño-southern oscillation. *Climate Dynamics* 13 (4), 275–284.
- Rogerson, M., Cacho, I., Jimenez-Espejo, F., Reguera, M. I., Sierro, F. J., Martínez-Ruiz, F., Frigola, J., Canals, M., 2008. A dynamic explanation for the origin of the western mediterranean organic-rich layers. *Geochemistry, Geophysics, Geosystems* 9 (7).
- Rohling, E., Foster, G. L., Grant, K., Marino, G., Roberts, A., Tamisiea, M. E., Williams, F., 2014. Sea-level and deep-sea-temperature variability over the past 5.3 million years. *Nature* 508 (7497), 477.
- Rohling, E., Medina-Elizalde, M., Shepherd, J., Siddall, M., Stanford, J., 2012. Sea surface and high-latitude temperature sensitivity to radiative forcing of climate over several glacial cycles. *Journal of Climate* 25 (5), 1635–1656.
- Rohling, E., Sprovieri, M., Cane, T., Casford, J., Cooke, S., Bouloubassi, I., Emeis, K., Schiebel, R., Rogerson, M., Hayes, A., Jorissen, F., Kroon, D., 2004. Reconstructing past planktic foraminiferal habitats using stable isotope data: a case history for mediterranean sapropel 5. *Marine Micropaleontology* 50 (1), 89 – 123.
- Rohling, E. J., Cane, T. R., Cooke, S., Sprovieri, M., 2002. African monsoon variability during the previous interglacial maximum. *Earth and Planetary Science Letters* 202 (1), 61–75.
- Rohling, E. J., Grant, K. M., Roberts, A. P., Larrasoána, J.-C., Dec. 2013. Paleoclimate Variability in the Mediterranean and Red Sea Regions during the Last 500,000 Years. *Current Anthropology* 54 (S8), S183–S201.
- Rohling, E. J., Hilgen, F. J., 1991. The eastern Mediterranean climate at times of sapropel formation: a review. *Geologie en Mijnbouw* 70, 253–264.
- Rohling, E. J., Jorissen, F. J., DE STIGTER, H. C., Oct. 1997. 200 Year interruption of Holocene sapropel formation in the Adriatic Sea. *Journal of Micropalaeontology* 16 (2), 97–108.
- Rohling, E. J., Marino, G., Grant, K. M., 2015. Mediterranean climate and oceanography, and the periodic development of anoxic events (sapropels). *Earth Science Reviews* 143, 62–97.
- Rohling, E. J., Rijk, S. D., 1999a. Erratum to holocene climate optimum and last glacial maximum

- in the mediterranean: the marine oxygen isotope record [marine geology 153 (1999) 5775]1pii of original article: S0025-3227(98)00020-6.1. *Marine Geology* 161 (2), 385 – 387.
- Rohling, E. J., Rijk, S. D., 1999b. Holocene climate optimum and last glacial maximum in the mediterranean: the marine oxygen isotope record. *Marine Geology* 153 (1), 57 – 75.
- Rossignol-Strick, M., 1983. African monsoons, an immediate climate response to orbital insolation. *Nature* 304 (5921), 46–49.
- Rossignol-Strick, M., 1985. Mediterranean Quaternary sapropels, an immediate response of the African monsoon to variation of insolation. *Palaeogeography, Paleoclimatology, Paleoecology* 49 (3-4), 237–263.
- Rossignol-Strick, M., 1987. Rainy periods and bottom water stagnation initiating brine accumulation and metal concentrations: 1. the late quaternary. *Paleoceanography* 2 (3), 333–360.
- Rossignol-Strick, M., 1999. The holocene climatic optimum and pollen records of sapropel 1 in the eastern mediterranean, 90006000bp. *Quaternary Science Reviews* 18 (4), 515 – 530.
- Rossignol-Strick, M., Nesteroff, W., Olive, P., Vergnaud-Grazzini, C., 1982. After the deluge: Mediterranean stagnation and sapropel formation. *Nature* 295 (5845), 105–110.
- Rossignol-Strick, M., Paterne, M., 1999. A synthetic pollen record of the eastern mediterranean sapropels of the last 1 ma: implications for the time-scale and formation of sapropels. *Marine Geology* 153 (14), 221 – 237.
- Ryan, W. B., Cita, M. B., 1977. Ignorance concerning episodes of ocean-wide stagnation. *Marine Geology* 23 (1-2), 197–215.
- Sachs, J. P., Repeta, D. J., 1999. Oligotrophy and nitrogen fixation during eastern mediterranean sapropel events. *Science* 286 (5449), 2485–2488.
- Sáenz, J., Rodríguez-Puebla, C., Fernández, J., Zubillaga, J., 2001. Interpretation of interannual winter temperature variations over southwestern europe. *Journal of Geophysical Research: Atmospheres* 106 (D18), 20641–20651.
- Sancetta, C., 1994. Mediterranean sapropels: Seasonal stratification yields high production and carbon flux. *Paleoceanography* 9 (2), 195–196.
- Schmiedl, G., Kuhn, T., Ehrmann, W., Emeis, K.-C., Hamann, Y., Kotthoff, U., Dulski, P., Pross, J., 2010. Climatic forcing of eastern mediterranean deep-water formation and benthic ecosystems during the past 22 000 years. *Quaternary Science Reviews* 29 (23), 3006 – 3020.
- Schmiedl, G., Mitschle, A., Beck, S., Emeis, K.-C., Hemleben, C., Schulz, H., Sperling, M., Weldeab, S., 2003. Benthic foraminiferal record of ecosystem variability in the eastern mediterranean sea during times of sapropel {S5} and {S6} deposition. *Palaeogeography, Palaeoclimatology, Paleoecology* 190, 139 – 164.
- Schrader, H., Matherne, A., 1981. Sapropel formation in the eastern mediterranean sea: Evidence from preserved opal assemblages. *Micropaleontology* 27 (2), 191–203.
- Scrivner, A. E., Vance, D., Rohling, E. J., 2004. New neodymium isotope data quantify Nile involvement in mediterranean anoxic episodes. *Geology* 32 (7), 565.
- Smith, A. C., Wynn, P. M., Barker, P. A., Leng, M. J., Noble, S. R., Tych, W., 2016. North atlantic forcing of moisture delivery to europe throughout the holocene. *Scientific reports* 6.
- Smith, D. J., Eglinton, G., Morris, R. J., 1986. The lipid geochemistry of a recent sapropel and associated sediments from the hellenic outer ridge, eastern mediterranean sea. *Philosophical Transactions of the Royal Society of London A: Mathematical, Physical and Engineering Sciences* 319 (1550), 375–415.
- Sodemann, H., Zubler, E., 2010. Seasonal and inter-annual variability of the moisture sources for alpine precipitation during 1995–2002. *International Journal of Climatology* 30 (7), 947–961.
- Spotl, C., Nicolussi, K., Patzelt, G., Boch, R., 2010. Humid climate during deposition of sapropel 1 in the Mediterranean Sea: Assessing the influence on the Alps. *Global and Planetary Change* 71, 242–248.
- Stommel, H., Bryden, H., Mangelsdorf, P., Dec 1973. Does some of the mediterranean outflow come from great depth? *pure and applied geophysics* 105 (1), 879–889.
- Struck, U., Emeis, K.-C., Vo, M., Krom, M. D., Rau, G. H., 2001. Biological productivity during sapropel s5 formation in the eastern mediterranean sea: evidence from stable isotopes of nitrogen and carbon. *Geochimica et Cosmochimica Acta* 65 (19), 3249 – 3266.
- Thunell, R. C., Williams, D. F., 1983. Paleotemperature and paleosalinity history of the eastern mediterranean during the late quaternary. *Palaeogeography, Palaeoclimatology, Paleoecology* 44 (1), 23 – 39.

- Toucanne, S., Minto'o, C., Fontanier, C., 2015. Tracking rainfall in the northern Mediterranean borderlands during sapropel deposition. *Quaternary Science Reviews* 129, 178–195.
- Tribovillard, N., Algeo, T. J., Lyons, T., Riboulleau, A., 2006. Trace metals as paleoredox and paleoproductivity proxies: an update. *Chemical geology* 232 (1), 12–32.
- Trigo, I. F., Bigg, G. R., Davies, T. D., 2002. Climatology of cyclogenesis mechanisms in the Mediterranean. *Monthly Weather Review*, 549–569.
- Trigo, I. F., Davies, T. D., Bigg, G. R., 2000. Decline in Mediterranean rainfall caused by weakening of Mediterranean cyclones. *Geophysical Research Letters* 27 (18), 2913–2916.
- Tsimplis, M. N., Josey, S. A., Mar. 2001. Forcing of the Mediterranean Sea by atmospheric oscillations over the North Atlantic. *Geophysical Research Letters* 28 (5), 803–806.
- Tzedakis, P., 2000. Vegetation variability in Greece during the last interglacial. *Netherlands Journal of Geosciences* 79 (2-3), 355–367.
- Tzedakis, P., Pälike, H., Roucoux, K., De Abreu, L., 2009. Atmospheric methane, southern European vegetation and low-mid latitude links on orbital and millennial timescales. *Earth and Planetary Science Letters* 277 (3), 307–317.
- Tzedakis, P. C., 1993. *Nature* 364, 437–440.
- Tzedakis, P. C., 2007. Seven ambiguities in the Mediterranean palaeoenvironmental narrative. *Quaternary Science Reviews* 26, 2042–2066.
- Vaks, A., Bar-Matthews, M., Ayalon, A., Matthews, A., Halicz, L., Frumkin, A., 2007. Desert speleothems reveal climatic window for African exodus of early modern humans. *Geology* 35 (9), 831–834.
- Vaks, A., Bar-Matthews, M., Ayalon, A., Schilman, B., Gilmour, M., Hawkesworth, C. J., Frumkin, A., Kaufman, A., Matthews, A., 2003. Paleoclimate reconstruction based on the timing of speleothem growth and oxygen and carbon isotope composition in a cave located in the rain shadow in Israel. *Quaternary Research* 59 (2), 182–193.
- Vaks, A., Bar-Matthews, M., Matthews, A., Ayalon, A., Frumkin, A., 2010. Middle-late Quaternary paleoclimate of northern margins of the Saharan-Arabian desert: reconstruction from speleothems of Negev desert, Israel. *Quaternary Science Reviews* 29 (19), 2647 – 2662, special Theme: Case Studies of Neodymium Isotopes in Paleoceanography.
- Vergnaud-Grazzini, C., Ryan, W. B., Cita, M. B., 1977. Stable isotopic fractionation, climate change and episodic stagnation in the eastern Mediterranean during the late Quaternary. *Marine Micropaleontology* 2 (Supplement C), 353 – 370.
- Visbeck, M., 2002. The ocean's role in Atlantic climate variability. *Science* 297 (5590), 2223–2224.
- Walker, G. T., Bliss, E., 1932. World weather. V. *Mem. Roy. Meteor. Soc.* 4, 53–84.
- Wallace, J. M., Gutzler, D. S., 1981. Teleconnections in the geopotential height field during the northern hemisphere winter. *Monthly Weather Review* 109 (4), 784–812.
- Wallace, J. M., Zhang, Y., Lau, K.-H., 1993. Structure and seasonality of interannual and interdecadal variability of the geopotential height and temperature fields in the northern hemisphere troposphere. *Journal of Climate* 6 (11), 2063–2082.
- Wanner, H., Brönnimann, S., Casty, C., Gyalistras, D., Luterbacher, J., Schmutz, C., Stephenson, D. B., Xoplaki, E., 2001. North Atlantic oscillation—concepts and studies. *Surveys in Geophysics* 22 (4), 321–381.
- Wassenburg, J. A., Immenhauser, A., Richter, D. K., Niedermayr, A., Riechelmann, S., Fietzke, J., Scholz, D., Jochum, K. P., Fohlmeister, J., Schröder-Ritzrau, A., Sabaoui, A., Riechelmann, D. F. C., Schneider, L., Esper, J., Aug. 2013. Moroccan speleothem and tree ring records suggest a variable positive state of the North Atlantic Oscillation during the Medieval Warm Period. *Earth and Planetary Science Letters* 375 (C), 291–302.
- Weldeab, S., Menke, V., Schmiedl, G., Mar. 2014. The pace of East African monsoon evolution during the Holocene. *Geophysical Research Letters* 41 (5), 1724–1732.
- Zanchetta, G., Drysdale, R. N., Hellstrom, J. C., 2007. Enhanced rainfall in the Western Mediterranean during deposition of sapropel S1: stalagmite evidence from Corchia cave (Central Italy). *Quaternary Science Reviews* 26, 279–286.
- Zavattarielli, M., Mellor, G. L., Jun. 1995. A Numerical Study of the Mediterranean Sea Circulation. *Journal of Physical Oceanography* 25 (6), 1384–1414.
- Zhao, Y., Colin, C., Liu, Z., Paterne, M., Siani, G., Xie, X., Dec. 2012. Reconstructing precipitation changes in northeastern Africa during the Quaternary by clay mineralogical and geochemical investigations of Nile deep-sea fan sediments. *Quaternary Science Reviews* 57 (C), 58–70.

- Zielhofer, C., Fletcher, W. J., Mischke, S., De Batist, M., 2017. Atlantic forcing of Western Mediterranean winter rain minima during the last 12,000 years. *Quaternary Science Reviews* 157, 29–51.
- Ziv, B., Dayan, U., Kushnir, Y., Roth, C., Enzel, Y., 2006. Regional and global atmospheric patterns governing rainfall in the southern Levant. *International Journal of Climatology* 26 (1), 55–73.

When Milankovitch cycles induce overprints on global pyrite records: Toward a better understanding of the sulfur cycle.

Quand les cycles de Milankovitch surimposent les processus globaux préservés dans la pyrite:
Vers une meilleure compréhension du cycle du soufre.

Abstract

Ce chapitre fait la synthèse des processus biologiques impliqués dans le cycle du soufre océanique. En effet, ce dernier joue un rôle important dans la régulation du climat global, puisqu'il participe à régulation de l'oxygène atmosphérique. Ainsi, comprendre les mécanismes qui contrôlent son fractionnement isotopique dans les sédiments est nécessaire pour bien appréhender l'émergence de la vie oxygénique Terrestre.

Dans les sédiments, les changements de composition isotopique du soufre sont généralement attribués à des processus biogéochimiques globaux (i.e. affectant l'intégralité de l'océan) de l'ordre de la dizaine de millions d'année. Cependant, les sédiments de PRGL1-4 ont révélés une impensable variabilité isotopique au cours des derniers 500 000 ans. Nous suggérons que cette variation résulte de processus sédimentaires. Et plus particulièrement reflètent une modification locale de la sédimentation.

Ces résultats remettent en question l'utilisation des isotopes du soufre préservés la pyrite comme indicateur de processus globaux (i.e. oxygène) par rapports aux conditions locales de sédimentation.

Contents

1	Biological Sulfur cycling.....	134
1.1	Sulfate reduction.....	134
1.2	Sulfur oxidation.....	137
1.3	Sulfur disproportionation.....	137
2	Geological Sulfur cycle.....	139
2.1	Generalities.....	139
2.2	The mineral record of the sulfur cycle.....	141
2.3	Variability in Sulfur isotopes proxies.....	145
3	Variability in modern environments.....	150
3.1	Study case of Papua New Guinea [Aller et al., 2008].....	150
3.2	Model prediction under sea-level changes [Fike et al. in review].....	153
4	Pyrite sulfur isotopes: a new proxy of glacial interglacial environmental changes.....	154
5	Implications for past sulfur records.....	160
6	Perspectives.....	161

List of Figures

- 37 Schematic of the processes involved in dissimilatory sulfate reduction. Step 1: environment sulfate transport through the cytoplasm envelope. Step 2: beginning of the sulfate reduction process after activation of APS by the Sat enzyme. Step 3: reduction of sulfate to sulfite (SO_3^{2-}). Step 4: sulfite interaction with DsrABC complex and the sulfur transfer protein DsrC. This last step induces production of a wide range of sulfur direct products. Slightly modified from Fike et al. 2015..... 135
- 38 Relationship between cell-specific sulfate reduction rate (csSRR) and sulfur isotopic fractionation during cultured sulfate reduction. We observe a clear decrease of sulfate fractionation (^{34}S ‰) at high csSRR. Data from Leavitt et al. 2013a and Sim et al. 2011a..... 136
- 39 Compilation of available data on the extent of sulfur isotopes fractionation associated with sulfate reduction in both pure cultures and natural populations. Also shown a compilation of available data on the depletion of ^{34}S preserved in sedimentary pyrite ($\delta^{34}\text{S}_{\text{SO}_4^{2-}} - \delta^{34}\text{S}_{\text{pyr}}$). Redrawn from Canfield (2001). 137
- 40 Major microbial sulfur cycling metabolisms and their redox transformations (with related valence). Blue line is related to the transformation of sulfate (SO_4^{2-} ; +6) to sulfide (H_2S ; -2); Green lines represent the transformation of sulfide to more oxidized sulfur states; Purple lines show disproportionation of elemental sulfur (S_0) to H_2S or SO_4^{2-} 138
- 41 **(A)** Depletion into pyrite ($\delta^{34}\text{S}_{\text{sulfate}} - \delta^{34}\text{S}_{\text{pyrite}}$) from various marine sediment compare to fractionation produced by microbial sulfates reducers within the same sediments. The 1/1 line is expected if sulfate reduction is the only processes that controlling the sediment composition, redrawn from (Canfield 2001). **(B)** Isotopic impact of disproportionation after Canfield and Thamdrup (1994). Sulfate reduction produces sulfide that is depleted in ^{34}S , subsequent sulfide oxidation (minimal isotopic fractionation) and disproportionation (yielding ^{34}S -enriched sulfate + ^{34}S -depleted sulfide) can cause increasing ^{34}S -depletion of the H_2S produced. **(C)** The $\delta^{34}\text{S}$ of pyrite produced by disproportionation is related to the ratio of H_2S to SO_4^{2-} generated during each cycle and the initial sulfate converted to sulfide in a closed system. This relationship between produced H_2S and $\delta^{34}\text{S}$ is represented for three different ratio of H_2S to SO_4^{2-} , where 3:1 has been reported in a pure closed system; 2:1 requires iron scavenging and 1.5:1 net stoichiometry has been observed in experiments (i.e. microbial culture; Canfield and Thamdrup 1996)..... 140
- 42 **(A)** Schematic of the geological sulfur cycle. The most relevant feature is the large seawater marine sulfate reservoir ($M_o = 1.3 \times 10^{21} \text{g}$, $\delta^{34}\text{S}_{\text{SO}_4} / \text{sim} + 21$ ‰). Most important sinks are (1) marine derived sulfates ($\delta^{34}\text{S}_{\text{SO}_4}$; evaporite and carbonate-associated sulfate; both sinks keep similar isotopic value to seawater) and (2) microbial sulfate reduction products ($\delta^{34}\text{S}_{\text{pyrite}}$; associated with isotopic fractionation of ~ 40 ‰). Input fluxes (F_{in}) are resulting from land weathering, volcanic and hydrothermal activity with a $\delta^{34}\text{S}_{\text{in}} \sim +3$ ‰. **(B)** Schematic showing the steady-state dependence of marine $\delta^{34}\text{S}_{\text{SO}_4}$ on the burial flux of pyrite (F_{pyrite}), isotopic composition of sulfate inputs into the ocean (F_{in}) and the presumed constant isotopic fractionation between sulfate and sulfide (ϵ_{pyrite}). Redrawn from Fike et al. 2015..... 141

43	Plot of weight percent of organic carbon versus weight percent of pyrite sulfur for modern marine sediments (non-euxinic), where organic carbon concentration and pyrite have attained quasi-steady values; in other words, where the C_{org} and S early diagenesis is complete. The dashed line around them encloses much more data from other studies. Redrawn from Berner and Raiswell (1983)	143
44	(A) Microbial sulfate reduction and sedimentary sulfur evolution during open-system at equilibrium. (B) Sulfate and sulfur evolution during closed-system sulfate reduction. High variability is observed as sulfides are growing from a pool that is evolving isotopically through time. After Fike et al. (2015)	144
45	(A) Estimates of seawater sulfate concentration based on the presence of gypsum evaporites in Proterozoic and fluid inclusion data from Phanerozoic marine evaporites. (B) Compilation of sulfate and sulfide $\delta^{34}S$ records. After Fike et al. (2015).	146
46	Schematics showing differences between open and closed systems with related impacts on sedimentary sulfur isotopes. In all case, the microbial sulfate rate is considered constant ($^{34}\epsilon$) in the sediment allowing production of H_2S , and the abundance and isotopic composition of the created sulfide is depth dependent. (A) Microbial reduction and consequences on the sedimentary record within an 'Open system'; (B) Schematic showing the isotopic evolution of sulfate and sulfide during an open system; (C) Microbial sulfate reduction and sedimentary sulfur evolution during closed-system, (D) Sulfate and sulfide evolutions during closed-system showing high variability as sulfides are growing from a pool that is isotopically evolving through time. Adapted from Fike et al. 2015.	149
47	(A) Location of 5 cores from Gulf of Papua, Papua New Guinea. (B) Presents depth profile of the shelf at locations G and H with projected cores depth and sediment remobilization layer. Slightly modified from Aller et al. 2008	150
48	(A) Porewater SO_4^{2-} profiles at 8 and 14 m, show constant concentration or linear decreases implying net reduction of SO_4^{2-} is complete at the end of the bottom reworked layer and that anaerobic oxidation of CH_4 occurs at the basal unconformity. The deeper core SO_4^{2-} profile shows presence of net reduction of SO_4^{2-} below the bioturbated zone and SO_4^{2-} decreases exponentially to a non-zero constant value. Porewater \sum_{CO_2} concentration (open symbols) and $\sum_{CO_2} \delta^{13}C_{org}$ (solid symbols) show significant ^{13}C enrichments in the upper few centimeters and substantial increase of $\delta^{13}C_{org}$ in the methanic zone. Data is from Aller et al., 2008. (B) $\delta^{34}S_{pyrite}$ depth profiles within sedimentary core spanning from 8 m to 50 m. This clearly suggests a depth dependence of $\delta^{34}S_{pyrite}$ characterized by an increase of $\delta^{34}S_{pyrite}$ with shallowing depth. Note that shallowest cores recorded 'super-heavy' pyrite. Data is from Fike et al., in prep.	151
49	Classic redox reaction zonation with depth and time in an accumulating sedimentary environment. Relative zonal depth depends of fluxes in oxidants and reductants. Unsteady redox stratification and diagenetic ingrowth in a surface mobile layer after a reworking event (t0) and influence of the isotopic sulfur cycle. Adapted from Fike et al. 2015.	152

50	Schematic view of the potential changes of environmental conditions on the $\delta^{34}\text{S}_{\text{pyrite}}$ core profile in a passive margin. (t1) : Stratigraphic cross section for shallow water sediments with a gradient of possible syn-depositional reworking processes. The red line represents a possible sediment core with a very low reworking leading $\delta^{34}\text{S}_{\text{pyrite}}$ model on the right box. These modeled values are characterized by relatively depleted values with low variability. (t2) : Following a seaward migration of the coastal line (drop of sea level) the resulting lowstand sediments are deposited in a more favorable reworking context. $\delta^{34}\text{S}_{\text{pyrite}}$ modeled with those high-energy conditions are more enriched and show a high variability. (t3) : Following an increase in Relative Sea Level, sediments are again deposited in a deep environment with a very low probability of reworking. The top schematic is a cross section of strata colored by predicted $\delta^{34}\text{S}_{\text{pyrite}}$ values. This clearly shows a sedimentary environment control of $\delta^{34}\text{S}_{\text{pyrite}}$ values, their scatters and any possible extremes values (super heavy pyrite). From Fike et al. (in review).	153
51	Individual pyrite grain μSIM investigation and expecting evolution of sulfur isotopes within pyrite grains. In a close system the sulfur isotopes in pyrites may have significant isotopes variability as they are growing from a pool that isotopically change with time (upper schematic representation). In contrast in an open system pyrite isotopic composition is not expecting to change due to constant replenishment of sulfate (lower schematic representation). Data from Meyer et al. 2017.	161
52	Multi-isotopic theoretical model showing the evolution of the isotopic composition of the residual sulfate (blue line) and instantaneous pyrite (black line), the green line represent the cumulative pyrite isotopic composition predicted by the calculation. From Sansjofre et al. 2016 Supplementary Information.	162
53	A steady-state model from Johnston et al. (2005). This model predicts the isotopic composition of sulfate (on the right) and sulfide (left part) as a function of the fraction of pyrite burial and sulfide re-oxidation.	163

List of Tables

9	Isotopic fractionation (‰) during the disproportionation of sulfite. Re-drawn from Canfield 2001.	139
---	---	-----

1. Biological Sulfur cycling

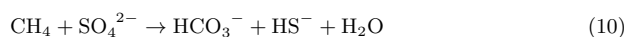
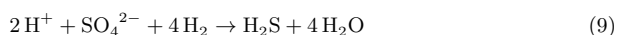
Sulfur is an essential component of all living cells, and assimilated sulfur is an important process in various biological pathways (construction of amino-acids, co-enzymes, vitamins and electron carriers). Since all those possible functions use sulfur, it is a ubiquitous component of most prokaryotic organisms (0.5 to 1 % of dry weight of prokaryotes; Zehnder and Zinder 1980; Canfield 2001). Sulfur found in cells is derived from the surrounding oxic environment, commonly as sulfate (SO_4^{2-}), but also as sulfide (FeS_2), thiosulfate ($\text{S}_2\text{O}_3^{2-}$), polysulfide (S_n^{2-}), and elemental sulfur (S_0).

Dissimilatory microbial processes change the oxidation state of sulfur, from a range of inorganic sulfur compounds, to gain energy. Three main dissimilatory pathways can be used by the wide taxonomic spectrum of microbes: sulfate reduction, sulfide oxidation, and sulfur disproportionation. They will be explained in detail in the following sections.

In aqueous environments (e.g. marine and/or lacustrine) the different sulfur metabolisms are spatially and temporally dependent on the supply of oxidized or reduced compounds. In marine environments, electrons come directly, or indirectly after the first step of degradation, from organic material produced by primary producers. Such variability in the origin of labile electron donors (e.g. organic matter) can explain the spatial variations observed in the environment, for example between the oxygenated water column and the top of the sedimentary sequence. However, other factors should be taken into account such as other sources of electron donors (e.g. redox stratification in the sedimentary column), bioturbation processes, or porosity of the sediment.

1.1. Sulfate reduction

Sulfate reducers are a geomicrobially and geochemically very important group of organisms that belong to the domain of Bacteria, but some sulfate reducing Archaea have also been reported. Most of the known examples of sulfate reducers have been laboratory cultured and described in the literature (Stetter et al. 2009; Speich and Trüper 2008; Burggraf et al. 1990). These organisms are very specialized nutritionally, indeed they gain energy for their growth by catalyzing exogenic chemical reactions in which organic carbon or gases (mainly H_2 or CH_4) are oxidized, while sulfate is reduced; following equation 8 to 10.



Sulfate reducing microorganisms are mainly distributed in anoxic environments containing sulfate where they anaerobically mineralize organic matter. Due to their diversity, they have been described on broad environmental conditions. For example, sulfate reducers were found in freshwater, as well as in brine environment (Brandt et al. 2001); and in a temperature range between -1.5°C to over 100°C (Sagemann et al. 1998; Jørgensen et al. 1990).

The knowledge of intracellular biochemistry of sulfate reduction has been greatly improved over the last years, see on **Figure 37** (Oliveira et al. 2008; Venceslau et al. 2014), it is simply and briefly described below:

- (i) First, microbes sulfate reducers transports sulfate from the environment into the cytoplasm through the cell envelope, via sulfate transporter proteins. These latter co-transport the sulfate anion with a proton or sodium ion using a passive transport (Cypionka 2013). This step is reversible. A considerable amount of sulfate can, by this transport, be concentrated into the cell. For example 1000 times ambient sulfate levels were reported in a freshwater low-sulfate environment (Cypionka 2013).

Equation n° 10:
corresponds to the
Anaerobic Oxidation
of Methane equation

- The transport into the cell will induce a fractionation from the parent sulfate pool ($\delta^{34}\text{S}_{\text{SO}_{4\text{in}}} - \delta^{34}\text{S}_{\text{SO}_{4\text{out}}} \sim -3\text{‰}$; Targgaard et al. 2011), which seems to be related to the expression of the sulfur fractionation during sulfate reduction (Habicht 2002).
- (ii) Inside the cytoplasm, sulfate reduction starts when sulfate is activated by the enzyme ATP sulfurylase (Sat, on **Figure 37**) to APS (adenosine 5-phosphosulfate).
 - (iii) Then, APS can be reduced to sulfite (SO_3^{2-}) by the enzyme APS-reductase (ApsAB), which is an intermediate key in the dissimilatory sulfate reduction.
 - (iv) Sulfite is reduced by a pair of enzymes (DsrABC complex, where DsrAB is a dissimilatory sulfite reductase and DsrC is a sulfur transfer protein) via a complex set of interactions that will produce a wide range of direct products (e.g. trithiosulfate, thio-sulfate and sulfide). Partially reduced sulfur bound to DsrAB can yield thiosulfate. Generally, four electrons are transferred by DsrAB, and a zero-valent sulfur is bound to DsrC that interacts with residues of DsrAB and forms S in an intermediate redox state, then interacts with DsrMKJOP complex at the cell membrane. During the transport of the S form, DsrC act as an electron acceptor and contributes to energy conservation in the cell. This last step is not perfectly understood, see (Oliveira et al. 2008) for a thorough review.

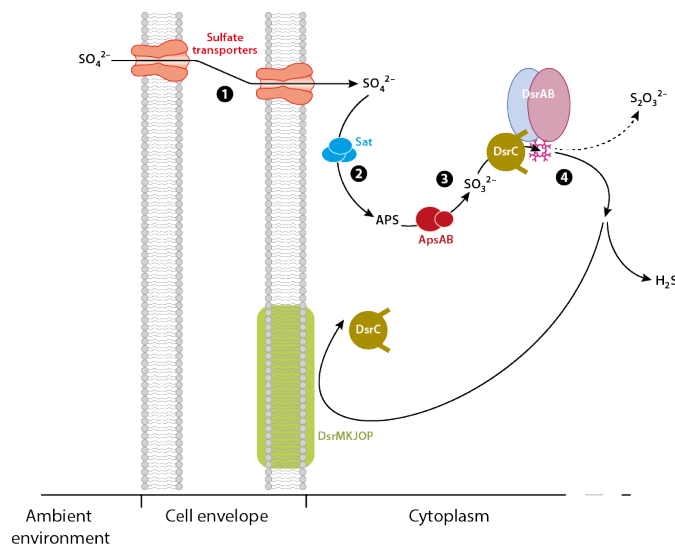


Figure 37

Schematic of the processes involved in dissimilatory sulfate reduction. Step 1: environment sulfate transport through the cytoplasm envelope. Step 2: beginning of the sulfate reduction process after activation of APS by the Sat enzyme. Step 3: reduction of sulfate to sulfite (SO_3^{2-}). Step 4: sulfite interaction with DsrABC complex and the sulfur transfer protein DsrC. This last step induces production of a wide range of sulfur direct products. Slightly modified from Fike et al. 2015.

The sulfur isotopic fractionations during all these steps are not well constrained. Rees in 1973 proposed that steps 2 and 3 are associated with fractionation of 25 ‰, whereas sulfate transport has an inverse discrimination of ^{32}S by a factor of 3 ‰. This was consistent with the observed culture fractionation around 47 ‰ (Canfield and Teske 1996). But the Rees model was not sufficient to explain the observed pure culture experiment results of > 65 ‰ (Sim et al. 2011b), or up to 55 ‰ in chemo stat culture (Lepland 2013), and during culture of mixing microbes from modern lacustrine waters (Canfield et al. 2010). During culture, isolated DsrAB produce an in-vitro fractionation of 15.3 ‰ (Leavitt et al. 2013b),

which is lower than the predicted values of isotopic modeling (Brunner and Bernasconi 2005; Rees 1973).

At low sulfate concentration, the rate at which sulfate enters the cell is reduced, consequently decreasing the rate of cell-specific sulfate reduction rate (csSRR). In such environments, limited sulfate supply reduces isotopic fractionation. The same processes are also noticeable during high cell-specific sulfate reduction rates, when sulfate becomes limiting due to high electron donor availability. Therefore, reduced fractionation is observed during high bacterial activity, **Figure 38**.

Maximum isotopic fractionation occurs during exchange in equilibrium between the internal and external sulfate pool (non-reversible exchange through the cell membrane). This happens when the cellular mechanism is reduced, e.g. low cell-specific sulfate reduction rate, and therefore the final step will be limiting. This explains why high fractionations are observed during low specific rates, **Figure 38**. Recent studies have suggested that slow rates allow sulfur isotope fractionation close to the thermodynamic equilibrium, whereas faster rates clearly show that there is a kinetic sulfur isotope fractionation (Wing and Halevy 2014).

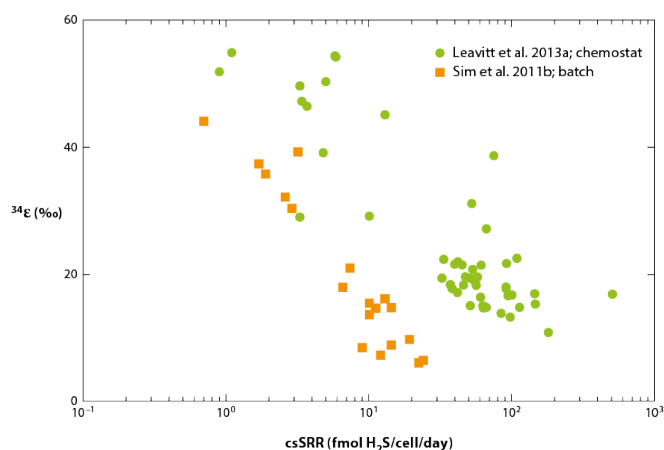


Figure 38

Relationship between cell-specific sulfate reduction rate (csSRR) and sulfur isotopic fractionation during cultured sulfate reduction. We observe a clear decrease of sulfate fractionation (^{34}S ‰) at high csSRR. Data from Leavitt et al. 2013a and Sim et al. 2011a.

Such knowledge of the sulfate-reducer organisms mainly results from exploration in batch cultures instead of nature environments observations because natural anoxic environments contain a wide variety of sulfate reducers and specific activities. Nevertheless, recent efforts have been conducted to address the isotopic fractionation by natural populations metabolizing at an in situ rate with naturally available organic substrates (Habicht and Canfield 1996; Habicht et al. 1998; Habicht 2002; Canfield 2001). The results obtained present a wide spectrum of environments from rapidly metabolizing microbial mats to slowly metabolizing natural populations of sulfate reducers in coastal sediments. Maximum fractionation occurs in coastal environments within the same range of pure culture studies, **Figure 39**. The data compilation from Canfield (2001) shows an upper limit to fractionation of around 45 ‰, this limit is however uncertain, and some model outcomes (Goldhaber and Kaplan 1980) and sediment-based studies suggest higher fractionation could be found in nature. This also shows that very low fractionation observed in cultures have not yet been found in the natural environment, which probably results from limited substrates inducing lower specific rates. However, Canfield (2001) reported high isotopic fractionation associ-

ated with limited organic supply in the natural environment, with a correspondence to low specific-rate of sulfate reduction.

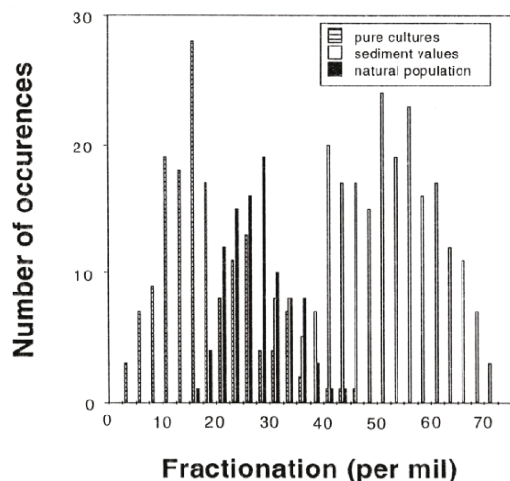


Figure 39

Compilation of available data on the extent of sulfur isotopes fractionation associated with sulfate reduction in both pure cultures and natural populations. Also shown a compilation of available data on the depletion of ^{34}S preserved in sedimentary pyrite ($\delta^{34}\text{S}_{\text{SO}_4^{2-}} - \delta^{34}\text{S}_{\text{pyr}}$). Redrawn from Canfield (2001).

1.2. Sulfur oxidation

As just discussed, sulfate reduction converts sulfate to sulfide, the blue line on **Figure 40**; Sulfur oxidation is the reverse process, the green line on **Figure 40**. Sulfide oxidation in marine environments is ubiquitous and follows sulfate reduction, where 90 % of the sulfide formed during sulfate reduction is re-oxidized (Canfield and Teske 1996). In nature, sulfur oxidation pathways are diverse, and poorly known, but three different pathways are described as being true sulfide oxidation and require introduction of an electron acceptor (e.g. O_2 ; NO_3^-) or fixation of organic carbon from CO_2 . **Figure 40** presents a schematic for major sulfur cycling metabolism and their redox states. The specific case of sulfur disproportionation intermediate compounds will be discussed in the next section, see section 1.3.

The biological oxidation of sulfide to elemental sulfur, or elemental sulfur to sulfate generally yields negligible fractionation. Abiotic oxidation can however induce non-negligible fractionation, as large as 5 ‰ (Fry et al. 1988), but during experiments of oxidation of elemental sulfur shows little fractionation as compared to the original sulfide, 1-2 ‰ (Fry et al. 1985; Zerkle et al. 2009). However, oxidative processes are known to more significantly impact $\delta^{34}\text{S}$ signals in natural environments frequently subject to oxidative reworking (e.g. shallow marine environments; Aller 2014).

1.3. Sulfur disproportionation

As mentioned above, most sulfide formed during sulfate reduction processes in natural environments are prone to being re-oxidized to sulfate and therefore be present in intermediate valence states. Example of intermediate oxidation states includes sulfite (SO_3^{2-}), elemental

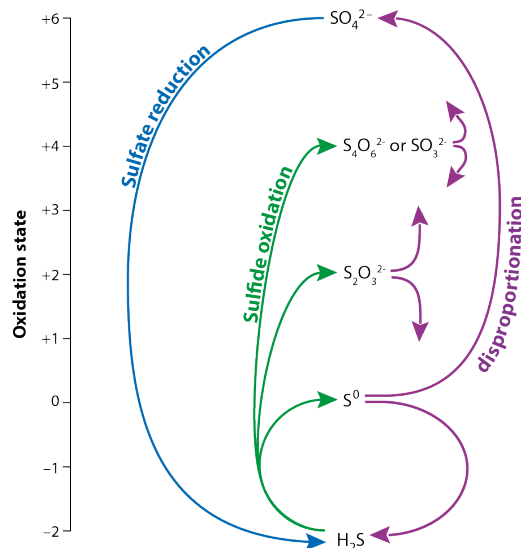


Figure 40

Major microbial sulfur cycling metabolisms and their redox transformations (with related valence). Blue line is related to the transformation of sulfate (SO_4^{2-} ; +6) to sulfide (H_2S ; -2); Green lines represent the transformation of sulfide to more oxidized sulfur states; Purple lines show disproportionation of elemental sulfur (S_0) to H_2S or SO_4^{2-}

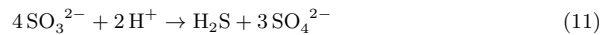
sulfur (S_0), thiosulfate ($\text{S}_2\text{O}_3^{2-}$) and tetrathiosulfate ($\text{S}_4\text{O}_6^{2-}$); see **Figure 40**. Organisms have evolved to take advantage of sulfur in intermediate valence states that are not stabilized in the environment but are rapidly transformed. Such organisms can use intermediate sulfur forms simultaneously as electron donors and acceptors: this is the disproportionation of sulfur (purple pathway on **Figure 40**; Bak and Pfennig 1987). Sulfur disproportionation means that some specific bacteria can disproportionate intermediate sulfur forms to sulfide and sulfate with no external electron donor or electron acceptor required, see **Figure 40**. The ability to disproportionate sulfur is possible by diverse groups of sulfate reducers with variable association in the disproportionation processes (Canfield et al. 1998). Nevertheless, disproportionation of S_0 has been a focus of the geochemical community due to easy accumulation of the S_0 form in sediments (Troelsen and Jørgensen 1982), which is known to be easily disproportionable (Canfield and Teske 1996). Both marine and fresh water culture experiments (Canfield and Thamdrup 1994; Canfield et al. 1998; Habicht et al. 1998) give us a better understanding of the fractionation associated with disproportionation of S_0 . Disproportionation of sulfide and thiosulfate is thermodynamically favorable under standard physiological conditions (sulfide concentration must be kept low, under 1 nM, for elemental disproportionation to yield sufficient energy to support cell growth). In addition, in most culture cases enrichment in iron or manganese is required (this buffers the sulfide concentration to low levels).

Disproportionation has been proposed as a mechanism that produces large fractionation where sulfide is depleted in ^{34}S , and sulfate enriched in ^{34}S . This is schematically illustrated in **Figure 41**. During disproportionation of elemental sulfur, there is no difference between disproportionation of marine or freshwater microbial communities, and thus no significant relationship between the extent of fractionation and cell-specific rate (Canfield et al. 1998). Larger fractionations have been observed during disproportionation of sulfite (Habicht et al. 1998, see **Table III.9**).

Isotopic fractionation during disproportionation of sulfide				
Culture	$\Delta(\text{SO}_3^{2-} - \text{H}_2\text{S})$	\pm	$\Delta(\text{SO}_3^{2-} - \text{SO}_4^{2-})$	\pm
Desulfovibrio sulfodimutans				
I	31.5	1.3	-9.2	0.6
II	37	1.4	-12	1.1
Desulfocapsa thiozymogenes				
I	20.5	1.3	-6.9	0.3
II	24	0.6	-8.5	0.2

Table 9 Isotopic fractionation (‰) during the disproportionation of sulfite. Redrawn from Canfield 2001.

The nearly 1 to 3 difference between disproportionation of sulfide and sulfate is consistent with the stoichiometric equation for the sulfide disproportionation pathway:



Habicht et al. (1998) also suggested that the magnitude of fractionation during disproportionation processes may be influenced by cell-specific rates, with higher fractionation during low cell-specific rates of disproportionation, as already discussed for sulfate reduction. In all experiments, sulfate reduction produces sulfide that is depleted in ^{34}S relative to the parent pool (up to 47 ‰; and possibly larger Leavitt et al. 2013a; Sim et al. 2011a,b). However, observed fractionations are not high enough to explain the depletion recorded in most sedimentary sulfide, as highlighted a decade ago by Habicht and Canfield (2001). In this study, authors compared the fractionation produced by natural sulfate reducers (ϵ_{SR}) with the magnitude of fractionation observed in natural sulfides phases (mostly pyrite) relative to sea-water sulfate ($\delta^{34}\text{S}_{\text{sw}} - \delta^{34}\text{S}_{\text{pyr}}$), see **Figure 41**. Their result provided the first evidence that sulfate reducers do not fractionate enough to explain the isotopic compositions recorded in sedimentary sulfides.

Using disproportionation pathway, the initial sulfide (remaining from sulfate reduction) may be oxidized to S_0 with minimal fractionation (Canfield et al. 1998). Subsequent disproportionation of S_0 produces sulfide that is more depleted in ^{34}S , and sulfate enriched in ^{34}S , see **Figure 41.B**. Through repeated cycles of sulfide oxidation to S_0 and S_0 disproportionation, **Figure 41.B**, increasingly ^{34}S -depleted sulfide can be generated. Because each cycle produces sulfate, which is supposed to leave freely in the overlying water column, and sulfide, the proportion of the initial sulfur remaining decreases during each iterative step. In a closed system, the amount of sulfide mineral at a given $\delta^{34}\text{S}$ is function of the ratio between $\text{H}_2\text{S}:\text{SO}_4^{2-}$ products (i.e. sulfide:sulfate) during the disproportionation processes, see **Figure 41.C**. The 3:1 net stoichiometry of disproportionation (already observed in Habicht et al. 1998) can then generate large depletion (> 60 ‰) while yielding more than 10 % of the initial sulfur in the system. The 2:1 sulfide to sulfate ratio required by iron scavenging can also produce large fractionation but decreases the yield of sulfide minerals. In practice lower ratios are observed, close to 1.5:1, where the missing sulfide is probably taken up by biomass (Canfield and Teske 1996), the observed product is lower in quantity but still produces large isotopic fractionation.

2. Geological Sulfur cycle

2.1. Generalities

The modern ocean sulfur cycle mainly includes two major sources and two major sinks of sulfur:

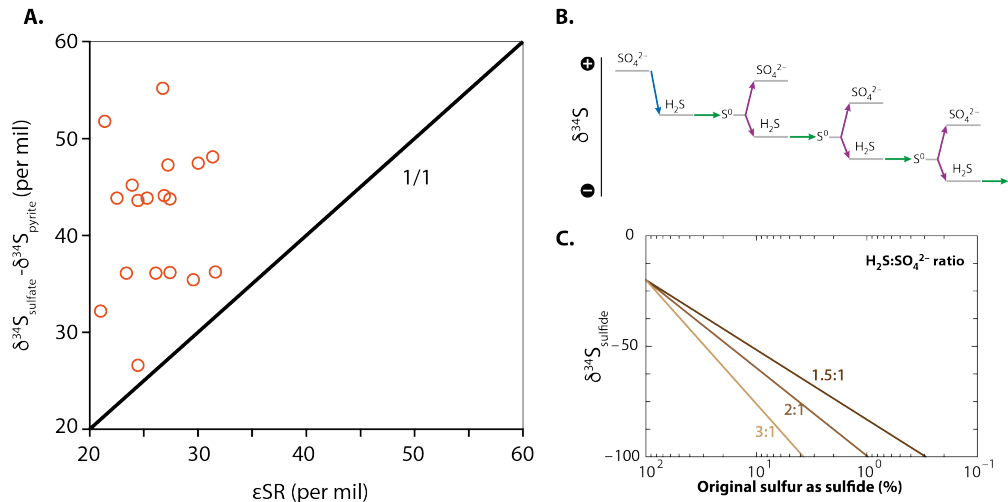


Figure 41

(A) Depletion into pyrite ($\delta^{34}\text{S}_{\text{sulfate}} - \delta^{34}\text{S}_{\text{pyrite}}$) from various marine sediment compare to fractionation produced by microbial sulfates reducers within the same sediments. The 1/1 line is expected if sulfate reduction is the only processes that controlling the sediment composition, redrawn from (Canfield 2001). (B) Isotopic impact of disproportionation after Canfield and Thamdrup (1994). Sulfate reduction produces sulfide that is depleted in ^{34}S , subsequent sulfide oxidation (minimal isotopic fractionation) and disproportionation (yielding ^{34}S -enriched sulfate + ^{34}S -depleted sulfide) can cause increasing ^{34}S -depletion of the H_2S produced. (C) The $\delta^{34}\text{S}$ of pyrite produced by disproportionation is related to the ratio of H_2S to SO_4^{2-} generated during each cycle and the initial sulfate converted to sulfide in a closed system. This relationship between produced H_2S and $\delta^{34}\text{S}$ is represented for three different ratio of H_2S to SO_4^{2-} , where 3:1 has been reported in a pure closed system; 2:1 requires iron scavenging and 1.5:1 net stoichiometry has been observed in experiments (i.e. microbial culture; Canfield and Thamdrup 1996).

- (i) **Weathering** of past sulfate and sulfide deposits on emerged lands inputs an estimated S flux of 1.0×10^{14} g/yr through rivers to the ocean (Tostevin et al. 2014). The oceanic sulfate reservoir has a long residence time (~ 13 Myr; Kah et al. 2004), and marine sulfate in the ocean is the fourth most abundant solute in seawater with a concentration of 28 mM (corresponding to 1.3×10^{21} g of S). Most sulfates are conservative under oxygenated environments with concentration changes resulting from evaporation and dilution (freshwater inputs),
- (ii) **Metamorphic processes and mantle degassing** also replenish the sulfate marine reservoir via input of hydrothermal (i.e. hydrothermal dissolved sulfur, and gaseous sulfur),
- (iii) **Burial** of marine sulfate as evaporite minerals (gypsum or anhydrite), as well as through carbonate associated sulfate (sulfate bound into the carbonate lattice, i.e. CAS; W Burdett et al. 1989), or barite (Paytan et al. 1998, 2002; Paytan 2004).
- (iv) **Burial of reduced sulfur**: Sulfur can also leave the ocean in sediments by the scavenging of hydrogen sulfide with iron or manganese during microbial sulfate reduction processes and by storage as sulfide, mainly pyrite (FeS_2). It is true that the availability of reactive iron also plays a role in the preservation of biogenic pyrite, and explains the close linkage between iron and sulfur geochemical cycles. After their formation, most sulfides will return to the sulfate ocean pool via re-oxidation ($> 90\%$; Jørgensen 1982). Pyrite and sulfate evaporites burials are the main mechanisms with which sulfur leaves the ocean, see **Figure 42**.

These two main sources and sinks control the sulfur and oxygen isotopic composition and mass balance of the seawater sulfate pool. The chemical reactions associated with these

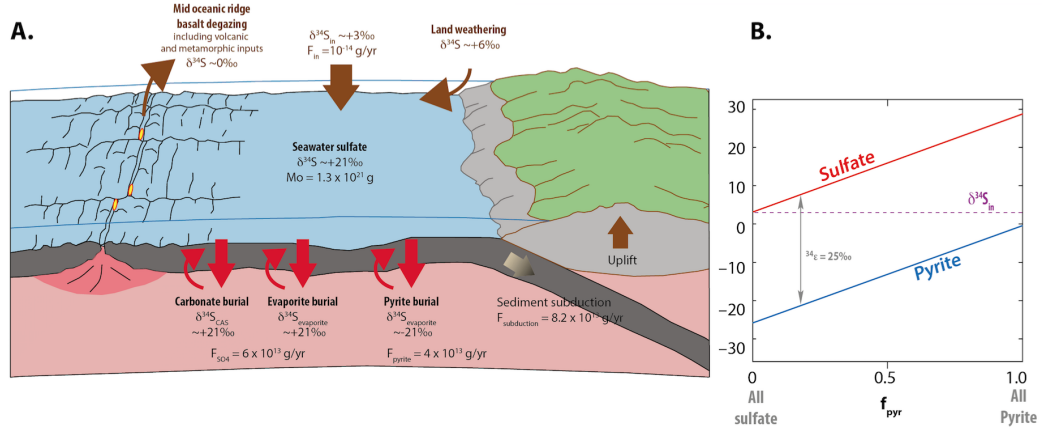


Figure 42

(A) Schematic of the geological sulfur cycle. The most relevant feature is the large seawater marine sulfate reservoir ($M_o = 1.3 \times 10^{21} \text{ g}$, $\delta^{34}S_{\text{SO}_4} / \text{sim} +21 \text{‰}$). Most important sinks are (1) marine derived sulfates ($\delta^{34}S_{\text{SO}_4}$; evaporite and carbonate-associated sulfate; both sinks keep similar isotopic value to seawater) and (2) microbial sulfate reduction products ($\delta^{34}S_{\text{pyrite}}$; associated with isotopic fractionation of $\sim 40 \text{‰}$). Input fluxes (F_{in}) are resulting from land weathering, volcanic and hydrothermal activity with a $\delta^{34}S_{\text{in}} \sim +3 \text{‰}$. (B) Schematic showing the steady-state dependence of marine $\delta^{34}S_{\text{SO}_4}$ on the burial flux of pyrite (F_{pyrite}), isotopic composition of sulfate inputs into the ocean (F_{in}) and the presumed constant isotopic fractionation between sulfate and sulfide (ϵ_{pyrite}). Redrawn from Fike et al. 2015.

fluxes affect alkalinity and the amount of oxygen in the ocean-atmosphere reservoir.

For many reasons, the extraction of relevant information about long-term secular variations in the isotopic composition of past sulfur species over geological times is difficult. However, two main processes are commonly used to explain such changes: the first one is related to variations in the flux and preservation of sulfide from sulfate reduction in marine sediments, and the second concerns the mean isotopic fractionation associated with microbial processes that generate reduced iron sulfide (pyrite) from a starting pool of sulfate. Moreover, additional variations could be induced by short-term and long-term changes in isotopic composition of the marine sulfate pool. Three parameters are linked in the standard steady-state description of isotopic mass balance of sulfur cycle:

$$\delta^{34}S_{\text{in}} = (1 - f_{\text{pyrite}}) \times \delta^{34}S_{\text{SO}_4} / f_{\text{pyrite}} \times \delta^{34}S_{\text{pyrite}} \quad (12)$$

It can be easily simplified if:

$$\epsilon_{\text{pyrite}} = \delta^{34}S_{\text{SO}_4} - \delta^{34}S_{\text{pyrite}} \quad (13)$$

Then :

$$\delta^{34}S_{\text{SO}_4} = \delta^{34}S_{\text{in}} + f_{\text{pyrite}} \times \epsilon_{\text{pyrite}} \quad (14)$$

Where f_{pyrite} is the fraction of total sulfur removed from the ocean as pyrite, and $\delta^{34}S_{\text{in}}$ is the isotopic composition of sulfur weathered from continent and delivered to the ocean, $\delta^{34}S_{\text{SO}_4}$ is the isotopic composition of seawater sulfate, $\delta^{34}S_{\text{pyrite}}$ is the average of pyrite sulfur removed from the ocean, and ϵ_{pyrite} is the isotopic offset from microbial processing. Note these parameters are controlling the isotopic composition of the marine sulfate pool, as illustrated in the **Figure 42**.

2.2. The mineral record of the sulfur cycle

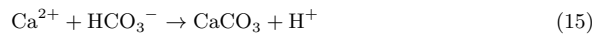
2.2.1. Sulfate. Geological records preserved three independent proxies allowing us to reconstruct past variations of $\delta^{34}S_{\text{SO}_4}$: sulfate-evaporite, barite, and CAS. Each proxy has its own

characteristics and limitations (i.e. accuracy, robustness, temporal and spatial continuity and extraction facilities; Fike et al. 2015). We also must keep in mind that environmental deposition conditions (redox condition, connectivity with the global open ocean, etc), and subsequent diagenetic processes play an important control on the preserved $\delta^{34}\text{S}_{\text{SO}_4}$. First investigations of sulfate records were conducted on sulfate-evaporites (Claypool et al. 1980; Holser 1977). Sulfate evaporites resulted from crystallization of gypsum and/or anhydrite from an extremely saline seawater, i.e. brine, with assumption of a minor fractionation of sulfur isotopes during crystallization processes (Holser and Kaplan 1966). Then, theoretical laboratory experiments were conducted and yielded an isotopic fractionation between seawater and crystallized minerals of 0 to +2.4 ‰ (Raab and Spiro 1991). Nevertheless, sulfate-evaporite formation processes require specific conditions such as evaporation rates exceeding the infill of marine sulfate. Therefore, they are mainly described in restricted basin with limited or no connection with the open ocean. Moreover, progressive crystallization of ^{34}S -enriched minerals from restricted seawater will result in a chemical evolution of the residual brine (^{34}S -depleted). Therefore, evaporites represent a spatially and temporally discontinuous episodic view of the past sulfur cycle.

Barites (BaSO_4) precipitate in various micro-environments such as open seawater, where they crystallize in isotopic equilibrium with ambient sulfate composition, or in marine hydrothermal vents, as well as diagenetically at the oxic-anoxic boundary in sediments where sulfate reduction takes place (Paytan et al. 2002), or in Ba-rich fluids. Pure marine barite can be distinguished from other forms using Sr-S coupled isotopic characterization and scanning electron microscopes image investigations, but this requires time. Barite records differ from evaporite because evaporite deposition is episodic, while barite can be continuously formed throughout geologic time. A continuous record was published throughout the Cretaceous (Paytan 2004). The only reason why the reported record is not continuous is because not enough analyses have been done.

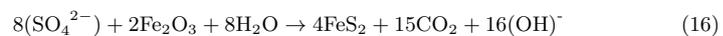
Carbonate associated sulfate (CAS) has become an important proxy for determining changes in the global sulfur cycle throughout geological times (Claypool et al. 1980). CAS is present as a substitution for the carbonate anion within the calcite mineral (Staudt and Schoonen 1995 for a summary). Isotopic variations in CAS have been utilized for environmental reconstruction during mass extinction events. CAS has been shown to accurately record the isotopic composition of surrounding seawater sulfate, and to preserve the signal in rocks (W Burdett et al. 1989). Because carbonates are nearly ubiquitous in marine rocks, the use of CAS records have greatly expanded the temporal resolution of available data, and the location measured. Kampschulte and Strauss (2004) have used CAS to expand the Phanerozoic's curve for oceanic sulfate isotopic composition, providing a more detailed record with small uncertainty.

CaCO_3 may also precipitate through cyanobacteria oxygenic respiration (sulfate reduction), Visscher et al. (2000). In such environments, microorganisms facilitate CaCO_3 precipitation changing $p\text{CO}_2$ via their metabolisms, and create a favorable chemical micro-environment for carbonate precipitation through active generation of Ca^{2+} . Interestingly, bacteria benefit from carbonate precipitation using generated protons on the outside of the cell membrane following the equation n°15.



In such cases, the CAS record could have been impacted if carbonate precipitation occurred in a modified sulfur isotopic micro-environment due to microbial metabolic activity.

2.2.2. Pyrite. Sulfide preserved in marine sediments is generally interpreted as coming from the oxidation of marine organic matter through sulfate-reducing bacterial activity. The overall process can be described through the equation n°16, and produce sedimentary pyrite.



Pyrite forms principally in the upper sedimentary sequence (shallow burial), via the reaction of detrital iron minerals with the H_2S that is produced by sulfate-reducing bacteria in interstitial environments. This process occurs under anoxic conditions, which are rapidly reached within an organic rich sedimentary column (i.e. even in well oxygenated normal marine condition). This happens because enough organic matter (OM) is deposited at the sediment/water interface, and acts as an oxygen-consuming barrier (resulting from oxygenic OM degradation). Pyrite is generally strongly depleted in ^{34}S , showing more or less negative $\delta^{34}S$ resulting from the preferential uptake of ^{32}S by sulfate-reducers. However, large isotopic variations are observed and strongly dependent on a variety of parameters, such as OM concentration, and reactivity, sulfate concentration and reduction rates, iron availability, connectivity with the overlying water column, etc.

In normal marine settings, the amount of metabolizable organic matter limits the microbial reduction process, as highlighted by Berner's works (Berner and Raiswell 1983; Berner 1984; Berner and Westrich 1985) in modern and ancient environments. This dependence is clearly expressed in the positive correlation between marine organic carbon and the amount of pyrite within sediments (**Figure 43**). Alternatively, reactivity of the available organic matter and iron availability also appears to be a limiting factor for pyrite formation.

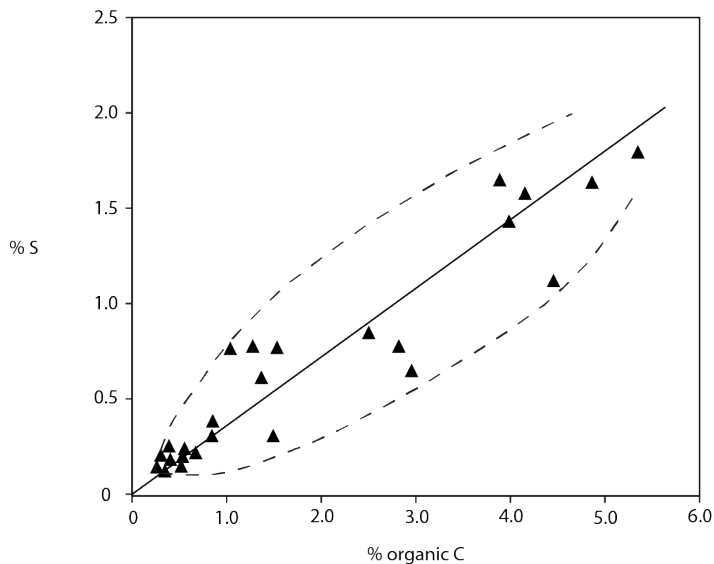


Figure 43

Plot of weight percent of organic carbon versus weight percent of pyrite sulfur for modern marine sediments (non-euxinic), where organic carbon concentration and pyrite have attained quasi-steady values; in other words, where the C_{org} and S early diagenesis is complete. The dashed line around them encloses much more data from other studies. Redrawn from Berner and Raiswell (1983).

In most cases, sulfate reduction appears near to the sediment/seawater interface allowing a constant supply of sulfate from the overlying column via diffusion processes. The supply of sulfate can also be enhanced through bioturbation activity. This scenario is characterized by "unlimited" sulfate availability which is described as being an 'open system'. Sometimes, the rate of sulfate reduction exceeds the sulfate supply, for example in "favorable living conditions" for sulfate reducers (i.e. with large amounts of easily metabolizable organic matter). If such conditions are combined with limited diffusion environments (low bioturbation and/or porosity, high permeability) then 'closed system' environments can be created, (Aller 2014; Canfield 2001). Under closed system environments, sulfate concen-

tration decreases and $\delta^{34}\text{S}_{\text{SO}_4}$ increases, due to Rayleigh-type distillation, see **Figure 44**. This distillation results in an exponential increase in $\delta^{34}\text{S}_{\text{H}_2\text{S}}$ which can be preserved in $\delta^{34}\text{S}_{\text{pyrite}}$ (i.e. at constant biological fractionation). Although the isotopic composition of created sulfides approaches the values of the initial sulfate pool, see **Figure 44.B**. Such sulfur isotopic enrichment can be easily address using secondary ion mass spectrometry (SIMS) in individual pyrite grain. Such approaches have already been used by Fischer et al. (2014) and allow us to better understand the degrees of biological participation in the complex history of mineralization.

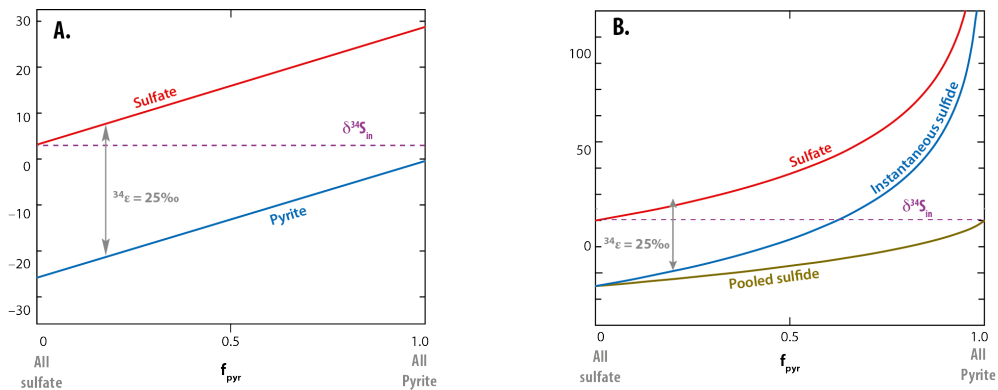


Figure 44

(A) Microbial sulfate reduction and sedimentary sulfur evolution during open-system at equilibrium. **(B)** Sulfate and sulfur evolution during closed-system sulfate reduction. High variability is observed as sulfides are growing from a pool that is evolving isotopically through time. After Fike et al. (2015)

2.3. Variability in Sulfur isotopes proxies

Various factors can affect the global sulfur cycle. Understanding past environmental conditions (shallow/deep basin's sedimentation) and how depositional environments were connected to the open ocean (i.e. global ocean chemistry/local basin) is a necessary step before interpreting past $\delta^{34}\text{S}$, and subsequently reconstructing the past sulfur cycle. Past $\delta^{34}\text{S}_{\text{SO}_4}$ records are sporadic and infer different geological histories in term of depositional alteration (Aller et al. 2010), post-depositional alteration and diagenetic evolution. The sulfate and sulfide response to these factors are different, and could give precious information for reconstructing the past sulfur cycle through geological time.

2.3.1. Sulfate. Variations in the isotopic composition of seawater sulfate throughout geologic time are interpreted as reflecting changes in the size of sulfate reservoir (Kah et al. 2004). In other words, they are related to changes in the proportion of oxidized versus reduced sulfur reservoirs. It is assumed that the isotopic difference between oxidized and reduced pool resulted from bacterial sulfate reduction, and is constant through time (i.e. a sulfur isotopic curve derived from sedimentary sulfides faithfully trace the approximate curve of past sea-water sulfate, Strauss 1997). If it was the same in the past, because today sulfate is the largest pool of oxidants in the ocean (modern seawater sulfate concentration is 28 mM), then secular variation is presumed to be very smooth through time. Nevertheless, evidence for lower concentrations (<1 mM) have been reported for early Earth history (Guo et al. 2009), and probably lower concentration during Archean times (Grotzinger and Kasting 1993). The first evidence for marine sulfate have been reported by Reuschel et al. (2012) in massive evaporite from the Tulomozero Formation dated from 2.1 Ga, then sulfate is presented in most evaporitic strata in greater concentration (>2 mM during Mesoproterozoic; Kah et al. 2004). However, changes in seawater sulfate concentration through time is poorly known, reconstruction of those variations is a critical point to address the past sulfur cycle over Earth history.

Our best understanding of past sulfate evolution comes principally from fluid inclusions in evaporites, **Figure 45**. Modeling of chemical evolution during evaporation of primary fluids resulting in evaporite provides clues to better estimate sulfate concentration evolution through the Phanerozoic (Brennan et al. 2004; Horita et al. 2002; Lowenstein et al. 2003; Timofeeff et al. 2006), see **Figure 45**. Additional approaches were taken to increase the temporal resolution, for example $\delta^{34}\text{S}_{\text{CAS}}$ stratigraphic variability has been used to estimate past ocean sulfate concentration (Kah et al. 2004; Gill et al. 2007, 2011; Hurtgen et al. 2009; Loyd et al. 2012). The use of this approximation for global ocean sulfate concentrations, even for strata with high $\delta^{34}\text{S}_{\text{CAS}}$ variability, would induce misunderstanding of the past sulfate evolution due to local processes and diagenetic overprints. In such case, deviation from global $\delta^{34}\text{S}_{\text{SO}_4}$ signal can easily result from low sulfate concentration environments that have shown important lateral gradients in abundance and isotopic composition of marine sulfate (Li et al. 2010; Poulton et al. 2010). In early Earth history, such cases should have occurred due to the low concentration of sulfate in the ocean (Grotzinger and Kasting 1993; Kah et al. 2004; Hurtgen et al. 2006; Gill et al. 2007; Hurtgen et al. 2009; Li et al. 2010; Poulton et al. 2010).

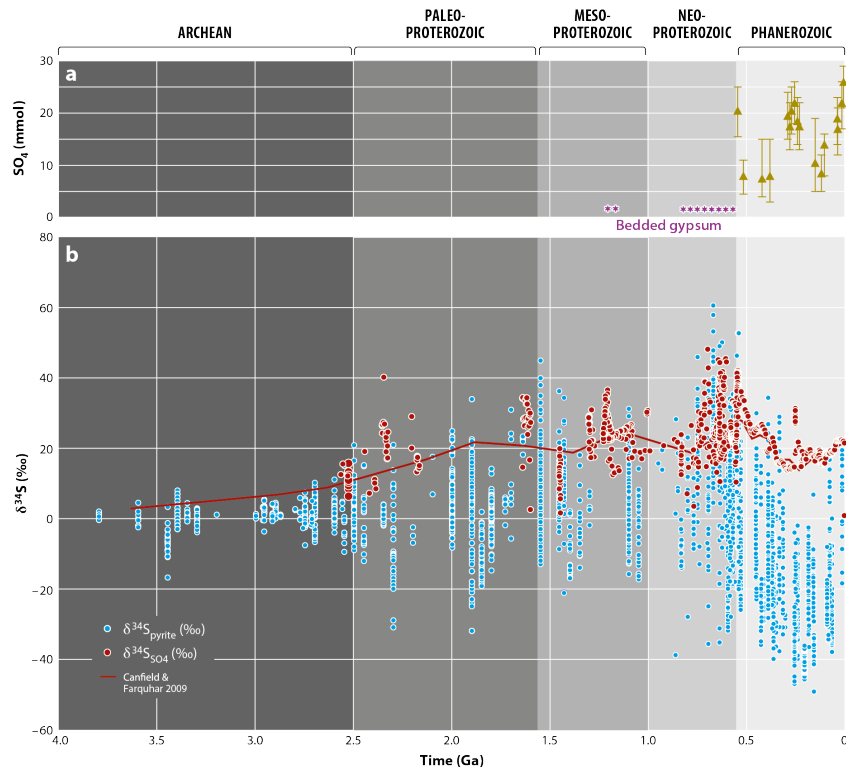


Figure 45

(A) Estimates of seawater sulfate concentration based on the presence of gypsum evaporites in Proterozoic and fluid inclusion data from Phanerozoic marine evaporites. (B) Compilation of sulfate and sulfide $\delta^{34}\text{S}$ records. After Fike et al. (2015).

Carbonate minerals are commonly recrystallized during burial, potentially altering their textural, geochemical, and isotopic properties (Veizer 1980; Banner and Hanson 1990; Kaufman et al. 1990). Thus, it is important to consider the possible effects that post-depositional processes may have had on the $\delta^{34}\text{S}_{\text{CAS}}$ time series data. Although considerable efforts have been made to identify potential diagenetic effects on $\delta^{13}\text{C}_{\text{carb}}$ and $\delta^{18}\text{O}_{\text{carb}}$, relatively little is known about the relevant processes for $\delta^{34}\text{S}_{\text{CAS}}$. In a study on Pleistocene limestones, Gill et al. (2008) demonstrated that, although meteoric diagenesis significantly reduced CAS concentrations in aragonite that had recrystallized to low-magnesium calcite, it had little to no effect on $\delta^{34}\text{S}_{\text{CAS}}$ of the recrystallized material. Similarly, Lyons et al. (2004) showed that $\delta^{34}\text{S}_{\text{CAS}}$ of modern marine carbonate muds records $\delta^{34}\text{S}_{\text{SO}_4}$ of overlying seawater even in sediments hosting active microbial sulfate reduction (MSR) and authigenic precipitation of carbonate from the MSR-associated alkalinity flux. Many CAS sulfur isotopes records based on bulk analyses show significant variation (Jones and Fike 2013). Meanwhile, determination of the source of bulk-rock analyses has been studied in detail in Present et al. (2015). They extracted CAS isotopic compositions of several sedimentary components from well-preserved Late Ordovician and Early Silurian-age limestones from Anticosti Island, Quebec, Canada. Mixtures of these components vary from 25 ‰ and can explain CAS-bulk analyses variations. On Anticosti Island, the CAS in micrite is ^{34}S -depleted relative to contemporaneous seawater, and may be explained by sulfide oxidation in pore fluids during early diagenesis, or incorporation of ^{34}S -depleted sulfate-rich dolomitizing fluids. The CAS

in components recrystallized during burial diagenesis is characterized by $\delta^{34}\text{S}$ values higher than contemporaneous seawater, and requires active sulfate reduction in Anticosti Island groundwater (Present et al. 2015). Promising advances in this approach have been done during the last 5 years, using high analytical technics such as MC-ICP-MS (Paris et al. 2013, 2014; Present et al. 2015) and SIMS (Jones and Fike 2013). Taken together, these approaches allow us to better understand natural variability observed on CAS samples, and give us opportunities to constrain the diagenetic history of samples.

Additionally, recent studies highlighted CAS isotopic offsets resulting from the chemical extraction in pyrite-rich samples, recent advances in this domain have been made towards solving this problem (Wotte et al. 2012; Marengo et al. 2008).

2.3.2. Sulfide. Our understanding of the evolution of the past sulfur cycle over Earth history, especially before the Paleo-Proterozoic, is mainly derived from the records of pyrite $\delta^{34}\text{S}$ from sedimentary strata (see **Figure 45**). Thus, reconstructed seawater $\delta^{34}\text{S}$ during Archean time is thought to be $\sim 0\text{‰}$ with minor variability (low pyrite variability), although this early Earth reconstruction assumes that pyrite was the dominant sink of sulfate in the ocean (Guo et al. 2009; Paris et al. 2014). During the Paleo-Proterozoic more reported data are available with no real change in the mean value ($\sim 0\text{‰}$) but with much more variability ($+25\text{‰}$ to -25‰ , see **Figure 45**). In contrast Meso-Proterozoic time shows more positive values that must reflect changes in the geochemical conditions during formation of pyrite via bacterial sulfate reduction (i.e. change in rate of sulfate reduction and/or sulfate limitation). The mean $\delta^{34}\text{S}_{\text{pyrite}}$ increase from 0‰ (i.e. Meso-Neoproterozoic) to $+20\text{‰}$ at the end of the Neo-Proterozoic is associated with an increase of $\delta^{34}\text{S}_{\text{SO}_4}$. Early Phanerozoic time is characterized by high isotopic pyrite signal, before beginning a continuous decrease until $\sim 300\text{ Ma}$, which is consistent with coeval reconstructed seawater signal. Beginning at 300 Ma , seawater sulfate composition decreases toward the modern isotopic composition (i.e. $+21\text{‰}$) indicating increasing sulfate concentration in the Ocean and increasing sulfate-pyrite ^{34}S fractionation (Canfield 2004). Phanerozoic time shows highly variable sulfur isotopes values at a given time with negative values and positive values that approximate the seawater composition in a single strata (Strauss 1997). This high variation could result from early to late diagenesis history, and limitation of sulfate for sulfate reduction, which is known to result in ^{34}S -enriched sulfide. Alternatively, such variation could also be explained by change in the ocean bottom water condition (i.e. oxygen availability) that records local to regional (i.e. entire basin anoxia for example) environmental condition during syndepositional pyrite formation. Pyrite sulfur isotope data presented in **Figure 45** are probably a mixture from various histories (i.e. primary syn-genetic and secondary diagenesis history).

Nevertheless, primary syn-genetic variation in $\delta^{34}\text{S}_{\text{pyrite}}$ can result from multiple causes on a broad spatial (i.e. lateral) scale. As we already mentioned, marine sulfide is directly connected to marine sulfate, thus any change in the parent pool (i.e. seawater sulfate) isotopic composition are equally transmitted to newly sulfide forms. However, changes in $\delta^{34}\text{S}_{\text{pyrite}}$ could also result from local biological or environmental factors. It appears that changes in the biological fractionation (near $0 < \varepsilon_{\text{pyr}} < 70\text{‰}$, Sim et al. 2011a; Leavitt et al. 2013a), or changes in the microbial community are dominant processes in the $\delta^{34}\text{S}_{\text{pyrite}}$ record. Because change in the rate of bacterial sulfate reduction, or the microbial community, are governed by very local processes on a very short time scale, it would not be consistent with lateral homogeneity in past and present $\delta^{34}\text{S}_{\text{pyrite}}$. Moreover, such biological overprints on the global sulfur cycle could explain extreme variability recorded in single sedimentary unit.

The shelf sediment distribution must be an important syn-genetic factor due to the strong control of the organic matter (i.e. electron donor) on the sulfate bacterial activity (i.e.

source, availability and reactivity, Jørgensen 2017; Canfield 2001). Indeed, it is difficult to access such isotopic gradients because they are spatially organized and dependent of the selected scale (i.e. km to mm). Nevertheless, several microbial mats studies have shown coherent spatial distribution within mat systems that seem to indicate a specific biological organization (Fike et al. 2009; Wilbanks et al. 2014; Visscher et al. 2000; Meyer et al. 2017). Large amplitude, spatially coherent $\delta^{34}\text{S}$ gradients (~ 10 to 20 ‰) were found at the chemocline, which are consistent with large geochemical changes and related to high microbial activity. However, other gradients were also reported deeper within mats where no substantial geochemical variations were observed. This probably resulted from change in the organic substrate (i.e. source/availability; Fike et al. 2009). In mat systems, ambient sulfate concentration appears strongly related to the magnitude of fractionation associated with sulfide production (i.e. smaller $[\text{SO}_4^{2-}]$ decreases the fractionation). This suggests that small-scale change in $\delta^{34}\text{S}_{\text{pyrite}}$ can be indicative of past sulfate concentration, even when the initial isotopic composition is still unknown, Fike et al. 2009.

There are several non-microbial syn-genetic processes that could also influence $\delta^{34}\text{S}$ trends and induce variability, see **Figure 46**. Sulfur cycling within natural sediment is dependent on the connectivity between porewater (i.e. parent sulfate pool during sedimentary sulfate reduction) and the overlying water column. In the literature, the connectivity at the sediment/water interface is used to describe open versus close system (Ohmoto et al. 1990; Canfield 2001; Hartmann and Nielsen 2012; Gomes and Hurtgen 2013, 2015). Indeed, during sedimentary sulfate reduction, microbial activity leads to a decrease in the porewater sulfate pool and increase in $\delta^{34}\text{S}_{\text{SO}_4}$ as sulfide (^{32}S enriched) is formed. Assuming a constant biological fractionation, this distillation process results in a parallel increase in $\delta^{34}\text{S}_{\text{H}_2\text{S}}$ that will be captured in $\delta^{34}\text{S}_{\text{pyrite}}$, **Figure 46.A** and **.B**. As already mentioned, this biological fractionation is mainly governed by the initial sulfate concentration, organic carbon source availability and reactivity, sedimentation rate, and sediment characteristics (i.e. permeability, porosity, density, Canfield 2001; Aller 2014), whereas the conservation of such process into pyrite depends on reactive iron availability (i.e. conversion of H_2S to pyrite; Berner 1984). Nevertheless, sediment studies from several different coastal environments (Kaplan et al. 1969; Canfield and Cappellen 1992; Brüchert and Pratt 1996; Werne et al. 2003; Raven et al. 2016), and direct observations obtained during microbial culture (Canfield 2001), reported isotopic shifts between sedimentary pyrite and coeval. Those observations suggest that the S-composition of pyrite cannot be inherited directly from the isotopic composition of porewater $\Sigma\text{H}_2\text{S}$, and challenge the idea that pyrite precipitation process generate small to zero fractionation from its sulfur source (i.e. H_2S ; Wilkin and Barnes 1996; Böttcher et al. 1999), see **Figure 46.C** and **.D**.

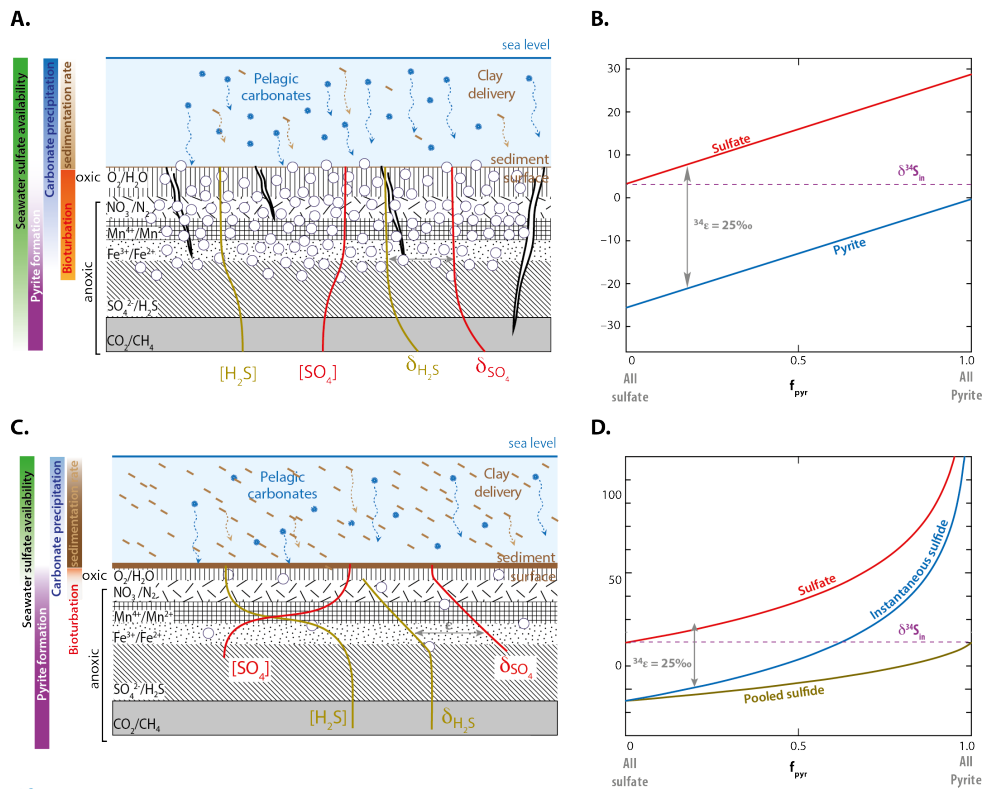


Figure 46

Schematics showing differences between open and closed systems with related impacts on sedimentary sulfur isotopes. In all case, the microbial sulfate rate is considered constant ($^{34}\epsilon$) in the sediment allowing production of H_2S , and the abundance and isotopic composition of the created sulfide is depth dependent. **(A)** Microbial reduction and consequences on the sedimentary record within an 'Open system'; **(B)** Schematic showing the isotopic evolution of sulfate and sulfide during an open system; **(C)** Microbial sulfate reduction and sedimentary sulfur evolution during closed-system, **(D)** Sulfate and sulfide evolutions during closed-system showing high variability as sulfides are growing from a pool that is isotopically evolving through time. Adapted from Fike et al. 2015.

Also, bioturbations processes such as irrigation of burrow tubes with 'fresh' (i.e. $[SO_4]_{sw}$ and seawater isotopic composition) and oxygenated seawater result in loss of sulfur from the sediment by oxidation of reduced sulfur compounds (mainly pyrite), and extra addition of organic carbon, (Jørgensen 2017; Aller 1982; Berner and Westrich 1985). Such processes induce an increase in bacterial sulfate reduction with subsequent decrease of microbial fractionation that creates a local isotopic gradient. Other processes are also known to remobilize surface sediments such as waves, tide-induced sediment mixing, and storms in the near shore area, Aller 2014.

Additionally to syn-genetic induced lateral and or horizontal changes in $\delta^{34}S_{pyrite}$, post deposition history (early to late diagenesis) can overprint original sulfur isotope signatures. This happens when sulfidic fluid migrates through strata with a high amount of iron, then sulfide mineralization occurs during diagenesis and/or during hydrothermal alteration.

3. Variability in modern environments

In modern cases, pyrite isotopic variations result from intrinsic sediment characteristics because of the long residence time of sulfate in the ocean (13 Myr, Kah et al. 2004). The resulting variations in $\delta^{34}\text{S}_{\text{pyrite}}$ in such environments arise from differences in the local depositional environments, not the ambient water chemistry. To better understand sulfur throughout Earth history, examination of modern environments can provide us clues to better understand the magnitude effects on sulfur from depositional environments versus biological effects. Depositional conditions can impact sedimentary $\delta^{34}\text{S}$ through several processes, such as (1) the physical sediments characteristics (i.e. sedimentation rate, grain size and shape, geochemical proprieties, amount of organic carbon or iron; Habicht and Canfield 1997; Aller 2014); (2) benthic ecology (i.e. bioturbation, microbial mats; Zhu et al. 2006; Canfield and Farquhar 2009; Aller et al. 2010) and (3) characteristics of environmental depositions (i.e. sediments remobilization, oxidative reworking; Aller et al. 2010; Aller 2014).

In the following section, we summarized two recent studies in order to highlight the potential effect of deposition conditions on $\delta^{34}\text{S}_{\text{pyrite}}$. The first one based on a geochemical investigation on Papua New Guinea multiple sediment cores (Aller et al. 2008, 2010). The second one present a numerical modeling based on the Papua New Guinea dataset. In both case, authors highlighted a strong $\delta^{34}\text{S}$ overprint of the depositional environment on the microbial fractionation.

3.1. Study case of Papua New Guinea [Aller et al., 2008]

Aller and colleagues published a paper in 2008 showing an interesting sedimentary case. Geochemical investigation of the organic carbon and sulfur cycles along the margin highlighted an important spatial variation according to depth of sediment deposition. A detailed discussion of the depositional environment, core description and associated pore-water chemistry can be found in Aller et al. 2008. The study has been conducted on shelf sediment of the Gulf of Papua (Figure 47).

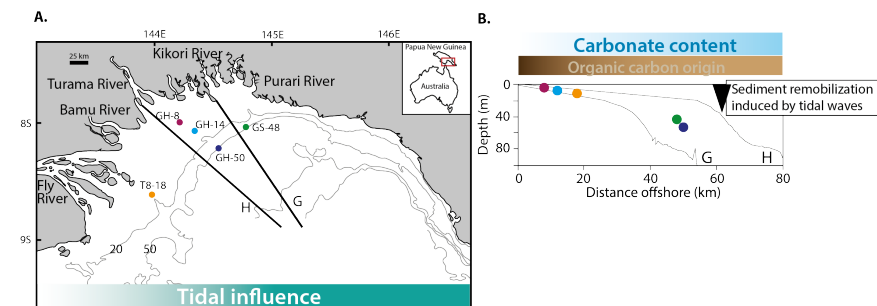


Figure 47

(A) Location of 5 cores from Gulf of Papua, Papua New Guinea. (B) Presents depth profile of the shelf at locations G and H with projected cores depth and sediment remobilization layer. Slightly modified from Aller et al. 2008

The shelf is characterized by numerous mountainous rivers supplying high amount of sediment and organic carbon. The shelf water column is warm, well oxygenated and bottom sediment diagenetically active. Most sediments are deposited on prograding clinoform deposits in <50 m water depth. The shelf presents disparities in the tidal influences (i.e. macrotidal to microtidal), nevertheless tidal waves induce sediment remobilization (inducing low bioturbation processes until 30 m). Spatial sedimentary organization is mainly governed by mangrove presence near the shore, which acts as a fine terrigenous sediment

trap. The seabed becomes progressively more carbonate rich and sandy seaward. Isotopic composition of organic carbon ($\delta^{13}\text{C}_{\text{org}}$) in surface sediments shows regular inshore/offshore changes from dominantly terrestrially-derived C_{org} ($\delta^{13}\text{C}_{\text{org}} \sim -26.6 \text{‰}$; dark brown on **Figure 47**) toward a dominantly marine planktonic source ($\delta^{13}\text{C}_{\text{org}} \sim -21 \text{‰}$, light brown on **Figure 47**), and ^{14}C age of organic carbon reveals mixing between recent (300 years) and aged soil C_{org} .

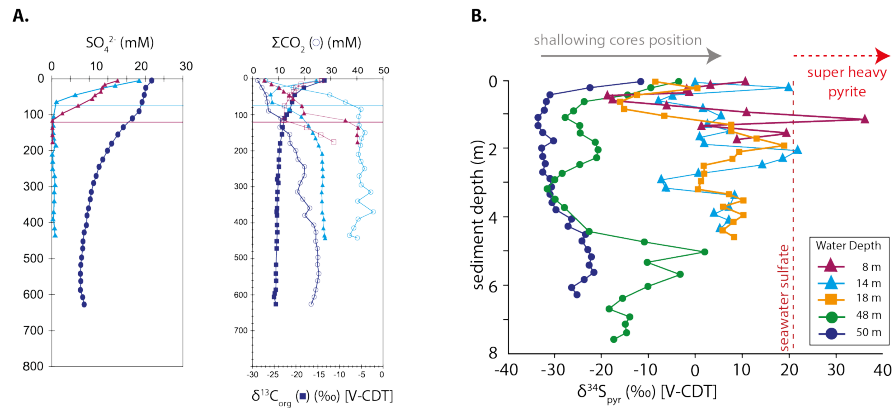


Figure 48

(A) Porewater SO_4^{2-} profiles at 8 and 14 m, show constant concentration or linear decreases implying net reduction of SO_4^{2-} is complete at the end of the bottom reworked layer and that anaerobic oxidation of CH_4 occurs at the basal unconformity. The deeper core SO_4^{2-} profile shows presence of net reduction of SO_4^{2-} below the bioturbated zone and SO_4^{2-} decreases exponentially to a non-zero constant value. Pore-water ΣCO_2 concentration (open symbols) and ΣCO_2 $\delta^{13}\text{C}_{\text{org}}$ (solid symbols) show significant ^{13}C enrichments in the upper few centimeters and substantial increase of $\delta^{13}\text{C}_{\text{org}}$ in the methanic zone. Data is from Aller et al., 2008. (B) $\delta^{34}\text{S}_{\text{pyrite}}$ depth profiles within sedimentary core spanning from 8 m to 50 m. This clearly suggests a depth dependence of $\delta^{34}\text{S}_{\text{pyrite}}$ characterized by an increase of $\delta^{34}\text{S}_{\text{pyrite}}$ with shallowing depth. Note that shallowest cores recorded 'super-heavy' pyrite. Data is from Fike et al., in prep.

Data reported in Aller et al. 2008 show formation and persistence through seasons of physically reworked seasonally variable surface layers in shallow environments. Multiple tracers ($\delta^{13}\text{C}_{\text{org}}$, $\Delta^{14}\text{C}_{\text{org}}$, ΣCO_2) show sub-oxic conditions within the mobile layer, which decrease seaward. Sulfate porewater profiles show concentration decreasing with depth, implying that net sulfate reduction is focused within the 'mobile layer'. Moreover, anaerobic oxidation of CH_4 occurs near the basal depositional unconformity, where we can observe the highest concentration of ΣCO_2 (see **Figure 48**).

The $\delta^{13}\text{C}_{\text{org}}$ downcore increase is consistent with the presence of a methanic zone. Mixing model evaluation of porewater ΣCO_2 and isotopic distribution show that a broad range, age and reactivity of C_{org} substrates from multiple sources (i.e. terrestrial soil, kerogen, vascular plant debris, freshwater plankton and marine biogenic production) are decomposed across the clinofolds. The remineralization pattern of terrestrial and marine C_{org} demonstrates the existence of a gradient across the shelf and toward the sediment column. Indeed, the mobile layers suboxic sediments mainly remobilize recent C_{org} , whereas the metagenic layer show very depleted values implying remobilization of kerogen, carbonate precipitation and aged sediment. Remobilization also show a clear spatial gradient of young and weakly decomposed terrigenous components over the shelf, implying complete disappearance/absence of young, labile C_{org} at core location near to the shelf break (i.e. 48 and 50 m below actual sea-level). Diagenetic processes must occur continuously during remobilization throughout the shelf break because depositional conditions do not allow expression of a vertical gradient within the sedimentary column. This is in contrast to shallow deposits where environmental conditions induce two different layers: a mobile layer overlying a metagenic

zone layer, where both layers are separated by an active geochemical and microbial discontinuity. Such spatial heterogeneities are also recorded in $\delta^{34}\text{S}_{\text{pyrite}}$ profiles collected within the same cores, **Figure 48**.

Deeper cores (48 and 50 m) show superficial enriched values, which are consistent with high microbial activity (Sim et al. 2011b; Leavitt et al. 2013a) across the superficial geochemical gradient (Fike and Grotzinger 2008; Wilbanks et al. 2014). Rapid cell-specific rates of sulfate reduction are consistent with the presence of a sufficient quantity of easily metabolizable marine planktonic C_{org} (Aller et al. 2008). Downcore values are more depleted (~ -25 ‰) and less variable, which are consistent with the consumption of SO_4^{2-} . Deeper, when porewater SO_4^{2-} becomes less abundant (i.e. consumed by sulfate reducers), $\delta^{34}\text{S}_{\text{pyrite}}$ are more enriched which is consistent with ^{34}S enrichment of the residual porewater sulfate pool. As for organic carbon, the situation is much more complex in shallow environment where the depositional processes induce an overprint on the biological sulfur pathway. Aller et al. (2008) show substantial and frequent reworking of the upper mobile layer of the sedimentary column. Moreover, the intensity of this reworking is strongly spatially controlled, that means increased intensity and impact of reworking processes when shallowing the core location. This is clearly recorded in the $\delta^{34}\text{S}_{\text{pyrite}}$ signal of shallow cores, which are substantially more ^{34}S -enriched than deeper cores, and present high sample to sample variability (see **Figure 48**). Such high variability towards enriched $\delta^{34}\text{S}_{\text{pyrite}}$ can be interpreted to result from various mixing sedimentary events, then subsequent oxidation steps of reduced sulfur forms (i.e. mainly pyrite; see **Figure 49**).

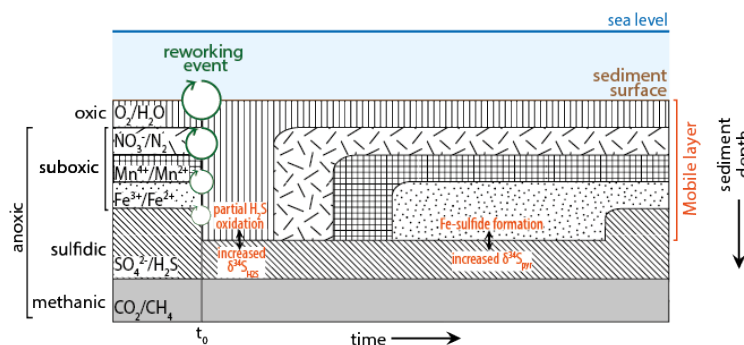


Figure 49

Classic redox reaction zonation with depth and time in an accumulating sedimentary environment. Relative zonal depth depends of fluxes in oxidants and reductants. Unsteady redox stratification and diagenetic ingrowth in a surface mobile layer after a reworking event (t_0) and influence of the isotopic sulfur cycle. Adapted from Fike et al. 2015.

In such cases, the previously stratified and undisturbed primary signal is affected. Indeed, during and after the reworking event we observe a juxtaposition of newly deposited oxic sediment on top of reduced, anoxic sediments (i.e. already containing pyrite) which can induce partial re-oxidation of sulfides and an increase of $\delta^{34}\text{S}_{\text{H}_2\text{S}}$. With time, oxygen is consumed and redox zones return to 'normal', then reactive iron (Fe^{2+}) can react with newly formed ^{34}S -enriched H_2S to form pyrite with elevated $\delta^{34}\text{S}_{\text{pyrite}}$ (Aller et al. 2008; Gao et al. 2013) (**Figure 49**). This can potentially result in the generation of 'heavy' to 'super-heavy' pyrite which are characterized by $\delta^{34}\text{S}_{\text{pyrite}}$ value higher than seawater $\delta^{34}\text{S}_{\text{SO}_4^{2-}}$. Such observation is consistent with the observations of Ries et al. 2009; Aller et al. 2010.

3.2. Model prediction under sea-level changes [Fike et al. in review]

Because of the increasing amount of information and interpretation of depositional controls on the $\delta^{34}\text{S}$ signature in modern environments, it is possible to extrapolate these results over an entire sedimentary shelf. Such approach has recently been used to generate a 2D predictive model of potential changes in sedimentary sulfur isotopic composition on a passive margin (Fike et al. in review), see **Figure 50**. This work, based on $\delta^{34}\text{S}_{\text{pyrite}}$ core profiles obtained on Papua gulf (Aller et al. 2010), was able to predict mean $\delta^{34}\text{S}_{\text{pyrite}}$, its scatter and magnitude of any excursion within a given sedimentary package, during sea level environmental changes.

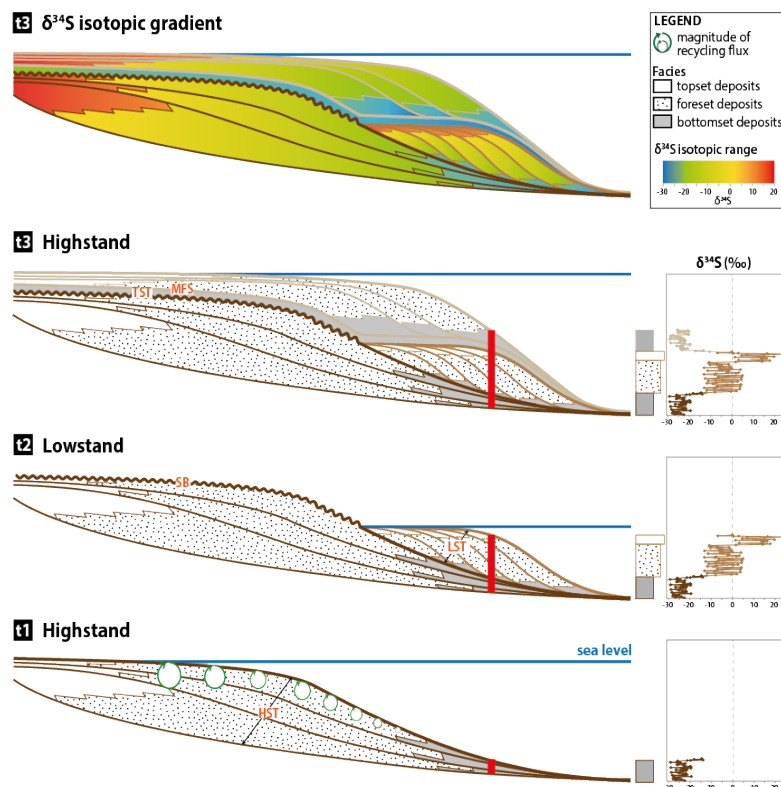


Figure 50

Schematic view of the potential changes of environmental conditions on the $\delta^{34}\text{S}_{\text{pyrite}}$ core profile in a passive margin. **(t1)**: Stratigraphic cross section for shallow water sediments with a gradient of possible syn-depositional reworking processes. The red line represents a possible sediment core with a very low reworking leading $\delta^{34}\text{S}_{\text{pyrite}}$ model on the right box. These modeled values are characterized by relatively depleted values with low variability. **(t2)**: Following a seaward migration of the coastal line (drop of sea level) the resulting lowstand sediments are deposited in a more favorable reworking context. $\delta^{34}\text{S}_{\text{pyrite}}$ modeled with those high-energy conditions are more enriched and show a high variability. **(t3)**: Following an increase in Relative Sea Level, sediments are again deposited in a deep environment with a very low probability of reworking. The top schematic is a cross section of strata colored by predicted $\delta^{34}\text{S}_{\text{pyrite}}$ values. This clearly shows a sedimentary environment control of $\delta^{34}\text{S}_{\text{pyrite}}$ values, their scatters and any possible extremes values (super heavy pyrite). From Fike et al. (in review).

The resulting sedimentological shelf organization is shown on **Figure 50**. The resulting shelf organization can be described as a superposition of sedimentary units separated by major discontinuities. The initial shelf organization ($t=1$ on **Figure 50**) was obtained in highstand conditions, which allows deposition of a sedimentary prism resulting from the interaction of fluvial inputs and marine processes, and deposition of the high stand track sedimentary unit on the shelf. On **Figure 50** we can observe a seaward decrease of terrestrial influence concomitant with the magnitude of the recycling flux on the depositional environment. Considering the red line as a potential core located within a very low reworking area, we can see on the right box a representative $\delta^{34}\text{S}_{\text{pyrite}}$ profile. Those predicted values are characterized by depleted ^{34}S values with low variability, which is coherent with respect to data obtained on the deeper part of the Papua Gulf (see data of the core collected at 50 mbsf in **Figure 50**). Following seaward migration of coastal sedimentary units during the sea-level drop most of the shelf underwent subaerial exposure/erosion ($t=2$ on **Figure 50**), allowing preservation of the low stand system (LST) at our core location. The LST is characterized by both vertical and horizontal reworking gradients leading to ^{34}S -enriched pyrite with high variability. Note that data predicted within the top set facies are characterized by very heavy $\delta^{34}\text{S}_{\text{pyrite}}$ (i.e. 'heavy pyrite') related to intense and continuous reworking processes, similar to mobile layer depositional environment (i.e. core collected at 8 and 14 mbsf on **Figure 50**). Back to high sea-level condition, $t=3$ on **Figure 50**, sediments are again deposited in deeper, quieter waters, showing similar $\delta^{34}\text{S}_{\text{pyrite}}$ values than $t=0$.

The top schematic is a cross section of sedimentary units with color-codes indicating predicted $\delta^{34}\text{S}_{\text{pyrite}}$ for local changes in depositional environment due to changing sea level. This study highlights the capacity to preserve in pyrite well-defined and stratigraphically coherent $\delta^{34}\text{S}$ excursions related to changes in local depositional conditions without any changes in the secular sulfur cycle (i.e. pulse of increase or decrease of pyrite burial).

4. Pyrite sulfur isotopes: a new proxy of glacial interglacial environmental changes.

Pyrite sulfur isotopes reveal glacial–interglacial environmental changes

Virgil Pasquier^{a,1}, Pierre Sansjofre^a, Marina Rabineau^a, Sidonie Revillon^{a,b}, Jennifer Houghton^c, and David A. Fike^c

^aLaboratoire Géosciences Océan, UMR CNRS-6538, Institut Universitaire Européen de la Mer, Université Bretagne Occidentale, 29280 Plouzane, France; ^bSEDISOR, Institut Universitaire Européen de la Mer, 29280 Plouzane, France; and ^cDepartment of Earth and Planetary Sciences, Washington University in St. Louis, St. Louis, MO 63130

Edited by John P. Grotzinger, California Institute of Technology, Pasadena, CA, and approved April 12, 2017 (received for review November 3, 2016)

The sulfur biogeochemical cycle plays a key role in regulating Earth's surface redox through diverse abiotic and biological reactions that have distinctive stable isotopic fractionations. As such, variations in the sulfur isotopic composition ($\delta^{34}\text{S}$) of sedimentary sulfate and sulfide phases over Earth history can be used to infer substantive changes to the Earth's surface environment, including the rise of atmospheric oxygen. Such inferences assume that individual $\delta^{34}\text{S}$ records reflect temporal changes in the global sulfur cycle; this assumption may be well grounded for sulfate-bearing minerals but is less well established for pyrite-based records. Here, we investigate alternative controls on the sedimentary sulfur isotopic composition of marine pyrite by examining a 300-m drill core of Mediterranean sediments deposited over the past 500,000 y and spanning the last five glacial–interglacial periods. Because this interval is far shorter than the residence time of marine sulfate, any change in the sulfur isotopic record preserved in pyrite ($\delta^{34}\text{S}_{\text{pyr}}$) necessarily corresponds to local environmental changes. The stratigraphic variations (>76‰) in the isotopic data reported here are among the largest ever observed in pyrite, and are in phase with glacial–interglacial sea level and temperature changes. In this case, the dominant control appears to be glacial–interglacial variations in sedimentation rates. These results suggest that there exist important but previously overlooked depositional controls on sedimentary sulfur isotope records, especially associated with intervals of substantial sea level change. This work provides an important perspective on the origin of variability in such records and suggests meaningful paleoenvironmental information can be derived from pyrite $\delta^{34}\text{S}$ records.

pyrite sulfur isotopes | glacial | interglacial | sedimentation rate | local environment changes

The sulfur biogeochemical cycle helps regulate Earth's surface redox conditions through a variety of abiotic and biological reactions (1). These diverse reactions are often associated with distinctive stable isotopic fractionations of sulfur species (2, 3). As such, changes in the sulfur isotopic composition ($\delta^{34}\text{S}$) of sedimentary phases over Earth history are often used to infer substantive changes to Earth's surface environment, including the rise of atmospheric oxygen, the oxygenation of the oceans, and episodes of metazoan evolution and mass extinction (2–6). Much of past efforts to reconstruct the ancient sulfur cycle has used sulfate evaporite minerals (gypsum and anhydrite), barium sulfate (barite), or carbonate-associated sulfate [i.e., sulfate bound into carbonate lattice, carbonate-associated sulfate (CAS)], all proxies commonly used to accurately reflect the $\delta^{34}\text{S}$ composition of seawater sulfate (2, 7). Additional constraints on ancient biogeochemical cycling have been placed through the analysis of $\delta^{34}\text{S}$ records from sedimentary pyrites, either in parallel with direct proxies for sulfate (4, 6, 8, 9), or on their own (10–13). Inferences about past biogeochemical cycling are based on the assumption that the $\delta^{34}\text{S}$ records reflect the isotopic composition of seawater sulfate and, further, that changes in these values indicate large-scale temporal changes in the global sulfur cycle. However, a subset of records of sulfur cycling from certain intervals

on Earth have shown substantial spatial and stratigraphic variability that is not easily reconciled with them reflecting the behavior of the global sulfur cycle (e.g., ref. 14). Rather, it has been suggested that some $\delta^{34}\text{S}$ records have the potential to be impacted by local depositional conditions (2), and, further, that these records may provide new insights into paleo-environmental conditions. This intriguing idea has, however, not yet been appropriately tested.

Here we examine the sulfur isotopic record preserved in pyrite ($\delta^{34}\text{S}_{\text{pyr}}$) from sediments from the Gulf of Lion deposited over the last 500,000 y associated with the last five glacial–interglacial transitions. Gulf of Lion is located in the northwestern Mediterranean basin and is characterized by a wide continental shelf (70 km) that was subaerially exposed during glacial periods over the Late Quaternary (15, 16). This study is based on borehole PRGL1-4 (Fig. 1), drilled in the framework of the European Union Profiles Across Mediterranean Sedimentary Systems (PROMESS) project (<https://www.pangaea.de/?q=PROMESS1>), which sampled a 300-m-long continuous record of the Bourcart and Hérault canyons' interfluvial sediment sequence on the upper slope of the Gulf of Lion (Fig. 1). The water depth of the core (298 m) ensures continued deposition under well-oxygenated conditions during glacial and interglacial periods with sedimentation rates that enable high-resolution records and where the changing proximity to the continental shelf results in variable detrital input. Given these characteristics, this drill core represents a record of glacial–interglacial deposition that is uniquely positioned to assess the environmental dependence of $\delta^{34}\text{S}_{\text{pyr}}$ signatures in marine sediments.

Significance

Changes in sulfur isotope ratios ($^{34}\text{S}/^{32}\text{S}$) of marine sulfur phases are often attributed to global biogeochemical perturbations. Sediments collected on the shelf of the Gulf of Lion revealed remarkable sulfur isotopic fluctuations in sedimentary pyrite over the last 500,000 years, ranging between -44.0‰ and 32.3‰ . We suggest this pattern is related to changes in the local environmental deposition, specifically, sedimentation modulating connectivity with the overlying water column and resulting microbial activity. Besides providing new understanding of an important and poorly constrained aspect of past glacial–interglacial transitions, our results are critically important because they question the degree to which changes in sulfur isotopes in pyrite reflect global biogeochemical processes versus local depositional conditions.

Author contributions: P.S., M.R., S.R., and D.A.F. designed research; V.P., P.S., and D.A.F. performed research; V.P. and J.H. contributed new reagents/analytic tools; V.P., P.S., and D.A.F. analyzed data; and V.P., P.S., M.R., S.R., J.H., and D.A.F. wrote the paper.

The authors declare no conflict of interest.

This article is a PNAS Direct Submission.

¹To whom correspondence should be addressed. Email: virgil.pasquier@univ-brest.fr.

This article contains supporting information online at www.pnas.org/lookup/suppl/doi:10.1073/pnas.1618245114/-DCSupplemental.



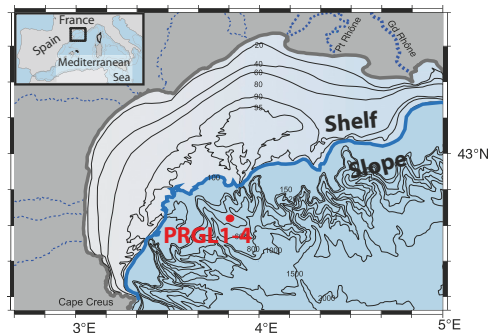


Fig. 1. Map of the Gulf of Lion with the position of the PRGL1-4 core (42.690°N, 3.838°E). The bold gray line highlights the present shoreline position, and the contours reflect modern water depths. The bold blue line corresponds to the shoreline position during the last glacial period (low sea level).

Results and Discussion

A total of 131 pyrite sulfur isotopes analyses have been performed along the 300-m PRGL1-4 core, spanning the last five glacial–interglacial transitions (Fig. S1 and Table S1). Throughout the core, pyrite shows extreme variations in $\delta^{34}\text{S}_{\text{pyr}}$, from -44.0‰ to 32.3‰ , whereas pyrite contents vary between 0.02 wt % and 1.69 wt %. No clear trend was observed between $\delta^{34}\text{S}_{\text{pyr}}$ and the pyrite content, nor between $\delta^{34}\text{S}_{\text{pyr}}$ and the iron content (Figs. S1 and S2). Complementary analysis of organic carbon isotopes ($\delta^{13}\text{C}_{\text{org}}$) was conducted, and these values vary between -25.3‰ and -21.8‰ , with no clear trends between $\delta^{13}\text{C}_{\text{org}}$ and total organic carbon (TOC) contents, which vary between 0.35% and 0.84%. Similarly, we do not observe any covariation between $\delta^{34}\text{S}_{\text{pyr}}$ and TOC (Figs. S1 and S2).

A clear distinction in pyrite $\delta^{34}\text{S}_{\text{pyr}}$ values is observed between glacial and interglacial periods (Fig. 2) as deduced from the oxygen isotope curve obtained from planktonic foraminifera (*Globigerina bulloides*) and the associated updated age model published on the same core (17). Distinctly different bimodal distributions are observed between glacial (*sensu stricto*, i.e., cold substages) periods with high $\delta^{34}\text{S}$ values and high isotopic variability (average $\delta^{34}\text{S} = -15.2\text{‰} \pm 9.0\text{‰}$, $n = 46$) and the interglacial (*sensu stricto*, i.e., warm substages) periods characterized by low $\delta^{34}\text{S}$ and low isotopic variability (average $\delta^{34}\text{S} = -41.6\text{‰} \pm 2.2\text{‰}$, $n = 19$; Fig. 2). The increased variability observed during glacial times provides insights into the suite of processes and their inherent temporal fluctuations that are likely to regulate the observed changes in $\delta^{34}\text{S}_{\text{pyr}}$. Specifically, the lowered sea level during glacial times brought the site of deposition closer to the shore and source of detrital materials. These shallower, more proximal settings are subjected to short-term, stochastic variations in depositional conditions (17), including sediment characteristics (organic carbon loading, sedimentation rates, physical reworking) and benthic ecology (bioturbation, presence of microbial mats) that can impact pyrite formation and eventual $\delta^{34}\text{S}$ composition. Within the glacial and interglacial sediments, the $\delta^{34}\text{S}$ values and variability can be further understood as a function of temperature, as reconstructed from alkenone records (18, 19). For example, warmer intervals during interglacial time are associated with more negative $\delta^{34}\text{S}$ values (Fig. 2).

Over the last two glacial–interglacial cycles, where the time reconstruction is best constrained, pyrite $\delta^{34}\text{S}$ values in PRGL1-4 are modulated by and track depositional conditions across glacial–

interglacial cycles (Fig. 3). During glacial times, higher $\delta^{34}\text{S}_{\text{pyr}}$ values are associated with lower sea levels and low $\delta^{13}\text{C}_{\text{org}}$ values, which are often attributed to greater input of terrestrial organic matter (20). Interestingly, because of their increased proximity to shore, glacial deposits are also associated with increased sedimentation rates of silty clay sediments (21) and are characterized by decreased porosity intervals (Fig. S3). In such nearshore environments, the rapid sediment burial dilutes TOC values. Nevertheless, a higher concentration of labile organic matter (supported by our TOC values) gets into the sediment without undergoing aerobic respiration. As such, a larger fraction of more easily metabolizable (i.e., less degraded by oxic processes) organic matter is available for sulfate reduction during glacial intervals (22).

In contrast, decreased and less variable $\delta^{34}\text{S}_{\text{pyr}}$ values are associated with the transition into and during interglacial times. These periods are associated with warmer temperatures and higher sea levels, as well as increased $\delta^{13}\text{C}_{\text{org}}$ values, indicative of increased marine input (23). Sediments deposited during interglacial periods are also associated with lower sedimentation rates (because of landward migration of the shoreline) and increased foraminiferal abundance, resulting in intervals of higher porosity (21) (Fig. S3). As sedimentation rates decrease, organic matter spends more time in the zone of aerobic respiration. Therefore, less (and less reactive) organic matter remains for sulfate-reducing bacteria under these conditions.

Stratigraphic variations in pyrite $\delta^{34}\text{S}$ are often interpreted to reflect changes in the global sulfur biogeochemical cycle, such as intervals of enhanced pyrite burial or variations in the marine sulfate reservoir (9, 24). However, in this case, these strata were deposited over an interval of 500 ky, much less than the residence

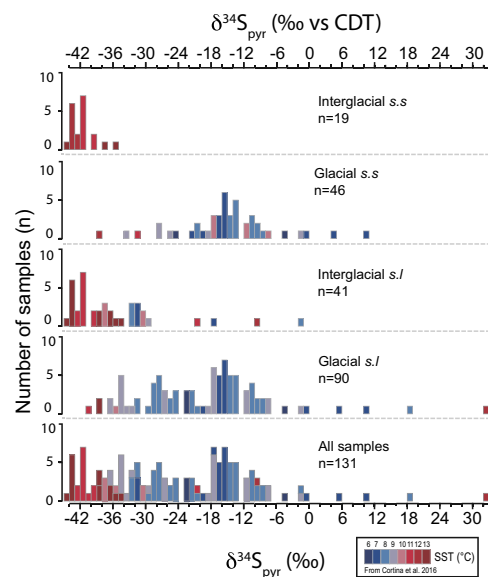


Fig. 2. Histogram of pyrite $\delta^{34}\text{S}$ (this study) as a function of glacial/interglacial periods, color-coded by temperature obtained from the relative composition of C_{27} unsaturated alkenones (18, 19). *Sensu stricto* (s.s.) refers to the warm substages of the interglacials and cold substages during glacials. The *sensu lato* (s.l.) includes all of the data within interglacial or glacial periods.

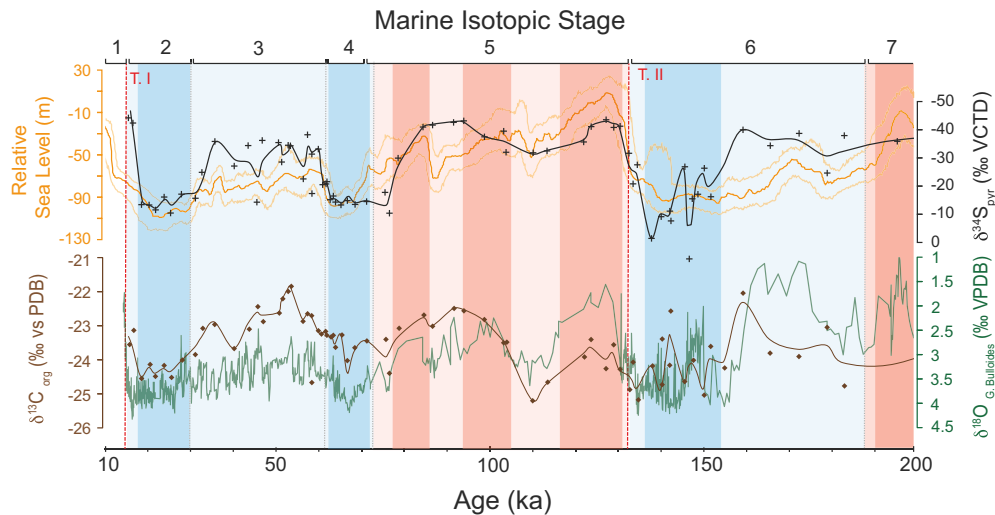


Fig. 3. Glacial–interglacial geochemical records. Shown are the $\delta^{34}\text{S}_{\text{pyr}}$ (black crosses; black line representing LOESS regression, this study), $\delta^{13}\text{C}_{\text{org}}$ (brown diamonds and brown line (local polynomial regression type LOESS, this study), reconstructed sea levels (orange) from the Red Sea, and $\delta^{18}\text{O}_{\text{G.Bullioides}}$ (green) for the last six Marine isotopic stages (10 ky to 200 ky). Also shown are relative sea level (orange line) superimposed with 95% of probability interval (light orange lines) from ref. 43 and $\delta^{18}\text{O}_{\text{G.Bullioides}}$, from refs. 17 and 21. Blue vertical bands represent the glacial times, with corresponding cold substages (i.e., *sensu stricto*) in darker blue. Red bands correspond to interglacial periods, with warm substages (i.e., *sensu stricto*) highlighted in dark pink. Vertical red dashed lines reflect glacial termination (T.) times according to ref. 44; vertical gray dashed lines reflect scheme of marine stages according to ref. 45.

time [13 My (25)] of sulfate in the modern ocean. While these sediments were deposited in the Gulf of Lion, the Mediterranean Sea maintained connectivity with the global ocean and retained marine sulfate abundances and isotopic compositions during glacial–interglacial periods, based on both the abundance and isotopic composition of sulfate pore water profiles (26) and the continuous sea water inflow of Mediterranean Sea by Atlantic water through the Gibraltar Strait since ~ 4.4 Ma (27, 28). Thus, continued connectivity with the ocean and the short timescale of deposition preclude any substantive change in the parent sulfate reservoir, such as might arise from prolonged variation in the burial flux of pyrite, during deposition of these sediments. How then is this variation in pyrite $\delta^{34}\text{S}$ to be interpreted?

Mechanistic Explanations. Two possible mechanisms present themselves to explain the observed data—both fundamentally driven by glaciation induced environmental changes: one reflecting changes in the inherent metabolic activity of sulfur cycling microbes in the sediments, and the other reflecting changes in the connectivity of pore waters to the overlying water column. In the former, isotopic fractionation during microbial sulfur cycling is typically dominated by microbial sulfate reduction (3), and a change in pyrite $\delta^{34}\text{S}$ can result from variations in the rate of cell-specific sulfate reduction (csSRR) in these sediments (29). Specifically, there is a well-documented relationship whereby faster rates of csSRR are associated with decreased isotopic fractionation between the parent sulfate and the produced sulfide (29, 30). Thus, our data could indicate faster csSRR during glacial times, possibly driven by enhanced input of more easily metabolizable organic matter [as supported by lower organic carbon isotopic values (Fig. S1)]. In contrast, slower csSRR would characterize interglacial times associated with more stable and more limited (both in abundance and reactivity) organic matter resources.

Assuming that pyrite is formed mainly in the pore water environment, as is expected under an oxygenated (noneuxinic)

water column (31), an alternative mechanism to explain our data involves a change in the connectivity of sedimentary pore waters where pyrites are forming with the overlying water column (32). Such a change could be the natural result of the increased sedimentation rates and decreased porosity during glacial times (Fig. S3), both of which act to more effectively isolate pore waters from ready communication with seawater. This decreased connectivity effectively isolates the local pore water sulfate reservoir, leading to increased pore water $\delta^{34}\text{S}_{\text{SO}_4}$ through ongoing microbial sulfate reduction (32). In turn, this microbial activity naturally leads to an increase in the resulting biogenic $\delta^{34}\text{S}_{\text{H}_2\text{S}}$, which eventually forms pyrite following reaction with available iron. The increased variability in $\delta^{34}\text{S}_{\text{pyr}}$ during glacial times can be understood as the natural response to increased short-term fluctuations in depositional conditions that characterize shallower water environments more proximal to the shore. During interglacial times, the return to slower sedimentation rates and higher porosity, driven in part by the admixture of foraminifera (Fig. S3), results in enhanced communication between pore water and seawater. In this relatively open system, the constant supply of seawater sulfate results in a stable, low value for pore water $\delta^{34}\text{S}_{\text{SO}_4}$ (and therefore in the resulting $\delta^{34}\text{S}_{\text{pyr}}$) in these intervals. Although the relationship between sedimentation rate and $\delta^{34}\text{S}_{\text{pyr}}$ indicates a dominant control by sedimentation (Fig. 4), it should be noted that these two mechanisms are not mutually exclusive. Indeed, all things being equal, increased csSRR will inherently lead to more closed system behavior because it represents enhanced sulfate consumption relative to the diffusive exchange of sulfate. Further, there is a general trend toward increasing rates of sulfate reduction with increasing sedimentation rate (33).

The magnitude and directionality of the relationship between water depth and pyrite $\delta^{34}\text{S}$ observed here agree with predictions previously made (2) but never rigorously tested and provide a powerful

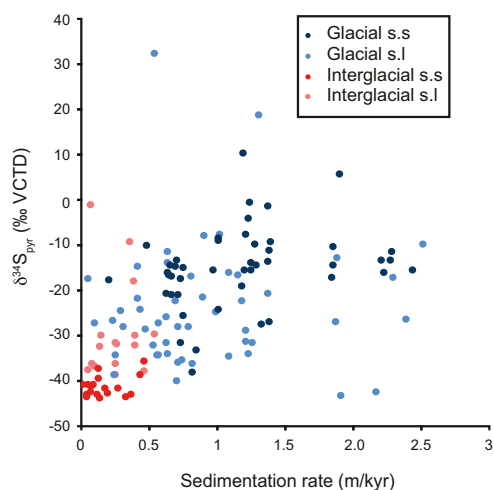


Fig. 4. The relationship between sedimentation rate (meters per kiloyear) and $\delta^{34}\text{S}_{\text{pyr}}$. Sedimentation rates are calculated using the linear relationship between depth in borehole and the update age model derived from ref. 17. Light/dark blue circles correspond to cold substages (i.e., respectively *sensu lato* and *sensu stricto*), and light/dark red circles refer to warm substages (i.e., respectively *sensu lato* and *sensu stricto*).

way to reconstruct paleoenvironmental conditions in sedimentary environments, particularly the degree to which sedimentary pore fluids may have been in communication with the overlying water column. In addition, the $\delta^{34}\text{S}_{\text{pyr}}$ data presented here also shed light on the possible origins of similar variability in this proxy in deep time.

Implication for Deep-Time Records. Many deep-time studies make use of direct proxies for seawater sulfate, such as CAS, which are generally thought to reflect marine sulfate with little fractionation (e.g., ref. 7; but see ref. 34). Indeed, studies using direct proxies for seawater sulfate (e.g., refs. 9, 24, 35, and 36) can provide powerful insights into ancient biogeochemical conditions. In many cases, however, no direct proxy of seawater sulfate is present and stratigraphic records of $\delta^{34}\text{S}_{\text{pyr}}$ are used to reconstruct global biogeochemical cycling and redox change (e.g., refs. 10–13). In other cases, the isotopic offsets between coeval $\delta^{34}\text{S}$ records from sulfate and pyrite are used to reconstruct marine sulfate levels or the types of microbial metabolism present (e.g., refs. 4 and 8). With few exceptions (e.g., ref. 6), these $\delta^{34}\text{S}_{\text{pyr}}$ records are not interpreted in the context of local depositional or facies change.

Interestingly, many of the reports showing positive $\delta^{34}\text{S}_{\text{pyr}}$ excursions in the rock record are also associated with shallowing-upward depositional sequences formed during sea level low-stands. The present study is particularly relevant for considering the ~10 to 30‰ positive excursions in $\delta^{34}\text{S}_{\text{pyr}}$ that are associated with the initiation and termination of the end-Ordovician Hirnantian glaciation and mass extinction (e.g., refs. 6 and 10–13). Depositional environments at this time experienced a magnitude

(~100 m) and timescale (~ 10^5 y) of sea level change that would have been comparable to those influencing the Pleistocene sediments of the Gulf of Lion. Our data suggest that, rather than reflecting a change in the global sulfur cycle, these $\delta^{34}\text{S}_{\text{pyr}}$ excursions could also be explained by local changes in depositional conditions, particularly changes in sedimentation that modulate connectivity with the overlying water column (e.g., Fig. 4). In this scenario, it is local sedimentological changes that impact how records of sulfur cycling get preserved in sedimentary records. The temporal coincidence of the Hirnantian $\delta^{34}\text{S}_{\text{pyr}}$ excursions, found in sections around the world associated with the end Ordovician glaciation, would then be the result of synchronous local changes in environmental conditions in basins around the world, changes driven globally by sea level fluctuations during the onset and termination of the Hirnantian glaciation. Local environmental controls could be relevant for explaining other stratigraphic $\delta^{34}\text{S}_{\text{pyr}}$ excursions in Earth history, particularly those associated with changing depositional facies and lacking a direct proxy for the marine sulfate reservoir (e.g., refs. 37–39). As such, the data presented here show that pyrite $\delta^{34}\text{S}$ can be a valuable proxy for reconstructing local paleoenvironmental and sedimentological conditions throughout Earth history.

Materials and Methods

Pyrite Sulfur ($\delta^{34}\text{S}_{\text{pyrite}}$ and S Content). Pyrite sulfur from the samples was extracted using the chromium reduction method (40–42). This method allows a recovering of all reduced inorganic sulfur present in sedimentary samples (pyrite, element sulfur, and iron monosulfide phases). During extraction, samples were reacted with ~25 mL of 1 M reduced chromium chloride (CrCl_2) solution and 25 mL of 6N HCl for 4 h in a specialized extraction line under a Nitrogen atmosphere. The liberated hydrogen sulfide was reacted in a silver nitrate (0.1 M) trap, recovering the sulfide as Ag_2S ; reproducibility was under 5% for repeated analyze. Residual Ag_2S were rinsed three times using Milli-Q water, centrifuged, and then the dried until complete dryness. The Ag_2S powders were homogenized before being analyzed; then 450 μg was loaded into tin capsules with excess V_2O_5 . The Ag_2S was analyzed measuring $^{34}\text{S}/^{32}\text{S}$ ratio following online combustion with a Thermo Delta V Plus coupled with a Costech ECS 4010 Elemental Analyzer at Washington University in St. Louis. Pyrite sulfur composition are expressed in standard delta notation as per mil (‰) deviations from Vienna Canyon Diablo Troilite with an analytical error of <0.5‰.

Organic Carbon Analyses ($\delta^{13}\text{C}_{\text{org}}$ and TOC). Before organic carbon and nitrogen analyses, the carbonated fraction was removed from bulk samples using excess 1.5 N HCl digestion for 48 h. During digestion, centrifuge tubes were placed in an ultrasonic bath to increase the mechanical separation of clay and calcium carbonates. After total dissolution, residues were washed three times with distilled water, centrifuged, and then dried at 50 °C. The residual powders were homogenized, and, before analyses, 30 mg were loaded into a tin capsule. Analyses were performed using an Elemental Analyzer (EA, Flash 2000; Thermo Scientific) coupled to an isotope ratio mass spectrometer (Delta V+ Thermo Scientific EA-IRMS) at the Pôle de Spectrométrie Océan (PSO). Carbon is given as delta notation as per mil deviation from Pee Dee Belemnite, with an analytical error of <0.2‰ (1 σ) for organic carbon isotopes. TOC was measured using the Thermal Conductivity Detector of the Flash EA 2000 (Thermo Scientific) at PSO.

ACKNOWLEDGMENTS. We thank the European PROMESS Scientific committee and colleagues at Ifremer for previous contributions of data acquisition, processing, interpretations, and permission to resample the borehole. We acknowledge C. Liorzou, who kindly helped during the analytical preparation of samples, and O. Lobeau, for stable isotope analyses assistance in Brest. This work was supported by the “Laboratoire d’Excellence” LabexMER (Grant ANR-10-LABX-19) and was cofunded by a grant from the French government under the program “Investissements d’Avenir,” and by a grant from the Regional Council of Brittany. Additional founding came from Actions Merges Program (Mediterranean Sea). The drilling operation was conducted within the European Commission Project PROMESS (Contract EVR1-CT-2002-40024).

- Garrels RM, Lerman A (1981) Phanerozoic cycles of sedimentary carbon and sulfur. *Proc Natl Acad Sci USA* 78:4652–4656.
- Fike DA, Bradley AS, Rose CV (2015) Rethinking the ancient sulfur cycle. *Annu Rev Earth Planet Sci* 43:593–622.
- Canfield DE (2001) Biogeochemistry of sulfur isotopes. *Rev Mineral Geochem* 43: 607–636.

- Fike DA, Grotzinger JP, Pratt LM, Summons RE (2006) Oxidation of the Ediacaran ocean. *Nature* 444:744–747.
- Riccardi AL, Arthur MA, Kump LR (2006) Sulfur isotopic evidence for chemocline upward excursions during the end-Permian mass extinction. *Geochim Cosmochim Acta* 70:5740–5752.
- Jones DS, Fike DA (2013) Dynamic sulfur and carbon cycling through the end-Ordovician extinction revealed by paired sulfate–pyrite $\delta^{34}\text{S}$. *Earth Planet Sci Lett* 363:144–155.

7. Kampschulte A, Strauss H (2004) The sulfur isotopic evolution of Phanerozoic seawater based on the analysis of structurally substituted sulfate in carbonates. *Chem Geol* 204:255–286.
8. Hurtgen MT, Halverson GP, Arthur MA (2006) Sulfur cycling in the aftermath of a 635-Ma snowball glaciation: Evidence for a syn-glacial sulfidic deep ocean. *Earth Planet Sci Lett* 245:551–570.
9. Gill BC, et al. (2011) Geochemical evidence for widespread euxinia in the later Cambrian ocean. *Nature* 469:80–83.
10. Yan D, Chen D, Wang Q, Wang J, Wang Z (2009) Carbon and sulfur isotopic anomalies across the Ordovician–Silurian boundary on the Yangtze Platform, South China. *Palaeogeogr Palaeoclimatol Palaeoecol* 274:32–39.
11. Zhang T, Shen Y, Zhan R, Shen S, Chen X (2009) Large perturbations of the carbon and sulfur cycle associated with the Late Ordovician mass extinction in South China. *Geology* 37:299–302.
12. Gorjan P, Kaiho K, Fike DA, Xu C (2012) Carbon-and sulfur-isotope geochemistry of the Hirnantian (Late Ordovician) Wangjiawan (Riverside) section, South China: Global correlation and environmental event interpretation. *Palaeogeogr Palaeoclimatol Palaeoecol* 337–338:14–22.
13. Hammarlund EU, Dahl TW, Harper D (2012) A sulfidic driver for the end-Ordovician mass extinction. *Earth Planet Sci Lett* 331–332:128–139.
14. Ries JB, Fike DA, Pratt LM, Lyons TW (2009) Superheavy pyrite ($\delta^{34}\text{S}_{\text{pyrite}} > \delta^{34}\text{S}_{\text{CAS}}$) in the terminal Proterozoic Nama Group, southern Namibia: A consequence of low seawater sulfate at the dawn of animal life. *Geology* 37:743–746.
15. Rabineau M, Berné S, Aslanian D, Olivet JL (2005) Sedimentary sequences in the Gulf of Lion: A record of 100,000 years climatic cycles. *Mar Pet Geol* 22:775–804.
16. Jouet G, Berné S, Rabineau M, Bassetti MA, Bernier P (2006) Shoreface migrations at the shelf edge and sea-level changes around the Last Glacial Maximum (Gulf of Lions, NW Mediterranean). *Mar Geol* 234:21–42.
17. Cortina A, Sierro FJ, Gonzalez-Mora B, Asioli A (2011) Impact of climate and sea level changes on the ventilation of intermediate water and benthic foraminifer assemblages in the Gulf of Lions, off South France, during MIS 11 in the northwestern Mediterranean Sea (Gulf of Lions). *Palaeogeogr Palaeoclimatol Palaeoecol* 309: 215–228.
18. Cortina A, Sierro FJ, Flores JA (2015) The response of SST to insolation and ice sheet variability from MIS 3 to MIS 11 in the northwestern Mediterranean Sea (Gulf of Lions). *Geophys Res Lett* 42:10366–10374.
19. Cortina A, Grimalt JO, Martrat B (2016) Anomalous SST warming during MIS 13 in the Gulf of Lions (northwestern Mediterranean Sea). *Org Geochem* 92:16–23.
20. Lamb AL, Wilson GP, Leng MJ (2006) A review of coastal palaeoclimate and relative sea-level reconstructions using $\delta^{13}\text{C}$ and CN ratios in organic material. *Earth Sci Rev* 75:29–57.
21. Sierro FJ, Andersen N, Bassetti MA, Berné S (2009) Phase relationship between sea level and abrupt climate change. *Quat Sci Rev* 28:2867–2881.
22. Canfield DE (1989) Sulfate reduction and oxic respiration in marine sediments: Implications for organic carbon preservation in euxinic environments. *Deep Sea Res A* 36:121–138.
23. Tesi T, Miserocchi S, Goñi MA, Langone L (2007) Source, transport and fate of terrestrial organic carbon on the western Mediterranean Sea, Gulf of Lions, France. *Mar Chem* 105:101–117.
24. Owens JD, Gill BC, Jenkyns HC (2013) Sulfur isotopes track the global extent and dynamics of euxinia during Cretaceous Oceanic Anoxic Event 2. *Proc Natl Acad Sci USA* 110:18407–18412.
25. Kah LC, Lyons TW, Frank TD (2004) Low marine sulphate and protracted oxygenation of the Proterozoic biosphere. *Nature* 431:834–838.
26. Böttcher ME, Bernasconi SM, Brumsack H-J (1999) Carbon, sulfur, and oxygen isotope geochemistry of interstitial waters from the Western Mediterranean. *Proc Ocean Drill Program Sci Results* 161:413–421.
27. Rohling EJ, et al. (2014) Sea-level and deep-sea-temperature variability over the past 5.3 million years. *Nature* 508:477–482.
28. Hernández-Molina FJ, et al. (2014) Onset of Mediterranean outflow into the North Atlantic. *Science* 344:1244–1250.
29. Sim MS, Ono S, Donovan K, Templer SP (2011) Effect of electron donors on the fractionation of sulfur isotopes by a marine *Desulfovibrio* sp. *Geochim Cosmochim Acta* 75:4244–4259.
30. Leavitt WD, Halevy I, Bradley AS (2013) Influence of sulfate reduction rates on the Phanerozoic sulfur isotope record. *Proc Natl Acad Sci USA* 110:11244–11249.
31. Censi P, Incarbona A, Oliveri E, Bonomo S, Tranchida G (2010) Yttrium and REE signature recognized in Central Mediterranean Sea (ODP Site 963) during the MIS 6–MIS 5 transition. *Palaeogeogr Palaeoclimatol Palaeoecol* 292:201–210.
32. Gomes ML, Hurtgen MT (2013) Sulfur isotope systematics of a euxinic, low-sulfate lake: Evaluating the importance of the reservoir effect in modern and ancient oceans. *Geology* 41:663–666.
33. Claypool GE (2004) Ventilation of marine sediments indicated by depth profiles of pore water sulfate and $\delta^{34}\text{S}$. *Spec Publ Geochem Soc* 9:59–65.
34. Present TM, Paris G, Burke A, Fischer W (2015) Large carbonate associated sulfate isotopic variability between brachiopods, micrite, and other sedimentary components in Late Ordovician strata. *Earth Planet Sci Lett* 432:187–198.
35. Fike DA, Grotzinger JP (2008) A paired sulfate–pyrite $\delta^{34}\text{S}$ approach to understanding the evolution of the Ediacaran–Cambrian sulfur cycle. *Geochim Cosmochim Acta* 72: 2636–2648.
36. Sansjofre P, et al. (2016) Multiple sulfur isotope evidence for massive oceanic sulfate depletion in the aftermath of Snowball Earth. *Nat Commun* 7:12192.
37. Goldberg T, Strauss H, Guo Q, Liu C (2007) Reconstructing marine redox conditions for the Early Cambrian Yangtze Platform: Evidence from biogenic sulphur and organic carbon isotopes. *Palaeogeogr Palaeoclimatol Palaeoecol* 254:175–193.
38. Feng LJ, Chu XL, Huang J, Zhang QR, Chang HJ (2010) Reconstruction of paleo-redox conditions and early sulfur cycling during deposition of the Cryogenian Datangpo Formation in South China. *Gondwana Res* 18:632–637.
39. Parnell J, Boyce AJ, Mark D, Bowden S, Spinks S (2010) Early oxygenation of the terrestrial environment during the Mesoproterozoic. *Nature* 468:290–293.
40. Canfield DE, Raiswell R, Westrich JT, Reaves CM (1986) The use of chromium reduction in the analysis of reduced inorganic sulfur in sediments and shales. *Chem Geol* 54: 149–155.
41. Tuttle ML, Goldhaber MB, Williamson DL (1986) An analytical scheme for determining forms of sulphur in oil shales and associated rocks. *Talanta* 33:953–961.
42. Burton ED, Sullivan LA, Bush RT, Johnston SG (2008) A simple and inexpensive chromium-reducible sulfur method for acid-sulfate soils. *Appl Geochem* 23:2759–2766.
43. Grant KM, et al. (2014) Sea-level variability over five glacial cycles. *Nat Commun* 5:5076.
44. Barker S, et al. (2011) 800,000 years of abrupt climate variability. *Science* 334:347–351.
45. Railsback LB, Gibbard PL, Head MJ (2015) An optimized scheme of lettered marine isotope substages for the last 1.0 million years, and the climatostratigraphic nature of isotope stages and substages. *Quat Sci Rev* 111:94–106.

Supporting Information

Pasquier et al. 10.1073/pnas.1618245114

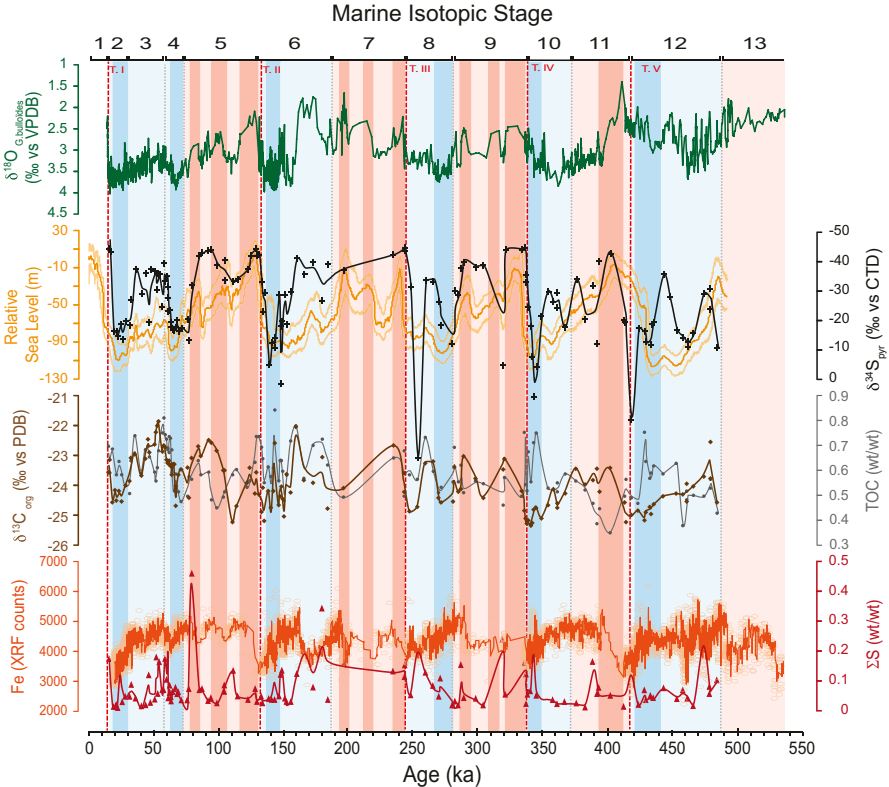


Fig. S1. The $\delta^{18}\text{O}_{\text{G. bullioides}}$ (green line from refs. 17 and 21) and $\delta^{34}\text{S}_{\text{pyr}}$ (black crosses and the black line represent local polynomial regression type LOESS between measured points, this study) associated with relative sea level (orange line) superimposed with 95% of probability interval (light orange lines) from ref. 43. Also shown are the $\delta^{13}\text{C}_{\text{org}}$ [brown diamonds and line (LOESS regression), this study] and associated TOC [gray line (LOESS regression) associated with gray circles]. Iron record from X-ray fluorescence core scanning (orange line) and total sulfide (TS, red line, this study) also are given. Blue bands represent the glacial times, with corresponding cold substages (i.e., *sensu stricto*) in darker blue. Red bands correspond to interglacial periods, with warm substages (i.e., *sensu stricto*) highlighted in dark pink. Termination (T.) is according to ref. 44. Scheme of marine stage is according to ref. 45.

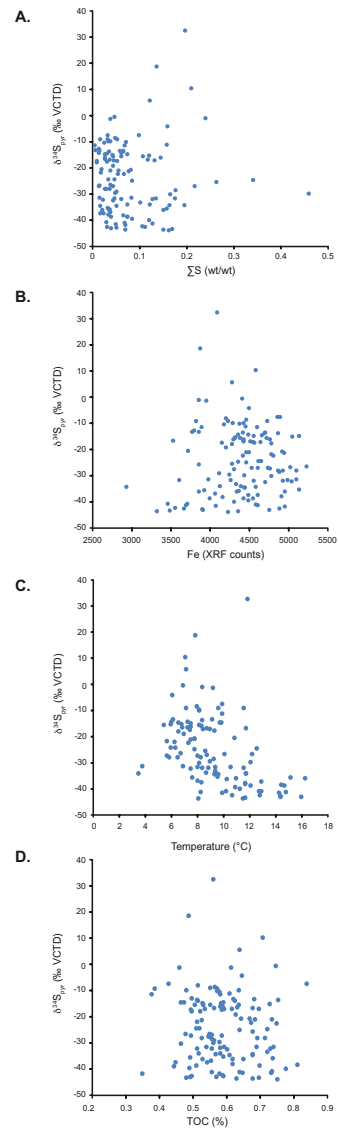


Fig. S2. (A) Cross-plot between $\delta^{34}\text{S}_{\text{pyr}}$ with associated total sulfur species present in sediment (TS wt %); (B) $\delta^{34}\text{S}_{\text{pyr}}$ with $\text{Fe}_{\text{XRF-counts}}$; (C) $\delta^{34}\text{S}_{\text{pyr}}$ against temperature obtained from the relative composition of C_{37} unsaturated alkenones from refs. 18 and 19; and (D) $\delta^{34}\text{S}_{\text{pyr}}$ with TOC within sediment (TOC wt %).

Table S1. Depth, estimated age, and associated geochemical information from samples from the PRGL1-4 borehole

PRGL1-4 depth, mbsf	Age, ky	S _{pyr} , %	δ ³⁴ S, ‰	δ ¹³ C, ‰	TOC, %
<i>Interglacial sensu stricto</i>					
65.56	84.5	0.25	-41.2	-22.7	0.64
66.15	86.7	0.26	-42.0	-23.0	0.58
67.21	91.8	0.11	-42.9	-22.5	0.59
67.51	94.2	0.14	-43.4	-22.6	0.48
68.16	98.8	0.08	-37.6	-22.8	0.45
68.80	103.4	0.31	-39.7	-23.5	0.49
72.09	124.0	nd	-41.1	-23.4	0.56
72.28	127.5	0.26	-43.8	-24.3	0.63
72.32	129.3	0.10	-41.1	-23.6	0.74
72.46	130.8	nd	-41.5	-24.3	0.74
123.81	196.1	0.58	-35.9	-24.1	0.49
127.01	234.6	0.47	-41.5	-22.7	0.65
127.65	242.8	0.41	-42.8	-23.6	0.50
127.83	243.4	0.55	-43.8	-24.2	0.68
160.90	320.7	0.18	-43.2	-23.1	0.57
161.62	334.1	nd	-43.3	-24.2	0.50
161.92	336.2	0.60	-44.0	-24.8	0.75
197.29	393.5	0.27	-39.0	-24.2	0.45
198.78	401.6	0.18	-41.9	-23.4	0.35
<i>Glacial sensu stricto</i>					
8.27	18.2	0.02	-13.6	-24.6	0.69
12.50	20.2	0.05	-13.5	-24.1	0.62
15.65	21.5	0.02	-11.8	-24.5	0.58
20.19	23.6	0.53	-16.4	-24.2	0.63
23.29	25.2	0.09	-10.7	-24.5	0.58
28.09	27.8	0.17	-17.3	-24.0	0.54
32.00	31.0	0.16	-15.8	-23.9	0.51
52.10	57.4	0.24	-38.4	-22.7	0.81
52.80	58.3	0.64	-31.8	-22.7	0.74
54.17	59.9	0.37	-33.5	-23.1	0.72
54.59	60.5	0.97	-25.8	-23.3	0.68
54.96	61.0	0.14	-21.2	-23.2	0.69
55.31	61.6	0.30	-21.0	-23.2	0.67
55.51	61.8	0.20	-21.3	-23.3	0.74
56.24	62.8	0.16	-15.3	-23.3	0.73
56.61	63.4	0.10	-16.8	-23.3	0.68
57.69	63.9	0.22	-14.6	-23.6	0.59
59.46	65.3	0.24	-14.1	-23.3	0.52
60.36	66.6	0.27	-15.0	-24.0	0.53
60.68	67.1	0.19	-17.6	-24.7	0.59
61.69	68.5	0.21	-13.7	-23.7	0.52
63.51	71.2	0.11	-14.8	-23.5	0.48
64.44	75.7	0.11	-18.0	-23.4	0.50
64.89	76.6	0.26	-10.5	-24.4	0.57
78.02	135.1	nd	-27.7	-25.2	0.55
82.52	138.3	0.14	-1.6	-24.2	0.62
85.67	140.6	0.12	-9.5	-24.7	0.57
88.28	142.4	0.58	-11.4	-24.2	0.61
88.72	142.8	0.12	-7.8	-22.6	0.84
93.24	146.1	0.16	-27.1	-24.7	0.56
95.12	147.0	0.45	5.4	-24.4	0.64
97.29	147.9	0.44	-15.7	-24.0	0.64
144.97	270.0	0.17	-24.6	-24.4	0.51
146.23	271.3	0.39	-15.8	-24.6	0.53
155.49	280.4	0.06	-9.3	-24.5	0.55
166.90	340.3	0.22	-15.7	-25.3	0.55
169.05	342.0	0.58	-4.4	-25.3	0.65
170.13	342.9	0.77	10.1	-24.8	0.71
172.49	344.8	0.17	-0.7	-24.8	0.75
177.21	348.8	0.16	-19.4	-25.1	0.63
213.01	423.5	0.05	-14.6	-24.8	0.47

Table S1. Cont.

PRGL1-4 depth, mbsf	Age, ky	S _{pyr} , %	δ ³⁴ S, ‰	δ ¹³ C, ‰	TOC, %
219.70	428.3	0.24	-13.8	-25.2	0.76
221.30	429.6	0.12	-10.2	-24.9	0.64
224.26	432.5	0.18	-8.7	-24.7	0.57
225.05	433.7	nd	-16.4	-25.0	0.59
226.09	435.3	0.13	-17.1	-24.6	0.62
Interglacial					
1.87	15.4	0.62	-43.5	-23.6	0.70
3.90	16.3	0.39	-42.6	-23.1	0.59
65.22	78.7	1.69	-30.2	-23.1	0.56
68.98	104.1	0.22	-32.2	-23.5	0.52
70.61	110.3	0.49	-32.0	-25.2	0.58
71.12	113.7	0.16	-32.7	-24.7	0.60
71.92	122.3	0.13	-36.4	-23.9	0.53
75.29	133.0	0.17	-31.8	-24.9	0.69
76.48	133.9	0.07	-20.9	-24.1	0.65
117.96	183.6	0.12	-38.2	-24.8	0.62
130.05	247.4	0.17	-29.9	-24.9	0.58
157.24	287.1	0.55	-36.5	-24.1	0.62
157.74	289.0	0.14	-38.8	-23.0	0.51
158.74	298.4	0.14	-37.1	-23.8	0.56
159.09	304.2	0.06	-37.7	-24.4	0.55
160.30	319.1	0.88	-1.4	-23.5	0.46
162.62	336.7	0.05	-31.6	-25.1	0.54
163.44	337.4	0.45	-34.3	-25.3	0.52
190.06	375.3	0.08	-32.4	-23.4	0.56
192.93	382.6	0.03	-18.2	-24.0	0.52
195.47	388.9	0.60	-30.3	-23.8	0.47
196.40	391.5	0.19	-9.4	-23.4	0.39
Glacial					
33.62	32.6	0.31	-25.1	-23.1	0.64
35.77	35.5	0.13	-36.1	-23.0	0.74
38.40	40.1	0.05	-27.4	-23.7	0.59
42.07	43.4	0.06	-34.7	-23.1	0.68
43.78	45.6	0.43	-17.2	-22.4	0.70
44.80	46.8	0.08	-36.3	-22.9	0.65
47.67	50.6	0.12	-35.6	-22.6	0.59
48.01	51.3	0.65	-28.8	-22.2	0.56
48.81	52.7	0.18	-34.7	-22.0	0.61
49.21	53.4	0.60	-34.5	-21.8	0.68
51.20	56.3	0.24	-22.7	-22.9	0.75
99.91	149.1	0.48	-17.3	-24.5	0.60
103.65	150.6	0.14	-26.8	-25.0	0.48
105.20	152.1	0.09	-16.3	-23.6	0.58
107.64	155.5	0.09	-28.2	-24.3	0.72
110.67	159.7	0.44	-40.2	-22.0	0.78
112.33	166.0	0.72	-34.5	-23.8	0.57
114.06	172.9	0.27	-39.0	-23.9	0.70
116.07	179.5	1.26	-24.8	-23.0	0.73
133.16	253.1	0.72	32.3	-24.7	0.56
136.45	259.2	0.47	-32.3	-23.3	0.73
140.50	265.6	0.30	-31.7	-23.2	0.60
155.89	281.7	0.10	-28.3	-23.4	0.69
156.64	284.7	0.05	-26.9	-24.2	0.55
164.51	338.3	0.20	-22.5	-25.2	0.67
181.02	353.6	0.13	-28.2	-24.7	0.53
182.99	358.0	0.12	-24.6	-24.1	0.52
184.38	361.3	0.06	-22.0	-24.7	0.52
184.41	361.5	nd	-27.6	-24.6	0.55
186.62	366.8	0.09	-15.1	-24.3	0.59
199.42	412.9	0.03	-17.6	-24.6	0.50
200.21	413.6	nd	-16.9	-25.2	0.57
206.09	418.1	0.50	18.4	-25.0	0.49

Table S1. Cont.

PRGL1-4 depth, mbsf	Age, ky	S _{pyr} , %	δ ³⁴ S, ‰	δ ¹³ C, ‰	TOC, %
230.87	442.7	0.27	-34.3	-24.4	0.58
234.33	448.1	nd	-26.1	nd	nd
237.53	453.1	0.13	-14.1	-24.3	0.63
240.50	457.7	0.25	-11.6	-24.3	0.38
243.72	461.2	nd	-8.2	-24.5	0.52
243.99	461.3	0.14	-10.1	-23.9	0.48
253.29	466.3	0.05	-13.0	-24.0	0.50
267.24	473.7	0.80	-27.3	-23.7	0.50
273.68	479.0	0.19	-29.2	-22.6	0.57
273.77	479.1	0.28	-21.7	-23.8	0.53
279.50	484.7	0.36	-7.8	-24.6	0.43

Sample depths are in meters below sea floor (mbsf). Ages come from the updated age model provided in ref. 17. S_{pyr} is the weight percent of sulfur as pyrite in the bulk sediment; δ³⁴S_{pyr} and δ¹³C_{org} are the sulfur and carbon isotopic compositions in pyrite and bulk organic matter, respectively. TOC % is the percent total organic carbon. nd indicates that the isotopic value or the abundance was not determined. Errors are given in *Materials and Methods*.

5. Implications for past sulfur records

Many local processes are strongly focused on the coastal and continental boundary region where biogeochemical interactions are the most intense and diagenetic processes are crucial in biogeochemical cycles but poorly understood. A better understanding of such shelf and deltaic environments are very important for future work because they represent 15 to 20 % of ocean sea floor, accumulating 90 % of sediments loaded and generated into the ocean and storing more than 50 % of bioactive elements in various forms. Moreover, they represent a very important bioactive community permanently interacting with remineralization processes (across a broad range of timescales), which contrasts with the deeper, open and quiet ocean. Indeed, in the light of such influences of depositional environment on the global sulfur biochemical cycle, we may have to revisit past geological records.

Indeed, paired $\delta^{34}\text{S}_{\text{SO}_4}$ and $\delta^{34}\text{S}_{\text{pyrite}}$ data is available and presents repeated isotopic fluctuation through geological times (Fike and Grotzinger 2008; Gill et al. 2007; Gorjan et al. 2012; Jones and Fike 2013; Kampschulte and Strauss 2004; Paytan et al. 1998, 2002 among others). Changes in $\delta^{34}\text{S}$ of seawater and sedimentary pyrite have mostly been interpreted to reflect changes in the fraction of sulfur removed from the ocean as pyrite, f_{pyr} . Because pyrite is depleted in ^{34}S relative to seawater sulfate from which it is formed, times of high $\delta^{34}\text{S}_{\text{SO}_4}$ are interpreted as times of high rates of pyrite burial. Although, some authors also invoked changes in the flux and isotopic composition of sulfate delivered to the ocean (i.e. $\delta^{34}\text{S}_{\text{in}}$) such as changes in area of shallow water and or riverine influx (Halevy et al. 2012; Wortmann and Paytan 2012; Markovic et al. 2015).

Assuming a constant biological fractionation through time, changes in f_{pyr} and or $\delta^{34}\text{S}_{\text{in}}$ would result in parallel changes in $\delta^{34}\text{S}_{\text{SO}_4}$ and $\delta^{34}\text{S}_{\text{pyrite}}$ (at least for globally averaged values), which occurred at reservoir timescale of sulfur flux into the ocean, approx. 13 Myr (Kah et al. 2004). Nevertheless, many sulfur isotope excursions occurred faster than this predicted time, which have been attributed to low sulfate concentration in the ocean at the time of pyrite formation. However, in some of these events there is no evidence for changes in sulfate seawater composition (i.e. $\delta^{34}\text{S}_{\text{SO}_4}$), and thus changes in the local depositional condition can be an alternative explanation. Such mechanisms have been recently reported at the end-Ordovician Hirnantian strata from Anticosti Island, Quebec, Canada. Hirnantian times are characterized by glaciation and associated ecological perturbation (i.e. mass extinction). Nevertheless, these strata preserve a parallel isotopic excursion in $\delta^{13}\text{C}_{\text{carbonate}}$ and $\delta^{13}\text{C}_{\text{org}}$ (Jones et al. 2011), with a significant positive excursion in $\delta^{34}\text{S}_{\text{pyrite}}$ which can be related to an increase in pyrite burial because $\delta^{34}\text{S}_{\text{SO}_4}$ are stable through the entire study area (Jones and Fike 2013). Authors interpreted such behavior as the result of low sea level during glaciation times, which is associated with changes in the sedimentation processes (supported by variation in $\delta^{13}\text{C}_{\text{org}}$) due to low sea level. Such changes may have modified depositional conditions (i.e. such as the type of organic matter loaded into the basin (i.e. source and availability), shelf exposure, modification of the chemocline within the sediment, and possible reworking processes which allowed modification of the biological fractionation associated with microbial sulfur cycling (ε_{pyr}).

This record highlights the potential for a large overprint of local changes in the isotopic fractionation during microbial sulfate reduction, which can be induced by ecological and environmental changes or the expression of that fractionation under closed system conditions. Moreover, such effect on the sulfur isotope record are much more rapid than the residence time of sulfur in the ocean and can't be explained by the 'classic' steady state view of the global sulfur cycle. It seems very interesting to carefully review our past interpretations that were based on sulfur isotope data, especially when paired measurements of seawater (i.e. $\delta^{34}\text{S}_{\text{SO}_4}$) and sedimentary ($\delta^{34}\text{S}_{\text{pyrite}}$) forms are not available, to better constrain times of rapid sulfur isotope excursions and subsequently provide new insights on ancient ocean chemistry.

6. Perspectives

In Pasquier et al. 2017, we proposed two different processes that can lead to the observed variability in $\delta^{34}\text{S}_{\text{pyrite}}$. The first one is related to changes in the inherent metabolism of microbial sulfur cycling microbes within the sediment (i.e. csSRR) or changes in the connectivity of porewater within the overlying water column (i.e. open vs closed system). In the near future, we would like to test the idea related to the connection between porewater and the water column using two different approaches: (i) SIMS mapping and (ii) multi Sulfur isotopes.

For SIMS, we plan to extract individual pyrite grains from bulk sediments presenting a wide range of $\delta^{34}\text{S}_{\text{pyrite}}/\delta^{13}\text{C}_{\text{org}}$ and different climatic contexts using a decantation technique. This will facilitate the detailed mapping of the structure and fabric within individual pyrite grains and the selection of target areas for micro-SIMS multi-sulfur isotope investigations. Indeed, in a closed system the sulfur isotopes in the pyrite (i.e. the reduced sulfur form) may present isotopic variability as they grow from a pool that is evolving isotopically with time. In contrast, in an open system with a constant replenishment of seawater sulfate the reduced sulfur product of microbial processes would not be expected to vary, as illustrated on the **Figure 51**.

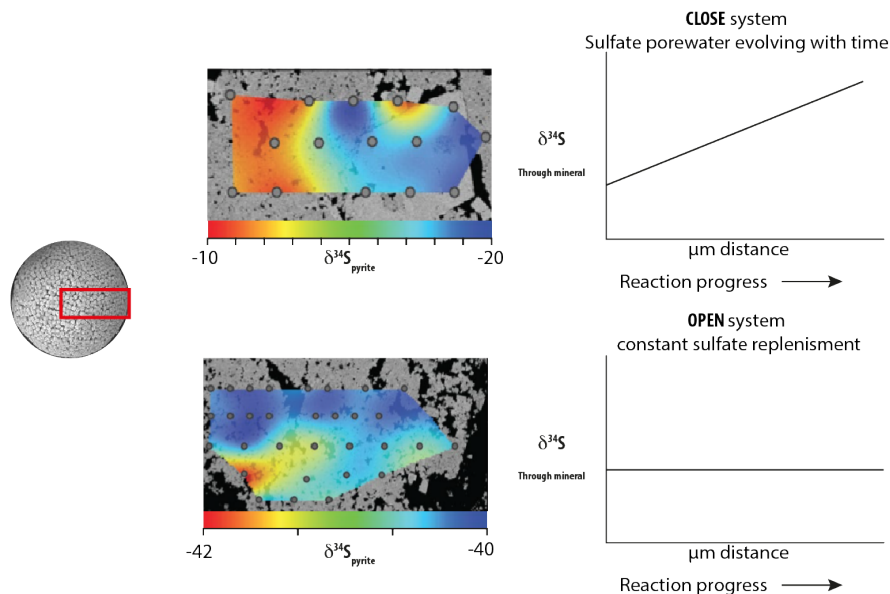


Figure 51

Individual pyrite grain μSIM investigation and expected evolution of sulfur isotopes within pyrite grains. In a close system the sulfur isotopes in pyrites may have significant isotopes variability as they are growing from a pool that isotopically change with time (upper schematic representation). In contrast in an open system pyrite isotopic composition is not expected to change due to constant replenishment of sulfate (lower schematic representation). Data from Meyer et al. 2017.

Multi sulfur isotope ratio (i.e. $^{33}\text{S}/^{32}\text{S}$) because Sulfur has four stable isotopes which can provide additional constraints on:

- (i) Open vs Close system (i.e. steady-state processes): it has been shown that the dynamic equations of mass balance and isotopic mass balance which govern pyrite isotopic composition (see equation n° 11, 12 and 13 for ^{34}S and ^{36}S) can predict in a $\Delta^{33}\text{S}$ versus $\delta^{34}\text{S}$ the isotopic evolution of produced FeS_2 under Rayleigh type distillation. A complete description of the methodology is reported in Sansjofre et al. (2016) which have used this approach during the terminal Neoproterozoic positive sulfur isotope excursion. Using this type of calculation, see **Figure 52**, will allow us to highlight the evolution of the isotopic composition of the residual pyrite during a Rayleigh type distillation and therefore better understand the distillation processes involved in the pyrite formation. This is a necessary step in our understanding of local vs global processes in the Gulf of Lion.

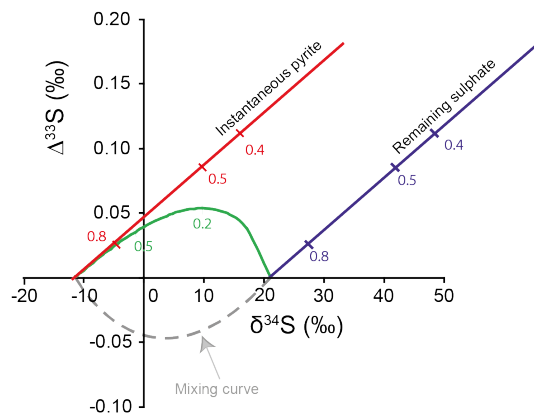


Figure 52

Multi-isotopic theoretical model showing the evolution of the isotopic composition of the residual sulfate (blue line) and instantaneous pyrite (black line), the green line represent the cumulative pyrite isotopic composition predicted by the calculation. From Sansjofre et al. 2016 Supplementary Information.

- (ii) biological reactions that fractionated sulfur isotopes as function of their mass (see **Figure 53**; Johnston et al. 2007; Johnston 2011; Leavitt et al. 2013a; Sim et al. 2011b). Because the different types of sulfur metabolisms impart differently the sulfur isotopes, deviation from the expected mass dependence are reported as 33Δ . Thus, high precision measurements allow identification of small deviation from the expected mass dependence which can be used to trace changes in microbial processes. Also, the minor isotope relationships (33λ) describe the metabolism-specific used during the sulfur cycle. Measured 33λ in modern microbial communities show values between 0.508 to 0.514 for sulfate reduction whereas higher values are reported for sulfur oxidative processes (Johnston 2011). Moreover, due to the critical importance of pyrite burial on Earth atmospheric condition, it is imperative to clarify the microbial processes at work during short timescale climate changes, leading to changes in sulfur cycle controlled by local processes.

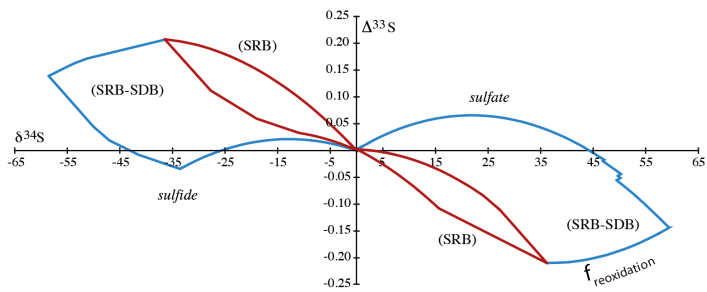


Figure 53

A steady-state model from Johnston et al. (2005). This model predicts the isotopic composition of sulfate (on the right) and sulfide (left part) as a function of the fraction of pyrite burial and sulfide re-oxidation.

LITERATURE CITED

- Aller, R. C., 1982. The Effects of Macrobenthos on Chemical Properties of Marine Sediment and Overlying Water. Springer US, Boston, MA, pp. 53–102.
- Aller, R. C., 2014. Sedimentary Diagenesis, Depositional Environments, and Benthic Fluxes, 8th Edition. Vol. 11. Elsevier Ltd.
- Aller, R. C., Blair, N. E., Brunskill, G. J., 2008. Early diagenetic cycling, incineration, and burial of sedimentary organic carbon in the central Gulf of Papua (Papua New Guinea). *Journal of Geophysical Research*.
- Aller, R. C., Madrid, V., Chistoserdov, A., Aller, J. Y., 2010. Unsteady diagenetic processes and sulfur biogeochemistry in tropical deltaic muds: implications for oceanic isotope cycles and the sedimentary record. . . et *Cosmochimica Acta*.
- Bak, F., Pfennig, N., Mar. 1987. Chemolithotrophic growth of *Desulfovibrio sulfodismutans* sp. nov. by disproportionation of inorganic sulfur compounds. *Archives of Microbiology* 147 (2), 184–189.
- Banner, J. L., Hanson, G. N., Nov. 1990. Calculation of simultaneous isotopic and trace element variations during water-rock interaction with applications to carbonate diagenesis. *Geochimica et Cosmochimica Acta* 54 (11), 3123–3137.
- Berner, R. A., 1984. Sedimentary pyrite formation: an update. *Geochimica et Cosmochimica Acta*.
- Berner, R. A., Raiswell, R., May 1983. Burial of organic carbon and pyrite sulfur in sediments over phanerozoic time: a new theory. *Geochimica et Cosmochimica Acta* 47 (5), 855–862.
- Berner, R. A., Westrich, J. T., 1985. Bioturbation and the early diagenesis of carbon and sulfur. *Am J Sci*;(United States).
- Böttcher, M. E., Bernasconi, S. M., brumsack, H.-J., 1999. 32. CARBON, SULFUR, AND OXYGEN ISOTOPE GEOCHEMISTRY OF INTERSTITIAL WATERS FROM THE WESTERN MEDITERRANEAN. *Proceedings of Ocean Drillings Program, Scientific results* 161, 413–421.
- Brandt, K. K., Vester, F., Jensen, A. N., Ingvorsen, K., 2001. Sulfate reduction dynamics and enumeration of sulfate-reducing bacteria in hypersaline sediments of the great salt lake (utah, usa). *Microbial Ecology* 41, 1–11.
- Brennan, S. T., Lowenstein, T. K., Horita, J., 2004. Seawater chemistry and the advent of biocalcification. *Geology* 32 (6), 473–5.
- Brüchert, V., Pratt, L. M., Jul. 1996. Contemporaneous early diagenetic formation of organic and inorganic sulfur in estuarine sediments from St. Andrew Bay, Florida, USA. *Geochimica et Cosmochimica Acta* 60 (13), 2325–2332.
- Brunner, B., Bernasconi, S. M., Oct. 2005. A revised isotope fractionation model for dissimilatory sulfate reduction in sulfate reducing bacteria. *Geochimica et Cosmochimica Acta* 69 (20), 4759–4771.
- Burggraf, S., Fricke, H., Neuner, A., Kristjansson, J., Rouvier, P., Mandelco, L., Woese, C. R., Stetter, K. O., Aug. 1990. *Methanococcus igneus* sp. nov., a Novel Hyperthermophilic Methanogen from a Shallow Submarine Hydrothermal System. *Systematic and applied microbiology* 13 (3), 263–269.
- Canfield, D., Cappellen, P. v., Jan 1992. How bioturbation may enhance the degradation rates of refractory sedimentary organics. Vol. 24:7.
- Canfield, D., Thamdrup, B., Feb. 1996. Fate of elemental sulfur in an intertidal sediment. *FEMS Microbiology Ecology* 19 (2), 95–103.
- Canfield, D. E., 2001. Biogeochemistry of sulfur isotopes. *Reviews in Mineralogy and Geochemistry* 43 (1), 607–636.
- Canfield, D. E., Dec. 2004. The evolution of the Earth surface sulfur reservoir. *American Journal of Science* 304 (10), 839–861.
- Canfield, D. E., Boudreau, B. P., Mucci, A., Gundersen, J. K., Mar. 1998. The Early Diagenetic Formation of Organic Sulfur in the Sediments of Mangrove Lake, Bermuda. *Geochimica et Cosmochimica Acta* 62 (5), 767–781.
- Canfield, D. E., Farquhar, J., 2009. Animal evolution, bioturbation, and the sulfate concentration of the oceans.
- Canfield, D. E., Farquhar, J., Zerkle, A. L., Apr. 2010. High isotope fractionations during sulfate reduction in a low-sulfate euxinic ocean analog. *Geology* 38 (5), 415–418.
- Canfield, D. E., Teske, A., Jul. 1996. Late Proterozoic rise in atmospheric oxygen concentration inferred from phylogenetic and sulphur-isotope studies. *Nature* 382 (6587), 127–132.

- Canfield, D. E., Thamdrup, B., 1994. The production of (³⁴S)-depleted sulfide during bacterial disproportionation of elemental sulfur. *Science*.
- Claypool, G. E., Holser, W. T., Kaplan, I. R., Sakai, H., Zak, I., 1980. The age curves of sulfur and oxygen isotopes in marine sulfate and their mutual interpretation. *Chemical Geology* 28, 199–260.
- Cypionka, H., May 2013. Solute transport and cell energetics. *Sulfate-Reducing Bacteria*, 151–184.
- Fike, D. A., Bradley, A. S., Rose, C. V., 2015. Rethinking the ancient sulfur cycle. *Annual Review of Earth and Planetary Sciences* 43.
- Fike, D. A., Finke, N., Zha, J., Blake, G., Hoehler, T. M., Orphan, V. J., Oct. 2009. The effect of sulfate concentration on (sub)millimeter-scale sulfide $\delta^{34}\text{S}$ in hypersaline cyanobacterial mats over the diurnal cycle. *Geochimica et Cosmochimica Acta* 73 (20), 6187–6204.
- Fike, D. A., Grotzinger, J. P., 2008. A paired sulfate–pyrite $\delta^{34}\text{S}$ approach to understanding the evolution of the Ediacaran–Cambrian sulfur cycle. *Geochimica et Cosmochimica Acta* 72, 2636–2648.
- Fike, D. A., Rose, C. V., Gao, J., Aller, R. C., in review. Spatial Heterogeneity in Sulfur Isotopes: Implications for Modern Environments and Paleoenvironmental Reconstructions. *Chemical Geology*.
- Fischer, W., Fike, D. A., Johnson, J. E., 2014. SQUID–SIMS is a useful approach to uncover primary signals in the Archean sulfur cycle.
- Fry, B., Gest, H., Hayes, J. M., May 1985. Isotope effects associated with the anaerobic oxidation of sulfite and thiosulfate by the photosynthetic bacterium, *Chromatium vinosum*. *FEMS Microbiology Letters* 27 (2), 227–232.
- Fry, B., Ruf, W., Gest, H., Hayes, J. M., Oct. 1988. Sulfur isotope effects associated with oxidation of sulfide by O₂ in aqueous solution. *Chemical Geology: Isotope Geoscience section* 73 (3), 205–210.
- Gao, J., Fike, D. A., Aller, R. C., Dec. 2013. Enriched Pyrite $\delta^{34}\text{S}$ Signals in Modern Tropical Deltaic Muds. AGU Fall Meeting Abstracts.
- Gill, B. C., Lyons, T. W., Frank, T. D., Feb. 2008. Behavior of Carbonate-Associated Sulfate during Meteoric Diagenesis and Implications for the Sulfur Isotope Paleoproxy. *Geochimica et Cosmochimica Acta* 72, 4699–4711.
- Gill, B. C., Lyons, T. W., Saltzman, M. R., 2007. Parallel, high-resolution carbon and sulfur isotope records of the evolving Paleozoic marine sulfur reservoir. *Palaeogeography, Paleoclimatology, Paleocology* 256, 156–173.
- Gill, B. C., Lyons, T. W., Young, S. A., Kump, L. R., Knoll, A. H., 2011. Geochemical evidence for widespread euxinia in the Later Cambrian ocean. *Nature* 469, 80–83.
- Goldhaber, M. B., Kaplan, I. R., Apr. 1980. Mechanisms of sulfur incorporation and isotope fractionation during early diagenesis in sediments of the gulf of California. *Marine Chemistry* 9 (2), 95–143.
- Gomes, M. L., Hurtgen, M. T., May 2013. Sulfur isotope systematics of a euxinic, low-sulfate lake: Evaluating the importance of the reservoir effect in modern and ancient oceans. *Geology* 41 (6), 663–666.
- Gomes, M. L., Hurtgen, M. T., May 2015. Sulfur isotope fractionation in modern euxinic systems: Implications for paleoenvironmental reconstructions of paired sulfate–sulfide isotope records. *Geochimica et Cosmochimica Acta* 157 (C), 39–55.
- Gorjan, P., Kaiho, K., Fike, D. A., Xu, C., 2012. Carbon-and sulfur-isotope geochemistry of the Hirnantian (Late Ordovician) Wangjiawan (Riverside) section, South China: global correlation and environmental event interpretation. *Palaeogeography, Paleoclimatology, Paleocology* 337–338, 14–22.
- Grotzinger, J. P., Kasting, J. F., Mar. 1993. New Constraints on Precambrian Ocean Composition. *The Journal of Geology* 101 (2), 235–243.
- Guo, Q., Strauss, H., Kaufman, A. J., Schroder, S., Gutzmer, J., Wing, B., Baker, M. A., Bekker, A., Jin, Q., Kim, S. T., Farquhar, J., May 2009. Reconstructing Earth’s surface oxidation across the Archean-Proterozoic transition. *Geology* 37 (5), 399–402.
- Habicht, K. S., Dec. 2002. Calibration of Sulfate Levels in the Archean Ocean. *Marine Geology* 298 (5602), 2372–2374.
- Habicht, K. S., Canfield, D. E., Jul. 1996. Sulphur isotope fractionation in modern microbial mats and the evolution of the sulphur cycle. *Nature* 382 (6589), 342–343.
- Habicht, K. S., Canfield, D. E., 1997. Sulfur isotope fractionation during bacterial sulfate reduction

- in organic-rich sediments. *Geochimica et Cosmochimica Acta*.
- Habicht, K. S., Canfield, D. E., 2001. Isotope fractionation by sulfate-reducing natural populations and the isotopic composition of sulfide in marine sediments. *Geology* 29 (6), 555–5.
- Habicht, K. S., Canfield, D. E., Rethmeier, J., Aug. 1998. Sulfur isotope fractionation during bacterial reduction and disproportionation of thiosulfate and sulfite. *Geochimica et Cosmochimica Acta* 62 (15), 2585–2595.
- Halevy, I., Peters, S. E., Fischer, W., Jul. 2012. Sulfate Burial Constraints on the Phanerozoic Sulfur Cycle. *Science* 337 (6092), 331–334.
- Hartmann, M., Nielsen, H., Mar. 2012. δ 34S values in recent sea sediments and their significance using several sediment profiles from the western Baltic Sea. *Isotopes in Environmental and Health Studies* 48 (1), 7–32.
- Holser, W. T., Jun. 1977. Catastrophic chemical events in the history of the ocean. *Nature* 267 (5610), 403–408.
- Holser, W. T., Kaplan, I. R., 1966. Isotope geochemistry of sedimentary sulfates. *Chemical Geology* 1, 93–135.
- Horita, J., Zimmermann, H., Holland, H. D., Nov. 2002. Chemical evolution of seawater during the Phanerozoic. *Geochimica et Cosmochimica Acta* 66 (21), 3733–3756.
- Hurtgen, M. T., Halverson, G. P., Arthur, M. A., 2006. Sulfur cycling in the aftermath of a 635-Ma snowball glaciation: evidence for a syn-glacial sulfidic deep ocean. *Earth and Planetary Science Letters* 245, 551–570.
- Hurtgen, M. T., Pruss, S. B., Knoll, A. H., May 2009. Evaluating the relationship between the carbon and sulfur cycles in the later Cambrian ocean: An example from the Port au Port Group, western Newfoundland, Canada. *Earth and Planetary Science Letters* 281 (3–4), 288–297.
- Johnston, D. T., May 2011. Multiple sulfur isotopes and the evolution of Earth's surface sulfur cycle. *Earth Science Reviews* 106 (1–2), 161–183.
- Johnston, D. T., Farquhar, J., Canfield, D. E., Aug. 2007. Sulfur isotope insights into microbial sulfate reduction: When microbes meet models. *Geochimica et Cosmochimica Acta* 71 (16), 3929–3947.
- Johnston, D. T., Farquhar, J., Wing, B. A., 2005. Multiple sulfur isotope fractionations in biological systems: a case study with sulfate reducers and sulfur disproportionators. *American Journal of Science* 305 (6–8), 645–660.
- Jones, D. S., Fike, D. A., 2013. Dynamic sulfur and carbon cycling through the end-Ordovician extinction revealed by paired sulfate–pyrite δ 34 S. *Earth and Planetary Science Letters* 363, 144–155.
- Jones, D. S., Fike, D. A., Finnegan, S., Fischer, W., Schrag, D. P., McCay, D., Jun. 2011. Terminal Ordovician carbon isotope stratigraphy and glacioeustatic sea-level change across Anticosti Island (Quebec, Canada). *Geological Society of America Bulletin* 123 (7–8), 1645–1664.
- Jørgensen, B. B., Apr. 1982. Mineralization of organic matter in the sea bed—the role of sulphate reduction. *Nature* 296 (5858), 643–645.
- Jørgensen, B. B., Sep. 2017. Bacterial Sulfate Reduction within Reduced Microniches of Oxidized Marine Sediments. *Marine Biology* 41, 7–17.
- Jørgensen, B. B., Zawacki, L. X., Jannasch, H. W., 1990. Thermophilic bacterial sulfate reduction in deep-sea sediments at the Guaymas Basin hydrothermal vent site (Gulf of California). *Deep-Sea Res* 37 (4), 695–710.
- Kah, L. C., Lyons, T. W., Frank, T. D., 2004. Low marine sulphate and protracted oxygenation of the Proterozoic biosphere. *Nature* 431, 834–838.
- Kampschulte, A., Strauss, H., Apr. 2004. The sulfur isotopic evolution of Phanerozoic seawater based on the analysis of structurally substituted sulfate in carbonates. *Chemical Geology* 204 (3–4), 255–286.
- Kaplan, I. R., Sweeney, R. E., Nissenbaum, A., 1969. Sulfur Isotope Studies on Red Sea Geothermal Brines and Sediments. In: Degens, E. T., Ross, D. A. (Eds.), *Hot Brines and Recent Heavy Metal Deposits in the Red Sea: A Geochemical and Geophysical Account*. Springer Berlin Heidelberg, Berlin, Heidelberg, pp. 474–498.
- Kaufman, A. J., Hayes, J. M., Klein, C., Dec. 1990. Primary and diagenetic controls of isotopic compositions of iron-formation carbonates. *Geochimica et Cosmochimica Acta* 54 (12), 3461–3473.
- Leavitt, W. D., Halevy, I., Bradley, A. S., 2013a. Influence of sulfate reduction rates on the Phanero-

- zoic sulfur isotope record. In: Proceedings of the National Academy of Sciences of the United States of America. pp. 11244–11249.
- Leavitt, W. D., Pereira, I. C., Bradley, A. S., Guo, W., Johnston, D. T., 2013b. Enzymatic constraints on the global S cycle: the fractionation factors of Dsr. *Mineralogy Magazine* 77, 1560(abstract).
- Lepland, A., Jan. 2013. Potential influence of sulphur bacteria on Palaeoproterozoic phosphogenesis. *Nature Geoscience*, 1–5.
- Li, C., Love, G. D., Lyons, T. W., Fike, D. A., Sessions, A. L., Chu, X., Apr. 2010. A Stratified Redox Model for the Ediacaran Ocean. *Science* 328 (5974), 80–83.
- Lowenstein, T. K., Hardie, L. A., Timofeeff, M. N., Demicco, R. V., 2003. Secular variation in seawater chemistry and the origin of calcium chloride basinal brines. *Geology* 31 (10), 857–4.
- Loyd, S. J., Marengo, P. J., Hagadorn, J. W., Lyons, T. W., Kaufman, A. J., Sour-Tovar, F., Corsetti, F. A., Jul. 2012. Sustained low marine sulfate concentrations from the Neoproterozoic to the Cambrian Insights from carbonates of northwestern Mexico and eastern California. *Earth and Planetary Science Letters* 339-340 (C), 79–94.
- Lyons, T. W., Kah, L. C., Gellatly, A. M., 2004. The Precambrian sulphur isotope record of evolving atmospheric oxygen. *The Precambrian Earth: Tempos and events: . . .*
- Marengo, P. J., Corsetti, F. A., Kaufman, A. J., Bottjer, D. J., Mar. 2008. Environmental and diagenetic variations in carbonate associated sulfate: An investigation of CAS in the Lower Triassic of the western USA. *Geochimica et Cosmochimica Acta* 72 (6), 1570–1582.
- Markovic, S., Paytan, A., Wortmann, U. G., 2015. Pleistocene sediment offloading and the global sulfur cycle. *Biogeosciences*.
- Meyer, N. R., Zerkle, A. L., Fike, D. A., Jan. 2017. Sulphur cycling in a Neoproterozoic microbial mat. *Geobiology*, 1–14.
- Ohmoto, H., Kaiser, C. J., Geer, K. A., 1990. Systematics of sulphur isotopes in recent marine sediments and ancient sediment-hosted base metal deposits. *Stable isotopes and fluid processes in mineralization* 23, 70–120.
- Oliveira, T. F., Vonrhein, C., Matias, P. M., 2008. The crystal structure of *Desulfovibrio vulgaris* dissimilatory sulfite reductase bound to DsrC provides novel insights into the mechanism of sulfate respiration. *Journal of Biological . . .*
- Paris, G., Fehrenbacher, J. S., Sessions, A. L., 2014. Experimental determination of carbonate-associated sulfate $\delta^{34}\text{S}$ in planktonic foraminifera shells. *Geochemistry, Geophysics, Geosystems* 15, 1452–1461.
- Paris, G., Sessions, A. L., Subhas, A. V., Adkins, J. F., May 2013. MC-ICP-MS measurement of $\delta^{34}\text{S}$ and $\Delta^{33}\text{S}$ in small amounts of dissolved sulfate. *Chemical Geology* 345 (C), 50–61.
- Pasquier, V., Sansjofre, P., Rabineau, M., Houghton, J., Fike, D. A., 2017. Pyrite sulfur isotopes reveal glacial– interglacial environmental changes. *Proceedings of the National Academy of Sciences of the United States of America* 114 (23), 5941–5945.
- Paytan, A., Jun. 2004. Seawater Sulfur Isotope Fluctuations in the Cretaceous. *Science* 304 (5677), 1663–1665.
- Paytan, A., Kastner, M., Campbell, D., Thiemens, M. H., 1998. Sulfur isotopic composition of Cenozoic seawater sulfate. *Science*.
- Paytan, A., Mearon, S., Cobb, K., Kastner, M., 2002. Origin of marine barite deposits: Sr and S isotope characterization. *Geology* 30 (8), 747–4.
- Poulton, S. W., Fralick, P. W., Canfield, D. E., Jun. 2010. Spatial variability in oceanic redox structure 1.8 billion years ago. *Nature Geoscience* 3 (7), 486–490.
- Present, T. M., Paris, G., Burke, A., Fischer, W., 2015. Large Carbonate Associated Sulfate isotopic variability between brachiopods, micrite, and other sedimentary components in Late Ordovician strata. *Earth and Planetary Science Letters* 432, 187–198.
- Raab, M., Spiro, B., Apr. 1991. Sulfur isotopic variations during seawater evaporation with fractional crystallization. *Chemical Geology: Isotope Geoscience section* 86 (4), 323–333.
- Raven, M. R., Sessions, A. L., Fischer, W. W., Adkins, J. F., Aug. 2016. Sedimentary pyrite $\delta^{34}\text{S}$ differs from porewater sulfide in Santa Barbara Basin: Proposed role of organic sulfur. *Geochimica et Cosmochimica Acta* 186 (C), 120–134.
- Rees, C. E., 1973. A steady-state model for sulphur isotope fractionation in bacterial reduction processes. *Geochimica et Cosmochimica Acta* 37, 1141–1162.
- Reuschel, M., Melezhik, V. A., Whitehouse, M. J., Lepland, A., Fallick, A. E., Strauss, H., Jan.

2012. Isotopic evidence for a sizeable seawater sulfate reservoir at 2.1Ga. *Precambrian Research* 192-195, 78–88.
- Ries, J. B., Fike, D. A., Pratt, L. M., Lyons, T. W., 2009. Superheavy pyrite ($\delta^{34}\text{S}_{\text{pyr}}$, $\delta^{34}\text{S}_{\text{SCAS}}$) in the terminal Proterozoic Nama Group, southern Namibia: A consequence of low seawater sulfate at the dawn of animal life. *Geology* 37 (8), 743–746.
- Sagemann, J., Jørgensen, B. B., Greeff, O., Apr. 1998. Temperature dependence and rates of sulfate reduction in cold sediments of svalbard, arctic ocean. *Geomicrobiology Journal* 15 (2), 85–100.
- Sansjofre, P., Cartigny, P., Trindade, R., 2016. Multiple sulfur isotope evidence for massive oceanic sulfate depletion in the aftermath of Snowball Earth. *Nature Communications* 7.
- Sim, M. S., Bosak, T., Ono, S., Jun. 2011a. Large Sulfur Isotope Fractionation Does Not Require Disproportionation. *Science* 333 (6038), 74–77.
- Sim, M. S., Ono, S., Donovan, K., Templer, S. P., 2011b. Effect of electron donors on the fractionation of sulfur isotopes by a marine *Desulfovibrio* sp. *Geochimica et Cosmochimica Acta* 75, 4244–4259.
- Speich, N., Trüper, H. G., Aug. 2008. Adenylylsulphate reductase in a dissimilatory sulphate-reducing archaeobacterium. *Journal of General Microbiology* 134, 1419–1425.
- Staudt, W. J., Schoonen, M. A. A., Jul. 1995. Sulfate Incorporation into Sedimentary Carbonates. In: *Geochemical Transformations of Sedimentary Sulfur*. American Chemical Society, Washington, DC, pp. 332–345.
- Stetter, K. O., Lauerer, G., Thomm, M., Neuner, A., Nov. 2009. Isolation of Extremely Thermophilic Sulfate Reducers: Evidence for a Novel Brandl of Archaeobacteria. *Science* 236, 822–824.
- Strauss, H., Aug. 1997. The isotopic composition of sedimentary sulfur through time. *Palaeogeography, Paleoclimatology, Paleocology* 132 (1-4), 97–118.
- Tarpgaard, I. H., Røy, H., Jørgensen, B. B., Jun. 2011. Concurrent low- and high-affinity sulfate reduction kinetics in marine sediment. *Geochimica et Cosmochimica Acta* 75 (11), 2997–3010.
- Timofeeff, M. N., Lowenstein, T. K., da Silva, M. A. M., Harris, N. B., Apr. 2006. Secular variation in the major-ion chemistry of seawater: Evidence from fluid inclusions in Cretaceous halites. *Geochimica et Cosmochimica Acta* 70 (8), 1977–1994.
- Tostevin, R., Turchyn, A. V., Farquhar, J., Johnston, D. T., Eldridge, D. L., Bishop, J. K. B., McIlvin, M., Jun. 2014. Multiple sulfur isotope constraints on the modern sulfur cycle. *Earth and Planetary Science Letters* 396 (C), 14–21.
- Troelsen, H., Jørgensen, B. B., Sep. 1982. Seasonal dynamics of elemental sulfur in two coastal sediments. *Estuarine, Coastal and Shelf Science* 15 (3), 255–266.
- Veizer, U. B. . J., 1980. Chemical Diagenesis of a Multicomponent Carbonate System–I: Trace Elements. *SEPM Journal of Sedimentary Research* Vol. 50, 1–18.
- Venceslau, S. S., Stockdreher, Y., Dahl, C., Pereira, I. A. C., Apr. 2014. The “bacterial heterodisulfide” DsrC is a key protein in dissimilatory sulfur metabolism. *BBA - Bioenergetics*, 1–17.
- Visscher, P. T., Reid, R. P., Bebout, B. M., Oct. 2000. Microscale observations of sulfate reduction: Correlation of microbial activity with lithified micritic laminae in modern marine stromatolites. *Geology* 28 (10), 919–922.
- W Burdett, J., Arthur, M. A., Richardson, M., Sep. 1989. A Neogene seawater sulfur isotope age curve from calcareous pelagic microfossils. *Earth and Planetary Science Letters* 94 (3-4), 189–198.
- Werne, J. P., Lyons, T. W., Hollander, D. J., Formolo, M. J., Sinninghe Damsté, J. S., Apr. 2003. Reduced sulfur in euxinic sediments of the Cariaco Basin: sulfur isotope constraints on organic sulfur formation. *Chemical Geology* 195 (1-4), 159–179.
- Wilbanks, E. G., Jaekel, U., Salman, V., Humphrey, P. T., Eisen, J. A., Facciotti, M. T., Buckley, D. H., Zinder, S. H., Druschel, G. K., Fike, D. A., Orphan, V. J., Feb. 2014. Microscale sulfur cycling in the phototrophic pink berry consortia of the Sippewissett Salt Marsh. *Environmental Microbiology* 16 (11), 3398–3415.
- Wilkin, R. T., Barnes, H. L., Nov. 1996. Pyrite formation by reactions of iron monosulfides with dissolved inorganic and organic sulfur species. *Geochimica et Cosmochimica Acta* 60 (21), 4167–4179.
- Wing, B. A., Halevy, I., Dec. 2014. Intracellular metabolite levels shape sulfur isotope fractionation during microbial sulfate respiration. *Proceedings of the National Academy of Sciences* 111 (51), 18116–18125.
- Wortmann, U. G., Paytan, A., Jul. 2012. Rapid Variability of Seawater Chemistry Over the Past 130 Million Years. *Science* 337 (6092), 334–336.

- Wotte, T., Shields-Zhou, G. A., Strauss, H., Oct. 2012. Carbonate-associated sulfate: Experimental comparisons of common extraction methods and recommendations toward a standard analytical protocol. *Chemical Geology* 326-327 (C), 132–144.
- Zehnder, A., Zinder, S. H., 1980. The sulfur cycle. *The Handbook of Environmental Chemistry*. Springer Verlag.
- Zerkle, A. L., Farquhar, J., Johnston, D. T., Cox, R. P., Canfield, D. E., Jan. 2009. Fractionation of multiple sulfur isotopes during phototrophic oxidation of sulfide and elemental sulfur by a green sulfur bacterium. *Geochimica et Cosmochimica Acta* 73 (2), 291–306.
- Zhu, Q., Aller, R. C., Fan, Y., Oct. 2006. Two-dimensional pH distributions and dynamics in bioturbated marine sediments. *Geochimica et Cosmochimica Acta* 70 (19), 4933–4949.

How climate affects early diagenesis?

Comment le climat affecte le diagenèse?

Abstract

Ce chapitre synthétique s'appuie sur les principaux résultats obtenus lors de cette étude pour discuter de l'impact du climat sur la diagenèse précoce. Ici, nous utilisons les variations de compositions isotopiques du soufre contenu dans la pyrite comme un indicateur des processus diagenétiques puisque cette dernière est formée post déposition. En effet, les processus microbiens qui entre en action lors de la précipitation des pyrites sont fortement influencés par la quantité de matière organique. Or, nous avons vu que dans le Golfe du Lion la quantité, l'origine et la préservation du carbone organique est tributaire des conditions climatiques. L'étude détaillée de cette relation ne semble pas permettre d'expliquer les variations isotopiques du cycle du soufre. Cependant, la cyclicité observée dans les isotopes du soufre suggère un important contrôle climatique. Ainsi, nous poursuivons l'exploration du contrôle sédimentaire suggéré dans le chapitre IV.

Contents

1	Organic matter content, origin and reactivity effect on early diagenetic processes [microbial view]	180
1.1	Organic carbon content	181
1.2	Organic carbon origin	182
1.3	Organic carbon reactivity and preservation state.....	185
2	Indirect regulation of early diagenesis by climate changes [sedimentary control]	188

List of Figures

54	Histogram of (A) TOC values and (B) pyrite $\delta^{34}\text{S}$ and $^{34}\epsilon$ as function of glacial/interglacial periods, color-coded by mean temperature from Cortina et al. (2015). Sensu-stricto refers to the warm substages of interglacial and cold substages during glacial. Sensu lato includes all data obtained within interglacial or glacial periods. Rainfall refers to data obtained during intervals of high runoff according to Pasquier et al. submitted	181
55	Histogram of (A) $\delta^{13}\text{C}_{\text{org}}$ values used as indicative of organic carbon origin and (B) pyrite $\delta^{34}\text{S}_{\text{pyr}}$ and $^{34}\epsilon$ as function of glacial/interglacial periods, color-coded by mean temperature from Cortina et al. (2015). Sensu-stricto refers to the warm substages of interglacial and cold substages during glacial. Sensu lato includes all data obtained within interglacial or glacial periods. Rainfall refers to data obtained during intervals of high runoff according to Pasquier et al. submitted. Tesi et al. (2007) mean values for the Rhone pro-deltaic and open marine sedimentation are also reported.	184
56	Histogram of (A) % of degraded organic matter from Cortina et al. (2016) and (B) pyrite $\delta^{34}\text{S}_{\text{pyr}}$ and $^{34}\epsilon$ as function of glacial/interglacial periods, color-coded by mean temperature from Cortina et al. (2015). Sensu-stricto refers to the warm substages of interglacial and cold substages during glacial. Sensu lato includes all data obtained within interglacial or glacial periods. Rainfall refers to data obtained during intervals of high runoff according to Pasquier et al. submitted.	186
57	Cross plot of $\delta^{34}\text{S}_{\text{pyr}}$ versus the percentage of sand preserved in PRGL-1-4 samples. Light/dark blue circles correspond to cold substages (i.e. respectively sensu-lato and sensu-stricto); and light/dark red circles correspond to warm substages (i.e. respectively sensu-lato and sensu-stricto).	188
58	Cross plot between the $\delta^{34}\text{S}_{\text{pyr}}$ with associated porosity/water content. Both porosity and water content are calculated from the gamma-ray MSCL sensor. Light/dark blue circles correspond to cold substages (i.e. respectively sensu-lato and sensu-stricto); and light/dark red circles correspond to warm substages (i.e. respectively sensu-lato and sensu-stricto).	189

We have shown in Chapter IV that sulfur stable isotopes were affected by glacial-interglacial transitions. We propose two mechanisms to explain these isotopic shifts, one is related to the lithology itself (physical parameters of the sediment) which influence the exposure time of the organic matter to oxidant, another one is the BSR csSRR rate which could be related to organic matter nature. In this chapter, we further investigate the role of the organic matter content, origin and its preservation in the sediments to test the hypothesis.

1. Organic matter content, origin and reactivity effect on early diagenetic processes [microbial view]

Marine sediments cover 70 % of the Earth surface. Organic matter is finely dispersed in these sediments in different concentrations and reactivity depending largely on the size of the organic matter source, water depth, and sedimentation rates (Hedges and Keil 1995). A part of shelf marine sediment organic matter is produced in-situ, i.e. the marine system, such as algal and the bacterial phytoplankton biomass, which is assumed to be fresh and easily metabolizable during early diagenetic processes. However, shelf marine sediments also receive inputs of terrestrial organic matter, mainly derived from plant materials rich in cellulose and lignin. This organic matter is known to be more resistant to decomposition and remineralization (De Leeuw and Largeau 1993). Regardless of sources, extensive recycling of organic matter occurs in oxic water column and, in general, it is admitted that only about 1 % of the organic carbon export reaches the seafloor on a global scale (Hedges and Keil 1995). This detrital organic matter serves as a main energy source (electron donors) for microorganisms living in marine sediments (Jørgensen and Boetius 2007), which are non-negligible agents of the early diagenesis.

The common view can be summarized as: in surface sediments, easily degradable organic matter is preferentially utilized by microorganisms (Jørgensen 1977, 2000), whereas less reactive organic matter has a greater potential to be buried in deeper sediments (Jørgensen 2000; Starnawski et al. 2017). Consequently, organic matter is strongly degraded and mineralized during early diagenetic processes. Therefore, a good understanding of the composition of sedimentary organic matter is important (i) to predict the contributions of the different organic matter sources (i.e. marine versus detrital) to the pool of total organic carbon that is later used by micro-organisms, but also (ii) to understand how each pool affects the rate of microbial communities (i.e. including Microbial Sulfate Reduction activity), and early diagenesis (i.e. post depositional processes).

The Gulf of Lion sediments are one of the modern key for better understanding the impact of organic matter composition on early diagenetic processes. As we saw in the third chapter, PRGL1-4 sediment have recorded periodic changes of organic matter composition (i.e. content, origin and reactivity) in response to climate fluctuations. Chapter IV highlighted a strong overprint of local environmental changes during early diagenetic processes involved in the reduction of sea-water sulfate, through MSR. Below we discuss the potential link between the organic matter content, composition, and reactivity and early diagenesis in the Gulf of Lion case (i.e. strongly suggested by earlier work e.g. Jørgensen 1982; Westrich and Berner 1984; Meyers 1994; Hedges and Keil 1995).

Culture experiments have shown that changes the cell-specific Sulfate Reduction Rate induce modification of the isotopic fractionation between the parent sulfate and the produced sulfide. A clear decrease in the isotopic fractionation (34) is associated with high csSRR (see chapter IV for more detailed explanations). Sulfate limitation would arrive from high local organic load. The last 500 kyr duration tells us just that the parent sulfate composition was the same as now (i.e. ~ 21 ‰; Paytan et al. 2002; Paytan 2004; Johnston

2011). Therefore, we assume that pore-water was at equilibrium with the overlying water column (i.e. regarding sulfates). We calculated the $^{34}\epsilon$ isotopic fractionation induced by microbial sulfate reduction (MSR) between the pore-water and the observed $\delta^{34}\text{S}_{\text{pyrite}}$ recorded in PRGL 1-4. We further compare $^{34}\epsilon$ which can trace MSR activity and more specifically csSRR to organic carbon content, origin and preservation state.

1.1. Organic carbon content

According to earlier studies, the amount of organic carbon reaching the sea-floor is commonly viewed as the principal regulator of the microbial activity because of the strong relationship between TOC and the electron donor availability (Macko et al. (1993) and references therein). The following sections try to combine this observation with TOC values recorded in the Gulf of Lion.

In borehole PRGL 1-4, TOC values show small variations between glacial (*sensu-stricto*; i.e. cold substages associated with low sea-level) and interglacial periods (*sensu-stricto*; i.e. warm substages associated with high sea level). Surprisingly, glacial *sensu-stricto* and interglacial *sensu-stricto* are characterized by the same mean TOC values (i.e. 0.63 %), see **Figure 54**. Considering migrations of the sedimentary system (i.e. seaward/landward, respectively) over the shelf, this result is unexpected.

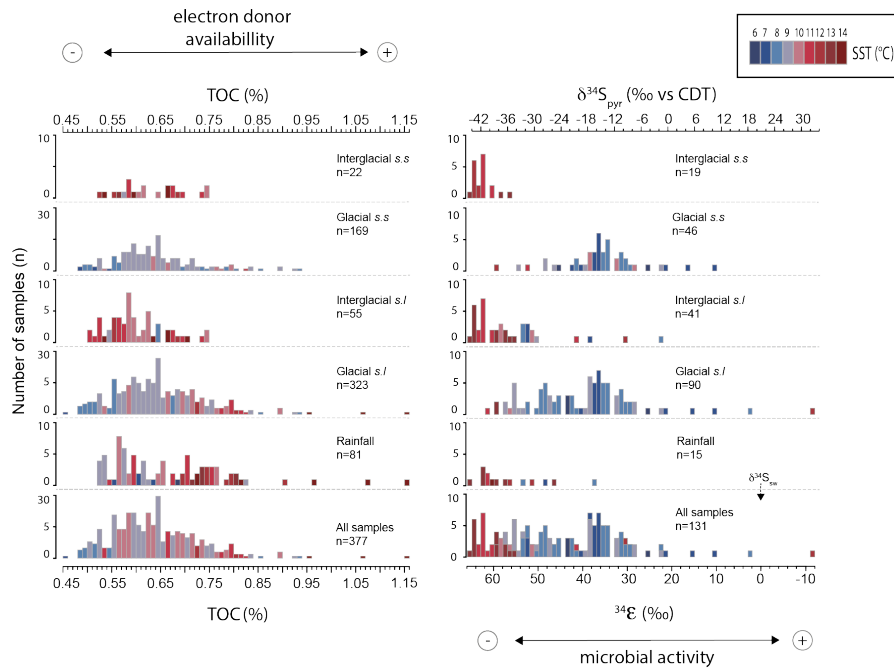


Figure 54

Histogram of (A) TOC values and (B) pyrite $\delta^{34}\text{S}$ and $^{34}\epsilon$ as function of glacial/interglacial periods, color-coded by mean temperature from Cortina et al. (2015). *Sensu-stricto* refers to the warm substages of interglacial and cold substages during glacial. *Sensu lato* includes all data obtained within interglacial or glacial periods. Rainfall refers to data obtained during intervals of high runoff according to Pasquier et al. submitted

Nevertheless, the variability of TOC values is higher during glacial times (i.e. 0.45

%) than during interglacial (i.e. 0.22 ‰). This can be explained by episodic fluxes of high organic carbon in pro-deltaic environments (i.e. flood events) and/or high spatial variability of the prodeltaic depocenters in response to small sea-level changes or as autocyclic phenomenon.

However, strong stratigraphic variations (> 76 ‰) in sulfur isotopes recorded in pyrite have been reported during this PhD. According to previous assumptions, they should reflect strong modulation of the microbial activity. Such huge changes in the microbial fractionation require important changes in the availability of electron donors (i.e. organic carbon) and therefore are hard to reconcile with the small changes in the TOC values.

We saw in Chapter III that the Gulf of Lion endured specific intervals of high river runoff not related to the first order global climatic changes (i.e. glacial/interglacial). Rain-fall events happened during precession minima insolation maxima of both interglacial and glacial. These periods are associated with higher TOC values when compared to surrounding sediments. Therefore we should expect enhanced MSR. But, in fact, they are associated with high $^{34}\epsilon$ values (see **Figure 54**), indicative of low MSR. We could therefore speculate that large freshwater inputs induced phytoplanktonic bloom which consumed the organic matter within the water column (supported by low $\delta^{15}\text{N}$ values (this study); but have been also observed in 2004 Rhone's flood event, Harmelin-Vivien et al. 2008). Therefore, the amount of organic carbon that reached the sea-floor was not enough to stimulate the MSR activities. Such proposition should be viewed cautiously because we assumed that csSRR was the main responsible factor for $^{34}\epsilon$ variations.

In the case of the Gulf of Lion, this finding shows that changes in microbial activities are not necessary synchronous with TOC variations. This confirm the idea of Berner and co-workers which have also highlighted the strong influence of the different pools of organic matter (i.e. relative lability) on the rate of degradation during early diagenesis (Berner et al. 1980; Westrich and Berner 1984).

1.2. Organic carbon origin

Previous studies have shown that the microbial degradation activity is dependent upon substrate composition (Berner et al. 1980; Westrich and Berner 1984). As we have just seen in the previous subsection, organic matter content variations in the sediment is likely insufficient to drive the MSR fluctuation in the Gulf of Lion. But we know that the origin of the organic matter has strong impact on its degradability.

Chapter III suggests that the origin (i.e. terrestrial versus marine) of organic carbon preserved in PRGL1-4 sediments is strongly modulated by climate changes, as is the $\delta^{34}\text{S}_{\text{pyrite}}$ fluctuation. Therefore, microbial changes may reflect the natural proportion of external input (i.e. terrestrial) and autochthonous production (i.e. Marine).

The general perception is that terrestrially-derived organic carbon is rather recalcitrant. As a consequence, sediment dominated by terrestrial inputs are expected to be less bio-reactive than sediments containing mostly autochthonous marine-derived organic matter, at least during early diagenesis. Therefore, the quality and quantity of sediment organic matter available for microbial processes is strongly influenced by the relative proportion of each organic carbon pools (i.e. terrestrial versus marine). In the following lines, the isotopic composition of organic carbon is used as a proxy of organic matter origin where low $\delta^{13}\text{C}_{\text{org}}$ are interpreted as indicative of high terrestrial inputs (i.e. prodeltaic environment around -25 ‰; Kim et al. 2006; Tesi et al. 2007). The present-day shelf break sedimentation has been characterized as an 'open marine' environment (Tesi et al. 2007). Therefore, its organic carbon isotopic composition is used to infer marine-derived organic matter origin (i.e. $\delta^{13}\text{C}_{\text{org}} \sim -22.7$ ‰).

Over the last 500 ka, PRGL1-4 sediments show a high variability of $\delta^{13}\text{C}_{\text{org}}$ ratio from -21.4 to -25.1 ‰ with an average value of -24.0 ± 3.6 ‰ (n= 377), see **Figure 55**. Such variability of $\delta^{13}\text{C}_{\text{org}}$ is the natural result of landward/seaward migration of the entire sedimentological system (i.e. river mouth, pro-deltaic accumulation, shelf and open marine sedimentation) in response to sea-level variation (Pasquier et al. submitted).

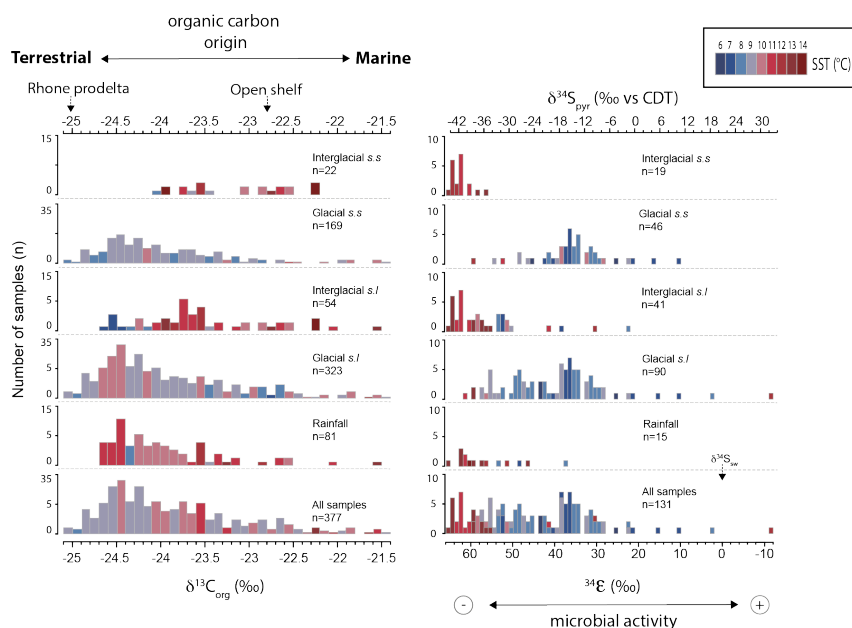


Figure 55

Histogram of (A) $\delta^{13}\text{C}_{\text{org}}$ values used as indicative of organic carbon origin and (B) pyrite $\delta^{34}\text{S}_{\text{pyr}}$ and $^{34}\epsilon$ as function of glacial/interglacial periods, color-coded by mean temperature from Cortina et al. (2015). Sensu-stricto refers to the warm substages of interglacial and cold substages during glacial. Sensu lato includes all data obtained within interglacial or glacial periods. Rainfall refers to data obtained during intervals of high runoff according to Pasquier et al. submitted. Tesi et al. (2007) mean values for the Rhone pro-deltaic and open marine sedimentation are also reported.

Consequently, glacial sediments (*sensu-stricto*) are characterized by lower isotopic ratios as expected with high terrestrial inputs in prodeltaic environment during low sea-level times. These sediments should also be more resistant to microbial degradation processes. As the sea-level rises, the landward migration of prodeltaic accumulation reduced terrestrial inputs to the outer shelf, and enhanced the deposition of marine-derived organic matter. This is consistent with (i) the increase in organic carbon isotopes preserved during interglacial sediments *sensu-stricto*, and (ii) the existence of condensed layers with a high concentration in foraminifera Sierro et al. (2009), see **Figure 55**. In terms of organic matters reactivity, this implies more bio-metabolizable organic matter during interglacial times. The latter should naturally increase the microbial activity during early diagenesis. Surprisingly, interglacial *sensu-stricto* (i.e. high $\delta^{13}\text{C}_{\text{org}}$) are characterized by low sulfur isotopic fractionation. In other words, fresh marine-derived organic carbon is associated with very low MSR activity. Also, maximum of MSR activity (i.e. lower $^{34}\epsilon$) happened during periods of high amount of terrestrial organic matter (i.e. low $\delta^{13}\text{C}_{\text{org}}$) whereas a larger proportion of terrestrial organics should have decreased the MSR. Periods of increased rainfall are characterized by high inputs of terrestrial organic matter, as in glacial times, see **Figure 55**. Based on previous statement they should have been

associated to higher $^{34}\epsilon$ (i.e. lower BSR activity), as observed on the **Figure 55**. This seems consistent with high inputs of more resistant organic matter (i.e. terrestrial origin). This suggest that MSR processes in PRGL1-4 sediments does not react sensitively to organic matter origin over the last 500 kyr.

Assuming that terrestrial inputs are associated with low reactivity in marine environment, we investigated the potential link between past changes in MSR productivity and past changes in organic matter origin (i.e. terrestrial versus marine). As long as terrestrial material is considered as refractory, the origin of the organic matter reaching the sediment interface cannot be considered as the most important parameter perturbing the sulfur stable isotope signal.

1.3. Organic carbon reactivity and preservation state

Bulk organic carbon preservation at the sediment interface has been shown to be directly impacted by the transport, sinking and settling particles times (Hartnett et al. 1998; Hedges and Keil 1995). These three parameters act in the same way, decreasing the reactivity of newly accumulated organic carbon at the sediment interface. Therefore, subsequent decrease in microbial activity is expected during early diagenesis.

As an example, low sea level conditions induce lower transport times (because sediment is rapidly transported within rivers directly to the outer shelf). At PRGL1-4 site low sea level conditions allowed prodeltaic sedimentation. The latter is characterized by a very high sedimentation rate. Such areas are known to bury a high amount of fresh (i.e. less degraded by oxic processes happening in the water column) terrestrial organic matter (Tesi et al. 2007; Cathalot et al. 2010). Therefore, we can expect high MSR activity. The situation is very different during interglacial times where high sea-level induced landward migration of terrestrial inputs (i.e. prodeltaic sediments). Warmer conditions also enhance the marine primary production and production of labile organic matter. Although, such 'fresh' organic matter spends long times in contact to oxygenic degradation processes (i.e. longer settling times due to higher water column, and very low sedimentation rate). Therefore, less reactive, but also more refractory organic matter is deposited at the sediment/water interface. So that, lower $^{34}\epsilon$ are expected.

In the Gulf of Lion, the reactivity of the organic matter has been approximated by Cortina et al. (2016). For this, they used n-alkanes preserved in sediment which are likely altered during diagenetic processes. Within the n-alkane fraction, microbial processes induce a break-down of long n-alkane chain (Eglinton and Hamilton 1967; Brittingham et al. 2017). In other words, fresh organic matter is mostly composed of C27 to C33 n-alkane whereas degraded organic matter lose their odd carbon, with n-alkane typically $> C29$. **Figure 56** shows the percentage of degraded organic matter of the PRGL-1 cores samples separated in function of glacial-interglacial context and color coded by mean sea-surface temperature.

This figure suggests that most of sediments deposited in the Gulf of Lion range between 10 and 40 % of degraded organic matter. In details, interglacial sediments (i.e. sensu-stricto) are characterized by lower proportion of degraded organic matter (i.e. 10 to 15 %) whereas glacial sensu stricto sediments range between 15 to 35 %.

Therefore, there is an apparent paradox between the times spend in contact of oxygenic processes (i.e. transport, settling) and the quality of the organic matter preserved at the sediment interface obtained with n-alkane. In other words, interglacial sensu-stricto are characterized by the highest sea-level conditions which increase the residence time of organic matter in the ocean (i.e. where most of the oxygenic degradation took place) while they

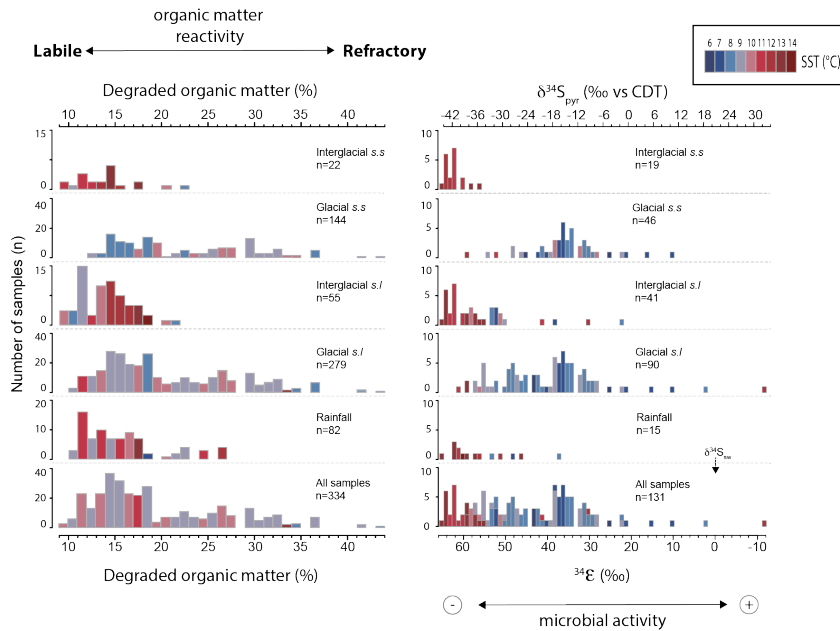


Figure 56

Histogram of (A) % of degraded organic matter from Cortina et al. (2016) and (B) pyrite $\delta^{34}\text{S}_{\text{pyr}}$ and $^{34}\epsilon$ as function of glacial/interglacial periods, color-coded by mean temperature from Cortina et al. (2015). Senu-stricto refers to the warm substages of interglacial and cold substages during glacial. Senu lato includes all data obtained within interglacial or glacial periods. Rainfall refers to data obtained during intervals of high runoff according to Pasquier et al. submitted.

show the lower percentage of degraded organic matter. The same assessment is clearly observed during glacial sensu-stricto, where more degraded organic matter is recorded in our samples. Regarding the reactivity/preservation of glacial sensu stricto sediment, the high MSR activity recorded with the $^{34}\epsilon$ unexpected. A close examination of the range of glacial sensu-stricto data allows the identification of a bimodal distribution. Such bimodal distribution may reflect two different type of organic matter:

- i A pool between 15 to 20 % which could result from rapid prodeltaic sedimentation and degradation,
- ii A pool of more degraded organic matter, ranging between 25 to 35 %. It might correspond to re-eroded and re-deposited material due to shelf aerial exposure and sea-level lowering (Rabineau et al. 2005). Thus, organic matter that have been subject to two phases of degradation.

In such case, the low degraded and well preserved organic matter should explain the high rate of MSR observed in our samples.

During interglacial sensu-stricto and rainfall events, sediments are characterized by low proportion of degraded material. Therefore they are assumed as more bio-easily metabolizable by microbes during early diagenesis. However, those intervals show high $^{34}\epsilon$ suggesting low MSR activity, see **Figure 56**.

Once again, the reactivity and preservation of the organic matter buried in the Gulf of Lion sediments cannot explain the observed shift in MSR activity. Therefore, the reactivity and preservation of the organic matter arriving at the sediment interface seems not to be

the primary mechanism explaining the stratigraphic expression of $\delta^{34}\text{S}_{\text{pyr}}$.

SUMMARY POINTS

The close examination of the organic carbon characteristics (i.e. content, origin and reactivity) point out some incongruities when compared to the recorded microbial activity preserved in the Gulf of Lion sediments.

1. Organic carbon content does not show any co-variations or tendency together with $^{34}\epsilon$ suggesting that MSR does not reacts very sensitively to variation of TOC inputs.
2. On the same base, we can suggest that the origin of the organic matter, terrestrial vs marine does not control on the first order the sulfur isotopic signal and the MSR activity.
3. An apparent paradox is observed between the expectations of MSR activity and the reactivity of the organic matter. Indeed, in the Gulf of Lion more refractory organic matter are associated with higher past bacterial activities.

2. Indirect regulation of early diagenesis by climate changes [sedimentary control]

Earlier sedimentological studies have highlighted a strong influence of climate changes over the Gulf of Lion shelf (Rabineau et al. 2005, 2006; Bassetti et al. 2008; Jouet et al. 2008; Sierro et al. 2009). One of the most important is probably the modulation of the shelf accommodation space by glacio-eustatic changes which governed the spatial and temporal distribution of sedimentary units. This also controlled the sediments physical properties associated within each sedimentary unit. The sedimentation rate and grain size are good examples: the Rhone pro-deltaic system is characterized by high rate of clastic fine sediments. As we move toward the shelf break, terrigenous clay no longer reach the upper slope and we observe a decrease of the sedimentation rate. Consequently, sediments are mainly composed of pelagic coarse grained skeletal material, i.e. mainly foraminifera shells, which increase the grain size.

During this PhD, we used PRGL 1-4 sedimentological parameters (i.e. sedimentation rates) and organic carbon isotopic compositions to document that (i) coastal-rivers pro-deltaic accumulations reached the shelf break during the last 5 glacial maxima, and (ii) marine derived products mainly composed interglacial sediments apart from specific intervals of high rainfall activity. In this present part of the general conclusion, we explored possible effects of changes in the physical sediment properties on the modulation of the sulfur stable isotope signal.

From existing literature, the general relationships between sediments proprieties (e.g grain size, available surface area, porosity, organic matter content) and benthic microbial community are well known. For example, Mayer (1994); Keil et al. (1998) reported that fine-grain sediments carry high organic matter content, and support a high microbial activity as compared to coarse grain. This means that the grain size is inversely correlated to available surface area, porosity, organic matter and microbial biomass.

A test for this possible relation is presented in the **Figure 57**, where $\delta^{34}\text{S}_{\text{pyr}}$ (i.e. used as indicator of MSR activity) is plotted against the % of sand (estimated by the sediment fraction higher than $63\ \mu\text{m}$, data from Frigola et al. 2012).

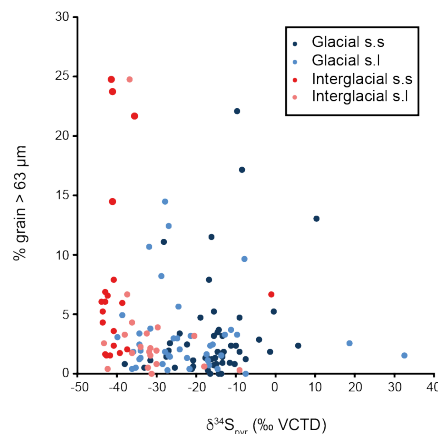


Figure 57

Cross plot of $\delta^{34}\text{S}_{\text{pyr}}$ versus the percentage of sand preserved in PRGL-1-4 samples. . Light/dark blues circles correspond to cold substages (i.e. respectively sensu-lato and sensu-stricto); and light/dark red circles correspond to warm substages (i.e. respectively sensu-lato and sensu-stricto).

In the case of the Gulf of Lion, no correlation between the percent of sand and the sulfur isotopic fractionation is observed, see **Figure 57**. Therefore, other parameters related to climate changes have to be considered to explain the observed variability in sulfur isotopes.

Taking advantage of the important database available on PRGL1-4, we were able to test the potential impact of two physical sediment properties on sulfate reduction processes: (i) the sediment porosity and (ii) the water content. Both parameters were measured using the gamma-ray MSCL sensor, therefore are linked by a constant coefficient. Although the relationship between the porosity/water content and $\delta^{34}\text{S}_{\text{pyr}}$ suggests a dominant control by the sedimentation, see **Figure 58**. Indeed, the observed co-variation has significant implication because porosity/water content are both related to the connectivity of the pore-water with the overlying column.

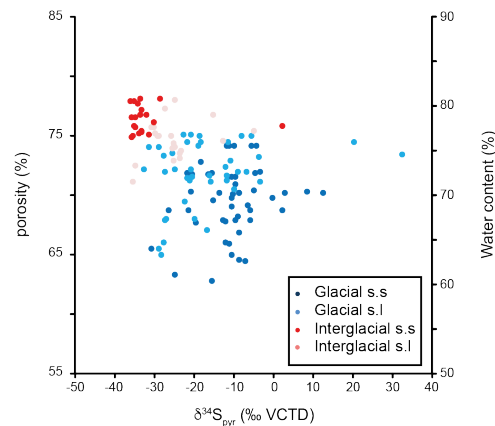


Figure 58

Cross plot between the $\delta^{34}\text{S}_{\text{pyr}}$ with associated porosity/water content. Both porosity and water content are calculated from the gamma-ray MSCL sensor. Light/dark blues circles correspond to cold substages (i.e. respectively sensu-lato and sensu-stricto); and light/dark red circles correspond to warm substages (i.e. respectively sensu-lato and sensu-stricto).

Sediments near the water-sediment interface commonly contains 70 - 90 % of water, but upon compaction the volume of water, commonly called porosity, usually decreases to 40 60 % within a few centimeters below the interface. Although, the compaction of sediment during the early diagenetic processes strongly depends on (i) the sedimentation rate which regulated the sediment aggradation and subsequent compaction, and (ii) sediment response to compaction (i.e. increase density, decrease porosity with depth) which affect the post deposition chemical history (i.e. early diagenesis).

In the Gulf of Lion, interglacial sediments are characterized by higher porosity (see **Figure 58**) and foraminifera content (Sierro et al. 2009). Therefore, the residence time of sea-water in pore environment is short in comparison to the rate of sedimentation. In other word, the communication between the porewater and the overlying column is maintained longer allowing rapid transport of chemical species across the sediment water interface. In sediment, exchanges at the sediment/water interface are caused by (i) advective processes such as bioturbation or bio-irrigation as well as (ii) the diffusional migration in pore-waters induced by difference in concentration between the two sides of the interface. Because microbial sulfate reduction processes consume porewater sulfate, they induce enhanced exchanges at the sediment interface. Such rapid exchanges can be

realized if the pore-waters are in contact with the overlying column (above the sediment water interface), or down in the sediment pore-water column. In such condition, sediments are in an open geochemical system, in the case of the sulfur cycle that is recorded by a permanent replenishment of porewater sulfate with overlying sea-water sulfate.

The reverse process is also true, decrease of pore-water porosity, as observed in the Gulf of Lion during glacial times, tends to limit connectivity of porewater water and transport between the porewater with the overlying environment. This turn the geochemical system near to a close state. In such case, the microbial consumption of porewater sulfate leads to isotopically increase of porewater composition (i.e. Rayleigh type distillation). The latter is transmitted to hydrogen sulfide and subsequent preserved in pyrite.

SUMMARY POINTS

In a prograding passive margin, like the Gulf of Lion, the natural variability in the sulfur isotopic compositions preserved in pyrites may reflect changes in sediment connectivity with the overlying water column during early diagenetic processes. Where the mechanisms that control the transport of chemical species across the sediment-water interface are strongly dependent of:

1. the rate of sedimentation (Pasquier et al. 2017).
2. the physical sediment properties such as the porosity and/or the water content. Especially, in the case of the Gulf of Lion, where positive $\delta^{34}\text{S}_{\text{pyrite}}$ are associated with local changes in the sedimentation (i.e. high sedimentation rate, lower porosity and lower water content) during sea-level low-stand; and vice versa.

Looking forward

In the light of all the results obtained during this PhD we highlighted global and local conclusions on both technics, and paleo climate/paleo environmental conditions. Many ideas emerged from this work, I tried to summarize some of the main interesting future work needed and possible future projects that would try to:

1. Characterize the organic matter loss during HCl acid digestion during sample preparation for organic carbon and nitrogen analyses. In our *Rapid Communication in Mass Spectrometry*, we draw attention to a preferential leaching of a labile terrestrial pool of organic matter. A further work would be to chemically characterize the pool of leachable organic matter. For this I would like to use GC-IRMS in order to identify the molecular composition of the lost pool (i.e. lignin, phenol, etc).
2. C and N isotopes along the PRGL-1 provide very interesting information about the Gulf of Lion coastal river paleo-hydrology. In order to better constrain the impact of the North Atlantic climate on Western Mediterranean climate, I would like to extend the isotopic characterization of the organic matter over the last deglaciation, but most importantly during the Holocene. Indeed, a high-resolution study will allow us to directly compare (i) the Gulf of Lion runoff with strong and well constrained NAO reconstructions, and (ii) abundant high resolution of speleothem records available over the North Mediterranean borderland (i.e. from the Western Atlantic coast to the Eastern Levant). Finally, such study will also give access to the youngest sapropel which is the best constrained in the entire Mediterranean basin.
3. Sulfur investigations shown anomalous sulfur isotopes signature that can only be explained by local processes on millennial timescales (i.e. changes in the sediment physical properties induced by climate changes). Consequently, understanding these Local vs Global processes over other margin location is crucial to better understand past Earth redox evolution. For this, I would like to work on IODP leg 201 (Peruvian shelf), another continental margin site on which a huge variety of chemical and biological analyses have been performed to understand sedimentary microbial activity. Samples are available via the International Ocean Discovery Program (IODP). Moreover, the access to borehole material was already assured by B.B. Jorgensen, co-chief scientist. Also, I would like to have access to a deep marine sedimentary sequence in the Western Mediterranean Sea to target the possibility of local post-depositional effects in a non-continental margin sedimentary sequence.
4. The local diagenetic process highlighted in this study still need to be better characterized and identify. This will be done using minor-sulfur isotopes and SIMS analysis. Both technics would provide important information in order to clarify geochemical processes involved in the stratigraphical variation of sulfur isotopes in the Gulf of Lion (i.e. open versus close isotopic system).
5. Finally, I would like to use the high amount of physical, and geochemical data already available on PRGL1-4 to run a diagenetic model. Such approach will help us to understand what is the part of the local (i.e. sedimentary modulation of porewater connection) versus global (i.e. change in seawater chemistry) involved over the last 500 kyr in the Gulf of Lion. Therefore, provides strong constrain on the modern sedimentary sulfur cycle.

LITERATURE CITED

- Bassetti, M. A., Berné, S., Jouet, G., Taviani, M., 2008. The 100-ka and rapid sea level changes recorded by prograding shelf sand bodies in the Gulf of Lions (western Mediterranean Sea). *Geochemistry, Geophysics, Geosystems* 9 (11), 1–27.
- Berner, W., Oeschger, H., Stauffer, B., 1980. Information on the CO₂ cycle from ice core studies. *Radiocarbon* 22 (2), 227–235.
- Brittingham, A., Hren, M. T., Hartman, G., 2017. Microbial alteration of the hydrogen and carbon isotopic composition of n-alkanes in sediments. *Organic Geochemistry* 107, 1–8.
- Cathalot, C., Rabouille, C., Pastor, L., Deflandre, B., 2010. Temporal variability of carbon recycling in coastal sediments influenced by rivers: assessing the impact of flood inputs in the Rhône River prodelta. *Biogeosciences* 7, 1187–1205.
- Cortina, A., Grimalt, J. O., Martrat, B., Rigual-Hernández, A., Sierro, F. J., Flores, J. A., 2016. Anomalous SST warming during MIS 13 in the Gulf of Lions (northwestern Mediterranean Sea). *Organic Geochemistry* 92, 16–23.
- Cortina, A., Sierro, F. J., Flores, J. A., 2015. The response of SST to insolation and ice sheet variability from MIS 3 to MIS 11 in the northwestern Mediterranean Sea (Gulf of Lions). *Geophysical Research Letters* 42, 10366–10374.
- De Leeuw, J., Largeau, C., 1993. A review of macromolecular organic compounds that comprise living organisms and their role in kerogen, coal, and petroleum formation. In: *Organic Geochemistry*. Springer, pp. 23–72.
- Eglinton, G., Hamilton, R. J., Jun, 1967. Leaf Epicuticular Waxes. *Science* 156 (3780), 1322–1335.
- Frigola, J., Canals, M., Cacho, I., Moreno, A., Sierro, F. J., Flores, J. A., Berné, S., Jouet, G., Dennielou, B., Herrera, G., Pasqual, C., Grimalt, J. O., Galavazi, M., Schneider, R., 2012. A 500 kyr record of global sea-level oscillations in the Gulf of Lion, Mediterranean Sea: new insights into MIS 3 sea-level variability. *Climate of the Past* 8 (3), 1067–1077.
- Harmelin-Vivien, M., Loizeau, V., Mellon, C., Beker, B., Arlhac, D., Bodiguel, X., Ferraton, F., Hermand, R., Philippon, X., Salen-Picard, C., 2008. Comparison of C and N stable isotope ratios between surface particulate organic matter and microphytoplankton in the Gulf of Lions (NW Mediterranean). *Continental Shelf Research* 28 (15), 1911–1919.
- Hartnett, H. E., Keil, R. G., Hedges, J. I., Devol, A. H., 1998. Influence of oxygen exposure time on organic carbon preservation in continental margin sediments. *Nature* 391 (6667), 572.
- Hedges, J. I., Keil, R. G., 1995. Sedimentary organic matter preservation: an assessment and speculative synthesis. *Marine Chemistry* 49 (2-3), 81–115.
- Johnston, D. T., 2011. Multiple sulfur isotopes and the evolution of Earth's surface sulfur cycle. *Earth-Science Reviews* 106 (1), 161–183.
- Jørgensen, B., 1977. Bacterial sulfate reduction within reduced microniches of oxidized marine sediments. *Marine Biology* 41 (1), 7–17.
- Jørgensen, B. B., Apr. 1982. Mineralization of organic matter in the sea bed—the role of sulphate reduction. *Nature* 296 (5858), 643–645.
- Jørgensen, B. B., 2000. Bacteria and marine biogeochemistry. In: *Marine geochemistry*. Springer, pp. 173–207.
- Jørgensen, B. B., Boetius, A., 2007. Feast and famine—microbial life in the deep-sea bed. *Nature reviews. Microbiology* 5 (10), 770.
- Jouet, G., Hutton, E. W., Syvitski, J. P., Berné, S., 2008. Response of the Rhône deltaic margin to loading and subsidence during the last climatic cycle. *Computers & Geosciences* 34 (10), 1338–1357.
- Keil, R. G., Tsamakis, E., Giddings, J. C., Hedges, J. I., 1998. Biochemical distributions (amino acids, neutral sugars, and lignin phenols) among size-classes of modern marine sediments from the Washington coast. *Geochimica et Cosmochimica Acta* 62 (8), 1347–1364.
- Kim, J. H., Schouten, S., Buscail, R., 2006. Origin and distribution of terrestrial organic matter in the NW Mediterranean (Gulf of Lions): Exploring the newly developed BIT index. *Geochemistry, Geophysics, Geosystems* 7 (11), 1–20.
- Macko, S. A., Engel, M. H., Parker, P. L., 1993. Early diagenesis of organic matter in sediments. In: *Organic geochemistry*. Springer, pp. 211–224.
- Mayer, L. M., 1994. Relationships between mineral surfaces and organic carbon concentrations in soils and sediments. *Chemical Geology* 114 (3-4), 347–363.

- Meyers, P. A., 1994. Preservation of elemental and isotopic source identification of sedimentary organic matter. *Chemical Geology* 114, 289–302.
- Pasquier, V., Sansjofre, P., Rabineau, M., Houghton, J., Fike, D. A., 2017. Pyrite sulfur isotopes reveal glacial– interglacial environmental changes. *Proceedings of the National Academy of Sciences of the United States of America* 114 (23), 5941–5945.
- Paytan, A., Jun. 2004. Seawater Sulfur Isotope Fluctuations in the Cretaceous. *Science* 304 (5677), 1663–1665.
- Paytan, A., Mearon, S., Cobb, K., Kastner, M., 2002. Origin of marine barite deposits: Sr and S isotope characterization. *Geology* 30 (8), 747–4.
- Rabineau, M., Berné, S., Aslanian, D., Olivet, J. L., 2005. Sedimentary sequences in the Gulf of Lion: a record of 100,000 years climatic cycles. *Marine Petroleum Geology* 22, 775–804.
- Rabineau, M., Berné, S., Olivet, J. L., Aslanian, D., 2006. Paleo sea levels reconsidered from direct observation of paleoshoreline position during Glacial Maxima (for the last 500,000 yr). *Earth and Planetary Science Letters* 252, 119–137.
- Sierro, F. J., Andersen, N., Bassetti, M. A., Berné, S., 2009. Phase relationship between sea level and abrupt climate change. *Quaternary Science Reviews* 28, 2867–2881.
- Starnawski, P., Bataillon, T., Ettema, T. J., Jochum, L. M., Schreiber, L., Chen, X., Lever, M. A., Polz, M. F., Jørgensen, B. B., Schramm, A., et al., 2017. Microbial community assembly and evolution in subseafloor sediment. *Proceedings of the National Academy of Sciences* 114 (11), 2940–2945.
- Tesi, T., Miserocchi, S., Goñi, M. A., Langone, L., 2007. Source, transport and fate of terrestrial organic carbon on the western Mediterranean Sea, Gulf of Lions, France. *Marine Chemistry* 105, 101–117.
- Westrich, J. T., Berner, R. A., 1984. The role of sedimentary organic matter in bacterial sulfate reduction: the g model tested. *Limnology and oceanography* 29 (2), 236–249.

Appendix 1:

The use of laser ablation: A New Hope in Brest.

Annexe 1:

L'utilisation de l'ablation laser: Un nouvel
espoir à Brest.

1. Scope of this project

One of the aims of this PhD was to search for new or apply different geochemical proxies (e.g. multi-element and/or different isotopic systems) on a long borehole in the western Mediterranean, spanning the last 5 glacial/interglacial cycles, in the search of a understanding of climate and sea-level variations and their effects on sedimentary records. Given this aim, I initially thought of using trace elemental composition of foraminiferal calcite shells because they are widely used as various proxies for past oceanic conditions.

As an example, measuring Mg/Ca and $\delta^{18}\text{O}$ within the same foraminifera population allows the application of Mg paleo-thermometer and acquisition of sea surface temperature (SST). This technic uses established (yet still under discussion) calibration equation, known as the Elderfield curve (Elderfield and Ganssen 2000). The latter show that $\delta^{18}\text{O}$ in foraminifera calcite ($\delta^{18}\text{O}_{\text{calcite}}$) is controlled by the calcification temperature and $\delta^{18}\text{O}$ of sea-water ($\delta^{18}\text{O}_{\text{sw}}$) which is itself controlled by salinity variation and continental ice volume. In order to obtain the calcification temperature, the $\delta^{18}\text{O}_{\text{sw}}$ is extracted. This is done using Mg/Ca-based SST estimation (Bemis et al. 1998). Also, because $\delta^{18}\text{O}_{\text{sw}}$ is related to salinity (i.e. sea surface salinity, SSS; Schmidt 1999), changes in the origin of surface water, i.e. changes in $\delta^{18}\text{O}$ of riverine runoff, make the use of $\delta^{18}\text{O}_{\text{sw}}$ -SSS relationship uncertain and challenges accurate determination of paleo sea surface salinity. However, Hall and Chan (2004) have recently shown that Ba/Ca in planktonic calcite provides a powerful tool to access past variability in regional riverine runoff. Following the methodology developed in Weldeab et al. (2007), the idea here, was to produce a foram-based reconstruction of Ba/Ca ratio throughout the core, because Ba incorporation in shell calcite varies linearly with changes in sea-water salinity (Lea and Spero 1994). The use of the present-day $\text{Ba}/\text{Ca}_{\text{sw}}$ $\text{Ba}/\text{Ca}_{\text{foram}}$ partition coefficient to produce SSS paleo reconstructions.

Because the beginning of my PhD happened at the same times of Aradhna Tripathi's CHAIR position (LabexMer), part of which was dedicated to set-up a method to measure trace element in foraminifera in Brest. Therefore, I integrated her 'IC-SIBP Team' as IUEM-member in charge of cleaning procedure on foraminifera.

2. Material

One huge advantage with working on PRGL 1-4 is that sediment samples were already prepared for foraminifera hand picking by F. Sierro and collaborators (from Salamanca) during the PROMESS consortium. This saved me a considerable amount of my time because this step is very time-consuming. Then, I went to Salamanca to visit F. Sierro, where I also quickly learned to identify key foraminifera species, and brought back samples in Brest.

Back in Brest, I realized that the amount of foraminifera (20 to 35 individual mono-specific tests) required for a standard trace elements determination using HR-ICP-MS was not available due to the high sedimentation rate during glacial times, at PRGL1-4 location. Therefore, I thought about using micro-analytical techniques such as laser ablation micro-sampling coupled to mass spectrometers (LA-ICP-MS) which provided new possibilities for my project.

Also, recent studies (Pena et al. 2005; Ferguson et al. 2008; Boussetta et al. 2011; Fehrenbacher et al. 2015 among others), pointed out several potential biases in the use of trace element (i.e. TE/Ca), especially in the Mediterranean Sea, where diagenetic processes induce deposition of a thin 'coating' of inorganic calcite on foraminifera shells. Those coatings have been known to be resistant to weak acid leaches and therefore require strong chemical cleanings, usually composed of 4 steps (see complete protocole at the end of this Appendix), which are briefly summarized here:

- **Foraminifera clay removal.** First, foraminifera were hand-picked from a specific fraction ($> 150 \mu$ in my case), with care being taken to select the well preserved and apparently 'clean' tests. Foraminifera shells were rinsed three times with ultra-pure Mili-Q water. Afterward, two methanol rinses with ultra-sonic bath were performed to carry out residual clays due to lower viscosity of methanol. Finally, one more Mili-Q rinse was performed to eliminate any methanol + clay residue.
- **Oxidative cleaning.** This step allows removal of residual organic matter preserved in foraminifera shells, which are known to contain high magnesium (Hastings et al. 1998). We used an alkali buffered (NaOH) hydrogen peroxide (H_2O_2) 1 % solution that reacted with samples in boiling water 2 x 5 minutes, samples were briefly sonicated to promote reaction at 5 minutes. After the oxidative step, three Mili-Q water rinses were used to eliminate any remaining H_2O_2 , and avoid any further reaction.
- **Reductive cleaning** aims to remove a variety of contaminants phases, such as Mn oxides. This step uses a mixture of hydrazine hydroxide, citric acid and ammonia hydroxide. As for the oxidative step, sample vials are placed under boiling water and sonicated briefly every 2 minutes for 30 minutes. Once the reductive step done, samples were subjected to a final rinse using Mili-Q water. This step is the most time consuming because of the extreme toxicity of reagents and the explosive characters of hydrazine on contact with oxidants.
- A weak HNO_3 leach (0.001 M) was done to eliminate any remaining contaminant phases that could still be attached to the shells.

This cleaning protocols have evolved from the Cd/Ca and Ba/Ca cleaning methods initially developed by Boyle, 1981; Boyle and Keigwin, 1985 and Lea and Boyle, 1991. However, there is a strong debate concerning the benefits of removing all these contaminants for TE/Ca ratio investigation (Brown and Elderfield 1996; Martin et al. 2002; Barker et al. 2003; Pena et al. 2005, 2008; Boussetta et al. 2011, 2012). Consequently,

the cleaning methods used differ between laboratories, and between depositional conditions.

For these two reasons, (i) low foraminifera concentration and (ii) inconsistencies in cleaning effects on Mediterranean Mg/Ca reconstruction, and because the 'Pole Spectrometrie Ocean' is equipped with a laser ablation system coupled to a HR-ICP-MS Element II, I decided to set up the laser ablation technique on foraminifera shells. My aim was also to try compare the different methods (chemical cleanings and Laser Ablation).

3. Objectives

- 1/ Set-up foraminifera cleaning in Brest clean room and start foraminifera cleaning,
- 2/ Set-up the micro-analytical foraminifera shells sampling using laser ablation coupled with high resolution plasma mass spectrometry (LA-HR-ICP-MS) with PSO instruments,
- 3/ Compare results obtained with LA-HR-ICP-MS and classic ICP-MS data,
- 4/ Produce a long record of the Rhone rivers paleo-hydrology, using Mg/Ca Ba/Ca and $\delta^{18}\text{O}$ measurements.

4. Set-up of foraminifera cleaning in Brest

This was done during the summer 2014, with advices from W. Doss (postdoctoral researcher from UCLA), in IFREMER clean labs (class 1000). During those two months, I was in charge of:

- Ordering material,
- Preparing the clean lab: cleaning of foram's vials, building foram's vial racks,
- Preparing the reagents and acid (see detailed protocols at the end of the present appendix).

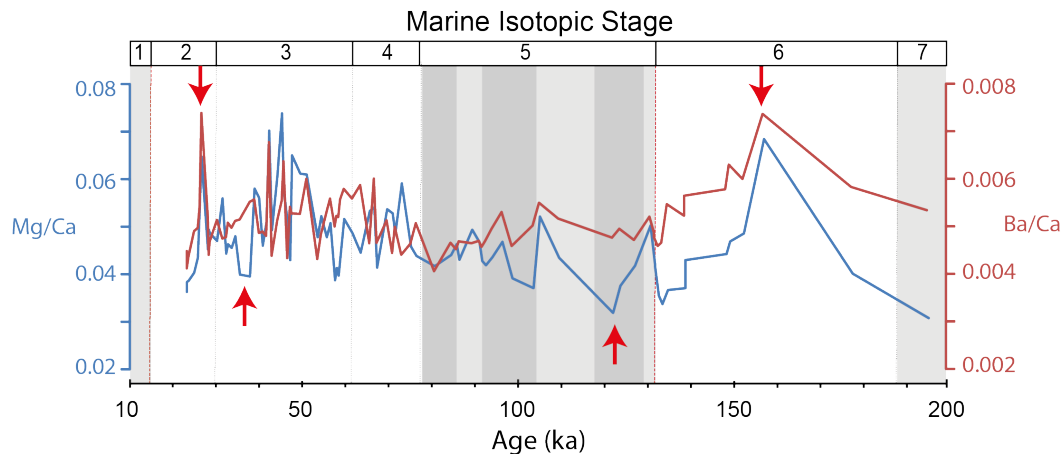


Figure 59

Downcore Mg/Ca and Ba/Ca records obtained from bulk carbonate leaching experiments using Rongemaille et al. (2011) methodology. Red arrows points toward the selected intervals used in this study.

In order to compare different cleaning procedures, I selected two different samples showing high and low Mg/Ca and Ba/Ca ratio during glacial and interglacial conditions, see **Figure 59**, using down core bulk carbonate leaching experiments. I picked approx. 50 individual shells, and I subdivided them into discreet cleaning sets and applied the cleaning

steps separately, see **Figure 60**. Shells of planktonic foraminifera *Globigerina ruber* (white variety) and *Neogloboquadrina packyderma* (dextral) were used in all experiments. I used two different approaches that aimed to: (i) compare the effect of each cleaning step on shell geochemistry of different specimens, (ii) directly compare efficiency of a cleaning step in removing surface contamination on the same shell, and (iii) compare data obtain with laser ablation versus the 'classic' ICP-MS measurements.

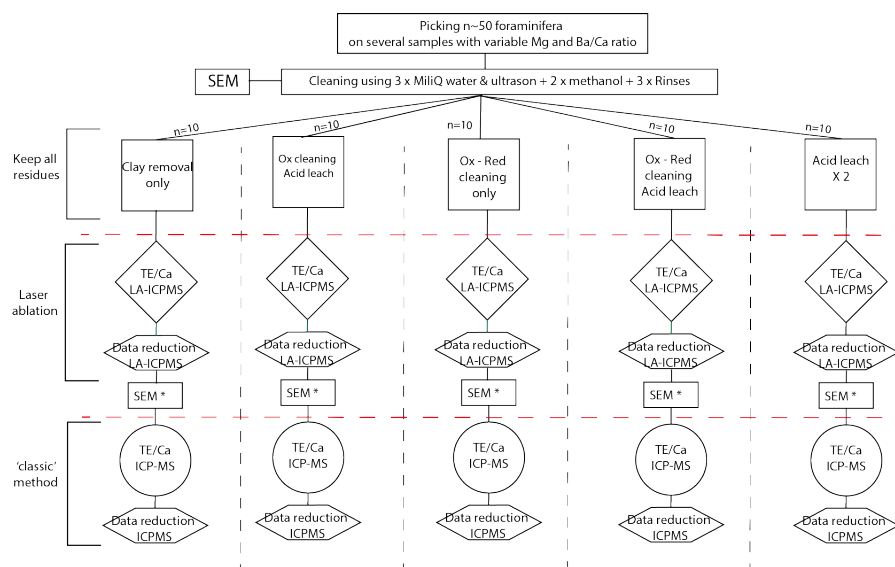


Figure 60

Methodologic approach developed in this project to better understand (i) efficiency of cleaning steps on foraminifera's shells chemistry, and (ii) eventual discrepancies between laser ablation and the 'classic' ICP-MS methodology.

5. Set-up of the laser ablation technic in Brest

This part was extremely time consuming because nobody had already tried laser ablation on micro-carbonates samples in Brest. Thankfully, the PSO is equipped with a deep UV laser (193 nm) system coupled with a HR-ICP-MS. Here in Brest, PSO engineers use the laser ablation for measuring trace elements in bulk silicate rocks, mostly for mantel processes, or carbonated matrix samples as fish ostracods where material is sufficiently big to perform long measurements.

The first step was to reproduce laser ablation conditions as described in Eggins et al. (1998) and 2003 using synthetic calcium-, sodium-, aluminosilicate glass standards NIST610 and NIST612.

After several long session of laser-ablation (March and April 2015), with the precious help of Claire Bassoulet (PSO engineer in charge of the Element II and laser ablation sampling), we finally obtained stable laser ablation condition using :

1. Laser spot of 40 μm ,
2. Laser fluence of 4.5 J/cm^2 ,
3. He flow (carrier flow) around 250 $\text{ml}\cdot\text{min}^{-1}$.

Then, we investigated the effect of the laser frequency on the mass spectrometer sample time integration, i.e. time between each mass scan realized by the mass spectrometer, in order to obtain the 'optimum condition' in the standard glass NIST 610. The idea here is

to tune the arriving of ablated material in the mass spectrometer with the time needed by the mass spectrometer to scan the entire range of elements, or in other words try to provide a constant impulse of material during one mass scan of the mass spectrometer. The results of this step are reported in **Figure 61** where we can clearly see the reduction of percentage of relative standard deviation (i.e. error; % RSD) when we decrease the mass spectrometer mass scan time, probably because decreased mass scan time lowers the injection of sample spike signal generated by laser ablation. Our best NIST 610 reproducibility was around 7 % which correspond to a laser repetition rate of 3 Hz using a mass-spectrometer sample time of 0.005 ms.

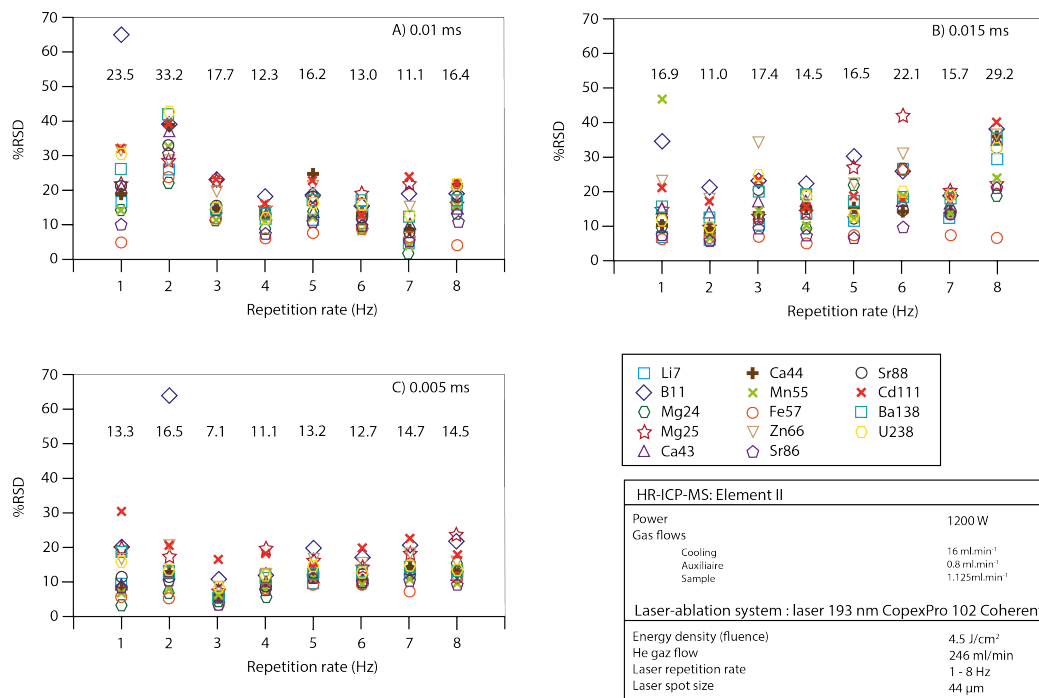


Figure 61

Relative standard deviation (RSDs in %) versus repetition rate of isotope data obtained under different 'sample time' mass spectrometer conditions: **(A)** correspond to 0.01 ms of sample time; **(B)** 0.015 ms and **(C)** 0.005 ms between individual mass-spectrometer mass scan. Within the right left box are reported the experimental condition of those experiments.

Since we obtained stable and reproducible results on NIST 610 (Fig.A.3) and NIST 612 (data not shown), we started to work on different foraminifera shells, see **Figure 62**.

At this stage (end of August 2015) of the analytical development, I was fairly confident about our HR-ICP-MS experimental set-up. Consequently, and also because I needed help for the data reduction, I contacted, by email, several researchers from European lab equipped with a laser ablation micro-sampling technic with foraminifera samples. Two of them: (i) Delphine Dissard from LOCEAN laboratory in Paris (IRD), and (ii) Aleksey Sadekov from the Godwin laboratory for paleoclimate research of the University of Cambridge, kindly answered me and proposed me to visit their laboratories and learn during few days the Art of laser ablation.

Therefore, I slightly changed my initial plan, and splitted my cleaned samples in two sets: one for data acquisition in Paris, the second for measurements in Cambridge. More than the possibility to learn laser ablation with highly qualified researchers, the collaboration was

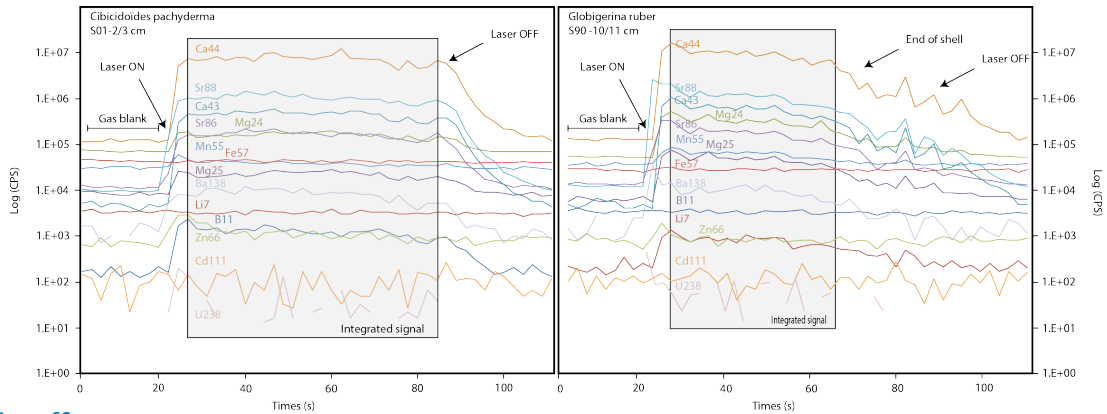


Figure 62
Time evolution of the signal intensities of several elements during ablation of a 40 μm hole into *C. pachyderma* shell (left box) and *G. ruber* shell (right box).

thought to bring the opportunity to start an inter-laboratories calibration using a single foraminifera-set; see **Figure 63**.

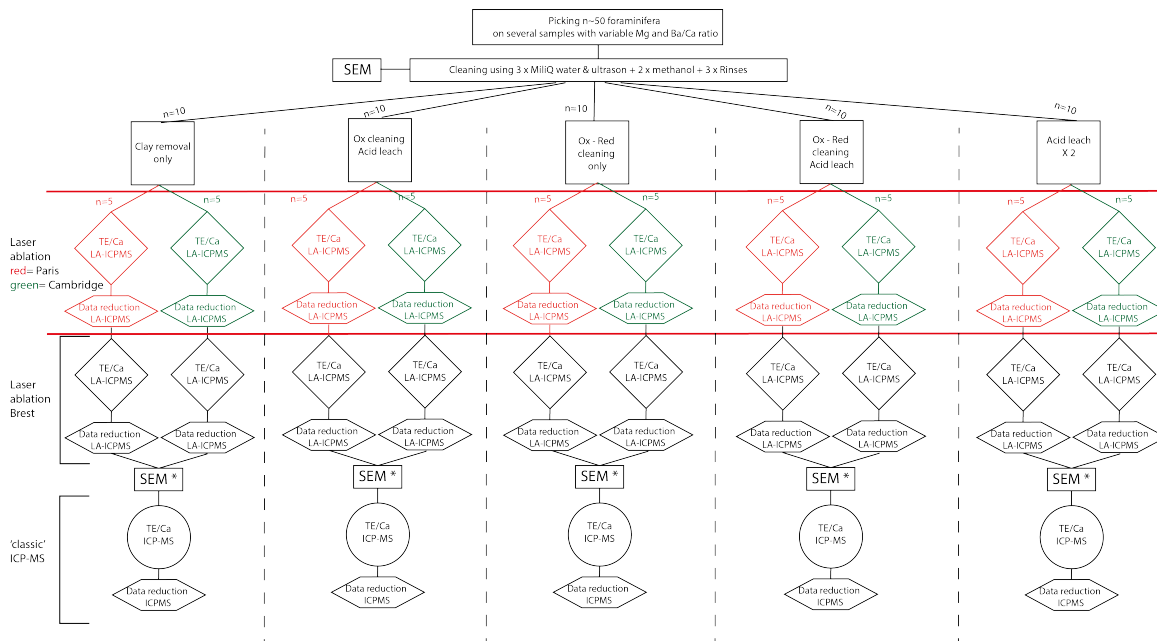


Figure 63
Methodologic approaches updated after five months of laser ablation works in Brest and the start of new collaborations with D. Dissard and A. Sadekov.

At the end of October 2015, I went 3 days in Paris to learn with Delphine Dissard, where the analytical set-up is totally different from the one in Brest. Indeed, they have a much bigger laser ablation cell which is pressurized and flushed of atmospheric gases (which is not the case in Brest). The Paris laser ablation system is coupled to a quadrupole ICP-MS instrument (Micromass Platform ICP). Moreover, Delphine does not work with sedimentary foraminifera shells but mostly use pure-cultured foraminifera, therefore she was not aware of

the effects of chemical cleaning because cultured foraminifera do NOT have any diagenetic overgrowths (coatings). Nevertheless, I learned a lot of information regarding the tuning of the mass spectrometer and the pre-sequence steps. Few of them are summarized here:

- Several total clean-up (i.e. purge) of the laser ablation cell are required before starting any measurements,
- Mass spectrometer tuning is done on NIST 610 raster (i.e. surface ablation) to obtain Th/ThO interference under 0.5 %,
- NIST 610 and 612 are analyzed in the 'analytical conditions' (i.e. downward holes) every 20 ablations to correct instrumental drifts (i.e. bracketing technic),
- Laser spot and energy have to be adapted to each calcite type (i.e. according to the foraminifera specie).

During this visit, Delphine also taught me how to use the data reduction software: Glitter which allows rapid selection of the best intervals for background and signal measurements. Using NIST 610 concentration of Pearce et al. (1997), and Ca as internal standard, Glitter software provides calculation (i.e. mean values obtained during user defined integration time, and errors) of the results for each analysis obtained during the LA-ICP-MS session. Using this technique, Ca is ideal because its concentration is assumed to be constant at 40 wt% in all calcitic foraminiferal tests. Such assumptions allow direct comparison of trace metal to Ca ratio obtained with the wet-chemical studies (i.e. 'classic' ICP-MS).

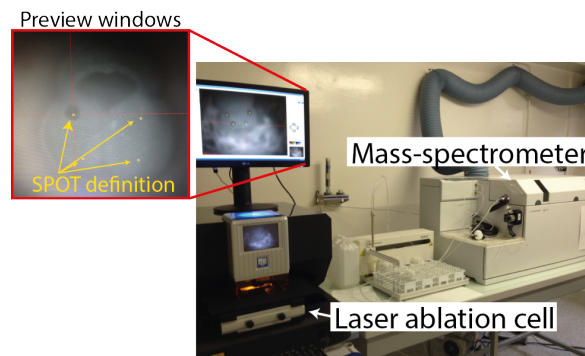


Figure 64

Laser ablation coupled to Quadrupole ICP-MS in Delphine Dissard lab (LOCEAN, Paris-Bondy).

One week after, I moved to Cambridge to work with Aleksey Sadekov for a week. Once there, the first half-day was devoted to meeting, discussion and establishment of the best strategy for the coming week. For me, this discussion was very interesting because I learned many things but the most important two were that :

1. To set-up a laser ablation with an Element II requires many skills, time and experience (which I did not have at all !),
2. The type of laser ablation cell that we have in Brest are not designed for laser ablation on foraminifera,
3. You DO NOT need to chemically clean the foram shells because the laser will do it for you,
4. You need at least 20 foraminifera shells, and each chamber must be analyzed at least four times to obtain a statistically robust Te/Ca ratio.

[At this point I felt totally desperate and stupid]

But in view of my motivation and all efforts I had made to get there, Aleksey proposed me to learn the Cambridge's way to prepare foraminifera for laser ablation using my 'useless' foraminifera (i.e. because (i) 5 foraminifera shells are not enough to obtain robust and publishable data and (ii) because of unnecessary chemical cleanings). Foraminifera chambers were first severed using a scalpel, and then cleaned by ultrasonication in methanol for 2-3 minutes to remove clays and other adhering detrital particles. Then the chamber surfaces were examined under a high-magnification stereo-microscope to check for the presence/absence of remaining surface contamination, and cleaned again when necessary. Once cleaned, foraminifera shell fragments were mounted on specific carbon tape, and stored prior to analyses. This step is essential for obtaining a 'clean' dataset but extremely time consuming. For example during one day and a half, I prepared only 20 shells which correspond to one sample.

The Cambridge equipment has been designed to increase the mass spectrometer sensitivity, and improve laser ablation. For example, they add N_2 in the carrier gases mixture which make the plasma hotter and therefore increase the stability and sensitivity of the detectors (i.e. increase by 8-fold sensitivity, but induce more interferences with Mn). The torch position tuning is performed using an automatic software which moves the torch position during a NIST 610 raster in order to obtain the lower Th/ThO ratio possible. After the first coarse tuning (i.e. change torch position 0.5 cm), the software re-injects the best torch position for a second tuning sequence (i.e. moving the torch about 0.1 cm) and a third very fine tuning is done where the torch moves are lower than the millimeter. Such sequential tuning is a necessary step to start acquisition with Th/ThO < 0.5 %. After the tuning, samples are placed under the ablation cell and photographed prior to the flushing of the cell. It is very important to flush the cell of atmospheric air because ^{43}Ca and ^{44}Ca are very sensitive to air (i.e. Argon), and variation of pressure within the cell injects air in the plasma during cell displacements. During the flush (> 2 hours), we can prepare our ablation spot on foraminifera shells using the very high-quality picture, which also allows laser's focus for each foraminifera surface. Aleksey also taught me the use of another software: Iolite which is a specific software developed for element ratio calculation with laser (contrary to Glitter which has been developed for U-Pb datation in Zircon) and does not need internal standard. As for Glitter, the user defines a blank and a sample interval but this time results are exported as a function of time.

Back to Brest, I finished the data-reduction step and played with both dataset in order to compare them (1 month). I was very frustrated because nothing convincing was observable when comparing the data sets probably because (i) the instrument configurations were very different between data acquired in Paris and Cambridge, (ii) the data processing technique used were different (I tried to reprocessed data obtained in Paris with Iolite, which I personally think more accurate and precise, but it was not possible because the software needs a specific file generated by the laser which is not usually created in Paris) and (iii) the number of analyses was not sufficient to observe real effect of the cleaning effects on foraminifera calcite.

Finally after almost one year (from March 2015, when I did my first laser ablation test in Brest and January 19 2016), I presented my conclusion to people involved in this project. The main conclusions are summarized here:

- i Set-up LA-HR-ICP-MS in Brest require:
 - (a) Engineer time
 - (b) Experience with Element II tuning and laser
 - (c) Modification of existing laser system ablation (i.e. at least buy a SQUID and if possible change the laser ablation cell)

- ii A strong data reduction software (i.e. Iolite)
- iii A high-magnification stereo-microscope for cleaning procedure

6. What about my TE/Ca PhD project?

After, these introductions to the art of laser (which is really something different from our 'classical' geochemistry view), I realized that my best option was to stop this project because:

- i Almost half of my PhD was done,
- ii In five days in Cambridge, I was able to generate 240 laser ablation spectre which represent less than the number of spectre required for one sample. Indeed, according to the methodology published in Sadekov et al. (2008), almost 300 ablations are required per samples (i.e. you need at least 20 foraminifera shells, where you will analyze at least 3 chambers with 5 laser spots per chamber),
- iii Because I did not have the necessary equipment for the cleaning and preparation of my samples in Brest, I had to be physically present in Cambridge to do this,
- iv Because I did not have the money to update the laser ablation system already existing in Brest.

I really liked to work with laser ablation technique, even if it is very time consuming and painful, because it is a very powerful tool which gives some precise dataset without any chemistry 'contaminations'.

Now with some hindsight, I am happy to have lost time learning this technique for many reasons. First, I met fantastic people both in Paris and Cambridge who have transmitted their knowledge to me without expecting anything in return which is becoming increasingly rare in the scientific world. Secondly, this teaching opened my mind to the use of laser ablation world and I hope to be soon able to use it again for investigation of the diagenetic effect on the carbonated associated sulfate.

[Finally but not least, only Jedris can use lightsabers !]

7. Foraminifera cleaning protocols

Clay removal [Siphon use new small pipet tip, suck up HCl and water first]

1. Fill with methanol (kept in fume hood), rap, settle, and siphon to $\sim 1/4$; Ultrasonicate 1-2 min
2. Repeat 3x w/ Q; 2x w/ methanol; 1x w/ Q reverse rack each time
3. Fill w/ Q and siphon most out

Reduction (oxide removal)

In fume hood, wearing safety goggles

1. Rinse pipet tip
2. 1) Add 100 μL Reducing Agent using repeater pipet (setting 2 and 2.5 mL syringe)
Note: if cleaning small samples with inserts, use 25 μL Reducing Agent (setting 1 and 1.25 mL syringe)
 - (a) When done with Red Agent, put in hazardous waste vial in fume hood leave bottle cap off in fume hood to evaporate
3. Cap tightly and cover rack, securing with tie wraps (push tubes up so that tops are flush with rack cover)
4. Put rack in hot bath 30 min, ultrasonicing for a few secs every 2 min
5. Allow to cool
6. Siphon off reagent
7. Rinse caps and fill tubes w/ Q, rap, settle, and siphon
8. *Bring back to flow bench:* Rinse caps again, fill, rap, settle and siphon 3x more

Oxidation (OM removal)

1. Add 250 μL Oxidizing Agent (in laminar flow bench) using repeater pipet (setting 5 and 2.5 mL syringe)
 - (a) Lasts ~ 8 squirts, refill after 7
2. Cap and cover (don't attach with tie wraps) and put in bath
3. Heat 5 min; ultrasonicate few secs; Heat 5 min; ultrasonicate few secs
4. Bring to laminar flow bench
5. Siphon off liquid from vial tops
6. Rinse caps and fill tubes w/ Q, rap, settle, and siphon; Repeat (check carefully for floating fragments during these steps)
7. Fill \sim halfway w/ Q, Heat 5 min, ultrasonicate, siphon; Repeat

Fill w/ Q and siphon

Sample transfer

Fill \sim halfway w/ Q. Centrifuge vials ~ 2 min

Cut tip off 50 μL pipet (use smaller)

Remove vial from rack, place pipet near to bottom of vial to draw up sample

Draw up samples and transfer to new, labeled tubes Push pipet to bottom of new vial to avoid bubble at bottom (rinse pipet between each sample)

Pipet 2x, then tap, then 3rd time, then check for leftovers

Weak acid leach (not for size 1 or single bugs)

Siphon out Q; Fill w/ Q and siphon again close vial if not leaching
Add 250 μL 0.001 N HNO_3 (unless very small sample) record in notebook
Ultrasonicate 30 sec, rap, settle, and siphon
Repeat 0-4x more (depending on sample size)
Fill w/ Q
Note approximate sample size (1, 2, or 3) and record
Rap, settle, and siphon
Remove \sim all remaining Q using 50 μL (smallest) pipet (rinse pipet between each sample)
Cap and store

8. Reagents and Materials needed for foraminifera cleaning

New supplies needed for each run crushed samples in μ 30 clean tubes
process blank ('PB') - optional
30 extra clean tubes
2 clean 60 mL bottles (kept in oven, filled w/ 0.5 N HCl)

Remember always use tip rinse for new pipet tips (acid/Milli-Q, x3)
when siphoning, check for forams at surface of liquid, or clogging tip (careful!)
minimize amount of time that open tubes are outside the laminar flow bench (only during Reduction step)
change gloves often
watch for droplets on pipet tips
beware dust!

1. Wipe down surfaces bench and hood
2. Rinse two 60 mL bottles (dump acid in fume hood waste jug)
3. Heat Milli-Q in evaporating dish (~ 85 °C, dial ~ 3 -3.5) w/ watch glass (rinse dish and watchglass first)
4. Fill ultrasonicator with fresh Q, insert wire rack, and place to left of flow bench
5. Fill tip rinse HCl and Replace tip rinse Q
6. Check siphon flask (under sink)

Reagent preparation (in 60 mL bottles) DO IN FUME HOOD

1. Reducing agent ('Red' 60 mL bottle)
2 mL citric acid solution (2.5 g citric acid dissolved in 50 mL NH_4OH) + 2 mL NH_4OH + 150 μL anhydrous hydrazine (*do all of this in fume hood, wearing safety goggles, and chemical gloves when opening hydrazine; hydrazine is volatile, toxic, and explosive when mixed with oxidizers!*)
 - (a) Citric acid solution is premade, kept in fume hood (careful, low viscosity and drips)
 - (b) NH_4OH kept below fume hood
 - (c) Hydrazine kept below fume hood put this pipette tip in back beaker in fume hood
 - (d) LEAVE IN FUME HOOD when done
2. Oxidizing agent
10 mL 0.1 N NaOH + 40 μL H_2O_2 (or more, if high OM content)
 - (a) NaOH kept in laminar flow bench
 - (b) H_2O_2 kept below right of sink

LITERATURE CITED

- Barker, S., Greaves, M., Elderfield, H., 2003. A study of cleaning procedures used for foraminiferal mg/ca paleothermometry. *Geochemistry, Geophysics, Geosystems* 4 (9).
- Bemis, B. E., Spero, H. J., Bijma, J., Lea, D. W., 1998. Reevaluation of the oxygen isotopic composition of planktonic foraminifera: Experimental results and revised paleotemperature equations. *Paleoceanography* 13 (2), 150–160.
- Boussetta, S., Bassinot, F., Sabbatini, A., Caillon, N., Nouet, J., Kallel, N., Rebaubier, H., Klinkhammer, G., Labeyrie, L., 2011. Diagenetic mg-rich calcite in mediterranean sediments: Quantification and impact on foraminiferal mg/ca thermometry. *Marine Geology* 280 (1), 195–204.
- Boussetta, S., Kallel, N., Bassinot, F., Labeyrie, L., Duplessy, J.-C., Caillon, N., Dewilde, F., Rebaubier, H., May 2012. Mg/Ca-paleothermometry in the western Mediterranean Sea on planktonic foraminifer species *Globigerina bulloides*: Constraints and implications. *Compte Rendus Geosciences* 344 (5), 267–276.
- Brown, S. J., Elderfield, H., 1996. Variations in mg/ca and sr/ca ratios of planktonic foraminifera caused by postdepositional dissolution: Evidence of shallow mg-dependent dissolution. *Paleoceanography* 11 (5), 543–551.
- Eggins, S., De Deckker, P., Marshall, J., 2003. Mg/ca variation in planktonic foraminifera tests: implications for reconstructing palaeo-seawater temperature and habitat migration. *Earth and Planetary Science Letters* 212 (3), 291–306.
- Eggins, S. M., Kinsley, L., Shelley, J., 1998. Deposition and element fractionation processes during atmospheric pressure laser sampling for analysis by icp-ms. *Applied Surface Science* 127, 278–286.
- Elderfield, H., Ganssen, G., 2000. Past temperature and delta18o of surface ocean waters inferred from foraminiferal mg/ca ratios. *Nature* 405 (6785), 442.
- Fehrenbacher, J. S., Spero, H. J., Russell, A. D., Vetter, L., Eggins, S., 2015. Optimizing la-icp-ms analytical procedures for elemental depth profiling of foraminifera shells. *Chemical Geology* 407, 2–9.
- Ferguson, J., Henderson, G., Kucera, M., Rickaby, R., 2008. Systematic change of foraminiferal mg/ca ratios across a strong salinity gradient. *Earth and Planetary Science Letters* 265 (1), 153–166.
- Hall, J. M., Chan, L.-H., 2004. Li/ca in multiple species of benthic and planktonic foraminifera: thermocline, latitudinal, and glacial-interglacial variation. *Geochimica et Cosmochimica Acta* 68 (3), 529–545.
- Hastings, D. W., Russell, A. D., Emerson, S. R., 1998. Foraminiferal magnesium in globigerinoides sacculifer as a paleotemperature proxy. *Paleoceanography* 13 (2), 161–169.
- Lea, D. W., Spero, H. J., 1994. Assessing the reliability of paleochemical tracers: Barium uptake in the shells of planktonic foraminifera. *Paleoceanography* 9 (3), 445–452.
- Martin, P. A., Lea, D. W., Rosenthal, Y., Shackleton, N. J., Sarnthein, M., Papenfuss, T., 2002. Quaternary deep sea temperature histories derived from benthic foraminiferal mg/ca. *Earth and Planetary Science Letters* 198 (1), 193–209.
- Pearce, N. J., Perkins, W. T., Westgate, J. A., Gorton, M. P., Jackson, S. E., Neal, C. R., Chenery, S. P., 1997. A compilation of new and published major and trace element data for nist srm 610 and nist srm 612 glass reference materials. *Geostandards and Geoanalytical Research* 21 (1), 115–144.
- Pena, L., Cacho, I., Calvo, E., Pelejero, C., Eggins, S., Sadekov, A., 2008. Characterization of contaminant phases in foraminifera carbonates by electron microprobe mapping. *Geochemistry, Geophysics, Geosystems* 9 (7).
- Pena, L., Calvo, E., Cacho, I., Eggins, S., Pelejero, C., 2005. Identification and removal of mm-mg-rich contaminant phases on foraminiferal tests: Implications for mg/ca past temperature reconstructions. *Geochemistry, Geophysics, Geosystems* 6 (9).
- Rongemaille, E., Bayon, G., Pierre, C., Bollinger, C., Chu, N. C., Fouquet, Y., Riboulot, V., Voisset, M., Jul. 2011. *Chemical Geology*. *Chemical Geology* 286 (3-4), 196–206.
- Sadekov, A., Eggins, S. M., De Deckker, P., Kroon, D., 2008. Uncertainties in seawater thermometry deriving from intratest and intertest mg/ca variability in globigerinoides ruber. *Paleoceanography* 23 (1).
- Schmidt, G. A., 1999. Error analysis of paleosalinity calculations. *Paleoceanography* 14 (3), 422–429.

Weldeab, S., Lea, D. W., Schneider, R. R., Andersen, N., 2007. 155,000 years of west african monsoon and ocean thermal evolution. *science* 316 (5829), 1303–1307.

Appendix 2:

CarboFlux: detritic versus biogenic.

Annexe 2:

CarboFlux: Détritique versus biogène.

This work is still in progress and more time will be spent on the understanding of the obtained data-set during the coming weeks.

1. Scope of this project

The sedimentary flux is a critical parameter to understand the generation of sediment accumulations and shelf stratigraphy. It is the fundamental parameter in the 'Source to Sink' approach, even if sediment fluxes are probably one of the most difficult parameters to reconstruct over times.

The sediment flux can be defined as the sum of solid particles and dissolved chemical elements transmitted from the continent, into oceanic basins, mainly by running water. The water flux connecting land and ocean reservoirs of the global hydrologic cycle is usually known as the runoff. [Even if the amount of continental rain is negligible compared to the ocean reservoir, the flux of water from land to ocean is considerable and essential in changing ocean bulk chemistry, nutrient loading and biological productivity.]

There are two strategies for evaluating the yield and mechanical denudation based on the export sediment: use the rate of filling of the oceanic basin and/or calculate the volume of sediment accumulated within the sedimentary basin. Both strategies estimate the volume of sediments in the sink zones of the sediment routing system using isopachs and cross-sections derived from borehole and seismic reflection lines. An average solid accumulation rate can be calculated depending on (i) the seismic penetration and borehole depth, after correction of the effect of compaction of the stratigraphic sequence, and (ii) physical proprieties of sedimentary units (i.e. density, porosity, chemical composition for example; Cremer et al. 1992; Auffret et al. 2002; Andrews and Eberl 2007). Recent basin scale sedimentology studies allow fine estimation of sedimentary fluxes over times; see Guillocheau et al. (2012) or Leroux et al. (2015).

In the same times, sediment provenance studies using geochemical and isotopic tracers give new insight into the weathering conditions, transport and deposition of on-shore and offshore sediment accumulation, see Révillon et al. (2011). These studies have focused on sand, coarse and fine silt, and clay fractions resulting from the weathering of crystalline, metamorphic and volcanic units.

Although, carbonated lithologies are part of most watersheds they are not often, or not at all, taken into account in sedimentary flux studies. Carbonates, which are a significant component of margin sediments are always considered as the result of marine biogenic production. The question here is: **are we sure of this hypothesis?**

Bulk sediment accumulation rates is defined as a sediment thickness by unit of time, in cm.ka-1. Also, we know that the weight of the sedimentary column caused an increasing compaction. Therefore, the sedimentation rate become quickly inadequate to quantify sedimentary inputs. To discard the compaction problem authors integrated the particle density in sediment accumulation rate. Thus, flux calculation uses the weight of particles per unit of area and times ($\text{g.cm}^{-2}.\text{ka}^{-1}$). Using this approach, it is possible to determine different components in a given sediment (i.e. terrigenous, biogenic, dissolved fraction). Determining terrigenous fluxes, or mass accumulation rate, using sedimentary sequence is commonly based on the application of the equation 16 proposed by Auffret et al. (2002).

$$MAR = LSR \times D_{\text{dry}} \times (1 - \text{carbonate content}) \quad (16)$$

Where LSR is the linear sedimentation rate in cm.kyr^{-1} , and D_{dry} correspond to the dry bulk density in g.cm^{-3} .

Since there is no evidence of diagenetic neo-formation resulting of anaerobic oxidation of methane (which product calcium carbonate during degradation of organic matter), the non-carbonated fraction is considered to represent the terrigenous component. In such case, authors simplified the terrigenous fraction, which is the result of land erosion transport in sedimentary basin by rivers or wind, and defined it as the land non-carbonated flux. In opposition to the marine biogenic production which is assumed to be only carbonated (i.e. mollusks, bivalves, nannofossils, foraminiferas among others). Such approach is commonly used but remains a coarse approximation since the detrital origin of carbonates is not taken into account, just like considering the marine production as carbonated only (i.e. organic matter, algae, sponges, diatoms). In the Gulf of Lion previous studies have shown that sediments are composed of $\sim 30\%$ of carbonated fraction, even during glacial times where the biogenic production is assumed to be reduced. Knowing the fact that the watershed is composed of abundant carbonated units, see **Figure 65**. We can question whether the sedimentary fluxes calculations are biased. The question is among this 'bulk-carbonated' fraction what is the real part of biogenic sediments, which are produced in-situ, against erosional products from the catchment area?

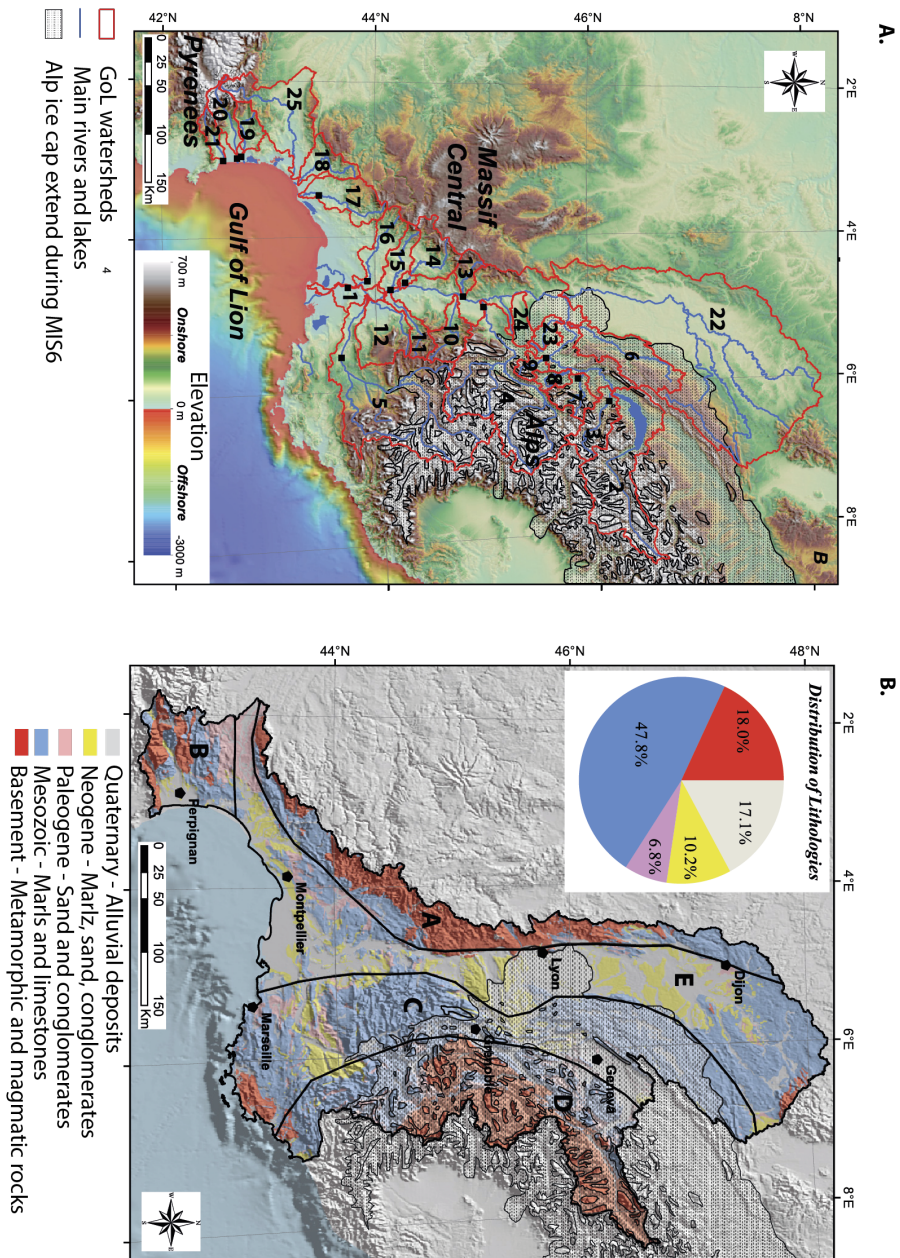


Figure 65

(A) Morphologic context in the Gulf of Lion and catchments. Names of catchments: 1) Rhone; 2) Leman; 3) Arve; 4) Isere; 5) Durance; 6) Ain; 7) Fier; 8) Bourget; 9) Guiers; 10) Drome; 11) Aygues; 12) Ouveze; 13) Eyrieux; 14) Ardeche; 15) Ceze; 16) Gard; 17) Herault; 18) Orb; 19) Agly; 20) Tet; 21) Tech; 22) Saone; 23) Bourbre; 24) Oron; 25) Aude. (B) Geological context and distribution of surface type rocks. The structural domains are: The structural areas are: A) Massif Central; B) Pyrenees; C) Alpine foreland; D) Inner part of the Alps; E) Plain. Maximum extension of ice cap from Delmas et al. (2009) and Coutterand (2010) for Alps and Pyrenees respectively. From Molliex et al. (2016).

Sedimentation in the Gulf of Lion results from the denudation of several catchments distributed in different structural domains covering a total drainage of $\sim 120\,000\text{ km}^2$ (**Figure 65**). Most of the sediments are carried by the Rhone river which provides 90 % of the sedimentary flux (Aloisi 1986; de Madron et al. 2000). The remaining supplies came from Languedocian rivers (Herault, orb, Aude, Tet and Tech respectively from east to west). The global catchment is composed of up to 50 % of carbonated rocks (Molliex et al. 2016) which represent $\sim 40\%$ of the total eroded then offshore transported (i.e. mean value calculated with a multi-approach quantification of denudation rate in the Gulf of Lion; refer to Molliex et al. (2016) for a thorough review). Those carbonated lithologies are mostly located in the Alp foreland, where the erosion rates have been estimated between 100 and 150 mm.k^{-1} . Most of these carbonated rocks have been deposited between Cretaceous and Neogene ages, with various proportions within every catchment as you can see on the **Figure 67**.

2. Geochemical approach

The main goals of this project are to (i) identify, (ii) characterize, and (iii) quantify the occurrence of detrital carbonates in the Gulf of Lion sediments.

For this we applied a geochemical approach coupling the use of element elements (trace and major) and radiogenic isotopes ($^{87}\text{Sr}/^{86}\text{Sr}$). Such methodology is based on the fact that the $^{87}\text{Sr}/^{86}\text{Sr}$ ratio of sea water has changed significantly over geological times (in response to the input of varying proportion of Sr delivered from continental crust and upper mantle sources through time). Carbonate mineral phase that precipitated under marine conditions record accurately the $^{87}\text{Sr}/^{86}\text{Sr}$ value of the sea-water from which it precipitated (Hodell et al. 1990, 1991; Hodell and Woodruff 1994; Veizer 1989; Veizer et al. 1999; McArthur 1994; McArthur et al. 2001). It was also reported that local riverine inputs did not alter the $^{87}\text{Sr}/^{86}\text{Sr}$ of sea water in the depositional environment. Therefore, using $^{87}\text{Sr}/^{86}\text{Sr}$ ratio we should be able to fulfill our objectives, see **Figure 66**.

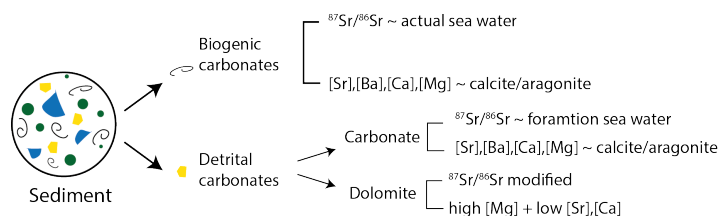


Figure 66

Schematic showing the methodological approach used in this project.

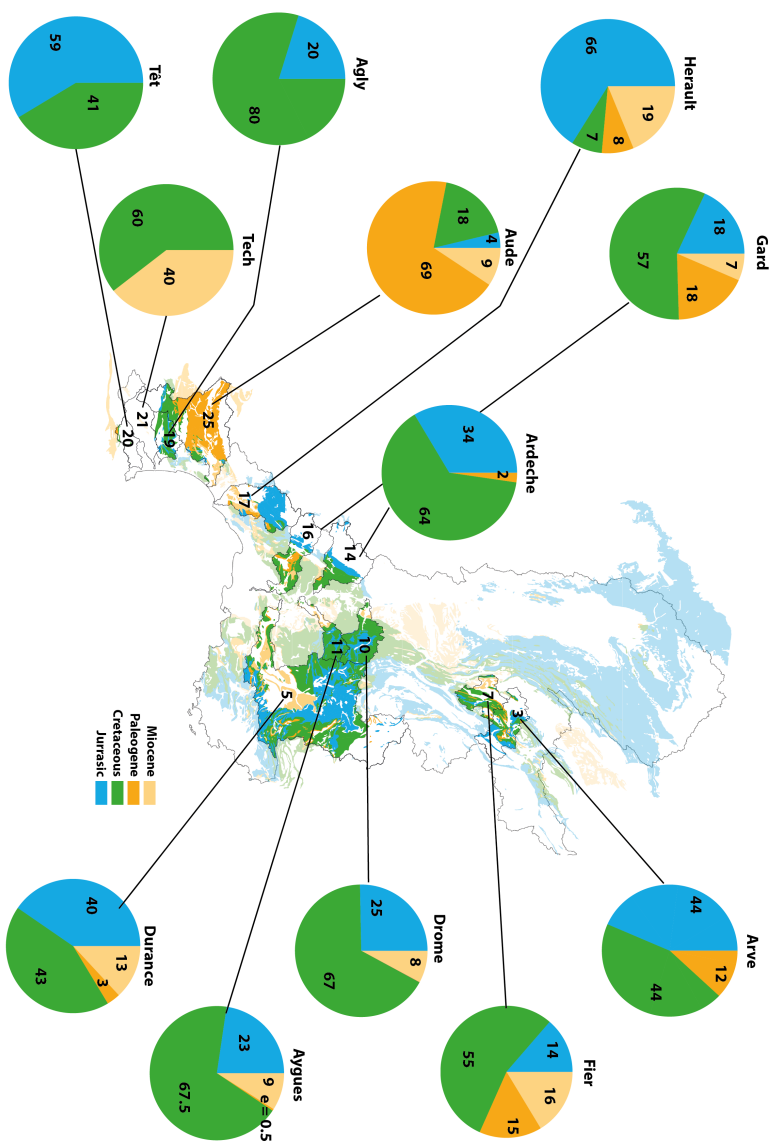


Figure 67

Distribution of carbonated rocks color-coded by age. The pie show the percentage of spatial extent of individual carbonated lithologies for selected catchments.

3. Identification of detrital carbonate in the Gulf of Lion sediments

The first, geochemical characterization has been done on PRGL 1-4 bulk sediments. For this study, it was necessary to choose an interval showing important variations in the detrital flux of carbonates and/or biogenic carbonates. Therefore, we selected 12 samples across the termination II (i.e. centred around 130 ka), where the percentage of calcium carbonate (% CaCO₃) range between 31 and 42 wt%, and which correspond to the transition between a glacial (i.e. high erosion in the catchment area that may induced higher detrital carbonate export) and interglacial conditions (i.e. where the biological production is important), see **Figure 68**.

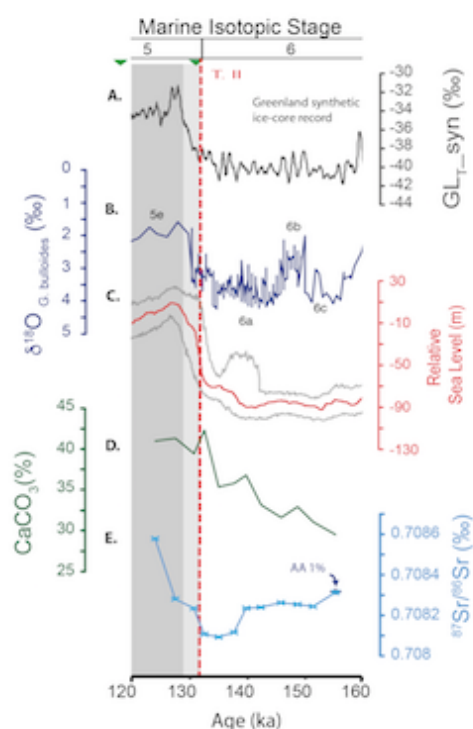


Figure 68

(A) Greenland synthetic $\delta^{18}\text{O}$ record ($\text{GL}_{\text{T-syn}}$; (Barker et al. 2011); (B) $\delta^{18}\text{O}$ of planktonic species [*G. bullodes*] (Sierra et al. 2009); (C) Red Sea sea level record (core KL09, red curve, grey line corresponds to with maximum probability 95%, ((Grant et al. 2014))); (D) % of CaCO₃ from bulk PRGL1-4 sediments (this study); (E) $^{87}\text{Sr}/^{86}\text{Sr}$ values obtained from the carbonated fraction of PRGL1-4 sediments (this study). Green triangles indicate position of age model tie-points. Grey bands indicate interglacial conditions s.l, dark grey bands indicate interglacial warm-periods. Termination (T.) according to (Barker et al. 2011). Scheme of marine stage according to (Railsback et al. 2015).

At this time, to go further in our investigation, the next step was to know the exact composition of the biogenic carbonated preserved in our samples. For that, I hand-picked biogenic carbonates (i.e. foraminifera and bivalve shells), in samples showing the maximum of amplitude in $^{87}\text{Sr}/^{86}\text{Sr}$, for individual shell Sr isotopic measurement. Samples were cleaned following the technic that I learned in Cambridge (i.e. samples were first severed using a scalpel, and then cleaned by ultrasonicing in methanol to remove clay.

Then samples were examined under a microscope for the presence of remaining surface contamination, and cleaned again when necessary). The application of laser ablation coupled to inductively coupled plasma spectrometry, in this case using a multi-collector mass spectrometer LA-MC-ICP-MS, for Sr isotopic measurements is easier than Te/Ca measurements because (i) biogenic calcite contains high amount of Sr, (ii) there is not interference between Sr isotopes and atmospheric air (i.e. ablation chamber do not need to be flushed), and (iii) MC-ICP-MS only focus on the masses of interest (i.e. no scan mass). Thanks to the help of E. Ponzevera this technic is routinely done in Ifremer. The ablated carbonates all display Sr isotopic compositions ($0.7092 \sim 0.0002$; mean value \pm SD) similar to the modern seawater values (0.70918; Veizer 1989), see **Figure 69**.

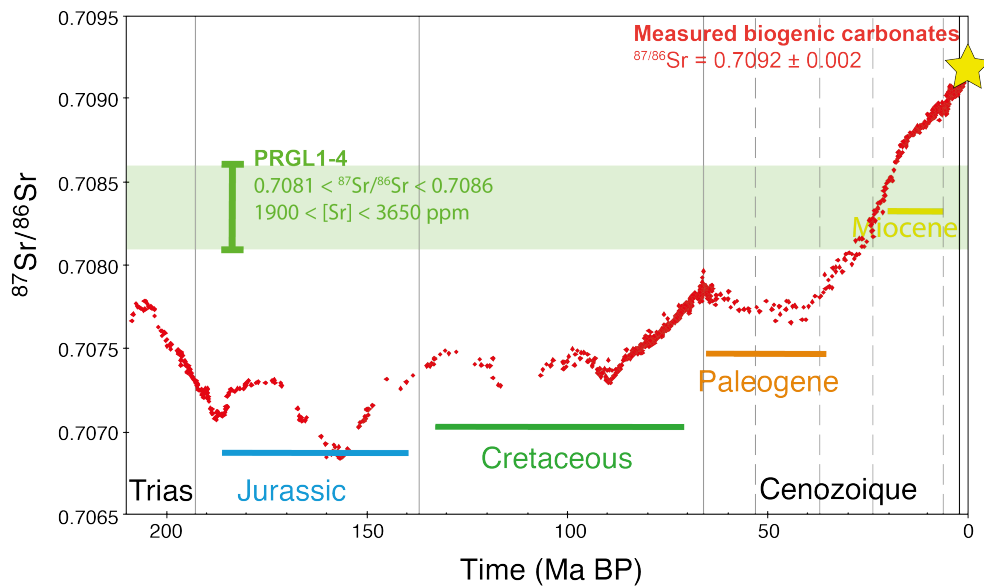


Figure 69

Evolution of the sea-water strontium isotopic composition through time from McArthur et al. (2001). The green band show the range of PRGL1-4 samples (i.e. carbonated fraction; this study). The yellow star indicate the Sr isotopic composition of biogenic carbonated obtained during this study. The colors horizontal bands give the mean composition of the mean carbonated units of the Gulf of Lion's watershed.

In this study, significant efforts have been done to measure accurate $^{87}\text{Sr}/^{86}\text{Sr}$ isotopic composition of various carbonated fractions in order to better understand the natural variability of $^{87}\text{Sr}/^{86}\text{Sr}$ in a bulk marine sample.

First our results show that the strontium isotopic of biogenic carbonates preserved in our samples range about 0.7092 ± 0.0002 , as observed in the modern global sea-water Veizer 1989. Therefore, we confirmed that modern carbonated in the Gulf of Lion are close to the isotopic composition of modern sea-water.

There is large $^{87}\text{Sr}/^{86}\text{Sr}$ isotopic composition in the bulk carbonated fraction, see **Figure 68**. All bulk $^{87}\text{Sr}/^{86}\text{Sr}$ isotopic composition are less radiogenic than sea-water composition, therefore can be explain by three different natural processes: (i) post-depositional processes, (ii) clay contamination, and/or (ii) mixing between biogenic carbonates and older carbonates from the catchment which less radiogenic according to their ages (**Figure 69**).

4. Characterization of carbonates preserved in Gulf of Lion marine sediments

By accepting that well-preserved foraminifera and bivalve shells calcite are a reliable proxy for seawater strontium isotopic (i.e. range in the composition of modern sea water), we therefore discard the diagenesis hypothesis. Because, (i) clay contamination lead to more radiogenic compositions (i.e. clay fractions are characterized by very high radiogenic composition, Révillon et al. 2011), and (ii) co-variation are observed between $^{87}\text{Sr}/^{86}\text{Sr}$ and [Al] (i.e. $R^2=0.02$, clay fraction is mainly composed of alumina-silicate, therefore the concentration in Al is often used as indicator of clay contamination). Therefore, the bulk carbonate isotopic compositions cannot reflect clay contamination during samples preparation. As a consequence, our PRGL 1-4 $^{87}\text{Sr}/^{86}\text{Sr}$ composition must reflect a mixing of two isotopically different sources of carbonates: (i) marine biogenic carbonate, and (ii) detrital carbonates exported into the Gulf of Lion.

In order to validate our hypotheses, we are build a precise and accurate mixing model between marine and detrital carbonate. Moreover, mixing models are powerful for quantification of the different end-member.

5. Characterization of carbonates from the watershed

To better understand the detrital carbonates component present in our marine sediments, we tried to characterize (i) river-bed samples and (ii) pure carbonated lithologies from the catchment.

First, we start to work on river-bed samples because they were available in Brest, thanks to the work of S. Molliex. We intentionally selected rivers showing various proportions of carbonated lithologies that may be exported into the Gulf of Lion. During selection of catchment river-bed samples, a significant effort has done to select rivers in each structural domain present in the Gulf of Lion catchment, see **Figure 70**. The methodology used was the same than marine sediment, except that 5 g of bulk river samples have been digested in order to obtain sufficient amount of calcium carbonate.

The modern river-bed sediments we analyzed show strontium isotope composition ranging between 0.707413 and 0.708085, and calcium carbonate content between 1 and 40 %, see **Figure 70**. We note that measured riverbed have less radiogenic compositions than modern $^{87}\text{Sr}/^{86}\text{Sr}$ values from the Rhone River reported in Albarède and Michard (1987). To ensure the reliability of our river dataset, we choose to exclude samples containing less than 5 % of CaCO_3 . Indeed, low carbonated samples were associated with high $^{87}\text{Sr}/^{86}\text{Sr}$. These very high radiogenic composition may result from contamination by non-carbonated minerals, see for example Tech and Tet samples in **Figure 70**. We also excluded the Hérault river which contains ~12 % of CaCO_3 because it is characterized by [Al/Sr] ratio up to 3 indicating clay contamination.

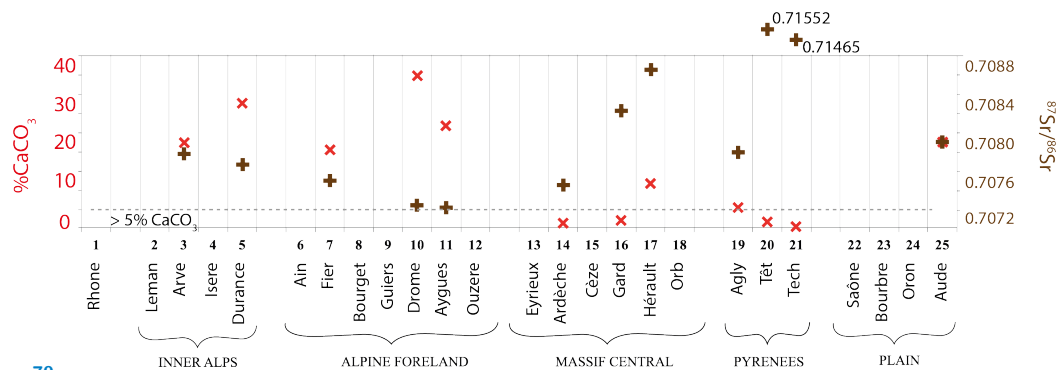


Figure 70

River-bed results. Red crosses indicated river bed's percentage of calcium carbonate, Brown crosses show the $^{87}\text{Sr}/^{86}\text{Sr}$ composition. For catchment location and name please refer to Figure 65.

The range of river-beds results is represented in McArthur's $^{87}\text{Sr}/^{86}\text{Sr}$ compilation of sea-water over the last 200 Ma, see **Figure 71**. On the same figure, we also reported the mean $^{87}\text{Sr}/^{86}\text{Sr}$ values obtained in PRGL1-4 sediments and the mean theoretical Sr isotopic composition of the catchment carbonated rocks.

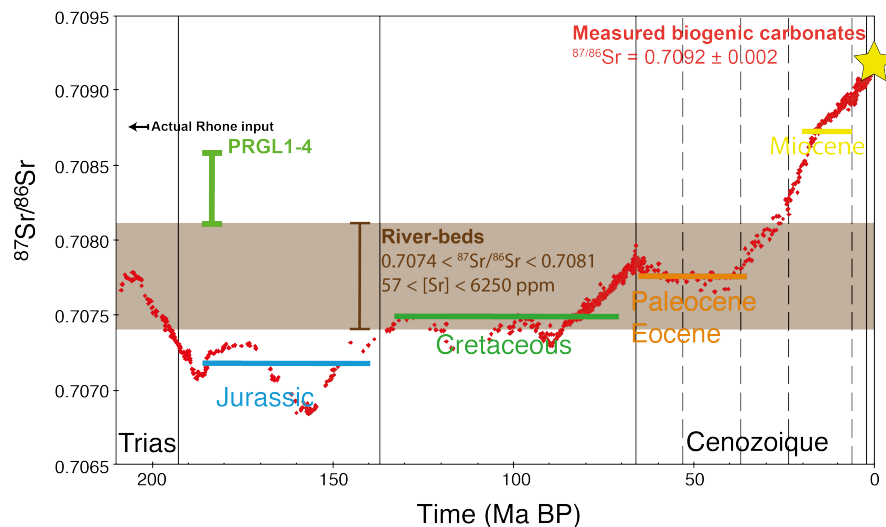


Figure 71

Evolution of the sea-water strontium isotopic composition through time from McArthur et al. (2001). The brown band show the range of river samples (i.e. carbonated fraction; this study) whereas the green brace report the PRGL1-4 isotopic composition. The yellow star indicate the Sr isotopic composition of biogenic carbonated obtained during this study. The colors horizontal bands give the mean composition of the mean carbonated units of the Gulf of Lion's watershed. The black arrow indicate the Rhone river strontium isotopic composition reported in Albarède and Michard (1987).

In this figure, we can clearly observe that measured Sr isotope composition of river-bed span between the mean compositions of the different end-members composing the catchments. This confirm that river beds are composed of mixture of the ancient carbonated rocks located in the catchment. Therefore, we can easily imagine that some of them can

be carried by rivers until the Gulf of Lion and consequently affected the bulk strontium isotopic values of sediments, as proposed earlier.

We can now use those data to construct an isotopic mixing model. This is shown in **Figure 72**, where the PRGL1-4 samples, rivers samples, and the mean foraminifera isotopic composition are also reported. In this figure, the PRGL1-4 have been color-coded according to sea surface temperature (SST) obtained on the same core, data from Cortina et al. (2016), see **Figure 72**. In this mixing model, we averaged river compositions (i.e. Sr isotopes and elemental concentrations) by main structural domains defined in **Figure 16**.

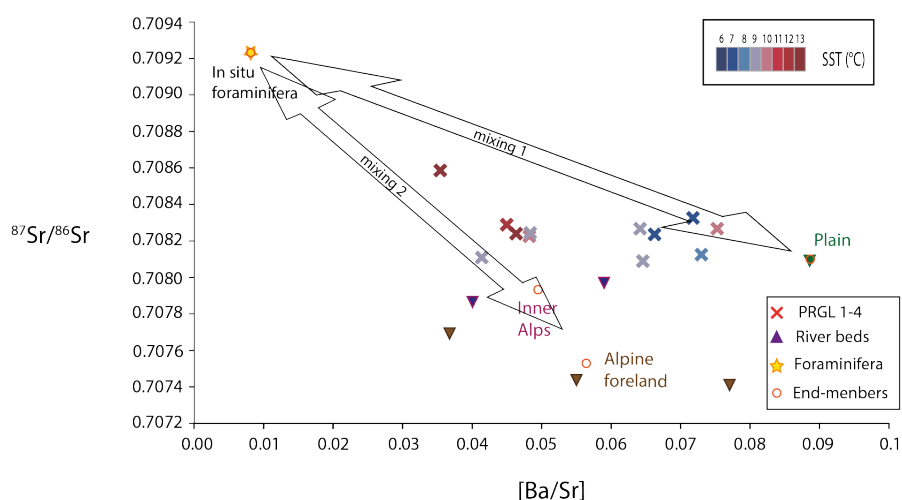


Figure 72

[Ba/Sr] ratio versus $^{87}\text{Sr}/^{86}\text{Sr}$ from PRGL1-4 carbonated fraction (crosses), in-situ biogenic production (yellow star), and river-bed samples (triangles). End-member composition from each structural domain is shown with red circles, two roughly isotopic mixing lines are represented between: (i) the biogenic end-member and the plain domain end-members, and (ii) the biogenic and the 'Alpine' end-member.

Figure 72 clearly suggests a geochemical mixing model between a biogenic end-member, defined here with the In-situ foraminifera composition, and detrital carbonates which composed the river samples from the different structural domains (i.e. Alpine foreland, Inner Alps, and Plain). The strontium isotopic composition of PRGL1-4 seems to be strongly impacted by the isotopic presence of two different pools: Plain, and Alps carbonates (i.e. defined as the Alpine end-member and composed of the inner alps and alpine foreland carbonates). Therefore, the isotopic strontium isotopic composition of the carbonated fraction preserved in PRGL1-4 may have been strongly impacted by watershed carbonated units exports by rivers.

A close examination of the PRGL1-4 samples in this mixing model, also allows the identification of a strong isotopic modulation according to sample's temperature. Samples characterized by warmer seawater conditions show an isotopic composition closer to the mixing between the biogenic and the 'Alpine' end-member. Whereas cold seawater samples reflect a higher proportion of the plain carbonates, see **Figure 72**. This could be the natural expression of several processes:

1. Change in the proportion between the biogenic compounds and the detrital carbonates. Indeed, during warm seawater conditions are associated with higher biological production of biogenic carbonates. This is consistent with a closer isotopic compo-

sition of PGL1-4 samples to the biogenic end-member. Following the same scheme, colder conditions characterize glacial times and subsequent low sea level conditions. Therefore, river accumulations are closer to our study site and more detrital carbonates would have been preserved in PRGL1-4 sediments,

2. Change in the detrital isotopic composition through time in response to climatic composition. Indeed, during glacial times (i.e. colder SST) the Alps catchment area is affected by the presence of the Alps ice-cap especially in the inner Alps and Alpine foreland, see **Figure 65**. Therefore, sediments from carbonated showing an 'Alpine' should have been less eroded, and carbonates from the plain structural domain were probably preferentially exported. This should explain why sediment deposited during cold conditions are very close to the plain end-member in **Figure 72**,
3. An intermediate situation between (i) and (ii).

Nevertheless, this figure does not allows us to decipher one of these hypothesis.

6. Looking forward

In order to confirm our last finding several strategy are in progress:

- I trying to re-calculate actual river-bed isotopic composition using:
 1. The percentage of each carbonated lithology extracted from the 1/1 000 000 geological cartography from the BRGM,
 2. Theoretical Sr isotopic composition of each lithology (i.e. minimum, mean, maximum values) using McArthur et al. 2001 compilation.

This step is necessary to better understand rivers response to ice-cap movements between glacial and interglacial. And obtain an estimation of a 'glacial' mean river composition.

- In order to better characterize what happened in the catchment area, in June, I went in the watershed collect samples. This have been done with the help of L. Mocochain during 3 days. I brought carbonates from each structural domains (~ 40 samples). Analyses are still in progress ...

LITERATURE CITED

- Albarède, F., Michard, A., 1987. Evidence for slowly changing $87\text{Sr}/86\text{Sr}$ in runoff from freshwater limestones of southern France. *Chemical Geology* 64 (1-2), 55–65.
- Aloisi, J.-C., 1986. Sur un modèle de sédimentation deltaïque: contribution à la connaissance des marges passives. Ph.D. thesis.
- Andrews, J. T., Eberl, D. D., 2007. Quantitative mineralogy of surface sediments on the Iceland shelf, and application to down-core studies of Holocene ice-rafted sediments. *Journal of Sedimentary Research* 77 (6), 469–479.
- Auffret, G., Zaragosi, S., Dennielou, B., Cortijo, E., Van Rooij, D., Grousset, F., Pujol, C., Eynaud, F., Siegert, M., 2002. Terrigenous fluxes at the Celtic margin during the last glacial cycle. *Marine Geology* 188 (1), 79–108.
- Barker, S., Knorr, G., Edwards, R. L., Parrenin, F., 2011. 800,000 years of abrupt climate variability. *Science* 334, 347–351.
- Cortina, A., Grimalt, J. O., Martrat, B., Rigual-Hernández, A., Sierro, F. J., Flores, J. A., 2016. Anomalous SST warming during MIS 13 in the Gulf of Lions (northwestern Mediterranean Sea). *Organic Geochemistry* 92, 16–23.
- Coutterand, S., 2010. Etude géomorphologique des flux glaciaires dans les Alpes nord-occidentales au pléistocène récent: du maximum de la dernière glaciation aux premières étapes de la déglaciation. Ph.D. thesis, Université Savoie Mont Blanc.
- Cremer, M., Grousset, F., Faugeres, J., Duprat, J., Gonthier, E., 1992. Sediment flux patterns in the northeastern Atlantic: variability since the last interglacial. *Marine Geology* 104 (1-4), 31–53.
- de Madron, X. D., Abassi, A., Heussner, S., Monaco, A., Aloisi, J. C., Radakovitch, O., Giresse, P., Buscaïl, R., Kerherve, P., 2000. Particulate matter and organic carbon budgets for the Gulf of Lions (NW Mediterranean). *Oceanologica Acta* 23 (6), 717–730.
- Delmas, M., Calvet, M., Gunnell, Y., 2009. Variability of Quaternary glacial erosion rates—a global perspective with special reference to the eastern Pyrenees. *Quaternary Science Reviews* 28 (5), 484–498.
- Grant, K. M., Rohling, E. J., Ramsey, C. B., Cheng, H., 2014. Sea-level variability over five glacial cycles. *Nature Communications* 5.
- Guillocheau, F., Rouby, D., Robin, C., Helm, C., Rolland, N., Le Carlier de Veslud, C., Braun, J., 2012. Quantification and causes of the terrigenous sediment budget at the scale of a continental margin: a new method applied to the Namibia–South Africa margin. *Basin Research* 24 (1), 3–30.
- Hodell, D. A., Mead, G. A., Mueller, P. A., 1990. Variation in the strontium isotopic composition of seawater (8 Ma to present): implications for chemical weathering rates and dissolved fluxes to the oceans. *Chemical Geology: Isotope Geoscience Section* 80 (4), 291–307.
- Hodell, D. A., Mueller, P. A., Garrido, J. R., 1991. Variations in the strontium isotopic composition of seawater during the Neogene. *Geology* 19 (1), 24–27.
- Hodell, D. A., Woodruff, F., 1994. Variations in the strontium isotopic ratio of seawater during the Miocene: Stratigraphic and geochemical implications. *Paleoceanography* 9 (3), 405–426.
- Leroux, E., Aslanian, D., Rabineau, M., Moulin, M., Granjeon, D., Gorini, C., Droz, L., 2015. Sedimentary markers in the Provençal basin (western Mediterranean): a window into deep geodynamic processes. *Terra Nova* 27 (2), 122–129.
- McArthur, J. M., 1994. Recent trends in strontium isotope stratigraphy. *Terra Nova* 6 (4), 331–358.
- McArthur, J. M., Howarth, R., Bailey, T., 2001. Strontium isotope stratigraphy: Lowess version 3: best fit to the marine Sr-isotope curve for 0–509 Ma and accompanying look-up table for deriving numerical age. *The Journal of Geology* 109 (2), 155–170.
- Molliex, S., Rabineau, M., Leroux, E., Bourlès, D., Authemayou, C., Aslanian, D., Chauvet, F., Civet, F., Jouët, G., 2016. Multi-approach quantification of denudation rates in the Gulf of Lion source-to-sink system (SE France). *Earth and Planetary Science Letters* 444, 101–115.
- Railsback, L. B., Gibbard, P. L., Head, M. J., 2015. An optimized scheme of lettered marine isotope substages for the last 1.0 million years, and the climatostratigraphic nature of isotope stages and substages. *Quaternary Science Reviews* 111, 94–106.
- Révillon, S., Jouët, G., Bayon, G., 2011. The provenance of sediments in the Gulf of Lions, western Mediterranean Sea. *Geochemistry, Geophysics, Geosystems* 12 (8), 1–20.
- Sierro, F. J., Andersen, N., Bassetti, M. A., Berné, S., 2009. Phase relationship between sea level and abrupt climate change. *Quaternary Science Reviews* 28, 2867–2881.

- Veizer, J., 1989. Strontium isotopes in seawater through time. *Annual Review of Earth and Planetary Sciences* 17 (1), 141–167.
- Veizer, J., Ala, D., Azmy, K., Bruckschen, P., Buhl, D., Bruhn, F., Carden, G. A., Diener, A., Ebner, S., Godderis, Y., et al., 1999. $^{87}\text{Sr}/^{86}\text{Sr}$, $\delta^{13}\text{C}$ and $\delta^{18}\text{O}$ evolution of Phanerozoic seawater. *Chemical Geology* 161 (1), 59–88.

Variations climatiques et glacio-eustatiques dans le Golfe du Lion : Une approche couplée des isotopes stables et radiogéniques.

De par sa position, Le golfe du Lion est un site idéal pour l'investigation des changements paleo-environnementaux et des processus affectant le dépôt sédimentaire. Les travaux antérieurs ont permis de mettre en évidence les impacts de la variabilité climatique et glacio-eustatique sur l'organisation stratigraphique de la marge, mais également sur les exports terrestres de matière organique.

L'étude isotopique du carbone organique et de l'azote de la matière organique dans les sédiments du forage PRGL1-4 nous a permis de mettre en évidence de forts exports fluviaux lors des interstades survenus au cours des 200 000 derniers millénaires. La mise en regard de cette découverte avec les enregistrements paleo-climatologiques terrestre et marin disponibles dans la région indique que ces forts exports fluviaux résultent d'une augmentation des précipitations le long de la bordure Nord Méditerranéenne. Grâce à la position de PRGL1-4, nous proposons que ces pluies soient le résultat d'une augmentation du passage de dépressions Nord Atlantique dans le bassin Ouest Méditerranéen.

Une caractérisation des isotopes du soufre préservés dans la pyrite sédimentaire a été réalisée. Les résultats obtenus ont permis de mettre en évidence une variation isotopique insoupçonnée, l'une des plus grandes observées de nos jours, dont la cyclicité semble indiquer un fort contrôle climatique. Nous proposons deux mécanismes influençant le fractionnement isotopique: une modulation de l'activité bactérienne par le climat, et/ou (ii) une modulation locale liée à la nature des sédiments impliqués dans la formation des pyrites en lien avec les variations eustatiques.

Mots clés: Golf du Lion, Bordure Nord Méditerranéenne, Variabilité glaciaire-interglaciaire, Flux sédimentaire, Isotope stables de la matière organique, Taux de sédimentation, Isotopes du soufre des pyrites, Changement environnementaux globaux vs locaux.

Climate and sea-level variations in the Gulf of Lion: coupling stable and radiogenic isotopes proxies.

By its position, the Gulf of Lion is an ideal location for investigation of past ecological changes and processes affecting the sedimentary deposition. Previous work has highlighted the impacts of climatic and glacio-eustatic changes on the GoL stratigraphic organization, but also on terrestrial exports of organic matter.

This isotopic study based on the organic carbon and nitrogen preserved in PRGL1-4 sediments highlights important rivers runoff during warm periods of the last 200 000 years. Regional intercomparison with terrestrial and marine records indicates that these river exports resulting from an increase of precipitation over the North Mediterranean borderland. Using PRGL1-4 location, out of Mediterranean cyclogenetic area, we suggest that these pluvial events occurred in response to enhance passage of North Atlantic atmospheric perturbation into the Western Mediterranean basin.

Pyrite sulfur isotopes investigation over the last 500 kyr have also been done. The stratigraphic variations (up to 76‰) in the isotopic data reported here are among the largest ever observed in pyrite, and are in phase with glacial-interglacial sea level. These results suggest that there exist important but previously overlooked depositional controls on sedimentary sulfur isotope records. Two different mechanisms influencing the isotopic fractionation can explain the observed dataset: a climatic modulation of the bacterial activity, and / or (ii) a local sedimentary modulation involve during early diagenetic formation of pyrite in relation with the eustatic variations.

Keywords: Gulf of Lion, North Mediterranean borderland, Glacial-Interglacial, Sedimentary flux, Organic matter stable isotopes, Sedimentation rate, Pyrite sulfur isotopes, Global vs local environmental changes.